Fakultät für Medizin

Institut für Molekulare Immunologie

The role of LTßR signaling in mediating hepatic metastasis formation

Paul Florian Vandersee

Vollständiger Abdruck der von der Fakultät für Medizin der Technischen Universität München zur Erlangung des akademischen Grades eines Doktors der Naturwissenschaften genehmigten Dissertation.

Vorsitzender: Prof. Dr. Marc Schmidt-Supprian

Prüfer der Dissertation:

1. Prof. Dr. Percy A. Knolle
2. Prof. Dr. Johann J. Hauner

Die Dissertation wurde am 17.06.2019 bei der Technischen Universität eingereicht und durch die Fakultät für Medizin am 05.11.2019 angenommen.

Table of Contents

1. Summary

Metastasis, the spread of tumor cells from a primary site to other organs, is the most common cause of cancer-related death. It is an inefficient multistep process, but while many new targeted cancer therapies are available, patients diagnosed with distant organ metastases are often not curable by current therapeutic options, facing terminal disease. The liver is one of the organs most commonly affected by metastasis, which represent the majority of hepatic malignancies. However, the mechanisms driving metastasis to the liver and metastasis in general are still poorly understood, making further research in this direction very important.

Inflammation has emerged as a new hallmark of cancer, with evidence showing its support in tumor initiation, progression and metastasis. Former publications of our group have revealed that the pro-inflammatory mediators lymphotoxin (LT) alpha (LTα) and beta (LTß) support liver cancer initiation and progression. However, their role in hepatic metastasis formation has not been shown yet.

Here, a distinct role for LT-signaling in establishing metastatic manifestations in the liver is described. Using a murine T-cell lymphoma model, a clear correlation between increased LT-signaling and secondary tumor manifestations in the liver is shown in mouse models and *in vitro*. Similar effects are shown in human samples and using further mouse models LT-signaling is shown to be primarily integrated by hepatic stellate cells (HSCs), who respond with a distinct activation pattern which increases cellular adhesion and the expression of MAdCAM-1 and MMP-9.

Database research revealed that many cancers express or overexpress LTs and that this correlates with decreased patient survival in some cases. Human sample analysis in this thesis shows that LT is highly expressed in secondary liver manifestations of lymphoma patients. L-CI.5s murine T-cell lymphoma cells show a strong correlation between the level of LT expression or LTßR activation and metastatic burden in the liver in experimental mouse models. These models also suggest that the source of LTßR activation is not relevant for the phenotype and that it can be induced in trans by a subset of high LT-expressing cells.

Experiments with mice lacking LTßR specifically in sinusoidal endothelial cells (LSECs), HSCs, Kupffer cells (KCs) or hepatocytes revealed that HSCs integrate the LT signals. This activates the HSCs in a distinct way, including the typical transition to a myofibroblast-like phenotype, but without inducing fibrosis. This is confirmed by *in vitro* experiments, which, furthermore, show that HSCs activated through LTßR enable increased adhesion and transmigration of tumor cells in an artificial endothelial model.

MMP-9 and MAdCAM-1 are among the most upregulated genes in HSCs after LTßR activation. *In vitro* assays show that MAdCAM-1 knockout in HSC-like cells significantly reduces the increased adhesion of tumor cells after LTßR activation and MMP-9 inhibition in these cells reduces tumor cell transmigration but not adhesion. MAdCAM-1 upregulation on HSCs might be involved in a retention mechanism that locks tumor cells within the space of Disse through adhesion to HSCs, preventing them from re-entering the circulation. MMP-9 secretion of HSCs could be involved in activating LSECs by remodeling the ECM in the space of Disse, inducing integrin-mediated LSEC activation. Evidence for LSEC activation and cappilarization after LTßR induction with increased expression of adhesion molecules is presented here, supporting this hypothesis.

In summary, the results in this thesis highlight a role for LTßR signaling in supporting tumor cell metastasis to the liver through a distinct activation of HSCs. This activation is not tied to fibrosis but supports tumor cell adhesion and transmigration, possibly through overexpression of MAdCAM-1 and MMP-9.

2. Zusammenfassung

Metastasierung, die Streuung von Tumorzellen eines Primärtumors in andere Organe, ist die häufigste Tumor-assoziierte Todesursache. Es ist ein ineffizienter, mehrstufiger Prozess, doch obwohl viele neue Krebstherapeutika verfügbar sind, können Patienten mit Metastasen in fernen Organen mit den verfügbaren therapeutischen Optionen oft nicht geheilt werden, sehen sich also einer unheilbaren, tödlichen Erkrankung ausgesetzt. Die Leber ist eines der Organe die am häufigsten von Metastasen betroffen sind, und diese machen den Großteil aller Lebertumore aus. Allerdings sind die Mechanismen welche der Metastasierung in die Leber, und Metastasierung generell, zu Grunde liegen noch sehr schlecht verstanden, was weitere Forschung in diese Richtung absolut notwendig macht.

Entzündungen haben sich als neues Schlüsselmerkmal von Krebserkrankungen hervorgetan, und es hat sich gezeigt, dass dies die Initiation, die Entwicklung und die Metastasierung von Krebserkrankungen beeinflusst. Frühere Veröffentlichungen unserer Gruppe haben gezeigt, dass die proinflammatorischen Mediatoren Lymphotoxin (LT) alpha (LTα) und beta (LTß) den Beginn und die Entwicklung von Leberkrebs unterstützen. Ihre Rolle bei der Bildung von Lebermetastasen wurde jedoch noch nicht gezeigt.

Hier wird eine eindeutige Rolle des LT Signalwegs bei der Etablierung metastatischer Manifestationen in der Leber beschrieben. Unter Verwendung eines murinen T-Zell Lymphommodells wird eine deutliche Korrelation zwischen erhöhter LT Signalgebung und sekundären Manifestationen in der Leber in Mausmodellen und *in vitro* gezeigt. Ähnliche Effekte werden in humanen Proben gezeigt und mit weiteren Mausmodellen wird demonstriert, dass die LT Signale in erster Linie von hepatischen Sternzellen (HSCs) integriert werden, die darauf mit einem besonderen Aktivierungsmuster reagieren, welches unter anderem die Zelladhäsion sowie die Expression von MAdCAM-1 und MMP-9 erhöht.

Datenbankrecherchen haben gezeigt, dass viele Krebserkrankungen LT exprimieren oder überexprimieren, und dass dies in einigen Fällen mit einer verringerten Überlebenserwartung der Patienten zusammenhängt. Eigene Analysen von humanen Proben haben gezeigt, dass LT in sekundären Lebermanifestationen von Lymphompatienten stark exprimiert wird. Murine L-CI.5s T-Zell Lymphomzellen zeigen in experimentellen Mausmodellen eine starke Korrelation zwischen dem Ausmaß der LT Expression, beziehungsweise der LTßR Aktivierung, und der metastatischen Belastung in der Leber. Diese Modelle legen auch nahe, dass die Quelle der LTßR Aktivierung für den Phänotyp nicht relevant ist, und dass dieser auch *in trans* durch eine kleine Gruppe von Zellen mit hoher LT Expression induziert werden kann.

Experimente mit Mäusen, denen LTßR spezifisch in sinusoidalen Endothelzellen (LSECs), HSCs, Kupffer-Zellen (KCs) oder Hepatozyten fehlt, zeigen, dass HSCs die LT Signale

integrieren. Dies aktiviert die HSCs auf eine besondere Art, welche den typischen Übergang zu einem myofibroblastenähnlichen Phänotyp einschließt, ohne jedoch Fibrose zu induzieren. Dies wird durch *in vitro* Experimente bestätigt, welche darüber hinaus zeigen, dass per LTßR aktivierte HSCs eine erhöhte Adhäsion und Transmigration von Tumorzellen in einem künstlichen Endothelmodell ermöglichen.

MMP-9 und MAdCAM-1 gehören zu den am stärksten hochregulierten Genen nach LTßR-Aktivierung in HSCs. *In vitro* Assays zeigen, dass MAdCAM-1 Knockout in HSC-ähnlichen Zellen nach LTßR-Aktivierung die erhöhte Adhäsion von Tumorzellen deutlich reduziert und Inhibition von MMP-9 im gleichen Modell die Transmigration von Tumorzellen, nicht aber die Adhäsion verringert. Die Hochregulierung von MAdCAM-1 in HSCs könnte an einem Retentionsmechanismus beteiligt sein, der Tumorzellen durch Adhäsion an HSCs im Disse-Raum festhält, und sie daran hindert wieder zurück in den Blutkreislauf einzudringen. Die MMP-9-Sekretion von HSCs könnte an der Aktivierung von LSECs beteiligt sein, indem MMP-9 im Disse-Raum die extrazelluläre Matrix (ECM) umgestaltet und dadurch eine Integrin vermittelte LSEC Aktivierung induziert. Unsere Ergebnisse zeigen eine Kappilarisierung der LSECs nach LTßR Induktion, mit erhöhter Expression von Adhäsionsmolekülen, was diese Hypothese stützt.

Zusammenfassend zeigen die Ergebnisse dieser Arbeit das LT Signalgebung die Metastasierung von Tumorzellen in die Leber durch eine spezielle Aktivierung von HSCs unterstützt. Diese Aktivierung ist unabhängig von Fibrose, aber unterstützt die Adhäsion und Transmigration von Tumorzellen, möglicherweise durch Überexpression von MAdCAM-1 und MMP-9.

Abbreviations

abbreviation(s)	full name
a-sma	alpha smooth muscle actin
BL	Burkitt's lymphoma
BMDC	bone marrow-derived dendritic cell
CAC	colitis-associated cancer
CAM	cell adhesion molecule
CCL	CC-chemokine ligand
cHL	classical Hodgkin's lymphoma
CIA	collagen induced arthritis
CLL	chronic lymphocytic leukemia
colI	collagen-I
CTC	circulating tumor cell
CXCL	chemokine (C-X-C motif) ligand
DC	dendritic cell
DEN	diethylnitrosamine
DLBCL	diffuse large B-cell lymphoma
DNA	deoxyribonucleic acid
DTC	disseminated tumor cell
EAE	experimental autoimmune encephalomyelitis
EBV	Eppstein-Barr virus
ECM	extracellular matrix
EGF	epidermal growth factor
EMT	epithelial-mesenchymal transition
FDC	mature follicular dendritic cell
GFAP	glial fibrillary acidic protein
HBV	hepatitis B virus
HCC	hepatocellular carcinoma
HCV	hepatitis C virus
HEV	high endothelial venule
HGF	hepatocyte growth factor
HL	Hodgkin's lymphoma
HSC	hepatic stellate cell
HVEM	herpesvirus entry mediator
IBD	inflammatory bowel disease
ICAM	intercellular adhesion molecule
ICC	cholangiocellular carcinoma
IEC	intestinal epithelial cell
IFN	interferon
Ig	immunoglobulin

IkB	inhibitor of kappa B
IKK	inhibitor of kappa B kinase
IL	interleukin
JNK	c-Jun N-terminal kinase
KC	Kupffer cell
LIGHT	homologous to lymphotoxins, exhibits inducible expression and competes with herpes simplex virus glycoprotein D for herpesvirus entry mediator, a receptor expressed by T lymphocytes
LMP1	latent membrane protein 1
LPS	bacterial lipopolysaccharide
LSEC	liver sinusoidal endothelial cell
LT	lymphotoxin
LTßR	lymphotoxin ß receptor
MAdCAM	mucosal vascular addressin cell adhesion molecule
MAP3K7, TAK1	mitogen-activated protein kinase kinase kinase 7
MCP1, CCL2	monocyte chemotactic protein 1
MDSC	myeloid-derived suppressor cell
MET	mesenchymal–epithelial transition
MIF	macrophage migration inhibitory factor
MMP	matrix metalloproteinase
mRNA	messenger RNA
NASH	non-alcoholic steatohepatitis
NF-kB	nuclear factor kappa-light-chain-enhancer of activated B cells
NHL	non-Hodgkin lymphoma
NIK	nuclear factor κB-inducing kinase
NKC	natural killer cell
NO	nitric oxide
PDAC	pancreatic ductal adenocarcinoma
PHL	primary hepatic lymphoma
PMN	pre-metastatic niche
RANKL	receptor activator of nuclear factor kappa-B ligand
RANTES, CCL5	regulated on activation, normal T cell expressed and secreted
rER	rough endoplasmatic reticulum
RNA	ribonucleic acid
ROS	reactive oxygen species
STAT3	signal transducer and activator of transcription 3
TAM	tumor associated macrophage
TCRBCL	T-cell rich B-cell lymphoma
TGFß1	transforming growth factor ß1
TIMP	tissue inhibitor of metalloproteinases
TLO	tertiary lymphoid organ
TLR	toll-like receptor
TNF	tumor necrosis factor

TNFR	TNF receptor
TRADD	tumor necrosis factor receptor type 1-associated death domain
TRAF	TNF receptor associated factor
Treg	regulatory T-cell
VCAM	vascular cell adhesion molecule
VEGFA	vascular endothelial growth factor A

3. Introduction

3.1 Liver and liver cancer

3.1.1 Epidemiology and etiology of liver cancer

Cancer is already the leading cause of death before the age of 70 in most highly developed countries and amongst the four leading causes of death in 113 of 179 countries today[1]. With its rapidly growing incidence and mortality rates it is, however, predicted to become the leading cause of death in all countries of the world within the 21st century[1].

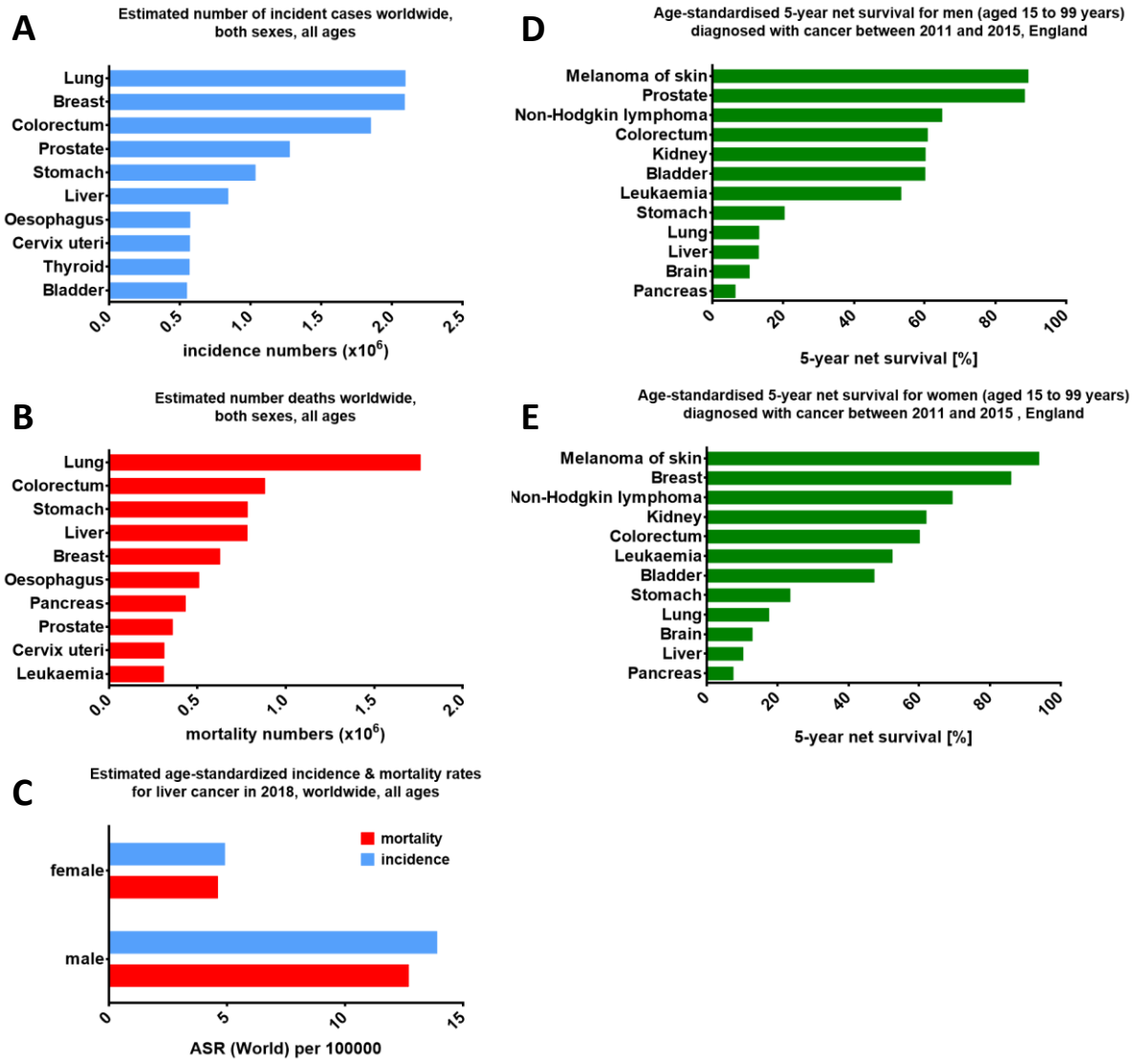

Figure 1: Incidence, mortality and overall survival rates of cancers worldwide
A) Estimated number of incident cases for the 10 most frequent cancers worldwide in 2018 for both sexes and all ages. Data is presented as incidence numbers (x10^6).

B) Estimated number of deaths for the 10 most mortal cancers worldwide in 2018 for both sexes and all ages. Data is presented as mortality numbers ($x10^6$).
C) Estimated age-standardized incidence (blue) and mortality (red) rates for liver cancers in 2018 in males and females of all ages worldwide. Data is presented as age-standardized rates (ASR) per 100,000.
D-E) Age-standardized 5-year net survival (%) for men (D) and women (E) (aged 15-99 years) diagnosed with a common cancer between 2011 and 2015 followed up until 2016 in England. Data is presented as 5-year net survival [%].
Data Source: GLOBOCAN 2018, © International Agency for Research on Cancer 2019. (A - C); Office for National Statistics, UK: Cancer survival in England: adult, stage at diagnosis and childhood – patients followed up to 2016. Release date: 29 June 2017 (D, E)

Liver cancer is estimated to be the sixth most common cancer and the fourth most common cause of cancer-related deaths worldwide in 2018, with an estimated 841,080 new cases diagnosed and an estimated 781,631 deaths this year (GLOBOCAN 2018)[1] (Figure 1A, B). Liver cancer is far more common in men, reflected by a 2 to 3 fold higher rate of incidence as well as mortality (Figure 1C). The 5-year overall survival rate is 12% (Figure 1D, E), but this is heavily influenced by the stage of the tumor at the time of diagnosis. While 5-year survival for patients diagnosed at an early stage is around 25-31%, it drops to only 3% for patients diagnosed with distant organ metastasis[2].

Liver cancer can be primary or secondary. Primary liver cancer starts in the liver, while secondary liver cancer has spread to the liver from another organ. Secondary liver cancer is far more common than primary liver cancer and accounts for around 95% of hepatic malignancies[3] (*World Cancer Report 2014*, World Health Organization, 2014. pp. chapter 5.6). Primary liver cancer mainly includes *hepatocellular carcinoma* (HCC), which comprises 75-85% of all cases, and *cholangiocellular carcinoma* (ICC), which comprises 10-15% of all cases[1]. Other types of liver cancer are very rare and include fibrolamellar carcinoma, angiosarcoma and hepatoblastoma[4]. The main risk factors for liver cancer are chronic infections with *hepatitis B* (HBV) or *C* (HCV), heavy alcohol intake, aflatoxin B1, hemochromatosis, obesity and diabetes type-2[1]. These risk factors, however, are highly influenced by region. While chronic HBV infection and aflatoxin exposure are the key factors in high-risk HCC areas like China and Eastern Africa, HCV infection is the key determinant in other high-risk areas like Japan and Egypt, but also for some low-risk HCC areas like Europe and North America[1,5,6] where obesity is another important and rising risk factor[7]. These differences are also reflected in recent trends of incidence rates in these areas. While the incidence of primary liver cancer has generally increased in many areas of the world between 1973 and 2007, it has actually declined in some countries, most notably in China and Singapore. On the other hand, there has been a steep increase of incidence in Western Europe and Northern America within the same timeframe[6]. Reasons for this are improved treatment options for HBV and decreased exposure to aflatoxin in China and Singapore on one hand, and an increase in obesity and HCV exposure on the other hand.

3.1.2 Liver physiology and functions

The liver is the largest solid organ in the human body, weighing around 1.4-1.5 kg in an adult. It has critical functions in the storage and metabolism of lipids, carbohydrates and proteins and therefore also plays a vital role in the nutrient supply of the body in general. In addition, the liver is crucial for detoxification of extraneous substances, bile acid production for the digestive system and has important immuno-regulatory functions[8].

It is situated in the upper right abdomen, right under the diaphragm and protected by the rib cage. It overlies the gallbladder and can be subdivided into four lobes, the bigger left and right lobes divided by the falciform ligament, and the smaller caudate and quadrate lobes. Two big blood vessels, the hepatic artery and the portal vein, converge in the liver funneling around 1.5 liters of blood into it every minute, which then leaves again mainly via the left, middle and right hepatic veins. The portal vein carries blood rich in digested nutrients from the gastrointestinal tract, spleen and pancreas, while the hepatic artery carries oxygen-rich blood to the liver.

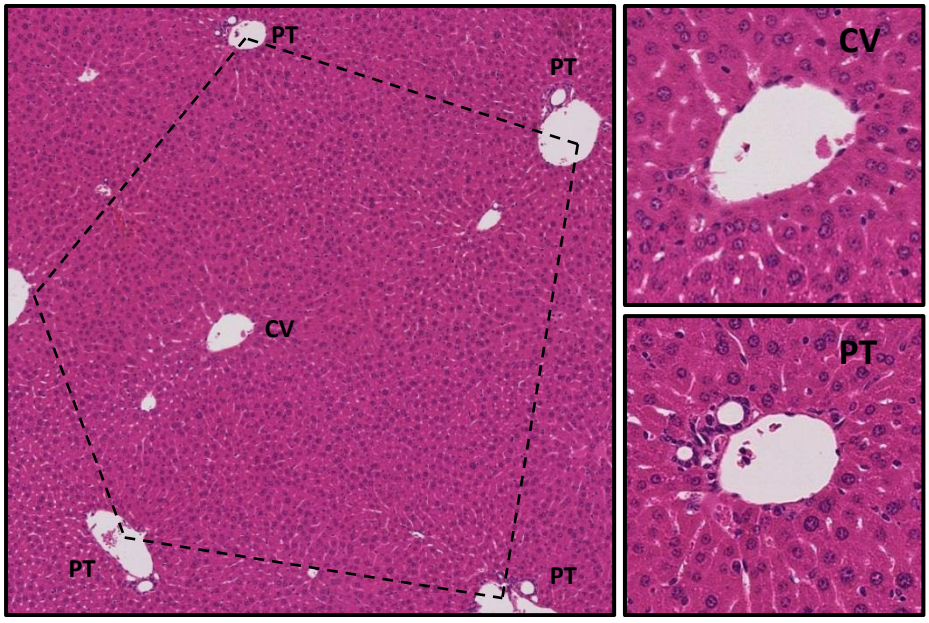

Figure 2: Histological H&E staining of a hepatic lobule
Picture of an H&E staining of a mouse liver sample depicting the structure of a hepatic lobule. The central vein (CV) in the middle is surrounded by multiple portal triads (PT) consisting of a branch of a portal vein, a hepatic artery and bile ducts. The small pictures on the right show higher magnifications of the central vein (top) and a portal triad (bottom).

An important feature of the liver is its unique capacity for regeneration, being able to recover its full mass and functions even with less than 33% of tissue remaining[9]. This evolutionary advantage is important for the liver, as it has vital functions for the body and a high exposure to harmful substances and blood-borne pathogens. The most common disorders of the liver are hepatitis mostly due to hepatitis B and C virus infections, acute and

chronic liver damage due to alcohol or drug abuse, as well as aflatoxin exposure, fatty liver disease and *non-alcoholic steatohepatitis* (NASH), haemochromatosis, cirrhosis and liver cancer[10].

3.1.3 Liver microenvironment and sinusoids

The main structural and functional units of the liver are the hepatic lobules (Figure 2). These are roughly hexagonal structures that consist of a central vein, portal triads, liver sinusoids and plates of hepatocytes. The central vein is located in the middle of each lobule (Figure 2, CV) and drains blood to the hepatic veins. The portal triads are running along each of the lobules corners and consist of terminal branches from the hepatic artery and the portal vein, bile ducts, a lymph vessel and a nerve fiber (Figure 2 C, PT). Between the portal triads and the central vein are plates of hepatocytes. The hepatocytes are the parenchymal cells of the liver and make up around 78% of the total tissue volume of the liver. They are the major functional cells of the liver and are responsible for most of the liver's many metabolic functions. Between the hepatocyte plates are the liver sinusoids. These are special blood vessels which funnel blood from the hepatic artery and the portal vein through the hepatocyte plates and towards the central vein (Figure 3). The sinusoids are the main access point of the hepatocytes to the hepatic blood flow and the non-parenchymal cells. The sinusoids contain the *liver sinusoidal endothelial cells* (LSECs), *hepatic stellate cells* (HSCs) and *Kupffer cells* (KCs) and build the interface through which these cells and the hepatocytes may communicate with each other[11] (Figure 3).

LSECs form the endothelial barrier of the sinusoids. They are highly plastic and pivotal for regulating the liver microcirculation. In contrast to regular endothelial cells LSECs possess a number of non-diaphragmed fenestrae that are arranged in sieve plates. These act like a filter, but they also contribute to LSEC permeability, facilitating hepatocyte oxygenation and exchange of macromolecules between hepatocytes and the circulation. In addition, they have no real basement membrane and are not tightly connected to neighboring endothelial cells[11,13]. Between the hepatocytes and the sinusoids lies the perisinusoidal space, called the space of Disse (Figure 3). It is mostly filled with *extracellular matrix* (ECM) but it also contains the HSCs[14,15]. Sitting in the space of Disse, the HSCs take a pivotal role in regulating interactions and communication between hepatocytes and non-parenchymal sinusoidal cells[16,17]. Furthermore they regulate the sinusoidal microenvironment through ECM deposition and metabolism, regulate sinusoidal lumen diameter and blood flow by contraction and are critical for retinoid storage and homeostasis[14,18,19]. A more recent discovery is their involvement in liver immunoregulation[20–22]. Apart from LSECs and HSCs, Kupffer cells are the third and final important cell type of the hepatic sinusoid. KCs are liver resident macrophages and play an essential role in immune regulation and inflammatory responses in the liver. They line the sinusoidal endothelial layer, where they are in a unique

position to capture signals from the blood and elicit appropriate responses from other liver cells[23,24].

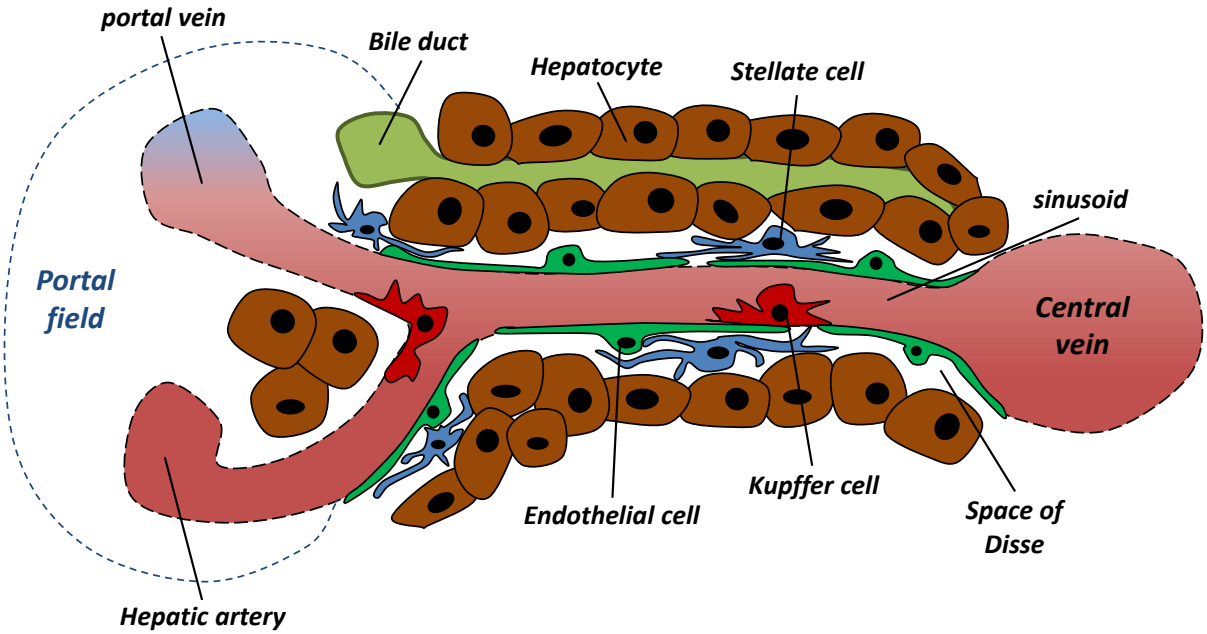

Figure 3: Hepatic sinusoid and surrounding microenvironment
Schematic depicting the functional units of a hepatic lobule. The portal field (to the left) includes branches from a hepatic artery, a portal vein and a bile duct. The hepatic sinusoid (in the middle) drains blood into the central vein (to the right). The sinusoid is wrapped with the highly specialized LSECs (green) and lined with the liver resident macrophages, the Kupffer cells (red). Beyond the endothelial wall is the space of Disse which separates the sinusoids from the layers of parenchymal hepatocytes, which form the bulk of the hepatic cells. The hepatic stellate cells are located within the space of Disse.
Figure is adapted from Frevert et al., 2005[12].

3.1.4 Hepatic stellate cells and their role in liver fibrosis

HSCs, also known as perisinusoidal cells or Ito cells, were first described by Kupffer in the 19th century and have since emerged as very versatile mesenchymal cells that are vital to the function of the liver in health and disease. As mentioned above, they are located in the perisinusoidal space of the liver, called the space of Disse[25] and comprise around 15% of cells in the liver[26,27]. They are most prominently known as quiescent vitamin A storing cells that activate upon liver injury, turning into contractile, proliferative, and fibrogenic myofibroblasts. Their role in liver injury and fibrosis has been studied extensively[14,19]. Beyond these well-established functions, recent research has started to uncover much more mechanisms of stellate cells, highlighting their involvement in hepatic development, regeneration, xenobiotic responses, intermediary metabolism and immunoregulation[15,25,28]. Thus, hepatic stellate cells are emerging as an important signaling hub within the sinusoidal environment, which requires tight regulation of cellular cross-talk and rapid responses to changing environmental cues from the liver[15,16].

Hepatic stellate cells in healthy liver

In their quiescent state, HSCs have oval or elongated nuclei and a spindle-shaped cell body with prominent dendritic cytoplasmic processes. These processes wrap around multiple liver sinusoids on one side and contact hepatocytes on the other side[17,29]. Having intimate contacts with the cells in their immediate vicinity, they facilitate sinusoidal communication and substance exchange[15]. In a healthy liver, HSCs are mostly known for their storage of vitamin A in cytoplasmic lipid droplets[30], where they store 50-80% of total body retinoids[19]. Nevertheless, recent studies suggest that a significant fraction of HSCs lack vitamin A[31,32]. Other well-established HSC-specific markers in the liver are desmin and *glial fibrillary acidic protein* (GFAP)[25]. In humans, desmin is mainly expressed in periportal stellate cells, but much less in pericentral HSCs[33]. In general, the HSC population is very heterogeneous with varying amounts of stored vitamin A, differing combinations of intracellular filaments and highly adaptive gene expression patterns[15,34]. HSCs also contribute to hepatocyte regeneration via secretion of *epidermal growth factor* (EGF)[35], *hepatocyte growth factor* (HGF)[36], epimorphin[37] and pleiotrophin[38]. A surprising and only newly discovered feature of hepatic stellate cells is their involvement in hepatic immunoregulation[20]. Stellate cells express *Toll-like receptors* (TLRs)[21] and can thus sense bacterial *lipopolysaccharide* (LPS), which stimulates the expression of a variety of chemokines, like *monocyte chemotactic protein 1* (MCP1, CCL2), *CC-chemokine ligand 21* (CCL21) and *regulated on activation, normal T cell expressed and secreted* (RANTES, CCL5)[28,39], that induce the infiltration of leukocytes. Interestingly, this activation does not lead to matrix deposition *in vitro*[15]. HSCs can also function as antigen-presenting cells[22,40,41] to stimulate lymphocyte proliferation or apoptosis[42].

Hepatic stellate cell activation

Liver injuries activate hepatic stellate cells through a variety of mechanisms. These mechanisms mostly revolve around changes of the extracellular matrix, paracrine signals from neighboring cells and necroptotic and apoptotic hepatocytes[15]. HSC activation is a process of continuous evolution from quiescent vitamin A-storing cells towards fibrogenic, proliferating and contractile myofibroblast-like cells[43]. This process is divided into two parts, the initiation and the perpetuation. During the initiation, early activating mechanisms cause the HSCs to acquire a phenotype that is much more sensitive and responsive to stimulation from growth factors and cytokines[44]. Activating events include paracrine signaling from *reactive oxygen species* (ROS), dying hepatocytes, injured cholangiocytes, inflammatory cells, de-differentiating LSECs and changing ECM[24,45–48]. Apoptotic bodies from dying hepatocytes can be phagocytosed by HSCs directly[45]. The perpetuation occurs if the injury is not cleared and the activating signals persist. In this case, paracrine and autocrine signaling loops drive HSCs to further evolve towards a myofibroblast-like phenotype that is marked by loss of vitamin A droplets, proliferation, contractility, chemotaxis, inflammatory signaling, fibrogenesis and ECM degradation[44]. ECM degradation is indeed just as important as ECM

deposition in the context of fibrogenesis, as both are needed to tip the balance between healthy ECM (e.g. collagen type-IV, laminin) and fibrotic scar ECM (e.g. collagen type-I and type-III) towards the latter. The balance between ECM degradation and ECM production is heavily controlled by HSCs through the expression of various *matrix metalloproteinases* (MMPs) and their inhibitors *tissue inhibitor of metalloproteinases 1* (TIMP1) and *2* (TIMP2). Increased contractility is also reflected by an upregulation of *alpha smooth muscle actin* (a-SMA) expression, which is the most reliable marker for HSC activation, as no other resident liver cell expresses it[15]. In their activated state HSCs have an enlarged *rough endoplasmatic reticulum* (rER) and well-developed Golgi[14]. Furthermore numerous microfilaments appear beneath the cell membrane[49] and they establish collagen fibers around themselves. If the liver injury subsides, HSC activation is resolved mainly through HSC apoptosis, but also through re-differentiation towards a quiescent phenotype[15,44].

3.1.5 Liver fibrosis, inflammation and cancer

Liver fibrosis is marked by an accumulation of ECM, mainly within the space of Disse and the portal tracts[50]. It is a part of the natural wound healing process and meant to encapsulate injured tissue[44]. Thus, fibrosis is also part of acute wound healing processes, but significant fibrosis usually accumulates only after years[44]. All sinusoidal cells take part in this process, which is quickly aggravated and perpetuated through autocrine and paracrine vicious cycles and inflammatory stimuli from invading immune cells[48,51,52]. Although other resident liver cells also contribute to ECM production during fibrosis, HSCs are the main source of ECM in the liver. Activation of HSCs can occur through various mechanisms as mentioned above (see 3.1.4). Activation of Kupffer cells and a de-differentiation of LSECs are also important for supporting the fibrotic phenotype[53–55]. The most potent pro-fibrogenic cytokine for HSCs is *transforming growth factor ß1* (TGFß1), making it a promising target for therapeutic treatments[56]. TGFß1 is also amongst the most prominent target genes upregulated during HSC activation, thus contributing to the autocrine perpetuation of HSC activation and fibrosis. Other important target genes include TGFß receptors, *collagen-I* (colI), MMP-2, TIMP-1 and -2 and a-SMA[15,44]. Fibrosis only occurs in the event of tissue damage. Although this may happen without underlying inflammation, as in the case of haemochromatosis, prolonged tissue damage is usually accompanied by inflammation[44], as inflammation is linked to tissue damage and regeneration[57]. As described earlier, HSCs are potent mediators of the hepatic immune system. Not only are they able to orchestrate the inflammatory response to tissue damage through the attraction of immune cells, but they also respond themselves to molecular cues from infiltrating immune cells. Many of the chemokines expressed by HSCs promote both inflammation and fibrogenesis[44,58]. Events that trigger liver inflammation are most importantly infection with HBV or HCV or hepatocyte death due to alcohol or drug abuse. The most important signaling mediator in this regard is *nuclear factor kappa-light-chain-enhancer of activated B cells* (NF-kB)[59]. Inflammation is not only a response to tissue damage, but prolonged inflammation may also cause significant tissue

damage itself, triggering hepatocyte death and compensatory wound healing processes accompanied by fibrosis[60–62]. Continuous liver fibrosis leads to liver cirrhosis, marked by a distortion of the liver architecture, inflammation and vascular dysfunction[44]. Furthermore, increased vascular resistance due to increased contractility of LSECs and HSCs leads to portal hypertension, a hallmark of liver cirrhosis[15,63].

Already in the 19th century Rudolph Virchow proposed that wound healing, inflammation and fibrosis might affect cancer formation and progression[64]. Since then, many studies have corroborated his hypothesis[65–67]. Chronic inflammation in general is linked, as an underlying mechanism, to 15-20% of all cancer-related deaths[68,69]. Although inflammation can be anti-tumorigenic, many of its effects support tumor growth and progression[70,71]. Hanahan and Weinberg summarized the hallmarks of cancer as self-sufficiency of growth signals, insensitivity to growth inhibitory signals, evasion of apoptosis, limitless replicative potential, tissue invasion and metastasis, sustained angiogenesis, re-programming of energy metabolism and evading immune destruction[72,73]. Most of these processes can be affected by inflammation[74,75]. The pro-inflammatory tumor stroma is a crucial contributor to cancer progression, by providing pro-proliferative, anti-apoptotic and angiogenic cues[76–78]. In general, cells and cytokines that mediate chronic inflammation also facilitate both tumor initiation and metastatic progression [79–83]. A good example is the activation of the NF-kB pathway that is frequently activated in chronically inflamed tissues and tumors alike [84]. In primary liver cancer, activated HSCs contribute to tumor progression and tumor vascularization through accumulation of tumor stroma and angiogenic cues[85,86]. Other reports also suggest a contribution of activated HSCs in hepatic metastases[87,88]. Interestingly, estrogens are anti-fibrotic in liver, which may explain the significantly lower risk of liver fibrosis and liver cancer in females compared to males[89].

3.2 Tumor metastasis

Tumor metastasis is the spread of tumor cells from the primary tumor to other organs. It is the main cause of cancer-related death. Stated differently, metastasis rather than the primary tumor is responsible for around 90% of all cancer-related deaths[72,79,90]. However, despite the vast body of knowledge available around the pathologic mechanisms that drive primary tumor formation, our knowledge of the mechanisms driving metastasis is poor[90]. Tumor metastasis is a highly inefficient process where only very few cells released from the primary tumor succeed in colonizing a new site[79,91,92]. This is ensured by a plethora of homeostatic mechanisms in healthy tissues which convey an inherent hostility towards invading tumor cells[90]. These mechanisms put a selective pressure on the rapidly growing, genomically unstable tumor cells. In this regard, cancer may progress through evolution of its genetically heterogeneous cell population driven by sequential environmental pressures[79,93,94]. Metastasis can thus be seen as a multistep process involving dedifferentiation, dissociation and local invasion of primary tumor cells followed by

intravasation into blood or lymph vessels, survival and transport in circulation, homing, attachment and arrest in microvessels of distant organs, extravasation into the parenchyma, proliferation and metastatic outgrowth into overt metastatic lesions[79,90,92,95] (Figure 4). Each of these steps is critical and can be rate-limiting[95].

3.2.1 The metastatic cascade

Dedifferentiation and acquisition of a pro-metastatic phenotype

The mutability and genetic heterogeneity of a cancer is directly linked to its metastatic potential[95,96], and the basis for the genetic heterogeneity of tumor cells is their intrinsic genomic instability which stems from DNA mutations, chromosomal rearrangements, telomeric crisis and epigenetic alterations[79,95,97–99]. In healthy tissues these changes are usually counteracted by telomere attrition and the expression of growth inhibitory, apoptotic and senescence pathways. Overcoming these cell-intrinsic barriers is a hallmark of all tumor cells[72]. Further pressures come from extrinsic barriers such as reactive oxygen species, hypoxia, immune surveillance, inhibitory cytokines, extracellular matrix components and interstitial pressure[79,100–103]. Many of these barriers limit the progression of primary tumors but also pose a challenge for disseminated metastasizing tumor cells. Tumor cells that can resist, co-opt or overcome these barriers can dominate the tumor and prime it for metastatic progression[79,95]. Despite many years of scientific progression, no recurrent genetic mutations have been found that might explain metastasis beyond those already present in the primary tumor[104,105]. This suggests that epigenetic changes and changes in the microenvironment are more important for metastatic progression than DNA mutations[90,106]. This hypothesis is corroborated by recent genomic studies showing a close genetic relationship between metastases and primary tumors, implying that all necessary genetic mutations for successful metastatic colonization have already been present in a fraction of primary tumor cells[107].

Dissociation and invasion

To progress to the invasive stage, tumor cells first need to detach from the primary tumor mass. Depending on the cell type and the site of the primary tumor, different mechanisms can lead to the ability of tumor cells to detach from the primary tumor, disobey the rules of tissue architecture and survive on their own [108]. Many primary tumors that progress towards a metastatic phenotype display a reduced or altered expression of cell adhesion molecules, often as part of an *epithelial-mesenchymal transition* (EMT) program[90,109,110]. The EMT is a program usually employed during embryogenesis or wound-healing[111]. It is marked by a loss of epithelial and a gain of mesenchymal properties and is frequently hijacked by tumor cells, granting them more malignant traits critical to dissemination, such as increased motility and invasiveness and the ability to degrade ECM components[112–114]. Furthermore, EMT can equip tumor cells with tumor-initiating capabilities[115–119], presumably a crucial trait

of disseminated tumor cells to form new colonies[90], and it has also been found to increase the resistance of tumor cells to cytotoxic treatment[120,121]. The EMT program is usually triggered by signals from the reactive tumor stroma and is generally reversible[90]. Furthermore, tumor cells often retain certain epithelial traits after their EMT, leaving them in an intermediate state between epithelial and mesenchymal poles[90,122–125].

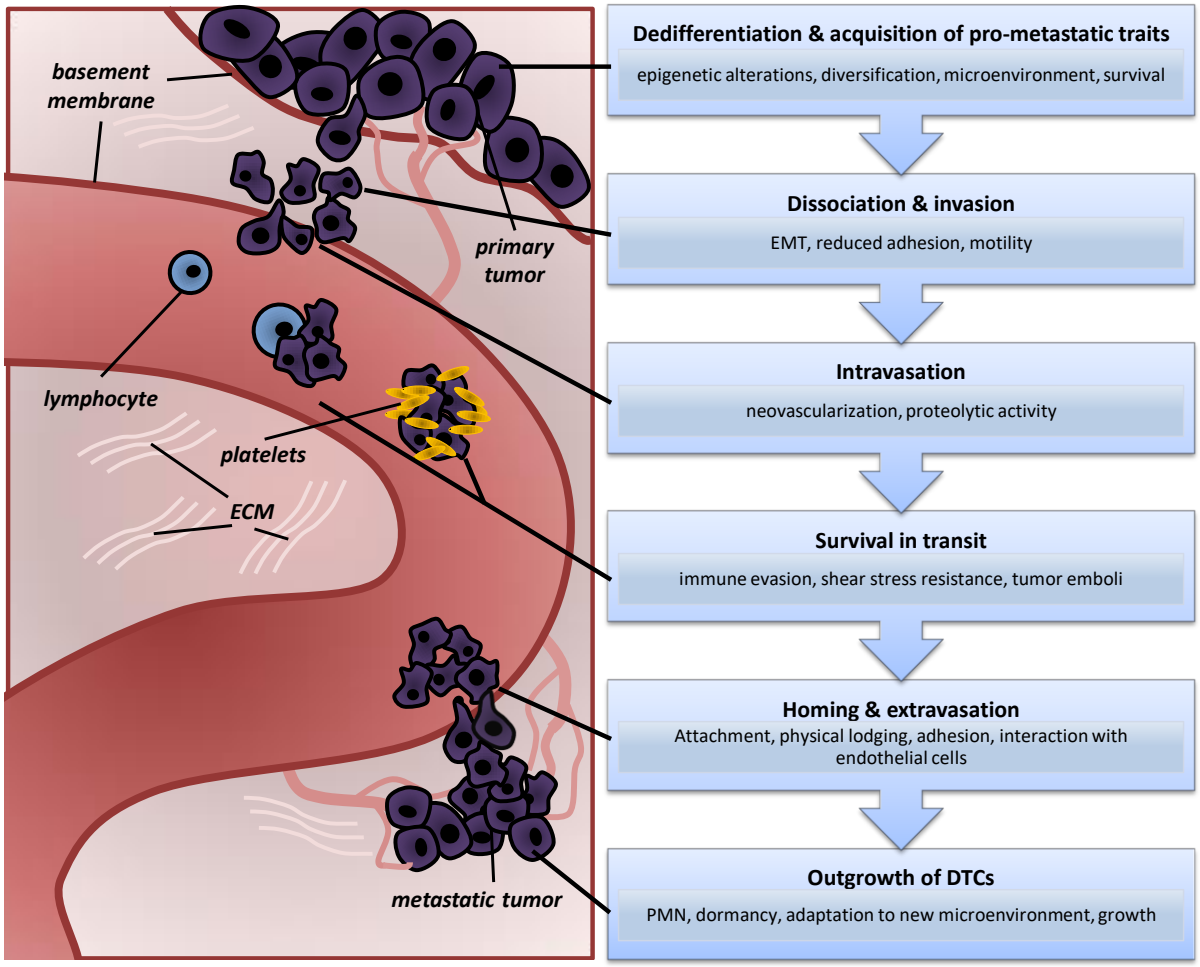

Figure 4: The metastatic cascade

Schematic depicting the principal steps of the metastatic cascade. Tumor cells at the primary site dedifferentiate and diversify through various mechanisms like epigenetic and microenvironmental changes. Subsets of tumor cells acquire pro-metastatic traits (resistance to anoikis, increased motility) that allow them to detach from the primary site and invade surrounding tissues. Leaky tumor neovasculature and proteolytic activity allow them to intravasate into the circulation. In the circulation CTCs form tumor emboli by attaching to other tumor cells, immune cells and platelets to protect themselves from immune surveillance and shear stress. These emboli can get physically stuck in the vasculature or else attach and adhere to endothelial cells through ligand-receptor interactions of adhesion factors or chemokines. CTCs leave the vasculature by extravasation which can be supported by ligand-receptor interactions of adhesion factors or chemokines, immune cells or physical force. Once in the new organ, DTCs require a suitable PMN, adapt to the new microenvironment or else enter dormancy. If they successfully adapt to the new microenvironment they can initiate growth and neovascularization to become a full-blown metastasis.

Figure is adapted from Cotran, R.S., Kumar, V., & Collins, T. (1999) Robbins Pathologic Basis of Disease. Philadelphia: W.B.Saunders, Co. pp.303

Once detached, metastatic tumor cells need to invade the adjacent tissue, which requires a migratory phenotype. Necessary molecular changes include dynamic cytoskeletal changes, actin-myosin contractions, focal contact disassembly, cell-matrix interactions and localized proteolysis. These mechanisms are mainly regulated by small GTPases, integrin-containing focal adhesions and membrane-bound proteases[126–128]. Recent findings suggest that many primary tumor cells invade surrounding tissues as part of large cohesive cell cohorts rather than as single cells[129]. The cells in these cohorts are genetically and phenotypically diverse, with cells at the leading edges showing more mesenchymal traits for migration and invasion, paving the way for cells at the rear that retain more epithelial traits to stay connected to the cells at the front[130–132].

Intravasation

To intravasate and reach the circulation, invading tumor cells eventually need to breach the epithelial basement membrane which is composed of proteoglycans and glycoproteins such as collagens, laminin or perlecan. Breaching the basement membrane requires proteolytic digestion of the membrane by extracellular matrix proteases[79]. Activity of these proteases is usually tightly controlled through localization, autoinhibition and secreted tissue inhibitors. Tumor cells can use various mechanisms to disrupt this control and proteolytically digest the basement membrane[127,133]. As the basement membrane as well as the extracellular matrix contains a variety of inactive, cleavable biomolecules, the tumor cell-initiated proteolysis may also generate various bioactive molecules that can modulate the tumor cells as well as the surrounding microenvironment. Although most of these molecules will promote tumor cell survival, proliferation, migration or angiogenesis, some may actually antagonize tumor progression[79,134]. Apart from increased motility and proteolytic activity, intravasation is often facilitated by the need of the growing primary tumor to establish its own neo-vasculature to ensure a proper supply of nutrients and oxygen beyond the diffusion limit of the existing blood vessels[135]. This tumor vasculature is usually leakier than regular vasculature, facilitating tumor cell intravasation[136,137].

Survival in transit, homing and extravasation

Once in the circulation, metastasizing tumor cells face several new stress factors like hydrodynamic flow, shear forces and the immune system[138]. To overcome these stress factors, *circulating tumor cells* (CTCs) may move in clusters[90] and also interact with platelets and host cells like neutrophils, macrophages and endothelial cells[90]. Aggregating into tumor cell clusters helps CTCs to evade the immune system, apoptosis, shield them from hemodynamic shear forces and helps with physical lodging within vessels[139]. Aggregating with platelets helps CTCs to evade the immune system[140,141], to protect against hemodynamic shear stress[142], to sustain EMT programs[143] and to help with adhesion and homing to vessel walls[144]. Aggregating with neutrophils helps CTCs to evade the immune system[145,146], survive the circulation, adhere to vessel walls and extravasate[147–149]. Anoikis,

cell death induced due to loss of adhesive supports, is an additional stress factor that may play a role, although it is likely that metastasizing tumor cells only spend mere minutes in the circulation, making anoikis a negligible factor[79,90,150]. Once again, the expression of more mesenchymal traits seems to correlate with increased treatment resistance and disease progression in CTCs[90]. Many CTCs will get physically stuck in a capillary bed of microvessels very quickly, especially as part of tumor cell clusters or emboli. Other possible means for initial target homing are interactions between cell surface receptors and ligands expressed by tumor cells and the target organ[79,95,151,152].

To finally leave the circulation, tumor cells need to breach the vascular wall once more in a process called extravasation. Some tumors will grow within the vasculature after getting stuck until they physically burst through the vascular wall[153]. Interactions with platelets[154], neutrophils[149] and monocytes[152] help CTCs to extravasate as well. Other known methods revolve around interactions between cell surface receptors and ligands expressed by tumor cells and the target organ vasculature[152,155,156]. A novel mechanism is marked by the induction of endothelial cell necroptosis[157].

The final step of the metastatic cascade is marked by proliferation and outgrowth of *disseminated tumor cells* (DTCs) in a distant organ. This step will be explained in more detail in the following section.

3.2.2 Seeding and outgrowth of disseminated tumor cells

Once the CTCs have successfully left the circulation, they still need to start proliferation and growth in the new organ to initiate a full-blown metastasis. This, however, is counteracted by the fact that they are missing the familiar microenvironment of their primary site, and by the homeostatic mechanisms of the non-receptive target organ[90]. Already in 1889 Stephen Paget proposed that disseminated cancer cells would only colonize compatible organ microenvironments in his seed-and-soil hypothesis[158]. Clinical observations have since corroborated this hypothesis[95,159–161]. Thus, it is well-appreciated today that metastatic outgrowth in the target organ requires the presence of a viable pre-metastatic niche within the target organ as well as the expression of suitable factors from the invading tumor cells[79,95,162,163]. The formation and evolution of the pre-metastatic niche is mostly driven by the primary tumor itself [162,164,165] . The pre-metastatic niche is, therefore, one consequence of the far-ranging systemic effects induced by the primary tumor[166]. Some of these effects are mediated by tumor-derived exosomes bearing DNA, mRNA or microRNA[167–169]. How the pre-metastatic niche is formed may vary greatly from tumor to tumor and organ to organ and concepts for its formation have only recently started to emerge. One of these concepts that is frequently observed involves the recruitment of hematopoietic progenitors[162] and immune cells[170] into the target organ. Another concept involves the induction of favorable gene expression in resident cells of the target organ[164]. If invading tumor cells don't find a suitable microenvironment in the target organ outright they can sometimes enter a state of

dormancy. In this quiescent state they exit the cell-cycle while keeping their proliferative and tumor-initiating potential[90,92,171,172]. Reasons for DTCs to enter dormancy include the inability to induce angiogenesis or active suppression by the immune system[173,174]. In general dormancy can be initiated as an active response to signals from the new microenvironment or due to the absence of cues the DTCs depended on in their primary site[175,176]. A novel concept related to dormancy is the dormant niche. These niches support DTC survival, their resistance to therapeutic agents and restrain their proliferation[177]. Recent findings suggest that these niches may otherwise be tissue-resident stem cell niches[178]. In lung, bone and brain it has been shown that the perivascular niche actively supports dormancy programs[179,180].

To colonize the target organ outright or to leave dormancy, the invading tumor cells need to acquire the capacity to productively interact with the new microenvironment[90]. To that end, tumor cells may release factors that modulate the extracellular matrix or stromal cells in the local microenvironment or express homing factors that recognize ligands in the pre-metastatic niche. Furthermore, cells in the microenvironment may release factors that directly or indirectly modulate properties or gene expression of the tumor cell[181–183]. The factors needed for successful colonization vary greatly depending on the target organ as every organ has its own unique structure and microenvironment[184–186]. It has been shown that the gene expression pattern of the same parental breast-cancer cell line for successful colonization of the bone is very different from the pattern needed for successful colonization of the lungs [187,188]. To successfully colonize the brain, disseminated tumor cells need to be able to penetrate the blood brain barrier and resist reactive astrocytes[189]. For successful colonization of the liver, on the other hand, extravasation might be less of a problem due to the fenestrated endothelium of the liver sinusoids[92], but evasion of resident immune cells is more important[190,191] as well as overcoming metabolic stress[192]. More general mechanisms include resistance to hypoxic stress[193], ways to surrogate adhesive interactions from the primary site[194,195], modulation of the ECM[196,197], recruitment of immune cells[198] and acute inflammatory responses[199]. Just like the target organ, the origin of the invading tumor cell also plays an important role, as cellular properties and gene expression patterns are significantly different between different cells of origin. The same oncogenic mutations may predispose different cells of origin to metastasize to different target organs[200]. Furthermore the developmental stage of the cell of origin at the time of transformation is also relevant[201], as this may significantly change its properties and gene expression pattern. In this regard, increasing evidence is being found that DTCs need certain stem cell traits to re-initiate tumor growth at distant sites[202,203]. These stem cell traits may be conferred by EMT programs[204,205] or acquired in a dormant niche[206,207].

Interestingly, while the traditional “linear progression” model suggests metastasis to be a late event in tumor progression, more recent studies have shown that dissemination and EMT can occur even before overt malignancy of the primary tumor mass[208–211]. This model is termed the “parallel progression” model[212]. However, it is still not known if and how DTCs

can evolve into fully transformed metastatic cells in a distant hostile microenvironment in the parallel progression model[90].

3.2.3 Primary and secondary lymphomas

Lymphomas are a group of cancers that develop from lymphocytes. There are many subtypes that can be divided into two main categories: *Hodgkin's lymphomas* (HL) and *non-Hodgkin lymphomas* (NHL). The vast majority are NHLs (~90%)[213,214]. HLs are characterized by the presence of Reed-Sternberg cells. These are giant, multinucleated cells that mostly derive from germinal center B cells. NHLs are all other lymphomas except HLs and they can be further divided into mature B cell neoplasms, mature T cell neoplasms, precursor lymphoid neoplasms and immunodeficiency-associated lymphoproliferative disorders. Further distinctions have to be made between primary and secondary and nodal and extranodal lymphomas. In the liver, primary lymphomas are defined as being restricted to the liver without evidence of extrahepatic involvement for at least six month[215,216]. Secondary lymphomas develop from tumor cells disseminated from another site and thus are usually a sign of advanced or late-stage disease[215]. Nodal lymphomas arise within lymph nodes, while extranodal lymphomas arise in tissues other than the lymph nodes, including organs without lymphoid tissues[217]. Around 25-40% of NHL patients have extranodal lymphoma. NHLs are the fifth leading cause of cancer in males and the seventh among women, accounting for 3-4 % of cancer–related deaths, in the United States[218]. Incidence rates have been rising constantly in the past two decades[219–221].

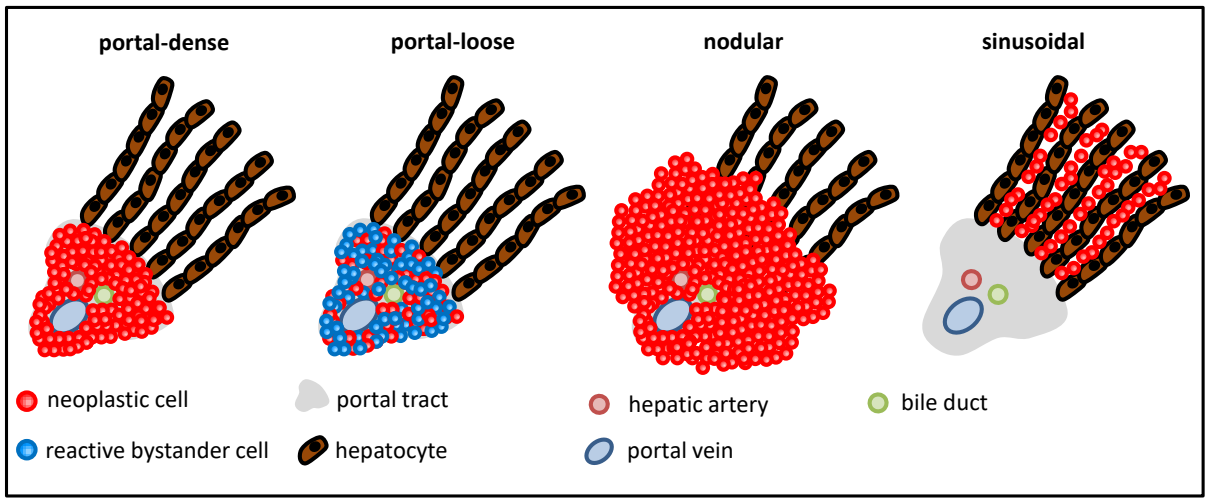

Figure 5: Infiltration patterns of lymphomas

Four different infiltration patterns of lymphomas can be observed. Portal infiltrates show lymphoma cells spread within the portal tracts, either densely packed or loose. Nodular infiltrates show lymphoma cells in densly packed nodules throughout the liver. Sinusoidal infiltrates show lymphoma cells loosely spread within the sinusoids.

Figure is adapted from Loddenkemper et al.,2006[222].

The liver is most often involved in lymphomas, aside from lymph nodes, spleen and bone marrow[222,223]. However, these are mostly secondary manifestations rather than primary manifestations, as *primary hepatic lymphoma* (PHL) is very rare, making up less than 1% of extranodal lymphomas[224–226]. Chronic hepatitis and cirrhosis have been shown to be relevant for the formation of PHL[227–229]. In the liver, the vast majority of both primary and secondary lymphoma manifestations are *diffuse large B-cell lymphomas* (DLBCLs), making up 63% of PHLs[224] and 45% of secondary manifestations[222]. Other frequent lymphoma entities in secondary hepatic lymphoma are *chronic lymphocytic leukemia* (CLL), *classical Hodgkin's lymphoma* (cHL) and *Burkitt's lymphoma* (BL)[222,223]. T-cell lymphomas are generally much rarer than B-cell lymphomas. In the liver they make up only around 12% of all NHLs, which is still higher than in many other organs, except skin and small intestine[222,230]. *T-cell rich B-cell lymphoma* (TCRBCL), a variant of DLBCL that consists of 10% large neoplastic B-cells and a dense infiltrate of non-neoplastic, reactive T-cells and histiocytes, is very rare in all extranodal sites except liver, where it makes up around 14% of all DLBCLs[222].

Most of the lymphomas in the liver have a characteristic infiltration pattern (Figure 5). Infiltrates can either be portal, nodular or sinusoidal[222,223]. Portal infiltrates show tumor cells densely clustered or loosely spread within the portal tracts. Nodular infiltrates show tumor cells densely clustered within nodules throughout the liver, while sinusoidal infiltrates show tumor cells loosely spread throughout the sinusoids. DLBCLs mostly show a nodular infiltration pattern, while B-CLLs and cHLs usually show portal infiltrates. T-cell lymphomas are amongst the few lymphomas that do not show characteristic infiltration patterns and are thus diagnostically more challenging[222].

3.2.4 The current lack of treatment options

Despite significant advances in the study and diagnosis of cancer and many novel targeted cancer therapies, patients diagnosed with distant organ metastases are in many cases not curable by current therapeutic options, facing terminal illness[90,95,231,232]. Therapeutic options for treatment of metastatic cancer are basically the same as for primary tumors[90]. This makes new strategies to fight distant organ metastases necessary. The main barrier to fighting metastases is the genetic and biological heterogeneity of tumor cells. This heterogeneity stems, on one hand, from the primary site, as there are more than 200 distinct cancer disease entities known in humans[90]. On the other hand, it stems from the metastatic process, as metastases evolving from a subpopulation of cells in the primary site have their unique clonal architecture and biology[233–235]. A further barrier is therapeutic resistance, which can be influenced by the highly specific organ microenvironment in metastatic sites[95,236] and also by chemotherapeutic agents themselves[237–239]. Furthermore, almost all currently available cytotoxic therapies target proliferating cells only, making dormant DTCs intrinsically more resistant[180,240]. All these barriers make generalized and empiric approaches to curing metastasis very hard. Therefore, in order to develop new

intervention strategies, it is important to understand the systemic, cellular and molecular mechanisms driving metastasis formation [95]. Of note, dormant DTCs can stay quiescent and undetected for years before eventually reinitiating proliferation and turning into an overt, full-blown metastasis, making the dormant phase prime for therapeutic intervention[90].

3.3 Cis- and transregulatory mechanisms during liver metastasis

The liver is one of the most common solid organs to be affected by metastasis, being a favourite site of dissemination for malignancies such as pancreatic cancer[241], colon cancer[238], breast cancer[242,243] and melanoma[244]. Metastatic tumors in the liver are indeed around twenty times more common than primary liver cancer. Unfortunately though, the mechanisms underlying liver metastasis are not yet fully understood[245], and reliable therapeutic options are lacking[242].

As already mentioned earlier, tumor metastasis is a very complex process that involves a multitude of cells and cellular interactions and its success is dependent on a plethora of regulatory mechanisms. These include cis-regulatory mechanisms between disseminated tumor cells and their current microenvironment as well as trans-regulatory mechanisms initiated by the primary tumor or immune cells to precondition the microenvironment of metastatic sites. These regulatory mechanisms shape the host tissue, its cellular composition and the tumor cells to determine sites and success of tumor metastasis[243,246]. Mechanisms involved in this process include, amongst others, expression of cytokines, chemokines and chemokine receptors, adhesion molecules, shedding of extracellular vesicles, ECM remodeling, immune deregulation, cell-cell and cell-ECM interactions[163,182,247] but also more abstract mechanisms like blood circulation patterns[246,248].

3.3.1 Metastatic niche formation and the impact of hepatic sinusoidal cells on liver metastasis

Sinusoidal cells and their microenvironment are a key factor for the successful colonization of tumor cells in the liver. Most of the sinusoidal cells can have pro- and anti-metastatic roles depending on the regulatory signals they receive[88]. The balance between pro- and anti-metastatic effects determines whether metastatic colonization will be successful, the tumor cells die or if they enter dormancy[88]. This balance can already be tipped towards a pro-metastatic effect by the primary tumor before disseminated tumor cells even arrive in the liver. Although the concept of *pre-metastatic niches* (PMNs) is hard to verify in a clinical setting, it is widely accepted in the scientific community[163,165]. The primary tumor can precondition and shape the PMN through a stepwise evolution with secreted factors and extracellular vesicles. These include pro-angiogenic factors such as *vascular endothelial growth factor A* (VEGFA)[249], which lead to vascular remodeling and hyperpermeability[250], and inflammatory cytokines and chemokines like TGFß and CCL2, which can activate

sinusoidal cells and attract immune cells[164,251]. Tumor-derived extracellular vesicles can contain exosomal microRNA or proteins[247,252]. *Pancreatic ductal adenocarcinoma* (PDAC)-derived exosomes expressing macrophage *migration inhibitory factor* (MIF) have been shown to educate Kupffer cells to express TGFß, leading to an activation of HSCs and a fibrinogenic and pro-metastatic environment[167]. Target organ and cell specificity of the extracellular vesicles are regulated through receptor expression on the vesicles themselves. Liver tissue may be targeted through expression of $a_v ß_5$ integrin, which binds to fibronectin[88].

LSECs have key regulatory functions in liver metastasis. Getting activated upon tumor cell entrapment within the sinusoids, they may induce tumor cell death through release of *nitric oxide* (NO) and ROS[253] or *tumor necrosis factor alpha* (TNFa)[254] and *interferon gamma* (IFNy)[255]. Furthermore they can attract immune cells like neutrophils, who in turn may activate tumoricidal activity in Kupffer cells and infiltrating T-cells[256]. On the other hand, activated LSECs may increase cell adhesion molecule (CAM) expression and induce EMT in cancer cells through fibronectin secretion. Both mechanisms help cancer cells with extravasation, migration and invasion[257], also shielding them from the toxic microenvironment of the sinusoidal lumen[258]. If pro- or anti-metastatic effects prevail is also regulated by the expression of surface receptors on the tumor cells[259,260].

Kupffer cells usually phagocytose and kill tumor cells in the sinusoidal lumen[261], but tumor cells that can survive the encounter may benefit from the activated KCs, as they can help with invasion, survival, proliferation and angiogenesis through secretion of various cytokines, growth factors and MMPs and the induction of CAM expression on LSECs[88,262].

Hepatic Stellate cells mostly serve pro-metastatic purposes. Activated HSCs secrete cyto- and chemokines that recruit immune cells like neutrophils, macrophages and *bone marrow-derived dendritic cells* (BMDCs) which help to shape the metastatic niche[263,264]. Furthermore, they support angiogenesis through secretion of VEGFA and Angiopoietin-1[265]. Their expression of a variety of MMPs is a key factor in tumor cell invasion and ECM remodeling[15,256]. ECM remodeling may release trapped molecules that can help with homing of BMDCs and CTCs. Furthermore, the composition of the ECM and its physical properties, such as stiffness, can induce signaling patterns in neighboring cells which may in turn support tumor cell seeding and outgrowth[266,267].

Not much is known about the role of hepatocytes in liver metastasis, but binding of tumor cells to hepatocytes has been identified as an early event in liver metastasis[268], and it has been shown that disseminated breast cancer cells can extend projections through the space of Disse to contact hepatocytes before leaving the sinusoidal lumen[269]. Binding of tumor cells to hepatocyte-derived ECM can initiate the expression of proliferation and survival genes and thus serve as an autocrine growth promotion mechanism for tumor cells[88,270].

3.3.2 The role of cell adhesion molecules in the progression of liver metastasis

Cell adhesion molecules play an important role in liver metastasis. Not only are they important for the initial homing of CTCs and organotropism[169], but they are also involved in tumor cell retention, trans-endothelial migration and invasion[258,271]. Furthermore certain cell adhesion molecules are involved in cellular signaling and may change cellular expression profiles considerably[272,273].

CTC homing to the liver is mediated, amongst others, through chemokine - chemokine receptor interactions[274]. *Chemokine (C-X-C motif) ligand 12* (CXCL12) expression in the liver may attract colorectal, prostate and breast cancer cells as well as melanoma cells expressing CXCR4[275,276]. E-selectin, *intercellular adhesion molecule 1* (ICAM1) and *vascular cell adhesion molecule 1* (VCAM1) expression on LSECs, mediated through inflammatory responses and *TNF receptor 1* (TNFR1)[277], is an important mechanism to bind and arrest CTCs at the sinusoidal endothelium[272]. The strength of the binding between CTCs and the vessel walls is crucial for successful arrest and subsequent trans-endothelial migration of CTCs[278] and consequently for CTC survival, as it allows them to escape the toxic environment of the circulation[258]. Due to the fenestrations in the liver sinusoidal endothelium, tumor cells can bind directly to ECM molecules within the space of Disse[279,280]. This is another important mechanism for CTC arrest in the liver, but it is also an important mechanism of outside-in signaling which can regulate apoptosis, proliferation, differentiation, migration and invasion, thus playing a critical role in metastasis[273,281]. Most of these tumor cell-ECM interactions are mediated by integrins, but cadherins, immunoglobulin superfamily members, proteoglycans, glypicans and syndecans are also important in this regard[282]. E-cadherin has been thoroughly studied in tumor metastasis for its role in EMT[112,283]. While E-cadherin loss is important in the early stages of carcinoma metastasis to enable dissociation, migration and dissemination via EMT, recent studies have shown that more epithelial traits, obtained via a *mesenchymal-epithelial transition* (MET), are beneficial for CTC survival and metastatic outgrowth in distant organs like the liver[284]. MET is usually marked by a re-expression of E-cadherin and can be triggered by the liver microenvironment[283].

3.3.3 The role of pro-inflammatory signaling and immune cells in liver metastasis

In recent years it has become evident that inflammation can be positively correlated with tumor progression[285,286] and metastatic dissemination[287,288]. Indeed, chronic inflammatory conditions are associated with increased risk of developing tumors and targeting of inflammatory mediators in the tumor microenvironment can decrease the incidence and spread of cancer in experimental models[289,290], while overexpression of inflammatory cytokines promotes tumor progression[285,288]. Similar findings have been reported for liver metastasis as well[291]. Pro-inflammatory mediators like TGFß and TNFα can activate sinusoidal cells to induce PMN formation, creating an environment that supports CTCs with

increased adhesion, proliferation, survival, migration and invasion[165,262]. Chemokines like CCL2, CCL5 and CXCL12 secreted by activated liver sinusoidal cells may help with CTC homing to the liver (s. 3.3.2), but also recruit macrophages, neutrophils, BMDCs, *myeloid-derived suppressor cells* (MDSCs) and other immune cells to the liver[169,264,292]. These recruited immune cells have a critical impact on the sinusoidal microenvironment and its metastatic capacity. Recruited blood-borne monocytes and macrophages can have pro- or anti-metastatic effects depending on their polarity. M1 macrophages are tumoricidal through secretion of large amounts of NO and TNFα[293], while M2 macrophages are pro-metastatic through their expression of pro-angiogenic and growth factors like VEGFα, *epidermal growth factor* (EGF) and TGFß[294]. Similarly, neutrophils may also exhibit pro- or anti-metastatic effects. They can kill tumor cells directly through cytolytic factors or indirectly by activating KCs or recruiting cytotoxic CD8+ T-cells[256,295]. On the other hand, they can contribute to the metastatic process by shaping the metastatic niche[249]. Furthermore, they can improve tumor cell retention by anchoring them to the vessel wall or through neutrophil extracellular traps[148]. Furthermore, they can contribute to CTC adhesion, proliferation and invasion through secretion of cytokines, chemokines, leukotrienes and MMPs[147,252]. MDSCs and *regulatory T-cells* (Tregs) have strong immunosuppressive properties, thus supporting tumor cell survival and immune evasion[296–299]. Platelets can help tumor cells in circulation to survive, by forming tumor cell-platelet clusters. These clusters are more resistant to the physical shear forces in the circulation, and the platelets also help with immune evasion[300].

3.3.4 Lymphotoxins

Cytokines play a pivotal role in immunity, as they are a means of communication for the highly mobile immune cells with themselves and with the surrounding tissues. Lymphotoxins belong to the tumor necrosis factor superfamily of cytokines, which plays a role in many pathways involving cell death, survival and differentiation but also development and maintenance of bone, neuronal, ectodermal and lymphoid organs[301,302]. There are two different lymphotoxin molecules, *lymphotoxin alpha* (LTα) and *beta* (LTß). LTα was initially described as a cytotoxic factor expressed in lymphocytes[303–305] and thought to be redundant with TNF[306]. Since then it has been shown to have functions very distinct from TNF. Like all TNF superfamily members, LTα is active only in a trimeric form and can form either homo- or heterotrimers with LTß[307]. As LTα unlike all other TNF superfamily members has no transmembrane domain, the $LT\alpha_3$ homotrimeric form is secreted[306,308] (Figure 6). It is mainly expressed by hematopoietic cells like B- and T-lymphocytes and *natural killer cells* (NKCs), but also by hepatocytes, melanocytes, acinar cells and kidney epithelial cells[60,309,310]. $LT\alpha_3$ does not bind to LTßR, but rather to TNFR1 and TNFR2[306] (Figure 6). LTß is, typical for TNF superfamily members, a type II transmembrane protein. Like LTα it is only active as a trimer and only forms heterotrimers with LTα, anchoring LTα to the membrane. It exists mainly as $LT\alpha_1ß_2$ (Figure 6), but can also form the much rarer $LT\alpha_2ß_1$ (~2%)

heterotrimer[306,311]. It is constitutively expressed on a low level in hematopoietic cells, but can also be expressed by many other tissues during acute inflammation[312]. $LT\alpha_1ß_2$ binds exclusively to LTßR, which requires cell-cell contact as $LT\alpha_1ß_2$ is membrane-bound. A third ligand of the LT network is *homologous to lymphotoxins, exhibiting inducible expression and competing with herpes simplex virus glycoprotein D for herpesvirus entry mediator, a receptor expressed by T lymphocytes* (LIGHT). It is very similar to LTα and LTß and binds to the *herpes virus entry mediator* (HVEM) and LTßR[313,314] (Figure 6).

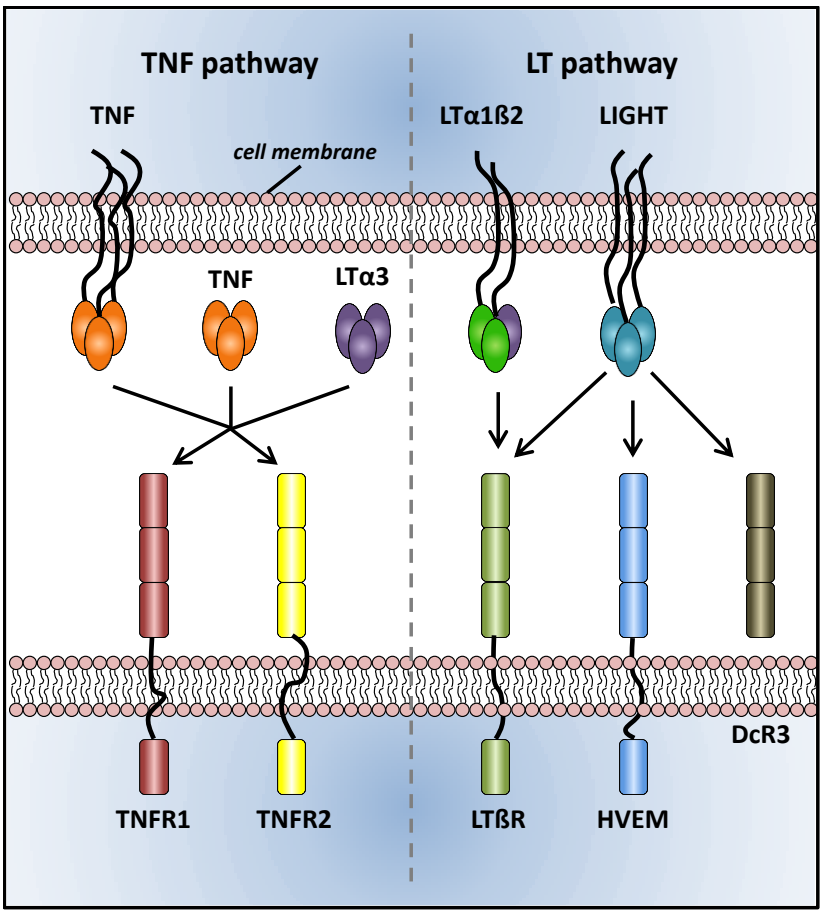

Figure 6: Ligands and receptors of the TNF/LT signaling pathways

The system can be parted into two pathways. The TNF pathway is activated through the two TNF receptors TNFR1 & 2, which bind TNF and LTα3. The LT pathway is activated by binding of $LT\alpha_1ß_2$ or LIGHT to LTßR. LIGHT can also bind to HVEM and DcR3.

Figure is adapted from Gommerman and Browning, 2003[321].

The cellular receptors involved in Lymphotoxin signaling are TNFR1, TNFR2, LTßR and HVEM[306] (Figure 6). Typical for the TNFR superfamily signaling is induced by clustering of these receptors through binding of the trivalent ligands[311]. Downstream signaling can lead to cell death mediated by the interaction of *tumor necrosis factor receptor type 1-associated death domain* (TRADD) with death domain containing receptors like TNFR1, or to activation of NF-kB mediated by *TNF receptor associated factors* (TRAFs) binding to TNFR2, LTßR or HVEM[306,315]. TNFR1 can also activate TRAF2 via TRADD. LTßR is a non-death receptor member of the TNFR superfamily and shares roughly 45% homology with TNFR1 and

TNFR2[316]. It contains a TRAF domain[317] and mainly activates NF-kB2 downstream, mediated by TRAF2 and TRAF3[317,318]. LTßR is expressed on many cell types like fibroblasts, epithelial cells and myeloid cells[319] but not on lymphocytes[320]. This suggests that the LTαß-LTßR axis provides a means of unidirectional communication between lymphocytes and the surrounding stromal and parenchymal cells[306].

The general role of lymphotoxins in health

Lymphotoxin signaling is involved in various important tasks revolving around the immune system. Most prominently, it plays a crucial part during development and maintenance of lymphoid organs[306], and mice lacking LTα, LTß or LTßR fail to develop lymph nodes, Peyer's Patches or mature *follicular dendritic cells* (FDCs)[322,323]. Development of secondary lymphoid organs is orchestrated by LTαß expressing inducer cells and LTßR expressing embryonic stroma organizer cells[324]. LT-dependent maintenance of lymphoid organs includes keeping the integrity of the marginal zone, function of stromal cells that recruit B-cells to the follicle, T-cell migration to the T-zone, creation of FDC networks and the formation of germinal centers[325,326]. This is achieved in part by regulating the expression of adhesion molecules like *mucosal vascular addressin cell adhesion molecule 1* (MAdCAM1), VCAM1 and ICAM1[327,328] and chemokines that regulate the tissue architecture. Accordingly, a defect in LTßR signaling leads to disrupted spleen and lymph node architecture, a reduction in *high endothelial venules* (HEVs), FDCs and lymphoid follicles[329,330]. Beyond these tasks, LT signaling is also involved in the development and maturation of NK-, NKT- and CD4 and CD8 T-cells[331–333] as well as the production of *immunoglobulin A* (IgA) through recruitment of B-cells to the lamina propria and the production of IgE through regulation of the T_H1:T_H2 ratio[334] and recruitment of *dendritic cells* (DCs) to secondary lymphoid organs[332]. Furthermore LT signaling is needed for lymphoid organ neogenesis during chronic inflammation[335] and for negative thymic selection of T-cells and development of central tolerance[336]. Decreased LT signaling leads to a lack of chemokine production, a disruption of the thymic architecture and decreased migration of thymocytes during the negative selection[336,337].

Due to these crucial tasks the expression of LTs is tightly regulated. While expression of LTs by lymphocytes is maintained in a constitutive manner within lymphoid organs[325], it is only induced after activation of lymphocytes outside of lymphoid organs[338]. This expression is regulated by cytokines like *interleukin 2* (IL2), Il4, IL7, CCL19 or CCL21[60,310]. Beyond the expression level, the availability of secreted $LT\alpha_3$, LIGHT as well as TNF is limited by decoy receptors like *decoy receptor 3* (DcR3) and shed forms of TNFR1 and TNFR2[306].

The general role of lymphotoxins in disease

Playing a critical part in the regulation and maintenance of the immune system, deficiencies or alterations in LT signaling can have severe consequences. Apart from disrupted microarchitecture of lymphoid organs mentioned above, a lack of LT signaling also inhibits the formation of *tertiary lymphoid organs* (TLOs) at sites of chronic inflammation[335]. TLOs

are similar to secondary lymphoid organs and appear at random sites in non-lymphoid organs that are affected by chronic inflammation where they help the immune system by offering a contact area for antigen presenting and responding cells and by sustaining inflammation[339]. Overexpression of LTs on the other hand can lead to the formation of TLOs at sites without chronic inflammation, leading to tissue damage and potentially cancer[335,340]. Increased LT signaling is also involved in certain autoimmune disorders. In *experimental autoimmune encephalomyelitis* (EAE), LTßR signaling is crucial for peripheral T-cell priming[341], while in *inflammatory bowel disease* (IBD) it is required for IgE[334] and IgA[342] production. It has also been shown to be involved in *collagen induced arthritis* (CIA)[343] and artherosclerosis[344] and in all of these diseases LTßR blocking agents can successfully be used as therapeutics[339,345,346], although an increased risk for developing non-Hodgkin's lymphomas has been reported as side-effect[347]. Due to their importance for the response of CD8 T-cells to alloantigens[348], LTs are also involved in the graft-vs-host response after transplantation[349]. Furthermore, LTs are involved in metabolic disease, type-II diabetes and dyslipidemia as they regulate expression of IL22 and microbial peptides that effect the microbial milieu in the gut[350,351], and also help during liver regeneration through induction of IL6 in hepatocytes[352] and by providing communication between LT producing hepatocytes and LTßR expressing HSCs[353].

Interestingly, a variety of viruses (mostly large DNA viruses like pox- and herpesviridae) can modulate the TNF/LT system in their favor through the expression of structural homologues as part of their systemic attack of the immune system[354]. *Eppstein-Barr Virus* (EBV), for instance, can activate TRAFs and subsequently NF-kB1 & 2 by expressing *latent membrane protein 1* (LMP1)[355] to ensure B-cell survival and differentiation. Herpes Simplex Virus uses HVEM as entry receptor by binding to it via glycoprotein D[356].

Lymphotoxins in cancer

Dysregulation of LT signaling is reportedly involved in various different cancer entities. Decreased levels of LTα correlate with a decreased risk of high-grade bladder cancer as well as lung and endometrial cancer[357–359] but also with a poor prognosis in DLBCL, highlighting that LT signaling has different functions depending on the tissue and the receptor type that it binds to. Increased LT levels in the liver have been shown to increase HCC incidence and LTßR is a key factor in hepatitis induced HCC[60]. As LTßR signaling has a direct role in proliferation, increased LTßR signaling can support tumor growth as has been shown for nasopharyngeal cancer, multiple myeloma, castration-resistant prostate cancer and leukemia, amongst others[360–363]. On the flip side, LTßR signaling has been shown to induce cytotoxicity in colon carcinoma cells[364], and LT signaling in NK cells supports anti-tumor surveillance[365]. In a murine T-cell lymphoma model, LT signaling was found to be involved in tumor cell homing to the bone marrow by inducing expression of chemokines and subsequently activating LTßR expressing stromal cells to support tumor cell outgrowth[366]. Lastly, lymphocyte derived LT has been shown to be involved in tumor angiogenesis[367].

3.3.5 Canonical and non-canonical NF-kB signaling

Nuclear factor 'kappa-light-chain-enhancer' of activated B-cells (NF-kB) is a group of transcription factors consisting of five members: RelA (p65), RelB, c-Rel, NF-kB1 (p50/p105) and NF-kB2 (p52/p100)[306,315]. As dimers they can bind to kB sites in promoter and enhancer regions to induce or repress transcription via their shared Rel homology domain[368]. NF-kB is widely regarded as one of the key regulators of inflammation, immunity and defense[315,369,370]. It is critical for the amplification and maintenance of inflammation, but also for its limitation and resolution[371,372], a key part of tissue homeostasis. More specifically, NF-kB is involved in proliferation[373,374], apoptosis[375], adhesion[376], development of cells and organs[368,377], cellular specialization[378], lymphocyte differentiation and mammary gland development[379,380]. Due to its central position in many important cellular signaling pathways, it can be activated by a vast variety of stimuli including ROS, antibacterial peptides, chemo- and cytokines as well as infection and physical and physiological stresses[370,381,382]. Considering that, it is not surprising that NF-kB can bind to almost all chemo- and cytokine promoters[383] and its dysregulation is involved in many disorders, including chronic inflammation, autoimmune diseases and cancer[370,384–386]. Interestingly, although most inflammatory conditions are correlated to increased NF-kB activity, decreased NF-kB activity can also increase inflammation in certain scenarios due to its role in the resolution of inflammation[387]. This is most commonly observed in injured tissues[388]. On a molecular level NF-kB is divided into a canonical and a non-canonical signaling pathway. The canonical pathway activates NF-kB1/Rel-A mediated by *inhibitor of kappa B kinase* (IKK) complex dependent degradation of *inhibitor of kappa B* (IκB), which otherwise keeps the NF-kB1/Rel-A complex in a latent form within the cytoplasma[306]. The critical IKK complex consists of the IKKα, IKKß and the regulatory IKKγ subunits. The non-canonical pathway activates NF-kB2/Rel-B mediated by *Nuclear Factor κB-inducing Kinase* (NIK) and IKKα phosphorylation[318,389]. It gets most notably activated by LTßR signaling[317,318] and results in the expression of genes more focused on lymphoid organ development and homeostasis than inflammation, as described earlier. Both pathways interact with each other, as NF-kB2 can attenuate the NF-kB1 response but is itself dependent on the NF-kB1 regulated expression of its p100 precursor molecule[306].

NF-kB in cancer

Cancer has been described as a wound that will not heal[390], and thus its close correlation to inflammation is widely accepted and has already been mentioned earlier in this manuscript. As a key regulator of inflammation, dysregulation of NF-kB is involved in the development and progression of many cancers[74,84,315,370]. Most of its effects are pro-tumorigenic, but it can also have anti-tumorigenic functions[370]. Dysregulation of NF-kB can be tumor cell intrinsic or linked to the tumor microenvironment[391]. NF-kB activating mutations in the tumor cell, like the loss of IκB[392] or inhibiton of NIK turnover[393] are mostly observed in hematological malignancies but have also been reported in glioblastoma[392,394]. Although NF-

kB activating mutations are rare in carcinomas, *receptor activator of nuclear factor kappa-B ligand* (RANKL) induced activation of IKKα in mammary epithelial cells has been shown to be important for breast cancer progression and metastasis[395,396]. Notably, RANKL signaling can also be initiated by regulatory T-cells in this case[397]. Another example is the NF-kB induced expression of anti-apoptotic genes in *intestinal epithelial cells* (IECs) in *colitis-associated cancer* (CAC), giving them a survival advantage[398]. In that setting, NF-kB signaling in myeloid cells also plays an important role by inducing pro-proliferative and pro-inflammatory factors like IL-6 and *signal transducer and activator of transcription 3* (STAT3)[398,399]. STAT3 and NF-kB have both similar anti-apoptotic properties[84,400] as they can interfere with p53 and p53-mediated genomic surveillance and control c-myc and cyclin D1 expression[400,401]. The effects of NF-kB signaling in the tumor microenvironment are very widespread and complex and are much more common than NF-kB dysregulation within the tumor cells[370]. One aspect is the increased expression of inflammatory chemo- and cytokines that shape and regulate the tumor stroma and provide growth and survival signals[70,370], another is the polarization of tumor associated macrophages (TAMs) from the cytotoxic M1 to the pro-tumorigenic M2 type[402]. Its activation in tumor associated fibroblasts entails a pro-inflammatory gene signature that leads to macrophage recruitment, neovascularization and tumor growth[403]. NF-kB induced expression of twist and snail could induce EMT in carcinoma cells[404]. In some situations decreased NF-kB signaling can have pro-tumorigenic effects as well, highlighting NF-kBs anti-tumorigenic capabilities. Inhibition of NF-kB in diethylnitrosamine (DEN) induced mice potentiates liver damage and HCC incidence as it inhibits NF-kBs anti-apoptotic effect in dying hepatocytes which in turn triggers STAT3 driven compensatory proliferation needed for the transmission of oncogenes[405,406]. Increased hepatocyte death, liver damage, fibrosis and HCC incidence is also observed in mice with a hepatocyte-specific knockout of IKKγ or *mitogen-activated protein kinase kinase kinase 7* (MAP3K7, TAK1), which are both required for NF-kB1/Rel-A activation[407,408]. It has to be noted that in models where increased NF-kB signaling is the cause of liver damage, inhibition of NF-kB decreases cancer incidence and progression as observed in mice overexpressing LTαß in hepatocytes[60]. Decreased NF-kB activation has been observed to enhance Ras-induced epidermal growth[409], possibly by inhibiting Ras-induced senescence[410]. In other cases, inhibition of IKKß has been observed to increase expression of pro-tumorigenic *c-Jun N-terminal kinase* (Jnk) family members in the liver[406].

Due to its many pro-tumorigenic effects, NF-kB is a promising target for anti-cancer therapy. But, although NF-kB inhibition has been very effective in treating cancer in many different mouse models, it had very little success in clinical trials[411]. Still, NF-kB inhibition could be useful in combination therapies, by sensitizing tumor cells to chemotherapy due to the inhibition of NF-kBs anti-apoptotic and antioxidant effects[412].

4. Aims of the thesis

It has become very evident in recent years that pro-inflammatory signaling is contributing to the progression of primary tumors as well as metastasis. Former publications of our group have shown that LTßR signaling specifically is involved in the initiation and progression of primary tumors, including HCC. However, there is currently no data indicating if this pathway is involved in metastatic spread of tumor cells to the liver. As liver metastases are representing the large majority of hepatic malignancies and metastases are far more life-threatening than primary tumors, this thesis aims to uncover a possible role for LTßR signaling in hepatic metastasis formation.

The lack of treatment options for patients diagnosed with distant organ metastases has induced a surge of new research projects aiming to increase our knowledge about the underlying mechanisms of metastasis, and identify possible new targets for therapeutic intervention. Agents that inhibit LTßR have already been developed and tested for clinical use against certain autoimmune diseases, so here, the aim is to evaluate if LTßR could be a promising target to combat liver metastasis formation.

Therefore, I want to investigate the mechanisms underlying LTßR signaling in the liver to fully understand its implications in liver metastasis. All four resident liver cell types express LTßR to some degree, so all of them could theoretically react to LT signaling from tumor cells or infiltrating immune cells. Here, our broad range of available animal models are used to generate different mouse lines that lack LTßR specifically in each resident liver cell type to find out which cells are important to integrate LT signaling in the setting of liver metastasis.

Finally, I want to find out how the responsive cells react to LTßR signaling and how they enable increased metastasis to the liver. This is a very important aspect of the thesis, as it is becoming increasingly evident that many mechanisms revolving around tumor progression and metastasis can act pro- or anti-tumorigenic depending on the circumstances. This has been shown for LTßR and NF-kB signaling already. Here, a mix of proteome and transcriptome screening methods is used as well as immunohistochemistry and functional *in vitro* assays to evaluate the effect of LTßR activation on the responsive cells in the liver and the pro-metastatic mechanisms they set in motion.

5. Materials & Methods

5.1 Materials

5.1.1 Chemicals & Reagents

Compound	Company
4',6-Diamidin-2-phenylindol (DAPI)	Thermo Fisher Scientific, Waltham, USA
Acetic Acid	Roth, Karlsruhe, Germany
Acetone	Merck, Darmstadt, Germany
Agarose	Biozym Scientific, Oldendorf, Germany
Albumin bovine fraction V	Biomol GmbH, Hamburg, Germany
Arginin	Sigma Aldrich, Taufkirchen, Germany
Asparagin	Sigma Aldrich, Taufkirchen, Germany
cell tracker green CMFDA	Invitrogen, Thermo Fisher Scientific, Waltham, USA
Citrate	Sigma Aldrich, Taufkirchen, Germany
Clodronate liposomes	Liposoma B.V., Amsterdam, Netherlands
Collagenase D	Roche, Penzberg, Germany
cOmplete™ Protease Inhibitor Cocktail	Roche Diagnostics, Penzberg, Germany
Dimethylformamide	Sigma Aldrich, Taufkirchen, Germany
Disodium hydrogen phosphate	Sigma Aldrich, Taufkirchen, Germany
DNAse I	Roche, Penzberg, Germany
EcoMount	Biocare Medical, Pacheco, USA
Endothelial cell growth supplement from bovine neural tissue	Sigma Aldrich, Taufkirchen, Germany
Eosin	Waldeck GmbH & Co.KG, Münster, Germany
ERK inhibitor SCH772984	Selleck Chemicals, Houston, USA
Ethanol absolute	Merck KGaA, Darmstadt, Germany
Ethylene glycol tetraacetic acid	Sigma Aldrich, Taufkirchen, Germany
Ethylenediaminetetraacetic acid	Sigma Aldrich, Taufkirchen, Germany
Eukitt® mounting medium	Sigma Aldrich, Taufkirchen, Germany
Evans Blue	Sigma Aldrich, Taufkirchen, Germany
Fast Start Universal SybrGreen ROX Mix 2x	Roche Diagnostics, Penzberg, Germany
Formamide	Sigma Aldrich, Taufkirchen, Germany
Glutaraldehyde	Merck, Darmstadt, Germany
Glycerol	Sigma Aldrich, Taufkirchen, Germany
Glycine	Sigma Aldrich, Taufkirchen, Germany
Heparine sodium salt, from porcine intestinal mucosa	Sigma Aldrich, Taufkirchen, Germany
Igepal-CA630	Sigma Aldrich, Taufkirchen, Germany

Isopropyl alcohol	Carl Roth, Karlsruhe, Germany
K3Fe(CN)6	Sigma Aldrich, Taufkirchen, Germany
K4Fe(CN)6	Sigma Aldrich, Taufkirchen, Germany
Kaisers Glycerin-Gelatine	Carl Roth, Karlsruhe, Germany
Ketamin	ACE Surgical supply, Brockton, USA
Magnesium chloride	Fluka Analytical, Seelze, Germany
MEK inhibitor UO126	Selleck Chemicals, Houston, USA
Methanol	Merck KGaA, Darmstadt, Germany
MMP-9 inhibitor Ro-28-2653	Glixx Laboratories, In.c, Hopkinton, USA
Monopotassium phosphate	Sigma Aldrich, Taufkirchen, Germany
Mowiol 4-88	Merck, Darmstadt, Germany
Nonidet-P40	Sigma Aldrich, Taufkirchen, Germany
Nycodenz	Axis-Shield, Dundee, Great Britain
Paraformaldehyde	Merck, Darmstadt, Germany
PBS liposomes	Liposoma B.V., Amsterdam, Netherlands
Phalloidin, Alexa 546-conjugated	Thermo Fisher Scientific, Waltham, USA
PhosSTOP™	Roche Diagnostics, Penzberg, Germany
Potassium chloride	Sigma Aldrich, Taufkirchen, Germany
Pronase E	Merck, Darmstadt, Germany
Proteinase K	Roche Diagnostics, Penzberg, Germany
Rac inhibitor EHT1864	Selleck Chemicals, Houston, USA
Sodium bicarbonate	Sigma Aldrich, Taufkirchen, Germany
Sodium carbonate	Sigma Aldrich, Taufkirchen, Germany
Sodium chloride	Sigma Aldrich, Taufkirchen, Germany
Sodium deoxycholate	Sigma Aldrich, Taufkirchen, Germany
Sodium dodecyl sulfate solution 20%	Sigma Aldrich, Taufkirchen, Germany
ß-mercaptoethanol (ß-MEtOH)	Sigma Aldrich, Taufkirchen, Germany
Tissue Tek O.C.T Compound	Sakura Finetek Europe B.V., Alphen aan den Rijn, Netherlands
Tris(hydroxymethyl)aminomethane	VWR International GmbH, Erlangen, Germany
Triton X-100	Sigma Aldrich, Taufkirchen, Germany
Tween-20	Bio-Rad, Hercules, USA
VECTASHIELD® Antifade Mounting Medium	Vector Laboratories, Burlingame, USA
X-gal	Promega, Fitchburg, USA
Xylazin	ACE Surgical supply, Brockton, USA

5.1.2 Buffers & Solutions

Buffer	Recipe
10x Electrophoresis Buffer	30.3*g* Tris-HCl, 144.2*g* Glycin, 10*g* SDS, fill to 1*l* with ddH_2O

10x HSc stock soultion	80*g* NaCl, 4*g* KCl, 0.882*g* NaH_2PO_4, 1.2*g* Na_2HPO_4, 2.4*g* HEPES, 3.5*g* $NaHCO_3$ - fill up to 1*l* with H_2O
10x tail lysis buffer	5*ml* 1*M* Tris-HCl, 25*ml* 1*M* KCl, 2.5*ml* Nonidet P-40, 2.5*ml* Tween-20, 15*ml* ddH_2O
10x TBST	0.5*M* Tris-HCl, 1.5*M* NaCl in ddH_2O, set pH to 7.6 with HCl
10x Trypsin EDTA solution (0.5%)	Gibco™, Thermo Fisher Scientific, USA
1x Cell Lysis Buffer	Cell Signaling Technology, Cambridge, UK
1x DPBS, sterile	Gibco™, Thermo Fisher Scientific, USA
1x PBS	135*mM* NaCl, 2.5*mM* KCl, 10*mM* Na_2HPO_4, 1.8*mM* KH_2PO_4
1x TAE	40*mM* TRIS-Cl, 20*mM* acetic acid, 1*mM* EDTA
40 mg/ml X-Gal stock (X-Gal staining)	1*g* X-Gal, 25*ml* Dimethylformamid
5x Nucleic Acid Sample Loading Buffer	BioRad, München, Germany
Ammonia water	40 *drops* 25% ammonium solution / 500ml ddH2O
BD Cytofix/Cytoperm™ Fixation/Permeabilization Solution	BD Bioscience, San Jose, USA
BD Perm/Wash™ Buffer	BD Bioscience, San Jose, USA
Blotting Buffer	3*g* Tris-HCl, 11.25*g* Glycin, 10*%* methanol - fill up to 1*l* with ddH_2O
Cell freezing medium	10% DMSO, 90% FCS
Clarity Western ECL Substrate	Bio-Rad, Hercules, USA
Collagenase D solution	560*mg* $CaCl_2$, 500*g* collagenase D - fill up to 1*l* with ddH2O
detergent solution (X-Gal staining)	2*mM* $MgCl_2$, 0,01% (m/V) Natriumdeoxycholat, 0,02% (V/V) Nonidet-P40, 1x PBS
Digestion solution	560*mg* $CaCl_2$, 300*mg* pronase E, 300*mg* collagenase D, 10*mg* DNAse I - fill up to 1*l* with ddH2O
DMEM	Gibco™, Thermo Fisher Scientific, USA
EGTA solution	190*mg* EGTA, 900*mg* Glc, 1*l* 1x HSc solution
Eosin Staining Solution	60*ml* Eosin Stock solution 430*ml* 96% ethanol 2.2*ml* glacial acidic acid
Eosin Stock Solution	4*g* Eosin 0.4*g* Phloxin 440*ml* ddH_2O
Evans Blue stock solution	20*mg/ml* Evans Blue dye, 1x PBS
FBS, heat inactivated	Gibco™, Thermo Fisher Scientific, USA
fixing solution (X-Gal staining)	2% paraformaldehyd, 0,2% glutaraldehyd, 1x PBS
gelatine solution, 2%, from bovine skin	Sigma-Aldrich, Taufkirchen, Germany
Gill's Hematoxylin I	American Master Tech Scientific, Lodi, USA
Harris Hematoxylin	American Master Tech Scientific, Lodi, USA
HBSS	Invitrogen, Thermo Fisher Scientific, Waltham, USA
HCl water	2.5ml 37% HCl solution / 500ml ddH2O

HEPES	Gibco™, Thermo Fisher Scientific, USA
IFF	2% FCS, 1% BSA, 1x PBS
M199	Sigma-Aldrich, Taufkirchen, Germany
Non-essential amino acid solution (NEAA)	Sigma-Aldrich, Taufkirchen, Germany
Penicillin-Streptomycin Solution (Pen/Strep)	Biochrom, Merck KGaA, Darmstadt, Germany
Ponceau S Solution	0.1% PONCEAU-S (w/v) in 5% acetic acid solution
Pronase E solution	560*mg* $CaCl_2$, 500*g* pronase E - fill up to 1*l* with ddH2O
ready-to-use X-Gal solution	X-Gal-stock 1:40, X-Gal-staining solution, always prepare freshly
REDTaq® ReadyMixTM PCR Reaction	Sigma Aldrich, Taufkirchen, Germany
Restore Western Blot Stripping Buffer	Life Technologies, Frankfurt, Germany
RPMI	Gibco™, Thermo Fisher Scientific, USA
scioExtract solution	sciomics GmbH, Heidelberg, Germany
Sörensen buffer	17.8*g* Na_2HPO_4 in 1*l* H_2O - titrate to pH 7.45 with 4.08*g* KH_2PO_4 in 0.3*l* -0.1*%* NaN_3
Thermo Scientific™ Spectra™ Multicolor Broad Range Protein Ladder	Thermo Fisher Scientific, Waltham, USA
Ultraglutamine	Lonza, Basel, Switzerland
washing solution (X-Gal staining)	2*mM* $MgCl_2$, 1x PBS
X-Gal-staining solution	5*mM* $K_3Fe(CN)_6$, 5*mM* $K_4Fe(CN)_6$, 2*mM* $MgCl_2$, Natrium-Deoxycholat 0.01%, NP40 0.02%, 1x PBS
Xylene solution	Medite GmbH, Burgdorf, Germany

5.1.3 Consumables

Product	Company
10% Mini-PROTEAN® TGX™ Precast Protein Gels, 15-well	Bio-Rad, München, Germany
384 well qPCR plates colourless, ABI type	Biozym Scientific GmbH, Oldendorf, Germany
96-,24-,12-,6-well plates polystyrene cell culture	Corning Life Sciences, Tewksbury, USA
Adhesive Microplate Seal, 135*x*80*mm*, Sheets	Biozym Scientific GmbH, Oldendorf, Germany
Aspiration pipette	Sarstedt, Nümbrecht, Germany
Cell scraper/spatula	TPP Techno Plastic Products AG, Trasadingen, Switzerland
Cell strainer 100µm	Corning Incorporated, Corning, USA

Cell-Star Serological Pipets 5*ml*/10*ml*/25*ml/50ml*	Greiner Bio-one, Frickenhausen, Germany
Conical Sterile Polypropylene Centrifuge Tubes 15*ml*/50*ml*	Thermo Scientific™ Nunc™, Ulm, Germany
Corning™ Costar™ Transwell™ permeable Supports	Thermo Fisher Scientific, Waltham, USA
Cover Glasses, round, Ø 13/15 mm	Menzel-Gläser, Braunschweig, Germany
Cryotubes 1.8*ml*	Thermo Scientific
Disposal Bags, autoclavable	Roth, Karlsruhe, Germany
Embedding Cassettes	Medite, Burgdorf, Germany
Extra Thick Blot Filter Paper, Precut	Bio-Rad, München, Germany
GentleMACS M-tubes	Miltenyi, Bergisch-Gladbach , Germany
Kimtech Science Professional tissues	Kimberly Clarke, Reigate Surrey, UK
Microtubes 1.1*ml* Z-gel	Braun-Melsungen, Melsungen, Germany
Mouse dissection tools (scissors, forecеps, scalpels)	Omnilab, München, Germany
Neolus Syringe Needles *gauge 18/20/24/26/27*	Terumo, Leuven, Belgium
Nitrex Nextgen examination gloves	Rösner-Mautby Meditrade, Kiefersfelden, Germany
Nitrocellulose Membrane, 0.2 µm	Bio-Rad, München, Germany
Omnican® F fine dosage syringe, 1.0 ml	Braun-Melsungen, Melsungen, Germany
Omnifix syringes 1ml/2ml/5*ml*/ 10*ml/50ml*	Braun-Melsungen, Melsungen, Germany
PCR tube stripes and lid strips	Biozym Scientific GmbH, Oldendorf, Germany
Perfusor fm perfusion pump	Braun, Melsungen, Germany
Pipette filter tips (10*µl*; 20*µl*; 100µl ; 200*µl*; 1000*µl*)	VWR International GmbH, Erlangen, Germany
Pipette tips (200*µl*/1000 *µl*)	VWR International GmbH, Erlangen, Germany
Reaction tubes (0.1*ml*/0.5*ml*/ 1.5*ml*/ 2*ml*)	Eppendorf, Hamburg, Germany
Rotilab syringe filters 0.22*µm*/ 0.45*µm*	Roth, Karlsruhe, Germany
Superfrost Plus Microscope Slides	Thermo Fisher Scientific, Waltham, USA
Surgical blades	Schreiber, Fridingen, Germany
Surgical disposable scalpels	Braun-Melsungen, Melsungen, Germany
Tissue culture flasks with filter lid (T15/T75/T175)	Greiner Bio-one, Frickenhausen, Germany
Transparent 96-well EIA/RIA plates	Corning Life Sciences, Tewksbury, USA
Vasofix safety, peripheral venous catheter	Braun, Melsungen, Germany

5.1.4 Mice

Mouse Line	Background	Supplier	Genetic Alteration
C57BL/6J	C57BL/6J	Charles River Germany GmbH, Sulzfeld, Germany	
DBA/2	DBA/2	Charles River Germany GmbH, Sulzfeld, Germany	
Alb-LTaß	C57BL/6J	intercrossed & bred in own facility	Overexpression of Lta & LTß under albumin promoter
GFAP-LTaß	C57BL/6J	intercrossed & bred in own facility	Overexpression of Lta & LTß under GFAP promoter
RIP-tag2	C57BL/6	Kristian Pietras, Lund University, Lund, Sweden	Overexpression of SV40 large T antigen under rat insulin promoter-1
Alb-Cre LTßR flox	C57BL/6J	intercrossed & bred in own facility	LTßR knockout in albumin expressing cells
VeCad-Cre LTßR flox	C57BL/6J	intercrossed & bred in own facility	LTßR knockout in Ve-cadherin expressing cells
NG2-Cre LTßR flox	C57BL/6J	intercrossed & bred in own facility	LTßR knockout in NG2 expressing cells
GFAP-Cre LTßR flox	C57BL/6J	intercrossed & bred in own facility	LTßR knockout in GFAP expressing cells
Lrat-Cre LTßR flox	C57BL/6J	intercrossed & bred in own facility	LTßR knockout in Lrat expressing cells
Lrat-TdTomato		Robert Schwabe, Columbia University, New York, USA	Expression of TdTomato under the Lrat promoter

5.1.5 Cell lines

Cell line	Origin	Supplier	Growth medium
10T1/2	murine embryonic fibroblasts	ATCC, Manassas, USA	DMEM, 10% FCS, P/S
10T1/2 LTßR	murine embryonic fibroblasts	CRISPR/Cas9 mediated LTßR deletion	DMEM, 10% FCS, P/S
10T1/2 MAdCAM-1	murine embryonic fibroblasts	CRISPR/Cas9 mediated MAdCAM-1 deletion	DMEM, 10% FCS, P/S
10T1/2 MMP-9	murine embryonic	CRISPR/Cas9 mediated MMP-9 deletion	DMEM, 10% FCS, P/S

	fibroblasts		
10T1/2 NIK	murine embryonic fibroblasts	CRISPR/Cas9 mediated NIK deletion	DMEM, 10% FCS, P/S
10T1/2 PX459	murine embryonic fibroblasts	CRISPR/Cas9 control construct	DMEM, 10% FCS, P/S
B16F10	murine melanoma	Dr. Anna Lorentzen, TU München, Germany	DMEM, 10% FCS, P/S
Eμ-myc	murine B-cell lymphoma	Prof. Ulrich Keller, TU München, Germany	RPMI, 10% FCS, P/S, 1x NEAA, 50μM ß-MEtOH
Eμ-myc LTa	murine B-cell lymphoma	plasmid mediated overexpression of LTa	RPMI, 10% FCS, P/S, 1x NEAA, 50μM ß-MEtOH
Eμ-myc LTß	murine B-cell lymphoma	plasmid mediated overexpression of LTß	RPMI, 10% FCS, P/S, 1x NEAA, 50μM ß-MEtOH
HUVECs	human umbilical cord endothelial cells	CellWorks, San Diego, USA	M199, 20% FCS, 2mM L-Glu, 0.25x P/S, 50*μg/ml* heparin, 30*μg/ml* endothelial cell growth supplement
L-CI.5s GFP	murine T-cell lymphoma	plasmid mediated overexpression of GFP	RPMI, 10% FCS, P/S, 10*mM* HEPES, 2*mM* L-Glu, 0.27*mM* Arg, 0.55*mM* Asp, 50*μM* ß-MEtOH
L-CI.5s LTa	murine T-cell lymphoma	plasmid mediated overexpression of LTa	RPMI, 10% FCS, P/S, 10*mM* HEPES, 2*mM* L-Glu, 0.27*mM* Arg, 0.55*mM* Asp, 50*μM* ß-MEtOH
L-CI.5s LTß	murine T-cell lymphoma	plasmid mediated overexpression of LTß	RPMI, 10% FCS, P/S, 10*mM* HEPES, 2*mM* L-Glu, 0.27*mM* Arg, 0.55*mM* Asp, 50*μM* ß-MEtOH
L-CI.5s P	murine T-cell lymphoma	Prof. Achim Krüger, TU München, Germany	RPMI, 10% FCS, P/S, 10*mM* HEPES, 2*mM* L-Glu, 0.27*mM* Arg, 0.55*mM* Asp, 50*μM* ß-MEtOH
L-CI.5s sh38	murine T-cell lymphoma	shRNA mediated knockdown of LTa	RPMI, 10% FCS, P/S, 10*mM* HEPES, 2*mM* L-Glu, 0.27*mM* Arg, 0.55*mM* Asp, 50*μM* ß-MEtOH
L-CI.5s sh39	murine T-cell lymphoma	shRNA mediated knockdown of LTa	RPMI, 10% FCS, P/S, 10*mM* HEPES, 2*mM* L-Glu, 0.27*mM* Arg, 0.55*mM* Asp, 50*μM* ß-MEtOH
L-CI.5s sh63	murine T-cell lymphoma	shRNA mediated knockdown of LTa & LTß	RPMI, 10% FCS, P/S, 10*mM* HEPES, 2*mM* L-Glu, 0.27*mM* Arg, 0.55*mM* Asp, 50*μM* ß-MEtOH
L-CI.5s sh88	murine T-cell lymphoma	shRNA mediated knockdown of LTß	RPMI, 10% FCS, P/S, 10*mM* HEPES, 2*mM* L-Glu, 0.27*mM* Arg, 0.55*mM* Asp, 50*μM* ß-MEtOH

L-CI.5s shNT	murine T-cell lymphoma	shRNA non-targeting control construct	RPMI, 10% FCS, P/S, 10*mM* HEPES, 2*mM* L-Glu, 0.27*mM* Arg, 0.55*mM* Asp, 50*µM* ß-MEtOH
LX-2	human hepatic stellate cells	RWTH Aachen, Germany	DMEM, 2% FCS, P/S
MC-38 GFP	murine colon carcinoma	PD Dr. Lubor Borsig, UZH Zürich, Switzerland	DMEM, 10% FCS, P/S
Sk-Hep1	murine sinusoidal endothelial cell-like	Prof. Percy Knolle - TU München, Germany	DMEM, 10% FCS, P/S

5.1.6 Commercial kits

Kit	Company
Bond Polymer Refine Detection	Leica Biosystems, Wetzlar, Germany
Bond Polymer Refine Red Detection	Leica Biosystems, Wetzlar, Germany
Cell Contraction Assay	Cell Biolabs, Inc., San Diego, USA
Immun-Star™ WesternC™ Chemiluminescent Kit	Bio-Rad, München, Germany
Pierce™ BCA Protein Assay Kit	Thermo Fisher Scientific, Waltham, USA
Proteome Profiler™ Human Phospho Kinase Array Kit	R&D Systems, Bio-Techne, Minnesota, USA
Qiaquick PCR purification Kit	Qiagen, Hilden, Germany
QuantiTect reverse transcription kit	Qiagen, Hilden, Germany
QuickLyse Mini Kit	Qiagen, Hilden, Germany
RNAscope 2.0 brown FFPE Assay kit	Advanced cell diagnostics, Hayward, USA
RNEasy Mini Kit	Qiagen, Hilden, Germany
TaqMan® Gene Expression Assay	Applied Biosystems, Foster City, USA
XTT Cell proliferation kit II	Roche, Penzberg, Germany

5.1.7 Antibodies

Target	Clone	Company	Reactivity	Dilution WB/ICC	Dilution IHC	ARC
a-SMA	1A4	Sigma	M		1:5000	30 min EDTA, 95°C
B220	RA3- 6B2	BD Bioscience	M		1:300	20 min EDTA, 100°C
CD3	SP7	NeoMarkers	M,H		1:300	20 min EDTA, 95°C

CD31	poly	Abcam	M;H	1:100		20 min EDTA, 100°C
CD31 PE-conjugated	MEC 13.3	BioLegend	M	2*µg/ml*		
Collagen IV		Cedarlane	M	1:50		Acetone 10 + formalin 31, 10 min enzymes 37°C
Desmin	D33	Dako	M,H		1:50	20 min citrate, 95°C
Erk 1/2	137F5	Cell Signaling Technology	M,H	1:1000		
F4/80	BM8	BMA Biomarkers	M		1:120	10 min enzymes, 37°C
FAK	poly	Cell Signaling Technology	H,M	1:1000		
GAPDH	14C10	Cell Signaling Technology	M,H	1:1000		
GFAP						
GFP	poly	Fitzgerald Industries International	M		1:1000	20 min EDTA, 95°C
Isotype control (ACH6)	Ha4/8	Biogen Idec	M	1*µg/ml*		
Isotype control (BS-1)	poly	Biogen Idec	H	1*µg/ml*		
isotype control (LTßR-Ig)	MOPC-21	Biogen Idec	H, M	1*µg/ml*		
ki67	SP6	NeoMarkers	M,H		1:200	30 min EDTA, 95°C
Lta	poly	R&D Systems	M	50*ng/ml*		
LTß	B27	Biogen Idec	H		1:1000	60 min EDTA, 100°C
LTßR	ACH6	Biogen Idec	M	1*µg/ml*		
LTßR	BS-1	Biogen Idec	H	1*µg/ml*		
LTßR	6D66	Santa Cruz	H	1*µg/ml*		
Ly6G	1A8	BD Pharmin- gen	M		1:600	30 min EDTA, 95°C
mLTßR-mIgG		Biogen Idec	M	1*µg/ml*		
mouse IgG, Alexa 488	poly	BD Bioscience	M	1:1000		
p100/p52	poly	Cell Signaling	M	1:1000		
Paxillin	poly	Cell Signaling Technology	H,M	1:1000		

Pdgfrß	28E1	Cell Signaling Technology	M,H	1:50		Acetone 10 + formalin 30
p-Erk1/2	D13.14.4E	Cell Signaling Technology	M,H	1:2000		
p-FAK 576/577	poly	Cell Signaling Technology	H,M	1:1000		
p-Paxillin	poly	Cell Signaling Technology	H,M	1:1000		
rabbit IgG, Alexa 488	poly	BD Bioscience	M	1:1000		
Rel-A	poly	NeoMarkers	M,H		1:500	20 min EDTA, 95°C
Rel-B	poly	Santa Cruz	M,H		1:400	20 min EDTA, 100°C
VCAM-1	M/K-2	Serotec	M	1:500		
Vimentin						

5.1.8 Primers

Primer	Mouse		Human	
	Forward	Reverse	Forward	Reverse
A20	TGGTTCCAATTTTG CT CCTT	CGTTGATCAGAGTC G TG	TCCTCAGGCTTTGT AT TTGAGC	TCTCCCGTATCTTCA C AGCTT
CCL17	TACCATGAGGTCAC TT CAGATGC	GCACTCTCGGCCTA C ATTGG	ACCGTTGGTGTTCA CC GCCC	GGCCCTTTGTGCCC AT GGCT
CCL19	GCCTCAGATTATCT GC CAT	AGACACAGGGCTC CT TCTGGT		
CCL2	TTAAAAAACCTGG AT CGGAACCAA	GCATTAGCTTCAGA TT TACGGGT	CTTCGGAGTTTGGG TT TGCTT	CATTGTGGCCAAG GA GATCTG
CXCL1	CTGGGATTCACCTC A AGAACATC	CAGGGTCAAGGCA AG CCTC		
CXCL10	AAGTGCTGCCGTC ATT TTCT	CCTATGGCCCTCAT TC TCAC		
CXCL13	ATATGTGTGAATCC TC GTGCCA	GGGAGTTGAAGAC AG ACTTTTGC		
IL-6			TCGAGCCCACCGG GA ACGAA	GCAACTGGACCGA AG GCGCT
LIGHT	TCCGCGTGCCTGG AA A	AAGCTCCGAAATA GG ACCTGG	CTGGCGTCTAGGA GA GATGG	CTGGGTTGACCTCG TG AGAC
LTa	TCCACTCCCTCAGA A GCACT	AGAGAAGCCATGT CG GAGAA	CCACCCTACACCTC CT CCTT	AGTCTGGGCAGCT GA AGGT
LTb	TACACCAGATCCAG G GGTTC	ACTCATCCAAGCGC C TATGA	GAGGACTGGTAAC GG AGACG	GGGCTGAGATCTG TTT CTGG

LTbR	GCCGAGGTCACAG AT GAAAT	CAGGACACTGGTG AA GAGCA	GAGAACCAAGGTC TG GTGGA	GAGCAGAAGAAGG C CAGTG
TGFß1	ATCCTGTCCAAACT A A GGCTCG	ACCTCTTTAGCATA GT AGTCCGC	CTAATGGTGGAAA CC CACAACG	TATCGCCAGGAATT GT TGCTG
TNFa	CGATGGGTTGTAC CTT GTC	CGGACTCCGCAAA GT CTAAG	GGCGCTCCCCAAG AA GACAGG	CCAGGCACTCACCT CT TCCCT
lacZ	CAAGCCGTTGCTG ATT CGA	GCTCATCCATGACC TG ACCAT		
aSMA	CCTGAGAAGCTTCT CC AGCTATGTG	AGCCCTGGTACCAT C ATCA	TAGCACCCAGCACC A TGAAGATCA	GAAGCATTTGCGGT G GACAATGGA
Desmin	GACGCTGTGAACC AG GAGTTC	GCGTTCTGCTGCTC CA AG	AGGACCGATTTGCC A GTGAG	GATGGGGAGATTG AT CCGGC
Vimentin			TGAGTACCGGAGA CA GGTGCAG	TAGCAGCTTCAACG G CAAAGTTC
FAP	CTTTGTGTTTCCTTC A GGTTTG	CTTTGGAGTTACCA CC CTGG		
TIMP-1	ACTCGGACCTGGTC A TAAGGGC	TTCCGTGGCAGGC AA GCAAAGT		
CCL5	TTT GCC TAC CTC TCC CTC G	CGA CTG CAA GAT TGG AGC ACT	CCC CTC ACT ATC CTA CC	TCA CGC CAT TCT CCT G
Col1a1	ACGCATGAGCCGA AG CTAAC	TTGGGGACCCTTAG G CCATT	GAG GGC CAA GAC GAA GAC ATC	CCG TTC TGT ACG CAG GTG A
ICAM-1	ACTGCTTGGGGAA CT GGAC	AGGCATGGCACAC GT ATGTA	ATGCCCAGACATCT G TGTCC	GGGGTCTCTATGCC CA ACAA
VCAM-1	GGCATCCTCACCTT AA TTGC	ACAGGTCTCCCATG C ACAA	GCTGCTCAGATTGG A GACTCA	CGCTCAGAGGGCT GT CTATC
PDGFR	TCAACGACTCACCA G TGCTC	TTCACAGGCAGGT AG GTGCT		
MMP-9	CTG GAC AGC CAG ACA CTA AAG	CTC GCG GCA AGT CTT CAG AG	TGT ACC GCT ATG GTT ACA CTC G	GGC AGG GAC AGT TGC TTC T
GFAP	CGGAGACGCATCA CC TCTG	TGGAGGAGTCATT CG AGACAA	GGCCTGTAGGTTGC TC CAGA	TTGCCCCCTGTAGT GA CAAG
PPARg	ATCATCTACACGAT G CTGGCC	CTCCCTGGTCATGA AT CCTTG		
Col4a4	GCCTGGTGTCGGG AT CAAAG	AGCTGGAGTCAAC AA AATGCC	AGA TAA GGG TCC AAC TGG TGT	AGG TAT GCC ATC TAA ACC TGG AA
Lama4	ATGAGCTGCAAGG AA AACTATCC	CTGTTTCGTTGGCT TC ACTGA	ACGCCAGGATAGC CA AGAAC	ATCACAGCTTATGG TT GGGCA
FN1	GCTCAGCAAATCGT G CAGC	CCATAGCAGGTAC AA ACCAGG		
MMP13	TGTTTGCAGAGCAC T ACTTGAA	CAGTCACCTCTAAG C CAAAGAAA		
IGF-2	GTG CTG CAT CGC TGC TTA C	ACG TCC CTC TCG GAC TTG G		

MAdCAM	CCTCTGCTGAGCCCTA CATC	CTTGTGGTAGGTTGCC AGGT		

5.1.9 Machines & Devices

Device	Source
7900HT Fast Real Time PCR System	Applied Biosystems, Foster City, USA
Ag Protect cryostat	Leica Microsystems, Wetzlar, Germany
Biofuge Fresco table top centrifuge	Heraeus, Hanau, Germany
BondMax II automated ICH/ISH stainer	Leica Microsystems, Wetzlar, Germany
ChemiDoc™ XRS System	Bio-Rad, München, Germany
FACS Canto II	BD Bioscience, Redmond, USA
GelDoc 2000	Bio Rad, München, Germany
gentleMACS™ Dissociator	Miltenyi, Bergisch Gladbach, Germany
Heating plate	Eltac, Germany
Heracell CO_2 Incubator	Thermo Scientific, Ulm, Germany
Herasafe biological safety cabinet	Thermo Scientific, Ulm, Germany
HLC sucking Pump	Ditabis, Pforzheim, Germany
Hybaid Shake'n Stack Hybridization oven	Thermo Scientific, Ulm, Germany
HybEZ oven	Advanced cell diagnostic, Hayward, USA
Hyrax M25 Microtome	Zeiss, Jena, Germany
IKAMAG RCT magnetic stirrer	IKA Werke, Staufen, Germany
Incubator	Memmert, Schwabach, Germany
Infinite F200 PRO microplate reader	Tecan, Männedorf, Switzerland
Infrared lamp	Philips, Amsterdam, Netherlands
Inverted microscope Axiovert 25	Zeiss, Jena, Germany
Ixus digital camera	Canon, Tokio, Japan
Megafuge 1.0	Heraeus, Hanau, Germany
Micro centrifuge MiniStar Silverline	VWR, Darmstadt, Germany
Microscope BX53	Olympus, Hamburg, Germany
Microscope camera DP72	Olympus, Hamburg, Germany
Microwave oven	Siemens, Germany
Milli-Q® Advantage A10 Ultrapure Water Purification System	Merck Millipore, Darmstadt , Germany
Mini-PROTEAN® Tetra Cell	Bio-Rad, München, Germany
Mini-PROTEAN® Tetra Handcast System	Bio-Rad, München, Germany
Nanodrop 2000 Spectrophotometer	Peqlab, Erlangen, Germany
Neubauer counting chamber	Paul Marienfeld GmbH & Co. KG, Lauda-Königshofen, Germany
Nugget Ice Machine AF10	Scotsman, USA

PCR thermal cycler	Biometra, Göttingen, Germany
pH-meter Inolab	WTW GmbH, Weilheim, Germany
PipetBoy	Integra Bioscience, Zizers, Switzerland
Power 300 Power Supply	Peqlab, Erlangen, Germany
Precision scale CP153	Sartorius, Göttingen, Germany
SCN400 slide scanner	Leica Microsystems, Wetzlar, Germany
SM30C shaker	Edmund Bühler GmbH, Hechingen, Germany
Sonoplus HD200 sonicator	Bandelin, Berlin, Germany
Stemi DV4 Stereo Microscope	Carl Zeiss AG, Oberkochen, Germany
Subcell Agarose Electrophoresis System	Bio-Rad, München, Germany
Thermomixer comfort	Eppendorf, Hamburg, Germany
Tissue drying oven TDO66	Medite, Burgdorf, Germany
Trans-Blot® Turbo Transfer System	Bio-Rad, München, Germany
UNITWIST RT shaker	UniEquip, Planegg, Germany
Varioklav autoclave	HP-Medizintechnik, Oberschlei*ß*heim, Germany
Vortexer Reax 200	Heidolph, Kelheim, Germany
Water bath	Memmert, Schwabach, Germany
Water bath B3	Thermo Haake, Karlsruhe, Germany

5.1.10 Software

Software	Company
Adobe Photoshop CS5	Adobe Systems, San Jose, USA
Digital Image Hub (DIH)	Leica Biosystems, Wetzlar, Germany
DIH- TissueIA	Leica Biosystems, Wetzlar, Germany
Mendeley Desktop	Elsevier, Amsterdam, Netherlands
GraphPad Prism	GraphPad Software Inc., San Diego, USA
Image Lab™	Bio-Rad, München, Germany
ImageJ	Open Source (NIH)
Magellan™ - Data Analysis Software	Tecan Group, Männedorf, Schweiz
Microsoft Office	Microsoft Corporation, Redmond, USA
NanoDrop2000	Thermo Fisher Scientific, Waltham, USA
PrimerBlast	Open Source (NCBI)
Quantity One™	Bio-Rad, München, Germany
SCN400 viewer	Leica Biosystems, Wetzlar, Germany
SDS 2.4 ™	Applied Biosystems, Foster City, USA
Genevestigator® V3	Nebion AG, Zürich, Switzerland
CellSense Dimensions 1.7	Olympus, Hamburg, Germany

5.2 Methods

5.2.1 Database research

Genevestigator

Compendium-wide analysis of expression levels of *Lta* and *Ltb* of all available neoplasms was performed using the Genevestigator® search engine (Nebion AG, Switzerland) following the user manuals instructions. *Homo sapiens* was chosen as species, the automatically chosen platform was kept and neoplasms was chosen as only condition. In the gene selection panel, either *Lta* (probeset: 206975_at) or *Ltb* (probeset: 1559754_at) were entered. Within the condition search tools, the cancer tool was selected. Results were exported into an excel file displaying path from root, neoplasm category, probeset, mean signal intensity as log2 value, median value, standard error, lower and upper whisker and lower and upper quartile for each of the 573 neoplasms included. Neoplasms were plotted and sorted according to their expression level using the *Prism* (Graphpad Software, Inc., USA) software. Neoplasms were manually grouped into lymphomas, leukemias or other tumor entities. *Raw data acquisition was done by Dr. Nicole Simonavicius, data processing and presentation was done by me.*

TCGA

Kaplan Meier plots were generated using the *Xena Functional Genomics Explorer* (https://xenabrowser.net, University of California, Santa Cruz). TCGA Large B-cell lymphoma (DLBC), TCGA Acute Myeloid Leukemia (LAML) or TCGA Ocular melanomas (UVM) were selected as studies. Gene expression of *LTA* or *LTB* was selected as first and second variable. Kaplan Meier Plot was selected from the dropdown menu above each gene. The option *2 groups* was used and then the plot was downloaded as pdf.

5.2.2 Molecularbiological methods

Protein lysate preparation from tissue samples

Protein homogenates from frozen tissue samples were homogenized using a GentleMACS dissociator (Miltenyi) and Cell Lysis Buffer (Cell Signaling Technology) with 1x c0mplete™ protease inhibitor (Roche) and 1x PhosSTOP™ phosphatase inhibitor (Roche) at a ratio of 100µl buffer per 10mg tissue sample. After homogenization, lysates were transferred into tubes and sonicated two times for 10-15 seconds at medium energy level and then centrifuged for 10 min at 4°C and 13,000 rpm in a *Heraeus Biofuge fresco* (Heraeus) table top centrifuge. Supernatant was transferred to a fresh tube and stored at -20°C until further used.

Protein lysate preparation from cell lines

Cells were washed once with ice-cold PBS and then lysed using Cell Lysis Buffer (Cell Signaling Technology) with 1x c0mplete™ protease inhibitor (Roche) and 1x PhosSTOP™ phosphatase inhibitor (Roche). 100µl lysis buffer were used for a 6-well plate and volumes adjusted accordingly for different plate/flask sizes. Cells with lysis buffer were incubated on ice for 5 min and then scraped, collected into a fresh tube and kept on ice. Cells were disrupted by pipetting lysates up and down several times and then vortexing them for 30-60 seconds. Finally, lysates were centrifuged for 10 min at 4°C and 13,000 rpm in a *Heraeus Biofuge fresco* (Heraeus) table top centrifuge. Supernatant was transferred to a fresh tube and stored at -20°C until further used.

Determination of protein concentration

Protein concentration was determined using a *Pierce BCA Protein Assay Kit* (Thermo Fisher Scientific) according to the manufacturer's instructions. Briefly, standard dilutions were prepared ranging from 25µg/ml to 2,000µg/ml protein in PBS. Samples were diluted 1:3 - 1:20 in PBS depending on expected protein concentration. Working reagent was prepared as described in the protocol. 25µl of sample or standard solution were incubated with 200µl of working reagent for 30 min at 37°C. Results were analysed using a *Tecan infinite200 pro* (Tecan Group Ltd.) at 560nm. Concentrations were determined by linear regression of standard curve absorption using Microsoft Excel.

Preparation of self-cast SDS-PAGE gels

Self-cast gels were made using a Mini-PROTEAN® Tetra Handcast System (Bio-Rad). Stacking gel (5% PAA) and separating gel (10% PAA) were prepared without adding TEMED. 1.5mm spacer plates and short plates were assembled and placed in the Mini-PROTEAN® Tetra Handcast System. TEMED was added to the separating gel solution and the gel was immediately added to the plates so that it filled roughly 80% of the volume. 1ml of isopropanol was added onto the gel. The gels were left to polymerize for 20 minutes. Then the isopropanol was removed, TEMED was added to the stacking gel solution and the stacking gel was immediately added onto of the polymerized separating gel. 1.5mm thick 15 well combs were gently pushed into the stacking gel and the gel was left to polymerize for another 20 minutes. Thereafter the gels were wrapped in tissue soaked with running buffer and then placed inside a sealed plastic bag to keep them from drying out.

Western Blots

Protein lysates were diluted to appropriate concentrations with lysis buffer and 5x SDS Loading buffer (Bio-Rad) was added. Samples were boiled for 5 min at 95°C, spun down shortly and then loaded into handcast or precast Mini-PROTEAN® Tetra Cell TGX™ (Bio-Rad) 10% SDS-PAGE gels. Spectra™ Multicolor Broad Range Protein Ladder (Thermo Fisher

Scientific) was used as standard. Electrophoresis was performed in a Mini-PROTEAN® Tetra Cell (Bio-Rad). The electrophoresis chamber was filled with 1x electrophoresis buffer and the gels were placed into the chamber. Gels were run at 30 mA for 10 min, and then the electric current was increased up to 60 mA. After completed electrophoresis, indicated by the standard ladder reaching the bottom, gels were taken out and equilibrated for 3 min in blotting buffer. Pre-cut Whatman paper blocks (Bio-Rad) and 0.2µm nitrocellulose membranes (Bio-Rad) were also shortly soaked in blotting buffer. Blotting was performed in a *Trans-Blot Turbo* (Bio-Rad) semi-dry blotting system by placing the gels onto the membrane between 2 stacks of soaked Whatman papers. Gels were blotted onto the membrane at 25V constant and up to 1.0 A for 30 min. Successful protein transfer was determined by a Ponceau-S stain. Ponceau-S was removed by washing once with 1x TBST, and membranes were blocked for at least 1 hour at room temperature with 5% BSA in 1x TBST. Afterwards membranes were shortly washed with TBST and primary antibodies (s. 5.1.7) diluted in 5% BSA in 1x TBST were added. Membranes were incubated with primary antibody solutions over night at 4°C with gentle rocking. Membranes were washed 3 times for 5 min with TBST and incubated with respective secondary antibodies (s. 5.1.7) diluted in 5% BSA in 1x TBST for 2h at room temperature and gentle rocking. Membranes were again washed three times with TBST for 5 min and then incubated with 2ml *Clarity Western ECL Substrate* (Bio-Rad) for 2 - 5 min. Chemiluminescence was measured and visualized by a *ChemiDoc XRS+* (Bio-Rad) with *ImageLab* software. Densitometric analysis was done using the *ImageLab s*oftware.

RNA isolation from tissue samples

Up to 20mg of frozen tissue samples were homogenized using 350µl of RLT buffer (Qiagen, RNeasy Mini Kit) and a *gentleMACS™* Tissue Homogenizer (Miltenyi Biotec). Total RNA was the isolated using an *RNEasy Mini Kit* (Qiagen) according to the manufacturer's instructions. Briefly, homogenized tissues were spun down at full speed for 3 min and the supernatant was transferred into a fresh microcentrifuge tube. 1 volume of 70% ethanol (50% ethanol for liver tissues) was added and the mix was transferred into an RNEasy spin column. Samples were spun down, flow-through was discarded and the column was kept. Subsequently, the column was washed with buffer RW1 and twice with buffer RPE. Thereafter, the columns were dried by centrifugation for 1 min at full speed. Finally, RNA was eluted by adding 30µl RNAse-free water directly onto the column and spinning it down into a fresh tube. Isolated RNA was stored at -80°C until further used.

RNA isolation from cell lines

Isolation of total RNA from cell lines was done using the *RNeasy Mini Kit* (Qiagen) according to the manufacturer's instructions. In brief, cells were washed once with PBS and then 350µl of buffer RLT were added. Cell lysates were collected and transferred to fresh tubes. One volume of 70% ethanol was added for RNA precipitation and solutions were transferred to

RNEasy spin columns. Samples were spun down, flow-through was discarded and the column was kept. Subsequently, the column was washed with buffer RW1 and twice with buffer RPE. Thereafter, the columns were dried by centrifugation for 1 min at full speed. Finally, RNA was eluted by adding 30µl RNAse-free water directly onto the column and spinning it down into a fresh tube. Isolated RNA was stored at -80°C until further used.

Reverse Transcription

RNA concentration was determined using a *NanoDrop 2000* photospectrometer (VWR). Generation of cDNA was performed using the *Qiagen QuantiTect* reverse transcription kit (Qiagen) according to the manufacturer's instructions. In brief, 1µg of RNA in 12µl RNase free water was incubated with 2µl of genomic DNA wipeout buffer for 10 min at 42°C. Thereafter, 6µl of master mix containing reaction buffer, primers and reverse transcriptase, were added and the mix was incubated for another 30 min at 42°C. Reverse transcription was stopped by incubating samples for 3 min at 95°C. Samples were diluted 1:40 with PCR-grade water and then stored at -20°C until further used.

Quantitative PCR analysis

Quantitative PCR analysis was performed using an *Applied Biosystems 7900HT* real time PCR cycler (Applied Biosystems) and *Fast Start Universal SybrGreen ROX Mix 2x* (Roche). In brief, 9µl of master mix containing 6µl of 2x SybrGreen Mix, 0.12µl of forward and reverse primers each (100µM stock concentration) and 2.76µl PCR-grade water, and 3µl of cDNA were added to each well of a 384 well plate. The standard cycling procedure consisted of a pre-heating step of 5 min at 95°C to activate hot start polymerase. Then, each cycling step consisted of 15 seconds double strand dissociation at 95°C and 15 seconds annealing and elongation at 60°C. In total 40 cycles were run. A melting curve ramping from 65°C to 95°C was added after the last cycle to control for primer specificity. Data analysis was performed using the SDS 2.4 software (Applied Biosystems). *RT-qPCR in figures 11, 12 and 14 was supported by Dr. Jan Kosla.*

lacZ TaqMAn

Quantitative lacZ gene expression analysis was performed using an *Applied Biosystems 7900HT* real time PCR cycler (Applied Biosystems) and *TaqMan lacZ gene expression assay* (Applied Biosystems). In brief, for each sample 1µl 20x TaqMan lacZ Gene Expression Assay, 10µl 2x TaqMan Universal Master Mix, 4µl cDNA sample (≙ 10ng cDNA) and 5µl RNAse-free water were pipetted into a fresh reaction tube for each well. Each sample and control was run in quatruplicates. The tubes were gently mixed and then 20µl were transferred per well of a 384-well reaction plate. The plate was sealed, briefly centrifuged and then placed into the PCR cycler. The standard cycling procedure consisted of a pre-heating step of 5 min at 95°C to activate hot start polymerase. Then, each cycling step consisted of 15 seconds double strand dissociation at 95°C and 15 seconds annealing and elongation at 60°C. In total

40 cycles were run. A melting curve ramping from 65°C to 95°C was added after the last cycle to control for primer specificity. Data analysis was performed using the SDS 2.4 software.

5.2.3 Histology and immunohistochemistry

Human samples

All study samples were obtained by informed consent and transferred, stored and archived in a de-identified manner using sample IDs. Identifiers that could link samples to corresponding patients were not transferred from the suppliers. Human liver samples from patients were obtained from the Department of Molecular Pathology, Universitätsspital Basel; the Department of Pathology, Universitätsklinikum Aachen; the Institute of Human Nutrition, Irving Medical Center, Columbia University and the Department of Hematology and Oncology, Klinikum rechts der Isar, Technische Universität München.

Hematoxylin-Eosin (HE) staining

Paraffin slides were baked 15 min at 70°C. Slides were deparaffinized by incubating them three times for 5 min in xylene solution and three times for 1 min in absolute ethanol. Afterwards slides were shortly washed with ddH_2O and immersed in Harris hematoxylin solution for 5 min. Following three ddH_2O washing steps, slides were dipped several times into ammonia water (40 drops 25% ammonium solution per 500ml ddH2O). Slides were washed with ddH_2O and dipped in HCl-water (2.5ml 37% HCl solution per 500ml ddH2O) 1-2 times. Slides were washed with running tap water and then once more dipped in ammonia water several times, washed again two times with ddH_2O and one more time with 70% ethanol. Slides were stained with eosin for 2 min and slides were subsequently washed with absolute ethanol three times. Subsequently, slides were dehydrated with xylene solution three times for 2 min and afterwards mounted with Eukitt medium. *Staining procedures were often supported by the technical staff.*

Immunohistochemistry

Paraffin sections were stained on a *Bond-MAX* immunohistochemistry robot (Leica Biosystems) with antibodies at concentrations listed in 5.1.7. For immunohistochemical detection *the Bond MAX DAB-kit* (Bond Polymer Refine Detection, Leica) was used, for double stainings in combination with the *Bond MAX Fast Red-Kit* (Bond Polymer Refine Red Detection, Leica). Depending on the primary antibody, citrate (H1) or EDTA (H2) based antigen retrieval was performed before staining. Slides were scanned using a *SCN400* slide scanner (Leica Biosystems) and analysed using *Tissue IA* image analysis software (Leica Biosystems). *Staining procedures were supported by the technical staff.*

In situ hybridization

RNA *in situ* hybridization was performed using the *RNAscope 2.0 brown FFPE Assay* (Advanced Cell Diagnostics) according to the manufacturer's protocol. Summarized, 2 µm paraffin-embedded tissue sections were baked in a dry oven for 1 h, 60°C, followed by de-paraffinization and blocking of endogenous peroxidases. Slides were cooked for 15 min in pre-treatment solution 2 and protease digestion was performed for 30 min using pretreatment solution 3. In situ probes specific for human *LTA*, murine *Lta*, *Vcam1*, Madcam*1* or *Tek* were incubated with the tissues for 2 hrs at 40°C in a hybridization oven, followed by signal amplification and detection according to manufacturer's protocol. Counterstaining was done using *Gill's Hematoxylin I* (American Master Tech Scientific, USA) and slides were mounted using *EcoMount* mounting medium (Biocare Medical) and scanned into digital images using a *Leica SCN400* Slide Scanner. *Staining procedures were supported by the technical staff.*

Analysis and quantification of immunohistochemical stainings

Immunohistochemical stainings were quantified either as positive cells per total cells or positive area per total area. The number of cells positively stained for nuclear or cytoplasmatic markers was determined using *SlidePath TissueIA* (Leica) image analysis software and was then normalized to the total cell number analyzed. Cell analysis algorithms were established once for each staining and then kept with the same settings for all groups of each staining. Alternatively, five different and independent areas were randomly selected, analyzed manually and normalized to the total analyzed tissue area using the *Digital Image Hub* viewer (Leica).

The area positively stained for cytoplasmatic, membrane-bound or extracellular markers was determined using *SlidePath TissueIA* (Leica) image analysis software and was then normalized to the total area analyzed. Area analysis algorithms were established once for each staining and then kept with the same settings for all groups of each staining.

Images for representation were either taken with an *Olympus BX53F Microscope* (Olympus) equipped with a *DP72 camera* (Olympus) using *CellSense Dimensions 1.7 software* (Olympus) or by scanning of whole tissue sections using a Leica *SCN400* slide scanner and *TissueIA* imaging software (Leica).

3D reconstruction

Cryo-blocks of liver samples of Lrat-TdTomato or Lrat-TdTomato Col-GFP mice were provided by the lab of Prof. Robert Schwabe (Columbia University, New York, USA). Anti-CD31 immunofluorescent staining was established by fixing 5 µm liver cryo-sections on glass coverslips in icecold 100% acetone for 10 minutes. Sections were then blocked for 10 minutes in 2% fetal calf serum (Gibco) in 1x PBS and then incubated for 60 minuntes with

anti-CD31 PE-conjugated antibody (BioLegend) diluted 1:100 in 1% BSA, 0.25% Triton-X100 in 1x PBS. Sections were then washed in 2% FCS in PBS solution and mounted with fluorescence mounting medium and then imaged using an *Olympus BX53 Microscope* (Olympus) equipped with DP72 *camera* (Olympus) using *CellSense Dimensions 1.7 software* (Olympus).

For 3D reconstruction, 30 consecutive cuts of each cryo-block were stained with CD31 or not further stained and then passed on to *Dr. Simone Joers from the lab of PD Dr. Fabian Geisler (Klinikum rechts der Isar, TU München, Germany) where the 3D reconstruction was done.*

5.2.4 Animal experiments

Mice

Mice were maintained under standard housing conditions and experiments were performed according to the German Animal Protection Law and approved by the Regierung von Oberbayern (TVA 55.2-1-54-2532-196-13) or the Regierungspräsidium Karlsruhe (TVA 35-9185.81/G-1/18). C57BL/6 and DBA/2 mice were bought from Charles River (Charles River Laboratories Germany GmbH, Sulzfeld, Germany). Transgenic mouse lines were bred and intercrossed within our mouse facilities.

Genotyping of transgenic mice

For genotyping of transgenic mice, tail biopsy samples were digested in 200 µl 1x tail lysis buffer containing proteinase K (20mg/ml, Roche) over night in a *Thermomixer comfort* (Eppendorf) at 56°C with vigorous shaking. Lysates were boiled for 15-30 minutes at 95°C and then centrifuged at 13,000 rpm for 3 min in a *Heraeus Biofuge fresco* (Heraeus) table top centrifuge and stored at 4°C. For long-term storage supernatant was transferred to a new tube and frozen at -20°C. 15µl of forward and 15µl of reverse primer stock (c = 100µM) were mixed and 1.6ml of PCR-grade water was added to prepare the primer mix solution. Then, 5µl of RedTaq Ready Mix PCR Reaction Mix (Sigma-Aldrich) were added to 4µl of primer mix. Finally, 2µl of tail lysate were added. PCR amplification was done in a PCR thermal cycler (Biometra) according to the mouse strain specific protocols. *Genotyping of transgenic mice was often done by the technical staff.*

Dissection and tissue preparation

Animals were euthanized using CO_2 as recommended by the German animal protection law. Skin and fur were moisturized with 80% ethanol. The abdomen was opened by a central cut. Organs were taken out, dissected as required and directly immersed in 4% PFA for paraffin embedding, immersed in Tissue Tek O.C.T. compound (Sakura Finetek) for cryo embedding or deep frozen in liquid nitrogen for RNA or protein analysis. Cryoblocks were evenly frozen by immersion in cold (-80°C) isopropyl alcohol. Frozen tissue samples were stored on -80°C

until further processing. Tissues for paraffin embedding were kept in 4% PFA for up to 5 days, then they were cut as required and stored in PBS on 4°C. Tissues were dehydrated overnight and then embedded in paraffin. A microtome was used for cutting paraffin embedded tissues into 2µm ultrathin sections adhered to Superfrost glass slides. Tissue cuts were incubated at 37°C overnight to allow dehydration before staining. *Dissection and tissue preparation of mice used for figures 11, 12, 13, 15, 16, 21 and 24 was fully or partly done by Dr. Nicole Simonavicius and Dr. Bastian Seubert.Dissection of mice was usually done in small groups with colleagues.*

Antibody and inhibitor treatments

ACH6 or IgG were injected intraperitoneally twice a week for two weeks prior to the experiment and once more on the day of the experiment. 50µg of antibody solved in 100µl PBS were injected with each injection. 100µg LTßR-Ig or MOPC21 in 200µl PBS were injected intraperitoneally once a day before and once a day after tumor cell injection.

Experimental metastasis

C57BL/6 and DBA/2 mice were purchased from Charles River Laboratories, Germany. Transgenic mice were bred in our own mouse facilities at the Helmholtz-Zentrum München or the DKFZ Heidelberg. C57BL/6 and DBA/2 mice of 8-12 weeks of age or transgenic mice of 10-24 weeks of age were intravenously injected with either $1.5x10^6$ cells for 24 hours (L-CI.5s, L-CI.5s GFP, L-CI.5s LTa, L-CI.5s LTß, L-CI.5s sh38, L-CI.5s sh39, L-CI.5s sh63, L-CI.5s sh88, L-CI.5s shNT), $1.0x10^4$ cells for 7 days (L-CI.5s, L-CI.5s GFP, L-CI.5s LTa, L-CI.5s LTß, L-CI.5s sh38, L-CI.5s sh39, L-CI.5s sh63, L-CI.5s sh88, L-CI.5s shNT), $0.5x10^6$ cells for 14 days (Eµ-myc) or $0.3x10^6$ for 20 days (MC-38 GFP). $0.4x10^6$ MC-38 GFP cells were injected for 16 days in case of the intrasplenic injection. Mice were sacrificed and livers, lungs, spleen, kidney, pancreas and thymus were resected and prepared as described above. Metastatic burden was evaluated using immunohistochemistry or X-gal stained liver lobes, as described below. *Intravenous injections were done by Dr. Bastian Seubert, Dr. Tracy O`Connor or Gaia Bianco.*

Metastases counting

Metastatic foci were counted macroscopically after X-gal staining of liver lobes or microscopically using immunohistochemical stainings. Macrometastases of the liver were counted using X-gal stained liver lobes. Liver lobes were observed through a dissecting microscope (Carl Zeiss) and macroscopically visible X-gal stained metastatic foci were counted manually on the frontside and backside of each liver lobe. *This was mostly done by Dr. Nicole Simonavicius.* Micrometastases and macrometastases were counted using H&E and ki67 stained tissue sections. Metastatic foci were identified by their strong hematoxylin staining without intermittent eosin stained areas as compared to the liver parenchyma and

by aggregations of ki67 positive cells. The number of metastatic foci was counted and then normalized to the analyzed tissue area.

The amount of seeded tumor cells in the liver 24h after tumor cell injection was counted using ki67, CD3, B220 and X-gal stained tissue sections. The amount of stained cells per total cells (ki67, CD3, B220) or stained area per total area (X-gal) was calculated using Tissue IA and DIH software (Leica Biosystems, Germany) using manually refined and specific algorithm preferences.

X-gal staining

Freshly dissected liver lobes or frozen liver pieces were put into a Greiner vessel with fixing solution for up to 30 minutes. The tissue was washed with PBS three times by filling the vessel with PBS and shaking gently. Then the vessel was filled with up to 5ml of ready-to-use X-Gal solution, such as to cover the whole tissue. The tissue was then incubated with the ready-to-use X-Gal solution for 3-7h at 37°C until blue stained metastatic foci were clearly visible. The tissues were then washed once more with PBS and then analysed.

X-Gal staining of freshly cut cryosections was performed by incubating the slides for 10 minutes in fixing solution and thereafter 10 minutes in washing solution. Then the slides were incubated for another 10 minutes in detergent solution before they were incubated over night with ready-to-use X-Gal solution at room temperature. Counterstaining with eosin was done by lowering the slides 2-3 times shortly into eosin solution and then washing them with water. The slides were then sealed with Kaisers Glycerin-Gelatine (Carl Roth). *Staining procedure was often supported by the technical staff.*

Clodronate treatment

C57BL/6 or DBA/2 mice were injected intraperitoneally with either clodronate or control (PBS) liposomes (Liposoma B.V.). 100µl of liposomes were injected three times over the course of eight days. Injections were done at days one, four and 6 and mice were sacrificed and dissected on day 8. Efficiency of clodronate treatment was measured using F4/80 stained liver tissue sections of clodronate liposome or PBS liposome treated mice. *This was done by Dr. Nicole Simonavicius.*

Vascular permeability assays

Permeability of the liver microvasculature was determined with Evans Blue dye extravasation technique (Reutershan *et al.*, 2006). Mice were pretreated with ACH6 for 7 days or left untreated prior to the experiment or were subjected to a 7 days experimental metastasis assay with L-CI.5s cells. 2mg Evans Blue dye in 200µl PBS were injected intravenously into the tail vein. 60 minutes later mice were sacrificed using CO_2 and the liver was perfused with 10ml of PBS using a peristaltic pump at 5ml/min to control liquid flow. The livers were dissected, photographed and then homogenized in 500µl PBS using a

gentleMACS Dissociator tissue homogenizer (Miltenyi Biotec). Evans Blue was extracted with 700µl formamide at 70°C for 48 hours. The suspension was centrifuged at 5000g for 30 minutes and 100µl of supernatant were analyzed spectrophotometrically with an *infinite f200 pro* (Tecan) microplate reader at 620nm and corrected against heme absorption measured at 740nm. Extravasated Evans Blue was calculated as µg/g liver tissue using a calibration curve. *This was done by Dr. Nicole Simonavicius.*

5.2.5 Cell culture, cell-based assays and microscopy

Cell lines

Parental LCI5s were provided by Prof. Achim Krüger (Insitut für Molekulare Immunologie, Klinikum rechts der Isar, TU München, Germany). Parental Eµ-Myc murine B-cell lymphoma cells were provided by Prof. Ulrich Keller (III. Medizinische Klinik, Klinikum rechts der Isar, TU München, Germany). LCI5s and Eµ-myc LT knockdown cells were created by Dr. Jan Kosla using shRNA transfection. LCI5s and Eµ-myc LT overexpressing cells were created by Dr. Jan Kosla using plasmid transfection. C3H 10T1/2 murine fibroblast cells were bought from ATCC. C3H 10T1/2 MAdCAm-1, NIK and LTßR knockdown as well as PX459 control cells were created by Dr. Jan Kosla using CRISPR/Cas9 guided excision. Human immortalized hepatic stellate cell line LX-2 was kindly provided by Prof. Weiskirchen (Institut für klinische Chemie und Pathobiochemie, RWTH Aachen, Germany). HUVECs were purchased from Cellworks (San Jose, USA). Sk-Hep1 human immortalized LSEC cell line was kindly provided by Prof. Percy Knolle (Institut für Molekulare Immunologie, Klinikum rechts der Isar, TUM, Germany). Primary murine hepatic stellate cells were freshly isolated by Dr. Silvia Affo (Columbia University, New York, USA) (RNA sequencing) or Dirk Wohlleber (Institut für Molekulare Immunologie, TU München, Germany) (RT-qPCR). MC-38 GFP murine coloncarcinoma cell line was kindly provided by Prof. Lubor Borsig (Institute of Physiology, University of Zurich, Switzerland).

Immunocytochemistry

10T1/2 or LX-2 cells were grown on sterile 13mm tissue culture coverslips placed in 24-well plates to the desired confluency. Antibody and inhibitor treatments were done as indicated in the figures. Antibodies and inhibitors were always diluted in the respective cell culture media. After reaching the desired confluency, cells were washed once with PBS and then fixed in 4% paraformaldehyde (in PBS, pH 7.4) for one hour at room temperature. Cells were then rinsed twice with PBS and once with IFF. Cells were permealized with 0.5% Triton X-100 in PBS for 10 minutes and then again rinsed twice with PBS and once with IFF. Thereafter, the cells were incubated with the primary antibody suitably diluted in IFF for 40 minutes at room temperature. Cells were then washed with PBS three times for 5 minutes and then incubated with a secondary Alexa488-conjugated antibody diluted 1/1000, Phalloidin 546 diluted 1/500 and DAPI diluted 1/10000 in IFF. Cells were washed again three times in PBS

for 5 minutes then the coverslips were dipped in water and drained on a paper tissue. The coverslips were mounted on a microscope glass slide with 4µl *Vectashield®* mounting medium (Vector Laboratories) and then sealed with nail varnish. Mounted samples were then visualized and analyzed using an Olympus *BX-53* fluorescence microscope (Olympus) with a *DP-72* camera (Olympus). For analysis of eccentricity and size 10 random pictures were taken and all single cells on each picture were analysed using Photoshop CS5 (Adobe Systems) software.

XTT assay

Cell viability and proliferation were tested using the XTT Cell proliferation kit II (Roche) according to the manufacturer's instructions. Briefly, cells were seeded into a 96-well plate in 100µl of culture medium and left to settle and attach overnight. Cells were then treated with antibodies and/or inhibitors at their indicated concentrations or left untreated. Immediately afterwards the 0 day time-point was measured. Therefore, 50µl of XTT labeling mixture were added to each well and left to incubate for 4 hours in a cell culture incubator at 37°C. Absorbance was measured using an an *infinite f200 pro* (Tecan) microplate reader at 492nm with reference wavelength set to 690nm. Further measurements were done on a daily basis for seven days in the same manner.

Contraction assay

Contractility of C3H 10T1/2 and LX-2 cells was measured using a Cell Contraction Assay (Cell Biolabs, Inc., CBA-201) according to the manufacturer's instructions. Briefly, cells were harvested and resuspended in the desired medium at $2x10^6$ cells/ml. The collagen lattice was prepared by mixing two parts of cell suspension with 8 parts of cold Collagen Gel Working Solution. 0.5ml of the cell-collagen mix were added per well of a 24-well plate and incubated for one hour at 37°C. After collagen polymerization, 1.0 ml of culture medium containing IgG, ACH6, IvIG or BS-1 was added atop each collagen lattice. Cultures were incubated for two days to develop stress. Then, contraction was initiated by gently releasing the collagen gels from the well walls using a sterile spatula. The collagen lattices were left in the wells to contract for 24 hours. Then a picture of the collagen lattices was taken using a digital camera and the contraction was measured as area of the collagen lattice versus the area of the well bottom.

Adhesion assay

C3H 10T1/2 or LX-2 cells were grown to near confluence in 12-well plates and then treated with antibodies (IgG/ACH6 or BS-1/IvIG) and inhibitors (NIKc2, Ro-28, EHT1864, UO126, SCH77) for 48 hours. Antibodies and inhibitors were refreshed after 24 hours. Tumor cells (LCI5s P, LCI5s shLTaß, LCI5s EGFP, LCI5s LTa, LCI5s LTß) were stained with cell tracker green CMFDA (Life Technologies) for 20 minutes, then recovered in their specific growth medium for at least 3 hours. Thereafter $2x10^5$ tumor cells were added in 10T1/2 medium (DMEM +

10%FCS + P/S) to the 10T1/2 cells for 30 minutes. Non-adherent cells were then aspirated, and wells were carefully washed 3 times with PBS to remove any remaining non-adherent cells. Then the remaining cells were fixed with 4% PFA for at least 1 hour. Five 4x pictures were taken on the green channel of a *CKX41* fluorescent microscope (Olympus) with an *Olympus XM10* camera and the *CellSense Dimensions* software (Olympus) for each well and pictures were analyzed with *ImageJ* using a batch analysis macro.

Migration assay

C3H10T1/2 or LX-2 cells were starved in DMEM + 2% FCS overnight. Cells were then detached with Trypsin/EDTA and then stained with 2µM cell tracker green CMFDA (Life Technologies) for 20 minutes and then recovered in DMEM + 2% FCS for at least 3 hours. Stained cells were then added to the upper chamber of a 24-well transwell dish (Thermo Fisher scientific) with 8 µm pore size and 6.5mm diameter in DMEM + 2% FCS, while the lower chamber contained 600µl DMEM + 10% FCS. Cells were left to migrate to the lower chamber for 24h. Then, cells remaining in the top chamber were removed using a cotton swab and the cells on the bottom side of the transwell membrane were fixed with 4% paraformaldehyde for 30 minutes. Transmigrated cells were then imaged using a 10× objective on a *CKX41* (Olympus) microscope with an *Olympus XM10* camera using the *CellSense Dimensions* software (Olympus). Seven randomly taken images per well were analyzed using the *ImageJ* software. All n values represent biological replicates performed as technical duplicates and averaged.

Trans-endothelial migration assay

Trans-endothelial migration was measured in transwell dishes (Thermo Fisher scientific) with 8 µm pore size and 6.5mm diameter. Inserts were coated with 0.1% gelatine (Sigma-Aldrich) for 30 min and then turned upside down to plate 3500 C3H 10T1/2 cells in 100µl DMEM + 10%FCS on the bottom side of the inserts and then inserts were placed in an incubator at 37°C. Medium was refreshed after 15 minutes if needed. After 30 minutes inserts were turned back around and put back into 24-well plates with 600µl HUVEC medium in the bottom well. 3.5×10^4 HUVECs (Cellworks, ZHC2301) were added in 10µl HUVEC medium and left to grow into a monolayer for 3 days. Medium was exchanged once during that time. Tumor cells were stained with 2 µM *Cell Tracker Green CMFDA* (Life Technologies) for 30 min and recovered in their specific growth medium for 3h. Cells were spun down and resuspended in HUVEC growth medium. 1×10^5 tumor cells were seeded into the top chamber and incubated as indicated and then fixed with 4% formaldehyde. Cells on the top of the membrane were removed with a cotton swab and membranes were mounted on a glass slide using *Mowiol* (Merck). Seven random images were obtained of Cell Tracker Green using a 10× objective on an *Olympus CKX41* with an *Olympus XM10* camera using the *CellSense Dimensions* software (Olympus). Cell numbers were quantified using

ImageJ. All n values represent biological replicates performed as technical duplicates and averaged; all experiments were normalized to an untransfected control.

Wound healing assay

LX-2 or C3H 10T1/2 cells were seeded into 12-well plates and incubated until they reached full confluency. Wells were divided into two groups and treated with either BS-1 or IvIG (LX-2) or ACH6 or IgG (10T1/2). Four scratches were cut through the monolayer in a foursquare pattern using a yellow 200µl plastic pipette tip. Pictures of the cuts were made at 10x resolution using an *Olympus CKX41* microscope with an *Olympus XM10* (Olympus) camera using the *CellSens Dimensions* software (Olympus). One picture was made per cut (4 per well) and the location was marked. Cells were then incubated at 37°C with 5% CO_2 for 24 hours. Thereafter, pictures of the cuts were taken again at the marked locations. Pictures were then analyzed using the *ImageJ* software. Wound healing potential was determined by dividing the area not covered by cells after 24 hours through the area not covered with cells at 0 hours for each picture series.

Atomic Force Microscopy

Atomic force microscopy measurements were done in collaboration with Prof. Dr. Jochen Guck (Institute of Cellular Machines, TU Dresden, Germany). C3H 10T1/2 cells were spread on glass-bottom dishes and kept in CO_2 independent medium. Cells were treated with IgG or ACH6 for 24 hours and then subjected an atomic force microscopy indentation measurement. An *Arrow™ T1 cantilever* (NanoWorld AG) tip with 5µm diameter was used. 6 positions per cell were measured on average and 70 cells were measured for each condition. Statistical significance was tested with a student's t-test.

Conditioned media

C3H 10T1/2 cells were seeded in 6-well plates and left to grow to around 50% confluency. Cells were then treated with ACH6 or IgG for 24 hours. Thereafter the medium above the cells was taken above and transferred into a 15 ml Falcon Tube. Medium from at least 3 different wells was pooled for each condition. Medium was then filtered through a 0.45 µm syringe filter (Roth) and frozen down at -20°C until further used.

Electron microscopy

Freshly prepared tissue was immersed in 3% glutaraldehyde solved in Sörensen buffer and fixed for 2h at room temperature. Afterwards, tissue was cut into small cubes of roughly 1mm x 1mm x 1mm size and fixed for a further 20h in 3% glutaraldehyde solution. After fixation, tissue cubes were immersed in Sörensen buffer and stored at 4°C until further processed. *Embedding, further processing and electron microscopy was performed at the lab of Prof. Marco Prinz (Institute of Neuropathology, University Hospital Freiburg, Germany).*

Isolation and culture of primary HSCs

Isolation of primary HSCs was done in collaboration with Dr. Dirk Wohlleber (Institut für Molekulare Immunologie, Klinikum rechts der Isar, TUM, Germany). Mice used for HSC isolation were at least 6 month old. Mice were anesthetized by intraperitoneal injection of roughly 100µl (according to their weight) Ketamin/Xylazin solution (3:1) and exposed to an infrared lamp. A small peripheral venous catheter (PVC) was inserted into the inferior vena cava (IVC) and immediately afterwards the portal vein was cut. The liver was perfused through the PVC at a rate of 5ml/min first with 10 ml EGTA solution, then with 10 ml pronase E solution and finally with 20 ml collagenase D solution. The livers were then resected and stored on ice in HBSS + 10% FCS. Livers of 2-3 animals were pooled and then the livers were transferred to a petridish and minced in a digestion solution containing pronase E, collagenase D and DNase. Cells were transferred into a 200ml flask with 100ml of the digestion solution and stirred at room temperature for 3-5 minutes. The digested livers were then filtered through a 100µm cell strainer and transferred to 50ml Falcon tubes. Then they were centrifuged at 500g for 7 minutes at 4°C. The supernatant was discarded and each pellet was washed with 10 ml HBSS containing 10ml FCS, Pen/Strep and 30µl DNAse I and then recollected in 50ml Falcon tubes. HBSS containing 10% FCS was added to fill the tubes up to 50ml and the tubes were centrifuged at 500g for 7 minutes at 4°C. Supernatant was discarded and the pellets again resuspended in 10 ml HBSS containing 10ml FCS, Pen/Strep and 30µl DNAse I. HBSS containing 10% FCS was added to fill the tubes up to 34ml and 13.5 ml Nycodenz solution were added. The solution was mixed well and transferred to four 15ml Falcon tubes (12ml each). 1ml of HBSS + 10% FCS was carefully added on top of each solution. Then the tubes were centrifuged at 1400g for 24 minutes at 4°C. No breaks were used to slow the rotor after the centrifugation. A white layer below the clear HBSS layer indicated the hepatic stellate cells. These were transferred to a 50ml Falcon tube with HBSS containing 10% FCS and soun down at 500g for 7 minutes at 4°C. The supernatant was discarded again and the pellet resuspended in DMEM containing 10% FCS, Pen/Strep and L-Glutamine. Cell count was determined using trypan blue staining to determine dead cells and a Neubauer counting chamber. Cells were then seeded into 6-well plates in a density of 0.5-1x10^6 cells per well.

5.2.6 Transcriptomics and proteomics

RNA sequencing

RNA sequencing (RNA Seq) of Lrat-TdTomato mice was done in collaboration with the lab of Prof. Robert Schwabe (Columbia University, New York, USA). Mouse preparation, HSC isolation and RNA Seq were done at the Columbia University. Data analysis was done by me. Lrat-TdTomato mice were treated with ACH6 or IgG for 2 weeks. 5 injections of 50µg antibody were used per mouse every 3rd or 4th day. Mice were then euthanized and HSCs were isolated. Isolated HSCs were pooled for each treatment group, lysed and RNA was

isolated. RNA samples were then sent to the RNA Seq core facility at the Columbia University. Data for each gene, including base mean, log2 fold change, fold change, standard error, p-value and adjusted p-value were send to us for further analysis.

Protein and phosphorylation profiling

Whole proteome and phospho-proteome profiling was done in collaboration with the sciomics GmbH (Heidelberg, Germany). LX-2 or C3H 10T1/2 cells were grown to around 50% confluency in T75 flasks and then treated with BS-1 or IvIG (LX-2 cells) or ACH6 or IgG (10T1/2 cells) for 48h. Cells were rinsed with ice cold PBS and then lysed using 300µl freshly prepared ready-to-use *scioExtract* (sciomics GmbH, Germany) solution per flask for 20 minutes on ice. Cells and extraction buffer were collected using a cell scraper and transferred into a 1.5 ml reaction tube. Samples were pipetted up and down carefully 20 times using a syringe with a 27 Gauge needle. The vessel was centrifuged at 15,000g and 4°C for 20 minutes. Using a syringe, the protein containing fraction, lying between the pellet at the bottom and the lipid fraction on top, was aspirated and transferred into a fresh reaction tube. The pellet and lipid layer were discarded. The protein sample was frozen down at -20°C and send to the *sciomics GmbH* for proteome and phospho-proteome profiling. A full report, including methods used, protein expression analysis and protein phosphorylation analysis was sent back thereafter. Protein expression and protein phosphorylation expression analysis contained cluster analysis, differential expression analysis, cellular component and biological process analysis.

Phospho-kinase array

The Proteome Profiler™ Human Phospho Kinase Array Kit (R&D Systems) was used following the manufacturer's instructions. Briefly, LX-2 or C3H 10T1/2 cells were grown to around 50% confluency and then treated with BS-1 or IvIG (LX-2 cells) or ACH6 or IgG (10T1/2 cells) for 4 hours. Then cells were lysed with Lysis Buffer 6, pipetted up and down several times and then rocked gently for 30 minutes at 4°C. Cells were spun down at 14,000g for 5 minutes and transferred to a fresh tube. Protein concentration was determined using a *Pierce BCA Protein Assay Kit* (Thermo Fisher Scientific) as described earlier (5.2.2). 1ml of Array Buffer 1 (blocking buffer) was added to each well of the 8-well multi-dish and for each sample one Part A membrane and one Part B membrane were added to a well each and then incubated for one hour on a rocking platform shaker. Meanwhile 500µg protein of each sample was diluted in 2ml of Array Buffer 1. Array Buffer 1 was removed from the wells and 1ml of each sample solution was added to a Part A and a Part B membrane each. Samples were incubated at 4°C on a rocking shaker overnight. Membranes were washed 3 times for 10 minutes in 1x Wash Buffer and the dish was cleaned. Part A membranes were then incubated for 2 hours at room temperature on a rocking shaker with 20µl of reconstituted Detection Antibody Cocktail A diluted in 1x Array Buffer 2/3. Part B membranes were incubated for 2 hours at room temperature on a rocking shaker with 20µl of reconstituted

Detection Antibody Cocktail B diluted in 1x Array Buffer 2/3. Membranes were washed again 3 times for 10 minutes in 1x Wash Buffer. Streptavidin-HRP was suitably diluted in 1x Array Buffer 2/3 and 1 ml was added to each membrane and incubated for 30 minutes on a rocking platform shaker. Membranes were washed again 3 times for 10 minutes in 1x Wash Buffer. Membranes were put onto a plastic sheet protector and 1 ml of Chemi Reagent Mix was added evenly onto each membrane. Membranes were covered with the top of the plastic sheet protector, air bubbles were removed from between the sheets and the membranes were incubated for one minute. Chemi Reagent Mix was removed, and any excess blotted off with an absorbent lab wipe. Membranes were wrapped in plastic wrap, air bubbles were smoothed out and chemiluminescence was measured and visualized by a *ChemiDoc XRS+* (Bio-Rad) with *ImageLab* software (Bio-Rad). Densitometric analysis was done using the ImageLab software.

5.2.7 Statistics

Statistical analyses were performed with *Prism software* (Graphpad Prism version 5.0a). The standard error of the mean (SEM) was calculated from the average of at least 3 independent samples per group. To evaluate statistical significance between two groups, data was subjected to Student's t test (unpaired or paired, two-tailed test). A p-value of less than 0.05 was considered significant. Xy scatter plots were evaluated by linear regression analysis with R2 representing the strength of the correlation. A p-value of less than 0.05 was considered significant.

6. Results

6.1 Lymphotoxin modulates lymphoma manifestations in the liver

6.1.1 LT expression positively correlates with secondary liver manifestations and disease severity in human lymphoma and leukemia patients

To find out whether lymphotoxin signaling is implicated in hepatic metastasis, first, lymphotoxin expression levels in human malignancies were investigated. The *Genevestigator* search engine (Nebion AG) was used to scan collective microarray data from 573 different tumor entities for expression levels of lymphotoxins (Figure 7). All datasets of human tumor tissues were included in the analysis and subjected to a search for the expression of *LTA* or *LTB*. The neoplasms were sorted according to their mean expression levels from highest (left) to lowest (right). Analysis of mean *LTA* expression of all neoplasms revealed that lymphomas (red bars) especially but also leukemias (green bars) were by far the highest *LTA* expressing entities on average (Figure 7A). The 30 highest *LTA* expressing entities contain 19 lymphomas and 4 leukemias and only 7 non-hematopoietic cancer types (Figure 7B). Thus, almost 77% of the top 30 *LTA* expressing entities are either lymphomas or leukemia. In total 56 of the 573 tumor entities (9.8%) included in the analysis were of lymphoid or hematopoietic origin. Expression levels for *LTB* were also highest in lymphomas and leukemia on average (Figure 7C), although to a lesser extent than for *LTA*. This is also reflected when looking at the 30 highest *LTB* expressing entities, which contain 5 lymphomas and 7 leukemias (Figure 7D), making up 40% of the top 30 *LTB* expressing entities.

The data from Figure 7 show clearly that lymphomas and leukemias express the highest levels of *LTA* and *LTB* on average. Next, it was investigated whether these genes were overexpressed in neoplastic tissues compared to healthy control tissues. a TCGA (The Cancer Genome Atlas) database search was performed. All available datasets for *LTA* or *LTB* overexpression in tumor tissues were included. Of the 33 tumor entities included in the search, only DLBCL (DLBC) showed a significant overexpression of *LTA* in tumor tissue (red dots) when compared to healthy control tissue (green dots) (Figure 8A, not all data shown). Others, such as AML (LAML) showed a trend towards increased *LTA* expression in tumor tissues, but no statistical significance was observed. Most showed no difference in expression levels and one (Testicular Germ Cell Tumors (TGCT)) showed decreased *LTA* expression in tumor tissues compared to healthy controls. For *LTB*, 19 of 33 tumor entities showed a significantly increased expression in tumor tissue (Figure 8B, not all data shown). Amongst those were DLBCL, AML as well as TGCT. One (Chromophobe renal cell carcinoma (KICH)) showed a decreased *LTB* expression in tumor tissue (not shown). The remaining 13

entities showed no significant changes. Certain tumors, such as adrenocortical carcinoma (ACC), showed almost no expression of *LTA* or *LTB* in either healthy or tumor tissue. Interestingly, TGCT showed an upregulation of *LTB* but also a downregulation of *LTA* in tumor tissue compared to healthy control tissue.

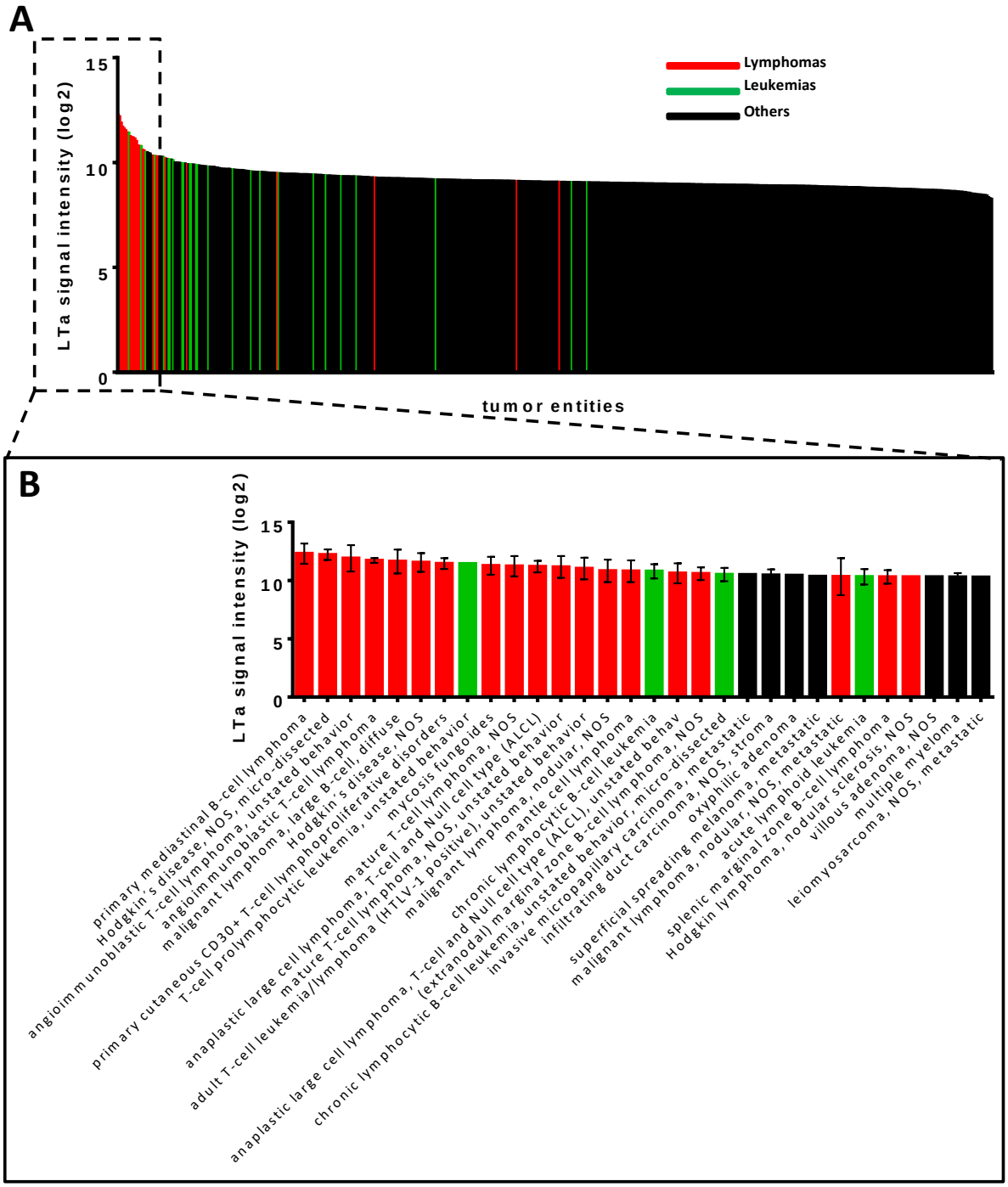

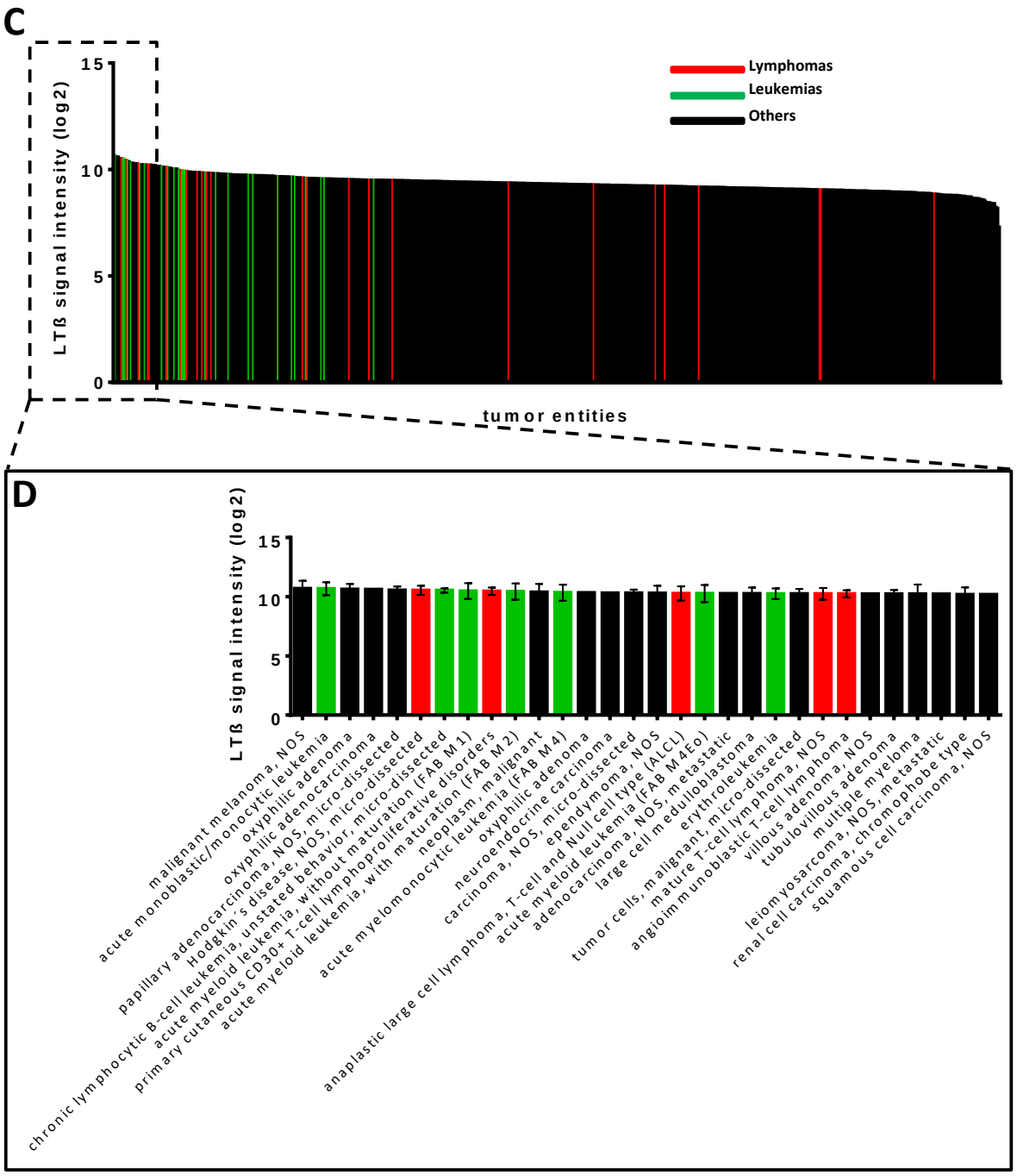

Figure 7: *LTA* and *LTB* expression levels of different tumor entities

Relative expression of *LTA* and *LTB* as extracted from the Genevestigator platform for 573 different types of neoplasms. Mean expression levels are shown as log2 signal intensity. Lymphomas are shown in red, leukemias are shown in green and other tumor entities in black.

A) Expression levels of *LTA* for all 573 types of neoplasms.

B) *LTA* expression levels of the 30 highest *LTA* expressing neoplasms.

C) Expression levels of *LTB* for all 573 types of neoplasms.

D) *LTB* expression levels of the 30 highest *LTB* expressing neoplasms.

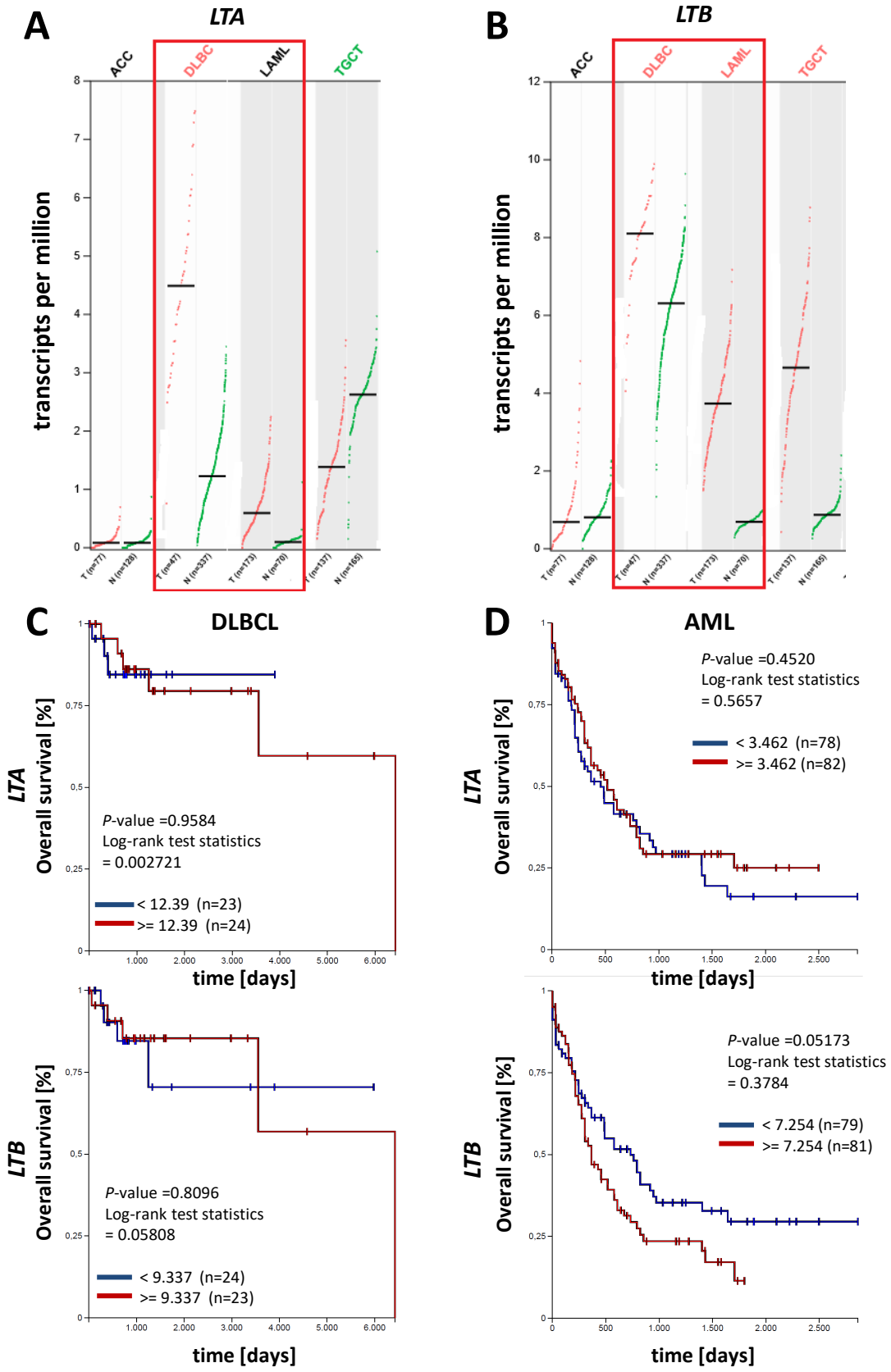

Figure 8: LT overexpression correlates with overall survival in human DLBCL and AML patients

A, B) mRNA expression levels of *LTA* **(A)** or *LTB* **(B)** as assessed by TCGA database research of samples from patients with ACC, DLBCL, AML or TGCT (red dots) and respective healthy control tissues (green dots). Mean expression levels are shown as transcripts per million. Each dot represents one sample.

C, D) Overall survival of DLBCL **(C)** or AML **(D)** patients with high (red graph) or low (blue graph) expression of either *LTA* (top) or *LTB* (bottom) as assessed by TCGA database research. Relative survival rate (Y axis) is plotted against time in days (X axis). Sample sizes for both groups and expression level thresholds for high or low expression are indicated in the graphs.

The data from Figure 8A and 8B show that some hematopoietic tumor entities (DLBCL, AML) not only express high levels of LTs, but also overexpress them in malignant tumor cells. Further TGCA database research was done to investigate whether the expression of LTs in these malignancies also correlates with overall survival of patients. Overall survival for patients with either DLBCL or AML was investigated. Patients were split into high (red bars) and low (blue bars) expressing groups based on their expression levels of either *LTA* or *LTB*. Unfortunately, the sample sizes were very low for DLBCL, ranging from 1-14 patients per group and time point. Still, a clear trend could be observed for a decrease in overall survival with higher *LTA* expression at late timepoints (past 3500 days) (Figure 8C). *LTB* does not seem to have an effect on patient survival (Figure 8C). For AML, no effect on overall survival can be seen with increased *LTA* expression, but a significant decrease in overall survival can be correlated with increased *LTB* expression already at early time points (~250 days) (Figure 8D).

To corroborate the data gathered from the database researches, tissues from human leukemia and lymphoma patients were analysed regarding their expression of LTs (Figure 9). Peripheral blood from CLL and AML patients was analysed using RT-qPCR, and the results were compared to peripheral blood from healthy control patients (Figure 9A). The expression of *LTA* was significantly increased in CLL patients. A similar trend was observed for *LTB* expression, but it did not reach statistical significance due to the large variation between samples.

Furthermore, *LTB* expression in human primary and secondary liver manifestations of various lymphomas was analysed via immunohistochemical staining of LTß (Figure 9B). Compairing LTß staining intensity of primary and secondary liver manifestations, LTß staining was found to be much stronger in secondary manifestations when compared to primary manifestations. These differences could be observed in cases of DLBCL, TCRBL, cHL and pTCL. There were a lot more secondary manifestations with medium to strong LTß expression, while most primary manifestations had low LTß expression. Taken together, these results corroborate that human lymphomas and leukemias can express high levels of LTs and that more advanced malignancies usually show a stronger LT expression.

LT is expressed in uveal melanoma and correlates with overall survival

Metastatic uveal melanoma is known to spread to the liver in the vast majority of cases[413,414]. This preference makes uveal melanoma an interesting subject for our studies. Searching the *Genevestigator* data on *LTA* and *LTB* expression in 573 neoplasms shown in Figure 7 revealed that *LTA* and *LTB* expression of uveal melanoma is above average

compared to all other neoplasms (Figure 10A). Immunohistochemical stainings against LTß of biopsies from liver metastases or primary sites of human uveal melanoma confirmed the expression of LTß in primary sites as well as hepatic metastases. Primary tumors as well as liver metastases show sites with low and sites with high expression of LTß (Figure 10B). The strength of LT expression correlates strongly with overall survival for *LTA* and *LTB* (Figure 10C, D). In both cases strong LT expression of primary uveal melanomas correlates significantly with reduced overall survival of patients according to TCGA research. Together these data indicate that LT is expressed in human uveal melanomas metastasizing to the liver, and that its expression in the primary site reduces overall survival of patients.

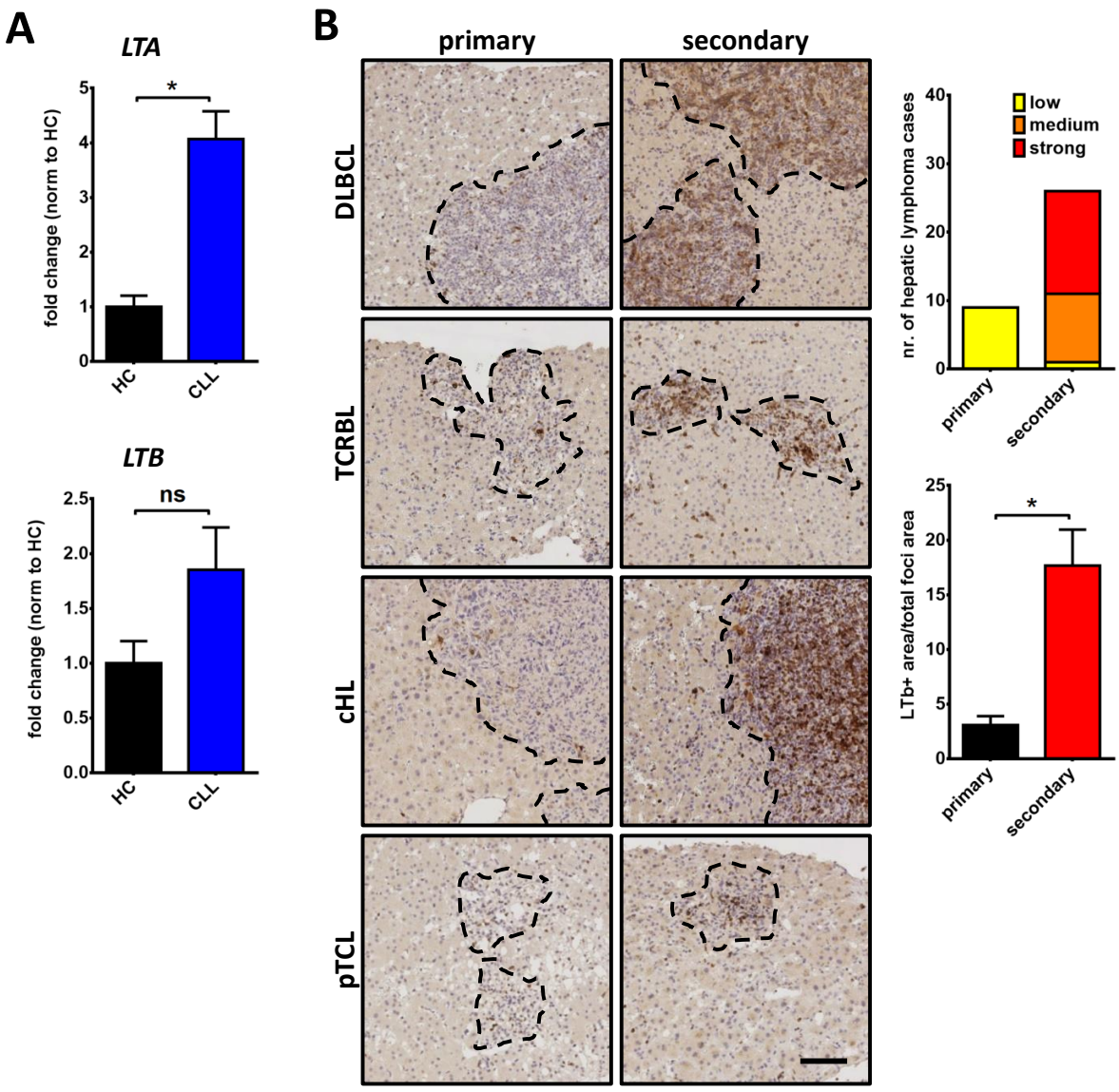

Figure 9: LT expression in human leukemias and lymphomas

A) Relative mRNA expression of *LTA* or *LTB* as assessed by RT-qPCR from human peripheral blood samples of CLL, AML or healthy control (HC) patients. mRNA expression was normalized to GAPDH housekeeping gene. Sample sizes are n=3 for HC and n=16 for CLL.

B) Representative pictures of immunohistochemical stainings against LTß of liver biopsies from patients with primary (left column) or secondary (right column) liver manifestations of DLBCL, TCRBL, cHL or pTCL. LTß expression was graded manually into low, medium and high expressing groups (upper graph) or calculated densitometrically using histological software (DIH) (lower graph). Sample sizes are n=9 for primary and n=29 for secondary manifestations. Scale bar is 100µm.
Data are expressed as number of cases with low, medium or high expression (upper right graph) or as mean + SEM. Statistical significance was calculated using Student's t-Test (* $p < 0.05$, ns=non-significant).

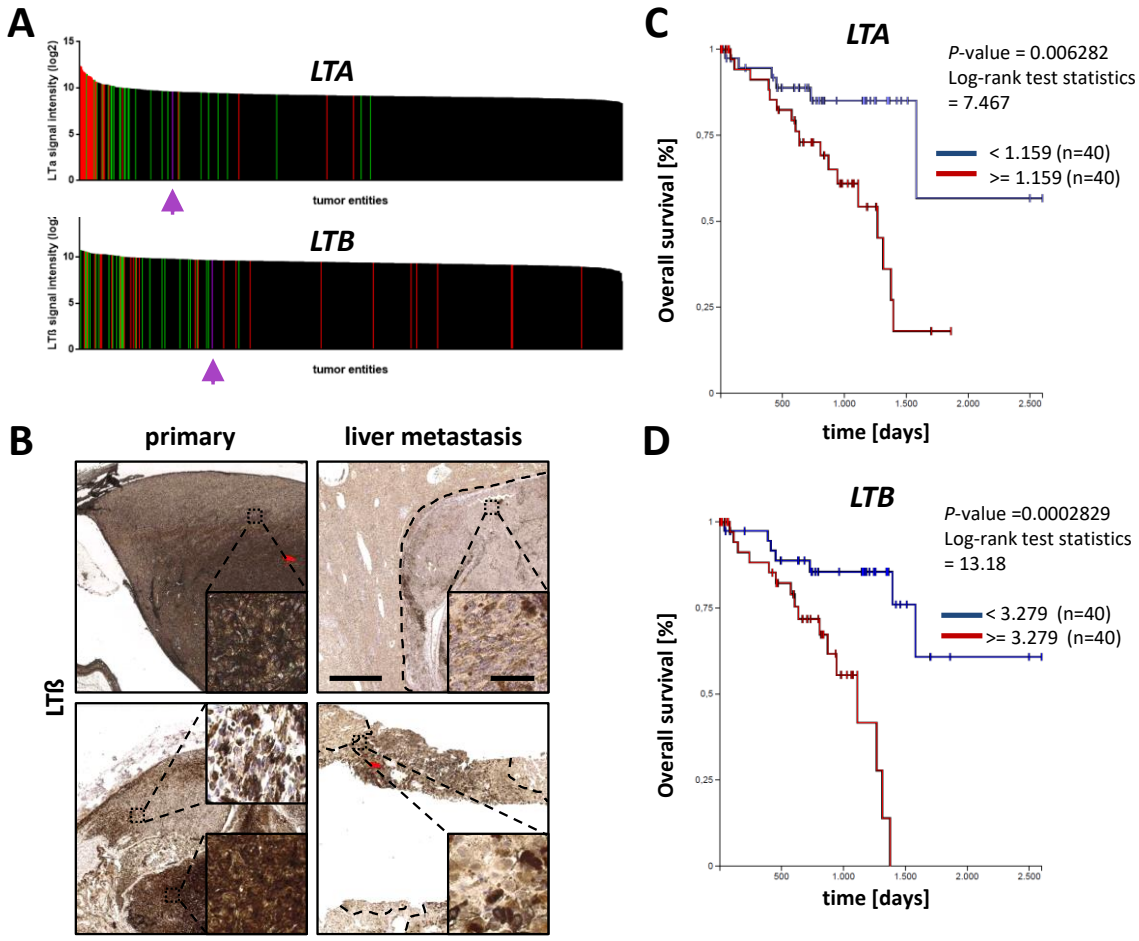

Figure 10: *LTA* and *LTB* expression correlates with overall survival in uveal melanomas
A) Relative expression of *LTA* and *LTB* as extracted from the Genevestigator platform for 573 different types of neoplasms. Mean expression levels are shown as log2 signal intensity. Lymphomas are shown in red, leukemias are shown in green and other tumor entities in black. Uveal melanoma is shown in purple and highlighted by a purple arrow.
B) Representative pictures of immunohistochemical stainings against LTß of eye biopsies from patients with primary uveal melanoma (left column) or liver biopsies from patients with liver metastases of uveal melanoma (right column). Insets show higher magnification of selected areas. Scale bars are 500µm and 50µm (inset).
C, D) Overall survival of uveal melanoma patients with high (red graph) or low (blue graph) expression of *LTA* **(C)** or *LTB* **(D)** as assessed by TCGA database research. Relative survival rate (Y axis) is plotted against time in days (X axis). Sample sizes for both groups and expression level thresholds for high or low expression are indicated in the graphs.

6.1.2 Functional interference of LT signaling in preclinical mouse models leads to a reduction of secondary lymphoma manifestations in the liver

L-CI.5s murine T-cell lymphoma cells show a high propensity to colonize the liver

To start with *in vivo* and *in vitro* research, a suitable preclinical model to study the role of lymphotoxins in secondary lymphoma manifestations in the liver was searched. One suitable model were the L-CI.5s murine T-cell lymphoma cells[415]. These highly metastatic lymphoma cells have a transgenic *lacZ* gene cassette, which allows for cell tracking using X-Gal staining solution[415]. To test the dynamics and general capability of these cells to metastasize to the liver, a timecourse experimental metastasis assay was performed. 5000 L-CI.5s lymphoma cells were injected into the tail vein of syngeneic DBA/2 mice and the mice were sacrificed 3 days, 5 days or 7 days thereafter (Figure 11A). Uninjected mice were used as a control. A staining against LTα was performed to analyse the formation of LT expressing metastatic foci (Figure 11B). Macroscopic tumor nodules expressing LTα could be found by 5 days after tumor cell injection. Furthermore, RelB translocation could be found in parenchymal (black arrows) as well as non-parenchymal (blue arrows) liver cells within the tumor nodules (Figure 11C). As expected, L-CI.5s cells within the metastatic nodules in the liver still expressed the T-cell marker CD3 (Figure 11D). To corroborate the results gained so far, RT-qPCR analyses of whole liver homogenates of these mice were done (Figure 11E). *LacZ* and *Lta* expression levels were increased significantly with the increase of tumor load after 5 and 7 days, respectively. A trend towards increased *Ltb* expression could also be seen, but statistical significance was not acquired. *Ltbr* expression levels did not change at all.

LTßR signaling interference reduces lymphoma manifestations in the liver

To investigate whether LT expression of L-CI.5s lymphoma cells has an effect on their ability to metastasize to the liver, several L-CI.5s knockdown cell lines were created. Either LTα (shLTα38, shLTα39) or LTß (shLTß88) or both (shLTαß63) were knocked down using shRNA. A non-targeting shRNA (shNT) was used as control. RT-qPCR analysis of these cell lines revealed a reduction in *Lta* expression levels of at least 50% in all four LT knockdown cell lines when compared to the non-targeting control (Figure 12A). *Ltb* expression was reduced in all four cell lines as well (Figure 12A). However, results were statistically significant only for shLTα39 and shLTαß63 when compared to shNT. ShLTα38 showed a 30% reduction and shLTß88 a 50% reduction, but both lacked statistical significance after 3 independent experiments. To supplement our results from the RT-qPCR we performed an ELISA assay against LTα (Figure 12B). The concentration of LTα in the supernatant of all four LT knockdown cell lines was 40-70% lower when compared to the shNT control. However, the results were not statistically significant for shLTß88. To make sure that the transgenic LT knockdown cells had no growth impairment, a *CellTiter-Blue™* cell viability assay was performed over a period of 7 days (Figure 12C). All four LT knockdown L-CI.5 cell lines

showed very similar growth kinetics when compared to the non-targeting control as well as the parental L-CI.5s, with a sharp increase in cell numbers between day 3 and day 5.

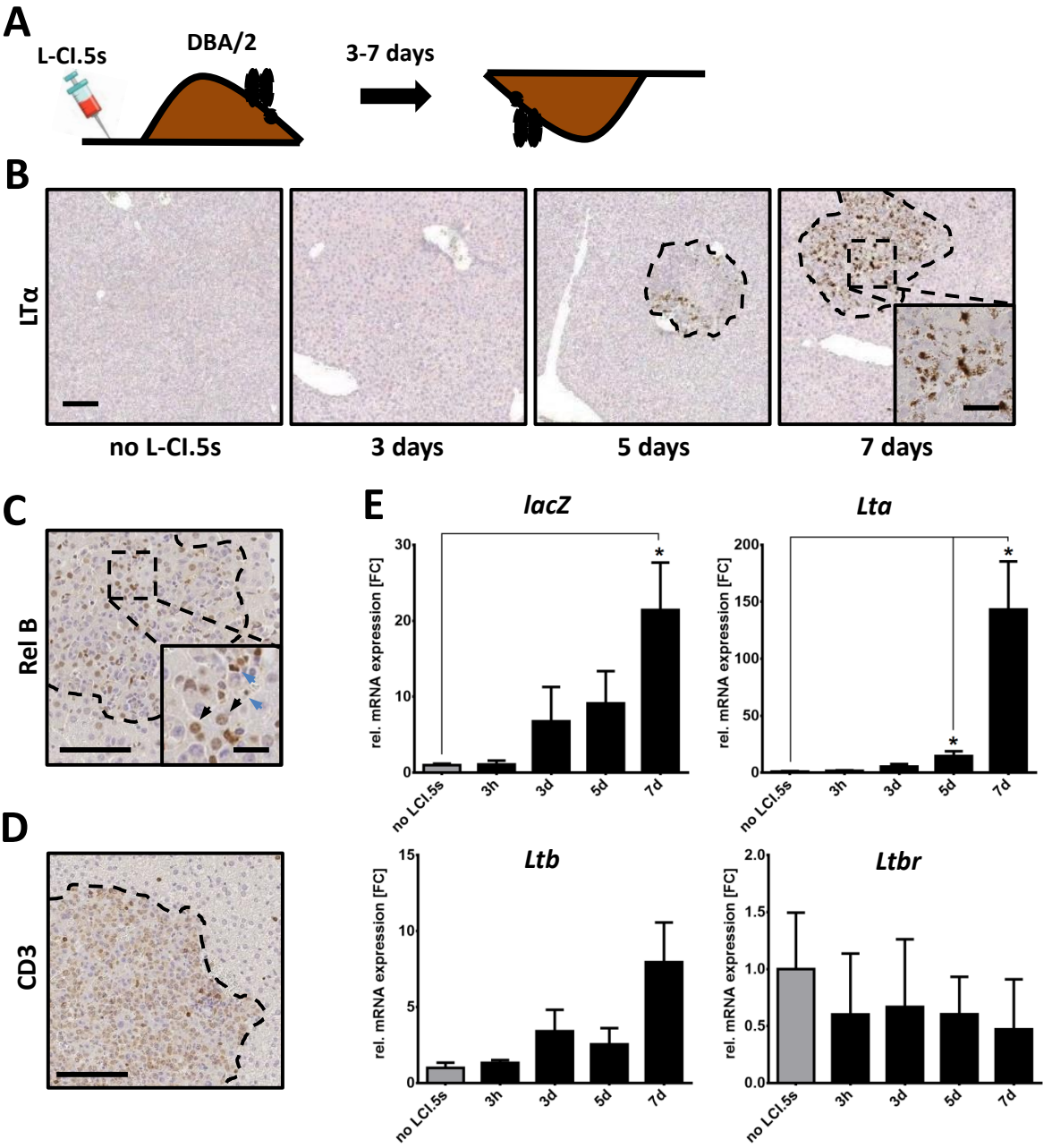

Figure 11: L-CI.5s lymphoma cells form liver manifestations in DBA/2 mice

A) Schematic of the experimental setup for the experimental metastasis assays. 5000 L-CI.5s were injected into the tail vein of DBA/2 mice. The mice were sacrificed 3, 5 or 7 days later.

B) Representative pictures of immunohistochemical stainings against LTα of paraffin-embedded liver samples from mice injected with 5000 L-CI.5s into the tail vein and sacrificed 3, 5 or 7 days later. Untreated mice were used as control. Inset shows higher magnification of selected area. Scale bars are 100µm and 20µm (inset).

C, D) Representative picture of immunohistochemical stainings against RelB **(C)** or CD3 **(D)** of paraffin-embedded liver samples from mice injected with 5000 L.CI.5s into the tail vein and sacrificed 7 days later. Inset shows higher magnification of selected area. Black arrows indicate RelB stained hepatocytes, blue arrows indicate RelB stained non-parenchymal cells. Scale bars are 100µm and 10µm (inset).

E) Relative mRNA expression of *lacZ*, *Lta, Ltb or Ltbr* as assessed by RT-qPCR of mice injected with no or 5000 L-CI.5s into the tail vein and sacrificed 3 hours, 3, 5 or 7 days later. mRNA expression was normalized to GAPDH housekeeping gene.
Data are expressed as mean fold change + SEM relative to the mean of the no L-CI.5s control. Sample sizes were n≥3 for all groups. Statistical significance was calculated for all timepoints against no L-CI.5s control using Student's t-Test (* $p < 0.05$).

Experimental metastasis assays were performed to investigate the capacity of LT knockdown L-CI.5s cells to metastasize to the liver. 5000 L-CI.5s of each strain were injected into the tail vein of untreated DBA/2 mice. The mice were sacrificed 7 days after and the amount of macrometastases in the liver was analyzed with H&E stainings (Figure 12E). L-CI.5s with reduced LT expression showed less liver macrometastases in general. The reduction was not statistically significant for shLTß88 and shLTαa38, but it was significant for shLTα39 and shLTαß63. Of note, shLTαß63 showed a much stronger reduction than the single knockdowns, with multiple animals showing no macrometastases in the liver at all. To test whether the effect was also visible at early timepoints the experimental setup was repeated, but mice were sacrificed after 24h already. Only shNT, shLTα38 and shLTαß63 cells were used for this experiment to reduce mouse numbers. The amount of micrometastases was analysed by staining whole liver lobes with X-gal staining solution and then counting the blue stained micrometastases (black arrowheads) using a dissecting microscope (Figure 12D). The results were similar to the 7 days experiment, with reduced micrometastases in shLTα38 and shLTαß63. Again, a strong and significant reduction was observed for shLTαß63 but not for shLTα38.

To corroborate the findings with a second model and evaluate if systemic depletion of LTs can reduce hepatic metastasis formation of L-CI.5s, the artificial decoy receptor LTßR-Ig was used to deplete LTs in experimental metastasis assays. Mice were treated 1 day before and 1 day after tumor cell injection with either LTßR-Ig or the control antibody MOPC21. 5000 L-CI.5s were injected into the tail vein of DBA/2 mice and the mice were sacrificed 7 days later (Figure 13A). The amounts of macrometastases in each liver were counted using histochemical H&E stainings. Mice treated with LTßR-Ig showed significantly fewer macrometastases in the liver than mice treated with MOPC21 (Figure 13A). A *CellTiter-Blue™* cell viability assay was performed over a period of 5 days (Figure 13B) to exclude reduced viability or growth impairment of LTßR-Ig treated cells as reason for reduced metastasis formation. Cells were treated with either MOPC21 or LTßR-Ig at the start of the experiment. There were no differences in growth kinetics of cells treated with MOPC21 or LTßR-Ig. Both showed slightly faster growth during the log-phase when compared to untreated cells.

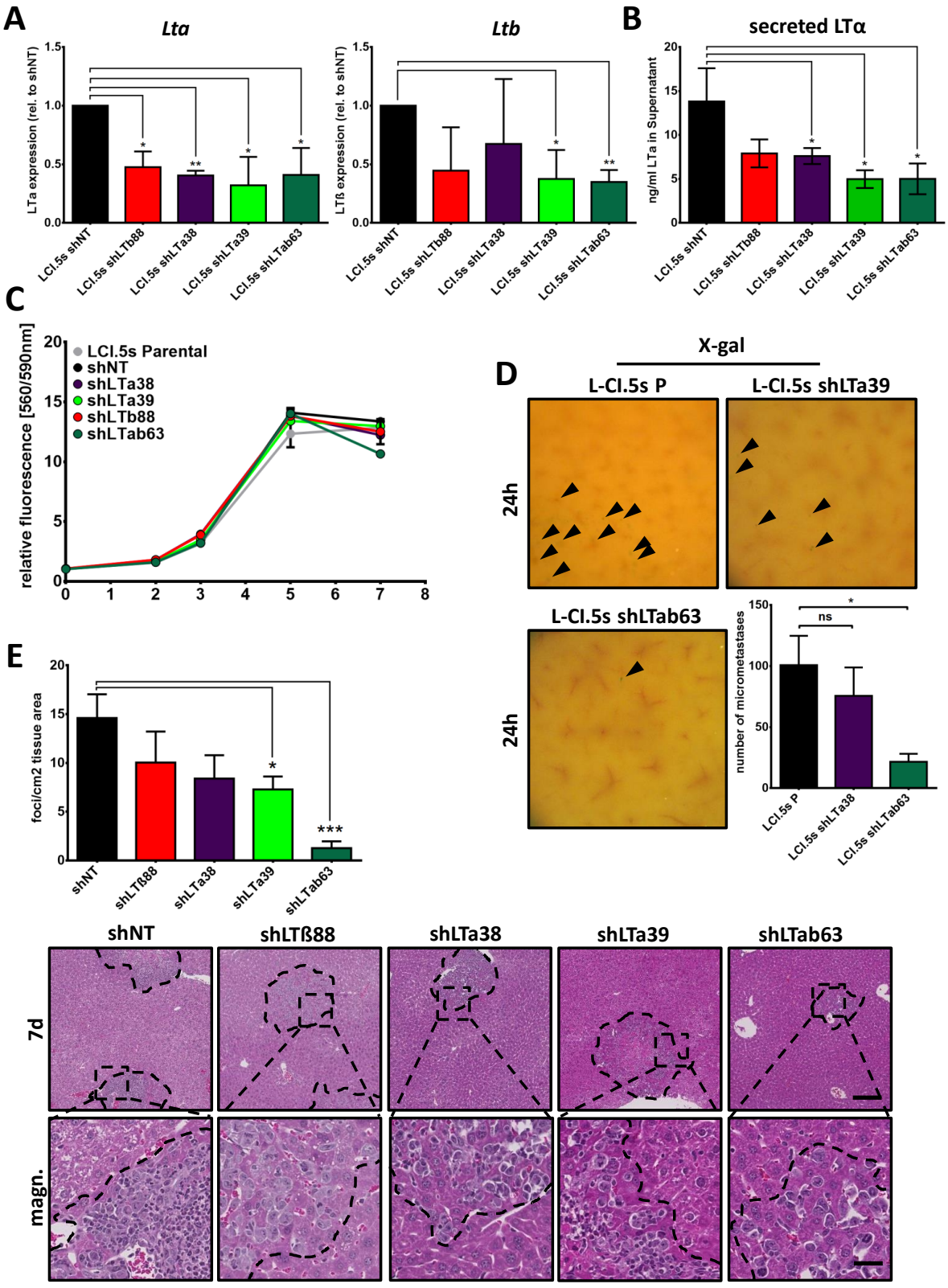

Figure 12: Knockdown of LT expression in L-Cl.5s lymphoma cells reduces liver metastasis

A) Relative mRNA expression of *Lta* or *Ltb* as assessed by RT-qPCR of cell lysates from L.Cl.5s shNT, shLTß88, shLTα39, shLTα38 or shLTαß63 cells. mRNA expression was normalized to GAPDH housekeeping gene. Sample sizes are n≥3 for all groups.

B) LTa protein secretion as assessed by ELISA of cell culture supernatant from L.CI.5s shNT, shLTß88, shLTα39, shLTα38 or shLTαß63 cells. Sample sizes were n≥3 for all groups.
C) Cell viability as assessed by CellTiter Blue assay of cell cultures from L.CI.5s shNT, shLTß88, shLTα39, shLTα38 or shLTαß63 cells over 7 days. Viability is expressed by mean fluorescence [560/590nm] and was measured at 0, 2, 3, 5 and 7 days. n≥3 replicates were done for all groups.
D) Representative macroscopical pictures of X-gal stained livers from DBA/2 mice injected with either L-CI.5s P, shLTα39 or shLTαß63 i.v. and sacrificed 24h later. Micrometastases were always calculated from the same lobes and are indicated by arrows. n=5 mice were used for all groups.
E) Representative histochemical pictures of H&E stainings of paraffin-embedded liver samples from DBA/2 mice injected with L-CI.5s shNT, shLTß88, shLTα39, shLTα38 or shLTαß63 i.v. and sacrificed 7 days later. Lower row shows higher magnifications of selected areas. Metastatic foci were annotated and counted manually and normalized to the tissue area analyzed. n=6 mice were used for all groups. Scale bars are 200µm and 40µm (magnification).
Data are expressed as mean + SD (A, B) or SEM (D, E). Statistical significance was calculated using Student's t-Test (* $p < 0.05$, ** $p < 0.01$, *** $p < 0.001$, ns=non-significant).

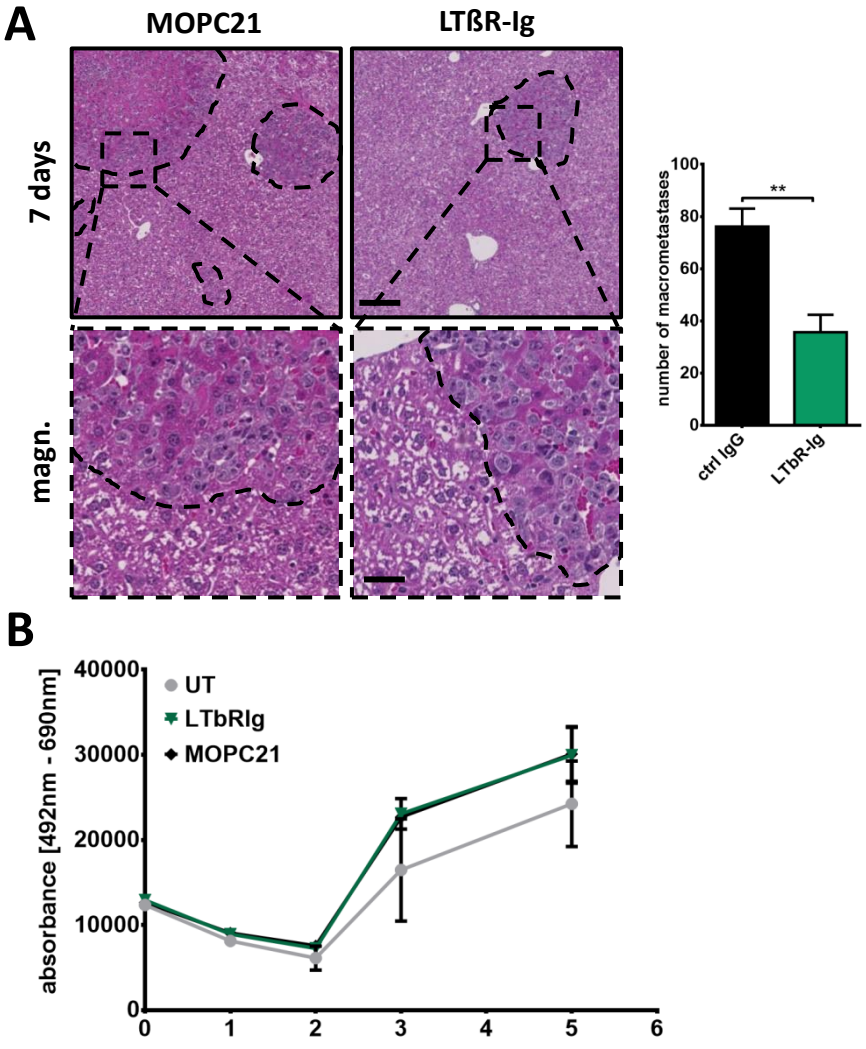

Figure 13: Antagonizing LTßR with LTßR-Ig reduces liver metastases of L-CI.5s cells
A) Representative histochemical pictures of H&E stainings of paraffin-embedded liver samples from DBA/2 mice pretreated for 1 day with LTßR-Ig or MOPC21, injected with L-CI.5s and sacrificed 7 days later. Lower row shows higher magnifications of selected areas. Metastatic foci were annotated and counted manually and

normalized to the tissue area analyzed. n=6 mice were used for both groups. Scale bars are 200µm and 40µm (inset).
B) Cell viability as assessed by CellTiter Blue assay of cell cultures from L.CI.5s untreated (UT) or treated with LTßR-Ig or MOPC21 for 5 days. Viability is expressed by mean absorbance [492-690nm] and was measured at 0, 1, 2, 3 and 5 days. n≥3 replicates were done for all groups.
Data are expressed as mean + SEM. Statistical significance was calculated using Student's t-Test (** $p < 0.01$).

6.1.3 Overactivation of LT signaling in preclinical mouse models leads to an increase of secondary lymphoma manifestations in the liver

To further investigate the role of tumor cell-derived LT and LTßR signaling in mediating liver metastasis of L-CI.5s, it was investigated whether increased LT expression and LTßR signaling can exacerbate metastasis formation in the liver. Stably LTß overexpressing L-CI.5s were created via plasmid transfection. LCI.5s LTß overexpressed LTß 7.7-fold compared to L-CI.5s parental cells, while LTα expression remained unchanged (Figure 14E). A 7-day experimental metastasis assay was performed using DBA/2 mice. Mice were injected with either 5000 L-CI.5s LTß or L-CI.5s EGFP (control) and sacrificed 7 days after (Figure 14A). Mice injected with L-CI.5s LTß showed a 5-fold higher number of macrometastases in the liver compared to L-CI.5s EGFP. To corroborate the data with a second model, the experiment was repeated with a murine B-cell lymphoma cell line derived from Eµ-myc mice[416] (Figure 14C). Eµ-myc cells are much less metastatic towards the liver and also express much less LTs compared to L-CI.5s. Nontheless, increasing LTß expression in these cells (Eµ-myc LTß) also led to a significantly increased number of metastatic foci in the liver after 14 days. A roughly 40% increase in the fraction of ki67+ cells within metastatic foci of mice injected with L-CI.5s LTß compared to L-CI.5s EGFP indicates, that L-CI.5s LTß have a small growth advantage compared to control cells *in vivo* (Figure 14B). However, the difference is much smaller than the difference in number of metastases. On the other hand, no increase in ki67+ cell fraction was observed in Eµ-myc LTß cells when compared to their control cells (Figure 14D).

To investigate whether tumor cell-derived LT is required for increased hepatic metastasis formation or if exogenous sources for LTßR activation can supplement it, DBA/2 mice were pretreated with either the LTßR agonizing antibody ACH6 or the control antibody IgG for 14 days and then subjected to an experimental metastasis assay with parental L-CI.5s for 7 days (Figure 15A). Mice pretreated with ACH6 showed a roughly 2-fold higher amount of liver metastases after 7 days compared to mice pretreated with IgG. Neither ACH6 nor IgG treatment had any measurable effect on the viability and growth of L-CI.5s *in vitro* up to 5 days after treatment initiation as assessed by XTT assays (Figure 15D). The fraction of ki67+ cells within the macrometastatic foci in the livers of ACH6 pretreated mice was not different compared to IgG pretreated mice (Figure 15B), indicating that the ACH6 treatment had no effect on tumor cell outgrowth. A 24h experimental metastasis assay was performed to investigate whether the pretreatment with ACH6 also affects early steps during liver colonization, like tumor cell seeding. Mice were pretreated with either ACH6 or IgG for 14

days, then injected with parental L-CI.5s and then sacrificed 24h afterwards (Figure 15C). Counting the amount of X-gal stained micrometastases on the liver lobes of each animal, the amount of micrometastases was found to be increased nearly 2-fold in the ACH6 pretreated mice compared to the IgG pretreated mice, similar to the 7 days experiment.

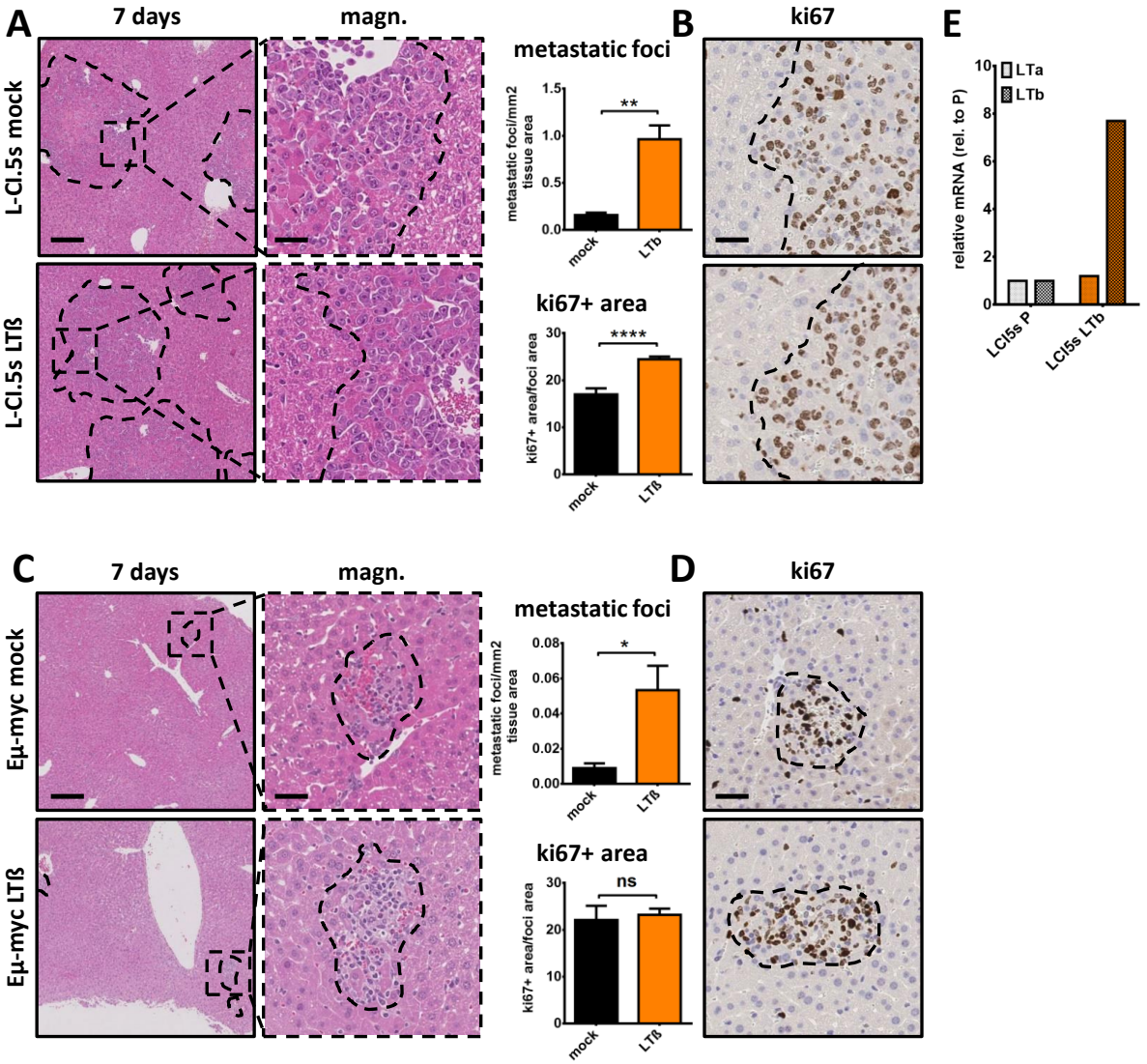

Figure 14: Overexpression of LTß in L-CI.5 and Eμ-myc lymphoma cells increases liver metastasis

A-D) Representative (immuno-)histochemical pictures of H&E **(A, C)** or ki67 **(B, D)** stainings of paraffin-embedded liver samples from DBA/2 mice injected with L-CI.5s **(A, B)** or Eμ-myc **(C, D)** EGFP (mock) or LTß cells and sacrificed 7 days (L-CI.5s) or 14 days (Eμ-myc) later. Right column (for H&E) shows higher magnifications of selected areas. Metastatic foci were counted manually and normalized to the tissue area analyzed. Ki67+ area was assessed using histological software (DIH) and normalized to the metastatic area analyzed. Sample size is n≥6 for all groups. Scale bars are 200μm and 40μm (magnification, ki67).

E) Relative mRNA expression of *Lta* or *Ltb* as assessed by RT-qPCR of cell lysates from L.CI.5s P or LTß cells. mRNA expression was normalized to GAPDH housekeeping gene. Sample size is n=1 for all groups.

Data are expressed as mean + SEM and statistical significance was calculated using Student's t-Test (* $p < 0.05$, ** $p < 0.01$, **** $p < 0.0001$, ns=non-significant).

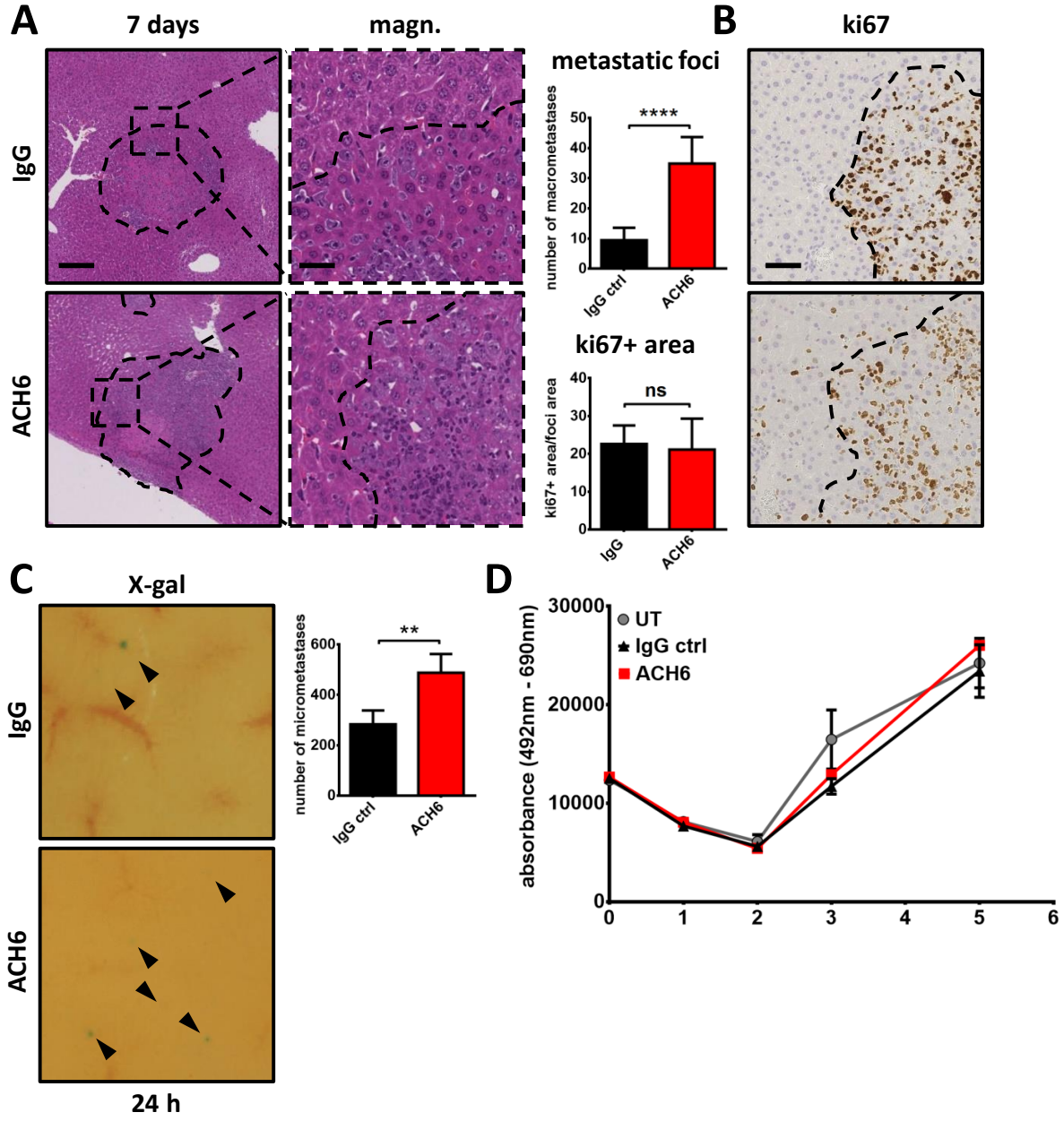

Figure 15: Pretreating mice with an LTßR agonizing antibody increases liver metastasis of L-CI.5 cells

A, B) Representative (immuno-)histochemical pictures of H&E **(A)** and ki67 **(B)** stainings of paraffin-embedded liver samples from DBA/2 mice pretreated for 14 days with ACH6 or IgG, injected with L-CI.5s and sacrificed 7 days later. Right column (for H&E) shows higher magnifications of selected areas. Metastatic foci were counted manually and normalized to the tissue area analyzed. Ki67+ area was assessed using histological software (DIH) and normalized to the metastatic area analyzed. Sample size is n≥6 for all groups. Scale bars are 200µm (HE), 40µm (inset) and 80µm (ki67).

C) Representative macroscopical pictures of X-gal stained livers from DBA/2 mice pretreated for 14 days with ACH6 or IgG, injected with L-CI.5s and sacrificed 24h later. Micrometastases were always calculated from the same lobes and are indicated by arrows. n=4 mice were used for all groups.

D) Cell viability as assessed by CellTiter Blue assay of cell cultures from L.CI.5s untreated (UT) or treated with ACH6 or IgG for 5 days. Viability is expressed by mean absorbance [492-690nm] and was measured at 0, 1, 2, 3 and 5 days. n≥3 replicates were done for all groups.

Data are expressed as mean + SEM. Statistical significance was calculated using Student's t-Test (** $p < 0.01$, **** $p < 0.0001$, ns=non-significant).

6.1.4 The source of LTs has no impact on the number of hepatic lymphoma manifestations

Lack of tumor cell-derived LT can be compensated by other sources of LTßR agonization

Delving further into the question whether the source of LTs affects the phenotype of increased liver metastases, two experiments with different methods to supplement LT signaling of L-CI.5s shLTαß were performed (Figure 16). In both cases 7 day experimental metastasis assays with DBA/2 mice were used. In the first experiment, the metastatic potential of L-CI.5s parental and L-CI.5s shLTαß cells pretreated with IgG or ACH6 for 14 days was compared (Figure 16A). ACH6 pretreatment for 14 days increased the number of metastatic foci in the liver for both cell lines, as expected. More importantly, ACH6 pretreatment allowed the L-CI.5s shLTαß cells to form a similar amount of liver metastases as the L-CI.5s parental cells with IgG treatment. This suggests that exogenous LT supplementation can alleviate the effects of reduced LT expression in L-CI.5s. As before, L-CI.5s shLTαß cells formed significantly fewer metastases as L-CI.5s parental cells. In the second experiment, a different model of LT supplementation of L-CI.5s shLTαß cells in experimental metastasis was used. GFP-expressing L-CI.5s parental (L-CI.5s GFP) cells were co-injected together with L-CI.5s shLTαß in equal amounts (Figure 16B). Solo injections of L-CI.5s GFP or L-CI.5s shLTαß were used as controls. To analyze the number of metastases formed by either the parental GFP expressing or the shLTαß cells, the amount of ki67+/GFP+ double-positive metastases, indicative of L-CI.5s GFP, was compared to the amount of ki67+/GFP- metastases, indicative of L-CI.5s shLTαß cells. Interestingly, the number of GFP+ and GFP- metastases was similar, indicating that the shLTαß cells benefited from the LT expressed by the parental cells to a similar degree as the parental cells themselves. This shows that the LT expressed from the tumor cells acts in trans, and high LT-expressing cells can support low LT-expressing cells during liver metastasis formation. The control mice that were solely injected with either L-CI.5s GFP or shLTαß showed a large difference in the number of hepatic metastasis, as already seen before.

Endogenous LT expression in mouse tissues can also compensate for lack of tumor cell-derived LT

Albumin-LTαß mice (Alb-LTαß) overexpress LTα and LTß constitutively in hepatocytes via the albumin promoter, and they have an increased propensity to develop primary HCC due to the increased LT expression[60]. RT-qPCR analysis of whole liver lysates of Alb-LTαß mice revealed that these mice express LTα 20-fold and LTß 7-fold compared to wild-type mice (Figure 17C). Expression of LTßR is not altered.

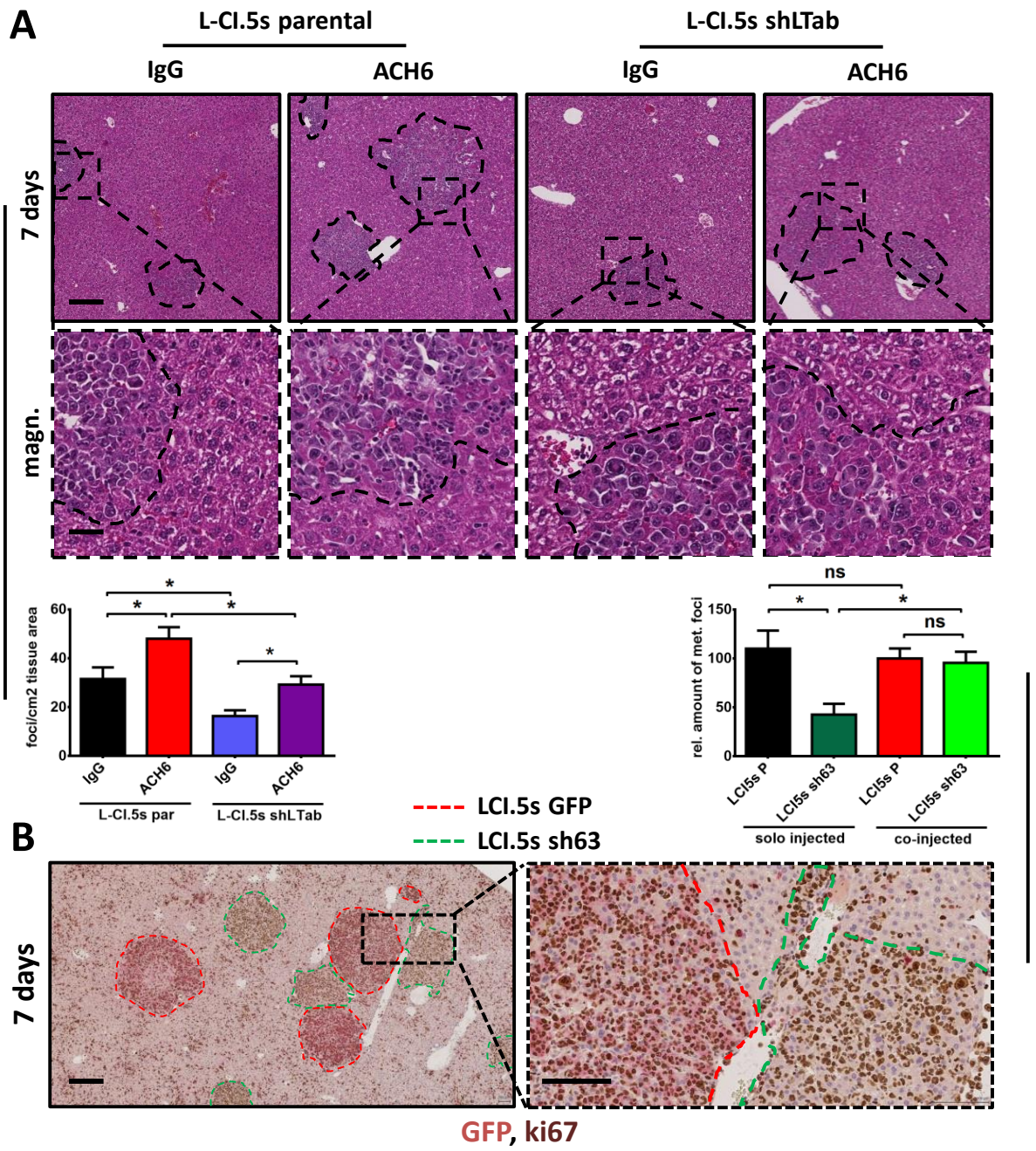

Figure 16: LT supplementation recovers phenotype in L-CI.5s shLTαß cells

A) Representative histochemical pictures of H&E stainings of paraffin-embedded liver samples from DBA/2 mice pretreated for 14 days with ACH6 or IgG, injected with L-CI.5s P or shLTαß and sacrificed 7 days later. Lower row shows higher magnifications of selected areas. Metastatic foci were counted manually and normalized to the tissue area analyzed. Sample size is n=4 for all groups. Scale bars are 200µm and 40µm (magnification).

B) Representative immunohistochemical pictures of GFP (red) + ki67 (brown) co-stainings of paraffin-embedded liver samples from DBA/2 mice injected with GFP-expressing L-CI.5s P or shLTαß or co-injected with both and sacrificed 7 days later. RIght picture shows higher magnifications of selected area. Ki67 single positive and ki67 + GFP double-positive metastatic foci were counted manually and normalized to the tissue area analyzed. Sample size is n=5 for all groups. Scale bars are 200µm and 160µm (inset).

Data are expressed as mean + SEM. Statistical significance was calculated using Student's t-Test (* $p < 0.05$, ns=non-significant).

To test whether the Alb-LTαß mice also show an increased propensity for hepatic metastasis formation, a short-term experimental metastasis assay was performed (Figure 17A). Alb-LTαß or wild-type control mice were injected with parental L-CI.5s and sacrificed 24h later. The Alb-LTαß mice showed a lot higher number of blue X-gal stained micrometastases on whole liver lobes compared to wild-type control mice. Plotting LTα expression of these mice against the amount of micrometastases, a significant linear correlation between LTα expression and the number of micrometastases could be observed, as indicated by a linear regression analysis (Figure 17B). Taken together, these results indicate that endogenous LT expression has similar effects on the metastasis formation of L-CI.5s as tumor cell-derived LT.

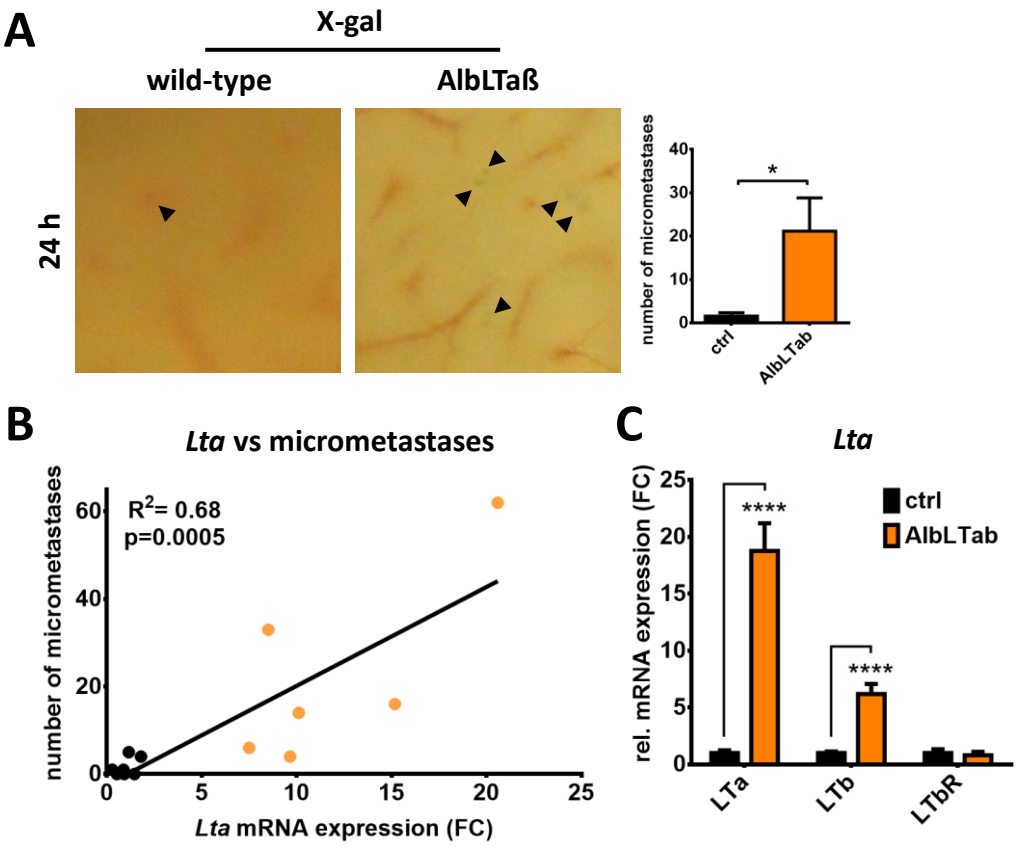

Figure 17: Hepatocyte-derived LT drives hepatic metastasis formation of L-CI.5 cells

A) Representative macroscopical pictures of X-gal stained livers from Alb-LTaß or wild-type mice injected with L-CI.5s and sacrificed 24h later. Micrometastases were always calculated from the same lobes and are indicated by arrows. n=7 mice were used for all groups.

B) Linear correlation between number of micrometastases (y axis, shown in A) and relative mRNA expression of *Lta* as assessed by RT-qPCR of whole liver homogenates of the same Alb-LTaß mice (x axis, shown in C). Ctrl animals are shown with black dots, Alb-LTaß animals are shown with orange dots. Correlation was analyzed by linear regression analysis showing r2 and p values.

C) Relative mRNA expression of *Lta* or *Ltb* as assessed by RT-qPCR of cell lysates from L.CI.5s P or LTß cells. mRNA expression was normalized to GAPDH housekeeping gene. Sample size is n=1 for all groups.

Data are expressed as mean + SEM and statistical significance was calculated using Student's t-Test (* $p < 0.05$, ** $p < 0.01$, **** $p < 0.0001$, ns=non-significant).

6.1.5 Increased LT signaling also increases liver metastasis in B-cell leukemia, colorectal cancer and spontaneous insulinoma models

GFAP-LTαß mice overexpress LTα and LTß constitutively via the GFAP promoter, which is expressed in various cells including hepatic stellate cells, pericytes and astrocytes. These mice show a higher number of hepatic metastases when injected with Eμ-Tcl1 cells after 14 days compared to wild-type control mice (Figure 18A). Eμ-Tcl1 cells are murine B-cell leukemia cells transgenic for *Tcl1* driven by the IgH enhancer Eμ[417]. The result corroborates our finding that endogenous LT expression can drive hepatic metastasis formation of tumor cells. Furthermore, it indicates that LTßR signalling is involved in formation of hepatic manifestations of B-cell leukemia.

To investigate if LTßR signalling affects hepatic metastasis formation of further tumor entities, a 16 day experimental metastasis assay using GFP-tagged MC-38 colon carcinoma cells was performed (Figure 18B). C57BL/6 mice were pretreated with either IgG or ACH6 for 14 days before injecting them intrasplenically with 400,000 MC-38 GFP murine colorectal carcinoma cells. Intrasplenic injection was used, as intravenous injection of MC-38 GFP cells mostly yields lung metastases with very few liver metastases (data not shown). ACH6 pretreatment increased the amount of liver metastases significantly as assessed by immunohistochemical stainings of GFP (Figure 18B). This was corroborated by RT-qPCR analysis of *Gfp* of whole liver homogenates from the same mice, showing a massive increase in *Gfp* mRNA in ACH6 compared to IgG pretreated livers (Figure 18B, lower bar graph). These results indicate that colon carcinoma cell metastasis to the liver is also affected by LTßR signalling.

RIP-tag2 mice express the SV40 large T antigen (Tag) under the rat insulin promoter-1[418]. This leads to the development of tumors originating from beta-cells in a very time-predictable manner. The RIP-tag2 mice form solid insulinomas from week 10 onwards and can start to metastasize a short while later. To recreate the conditions used for the experimental metastasis assays, the mice were pretreated with either IgG or ACH6 for 2 weeks beginning at 10 weeks of age (Figure 19A), shortly before they can start to metastasize. The mice were sacrificed two weeks later at 12 weeks of age and the metastatic burden in the liver was determined. ACH6 pretreatment significantly increased the number of metastatic foci in the liver by nearly 10-fold (Figure 19B). On the other hand, a slightly but significantly lower number of metastatic foci in the liver was observed when the mice were pretreated with LTßR-Ig for 2 weeks when compared to MOPC21 pretreated mice (Figure 19C). These data suggest that the spontaneous and endogenous insulinomas formed in RIP-tag2 mice have a higher propensity to metastasize to the liver after LTßR agonization.

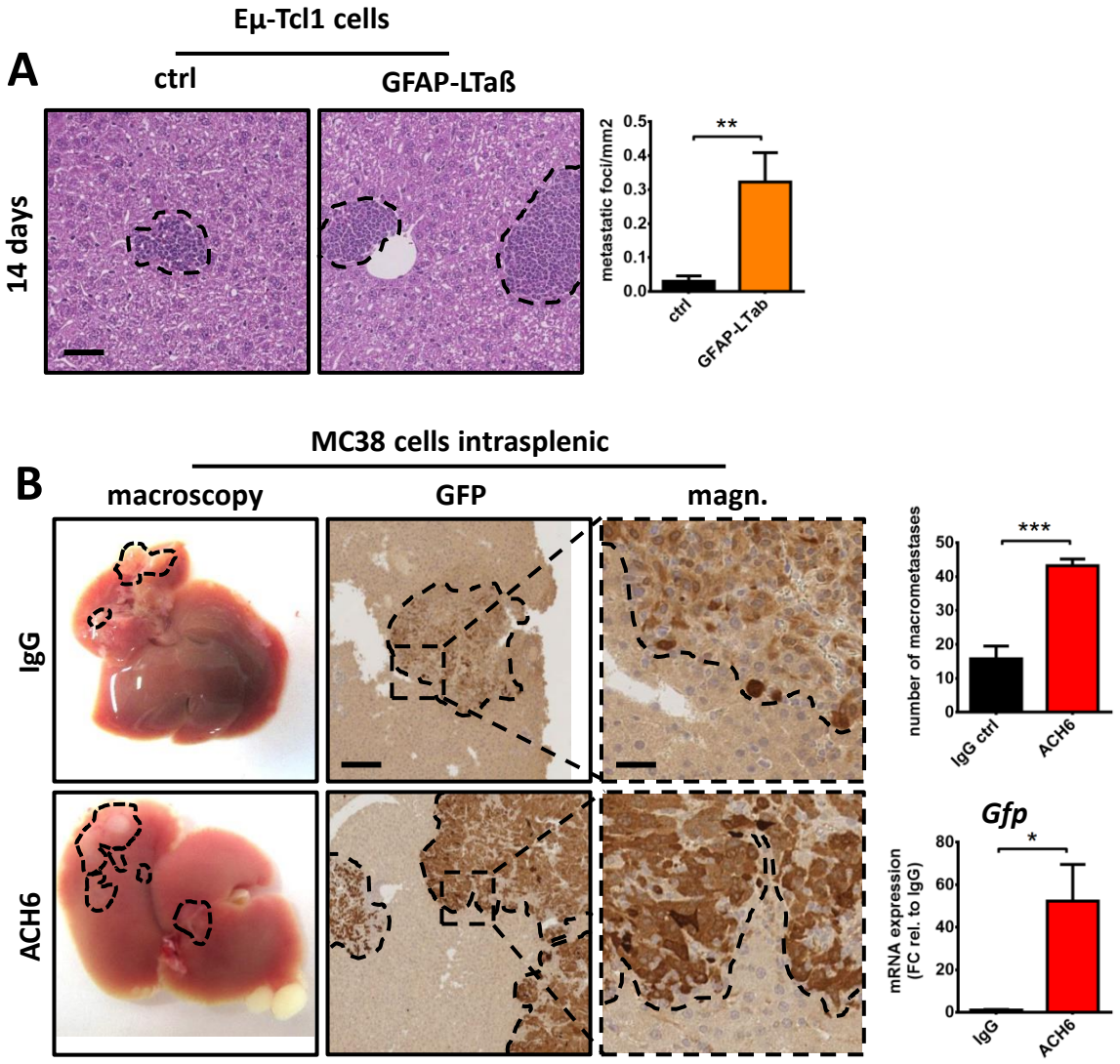

Figure 18: LT signaling also affects liver metastasis formation of Eμ-Tcl1 and MC38-GFP cells

A) Representative histochemical pictures of H&E stainings of paraffin-embedded liver samples from GFAP-LTαß or wild-type mice injected with Eμ-Tcl1 lymphoma cells and sacrificed 14 days later. Metastatic foci were counted manually and normalized to the tissue area analyzed. Sample size is n=5 for all groups. Scale bars are 80μm.

B) Representative macroscopical liver pictures or immunohistochemical pictures of GFP stainings of paraffin-embedded liver samples from C57BL/6 mice pretreated with ACH6 or IgG for 14 days injected with MC38-GFP cells and sacrificed 16 days later. GFP+ metastatic foci were counted manually. *Gfp* mRNA expression was also assessed by RT-qPCR of whole liver homogenates of the same mice and was normalized to GAPDH housekeeping gene. n=5 mice were used for all groups. Scale bars are 200μm and 40μm (inset). *Intrasplenic injection was performed by Dr. Lubor Borsig (UZH Zürich, Switzerland).*

Data are expressed as mean + SEM and statistical significance was calculated using Student's t-Test (* $p < 0.05$, ** $p < 0.01$, *** $p < 0.001$).

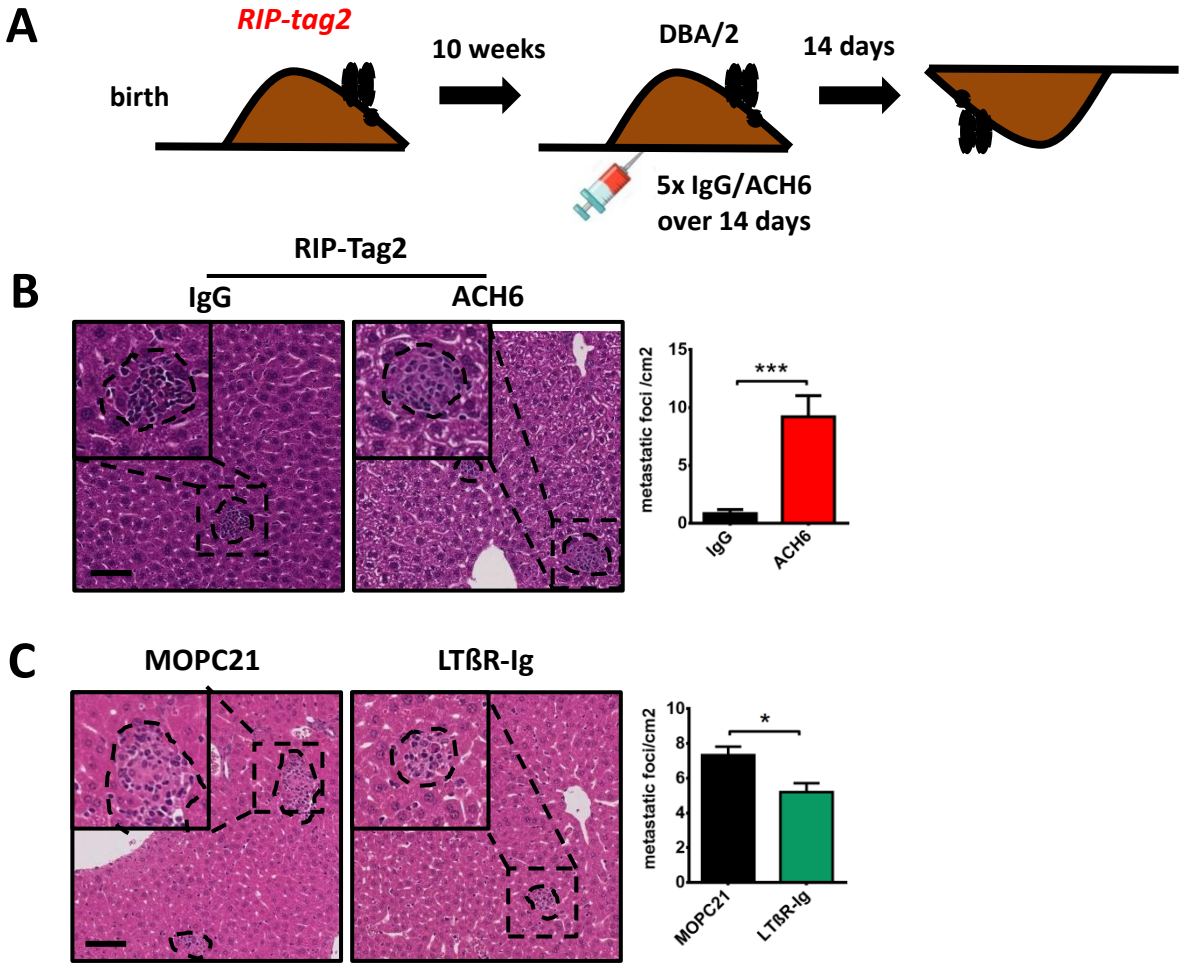

Figure 19: LTßR agonization increases spontaneous hepatic metastasis formation in Rip-Tag2 mice

A) Schematic of the experimental setup for the Rip-Tag2 spontaneous metastasis experiments. Rip-Tag2 mice were pretreated with IgG or ACH6 from 10 until 12 weeks of age by i.p. injection. Mice were injected with 50µg antibody every 3-4 days (5 total injections). The mice were sacrificed thereafter (12 weeks old).

B, C) Representative histochemical pictures of H&E stainings of paraffin-embedded liver samples from Rip-Tag2 mice treated with IgG or ACH6 **(B)**, or MOPC21 or LTßR-Ig **(C)** from 10 until 12 weeks of age and sacrificed thereafter. Insets show higher magnifications of selected areas. Metastatic foci were counted manually and normalized to the tissue area analyzed. Sample size is n≥6 for all groups. Scale bars are 80µm. *Animals were bred, treated and sacrificed at the lab of Kristian Pietras (Lund University, Sweden).*

Data are expressed as mean + SEM and statistical significance was calculated using Student's t-Test (* $p < 0.05$, *** $p < 0.001$).

Taken together, all above results show clearly that LT signalling affects liver metastasis formation of L-CI.5 lymphoma cells. It is clear, that the amount of LT expression is directly correlated to the amount of metastasis in the liver and that the source of LT is irrelevant for the outcome. Furthermore, the effect is not restricted to L-CI.5 lymphoma cells but can be observed in B-cell lymphomas, colon carcinomas and insulinomas as well.

6.2 Hepatic Stellate Cells integrate LT signals from the blood to orchestrate physiological changes in the liver sinusoids which facilitate secondary lymphoma manifestations

6.2.1 Functional interference of LTßR signaling in different liver cell types reveals that only HSC-specific LTßR signaling is needed to increase lymphoma manifestations in the liver

To determine the mechanism by which LT increases liver metastasis formation, the cell type integrating LT in the liver in this model first had to be identified. The liver consists of 4 major cell types: hepatocytes, liver sinusoidal endothelial cells (LSECs), hepatic stellate cells (HSCs) and Kupffer cells (KCs) (Figure 20A). For each cell type a treatment or mouse model to delete LTßR signaling in a cell-type specific manner was used (Figure 20B).

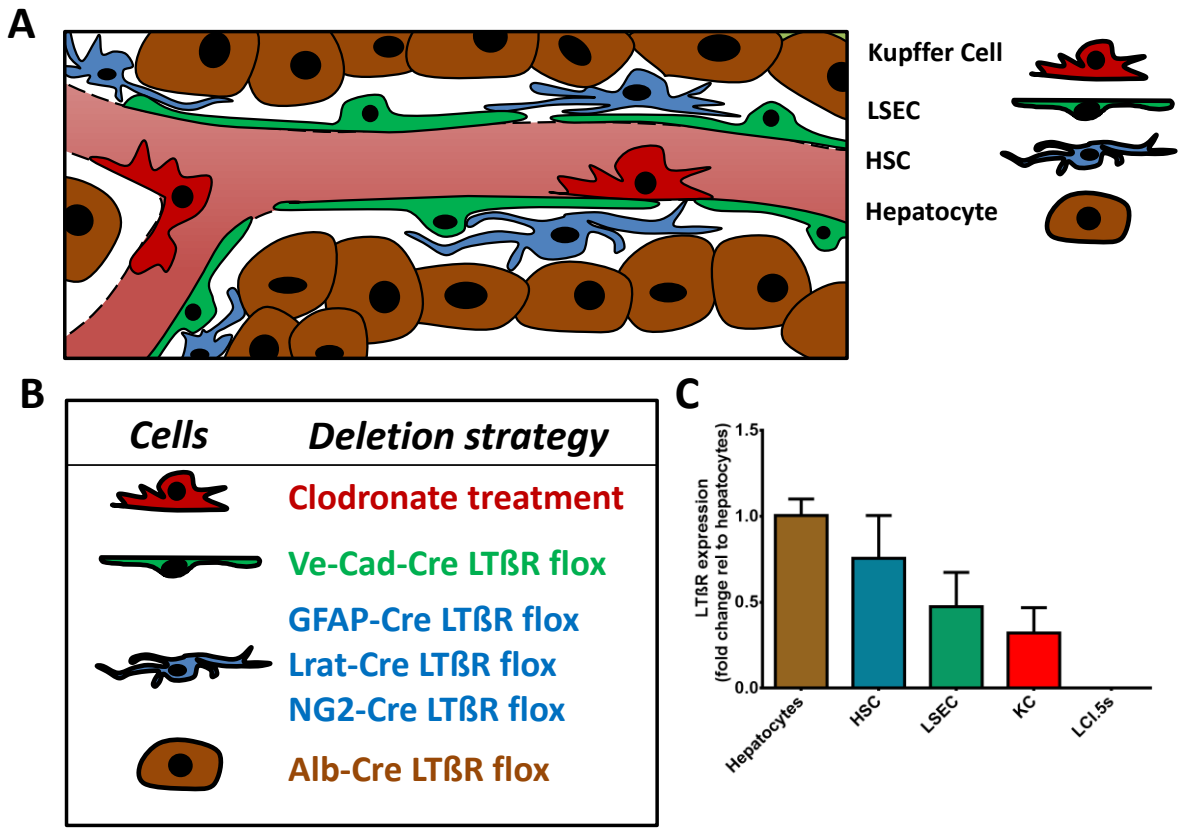

Figure 20: Strategy to identify the LT responsive cell type in the liver

A) Schematic depicting a hepatic sinusoid and the 4 major cell types of the liver. LSEC - liver sinusoidal endothelial cells, HSC - hepatic stellate cells.

B) List of strategies used to delete LTßR cell-type specific in all 4 major cell types of the liver. Ve-Cad - Ve-Cadherin, Alb – Albumin.

C) Relative mRNA expression of *Ltbr* as assessed by RT-qPCR of primary cell lysates from hepatocytes, HSCs, LSECs, Kupffer cells (KCs) and L-CI.5s. mRNA expression was normalized to GAPDH housekeeping gene. Sample size is n=3 for all groups. Data are expressed as mean + SEM.

Clodronate depletion was used to remove Kupffer cells entirely, and thus Kupffer cell-specific LTßR signaling as well. For LSECs, Ve-Cadherin-Cre (Ve-Cad-Cre) mice were intercrossed with LTßR loxP/loxP (floxed) mice to gain mice with endothelial cell-specific LTßR deletion. Albumin-Cre (Alb-Cre) mice were intercrossed with LTßR floxed mice to gain mice with hepatocyte-specific LTßR deletion. For hepatic stellate cells three different mouse models were used. LTßR floxed mice were intercrossed with either NG2-Cre, GFAP-Cre or Lrat-Cre mice. All three Cre models are specific for HSCs in the liver. LTßR was found to be expressed in all 4 major cell types of the liver as determined by RT-qPCR analysis of isolated primary hepatocytes, LSECs, HSCs and KCs, respectively (Figure 20C). LTßR is not expressed on L-CI.5 lymphoma cells, arguing against the possibility of autocrine signaling as a mechanism for increased liver metastasis formation of L-CI.5s.

Kupffer cells and Kupffer cell-specific LTßR signaling do not affect hepatic metastasis formation

To deduce whether Kupffer cell-specific LTßR signaling is needed for the LT-induced increase in liver metastasis, clodronate liposomes were used to remove Kupffer cells from the mice. C57BL/6 mice were chosen for this experiment and treated with ACH6 and clodronate or PBS control liposomes for 7 days (Figure 21A). ACH6 and liposomes were both administered intraperitoneously on an alternating 2-day schedule. Both were injected a total of 3 times. The clodronate treatment very efficiently removed Kupffer cells from the liver, as demonstrated by an F4/80 staining (Figure 21B). F4/80 staining in the liver was reduced to about 6% of the control mice in the clodronate treated mice. On the 8^{th} day of the experiment an Evans Blue assay was performed with the mice. Mice were injected intravenously with 100µl of 20 mg/ml Evans Blue and sacrificed 1 hour later. After perfusion with PBS, the livers were analysed for Evans Blue dye retention. No significant difference in the retained Evans Blue dye in the livers of clodronate-treated mice compared to the control mice was found. As LTßR agonization increases liver metastasis and Evans Blue dye retention compared to control mice (data not shown), this suggests that Kupffer cells do not play a role in the LT-induced increase in hepatic metastasis of L-CI.5s, although final proof has to be made with an experimental metastasis assay.

Hepatocyte specific LTßR signaling does not affect hepatic metastasis formation of L-CI.5s

To deduce whether hepatocyte-specific LTßR signaling is needed for the LT-induced increase in liver metastasis, Alb-Cre LTßR floxed mice were used. These mice express the Cre recombinase under the hepatocyte-specific albumin promoter, thus knocking out the loxP flanked LTßR gene specifically in hepatocytes. This was shown by a Western Blot against LTßR using cell lysates from isolated hepatocytes from either Albumin-Cre LTßR floxed mice or cre-negative littermate controls (Figure 22A). The signal intensity was clearly lower for Alb-Cre LTßR floxed mice when compared to their littermate controls. Signal intensity for the GAPDH control was similar throughout all samples.

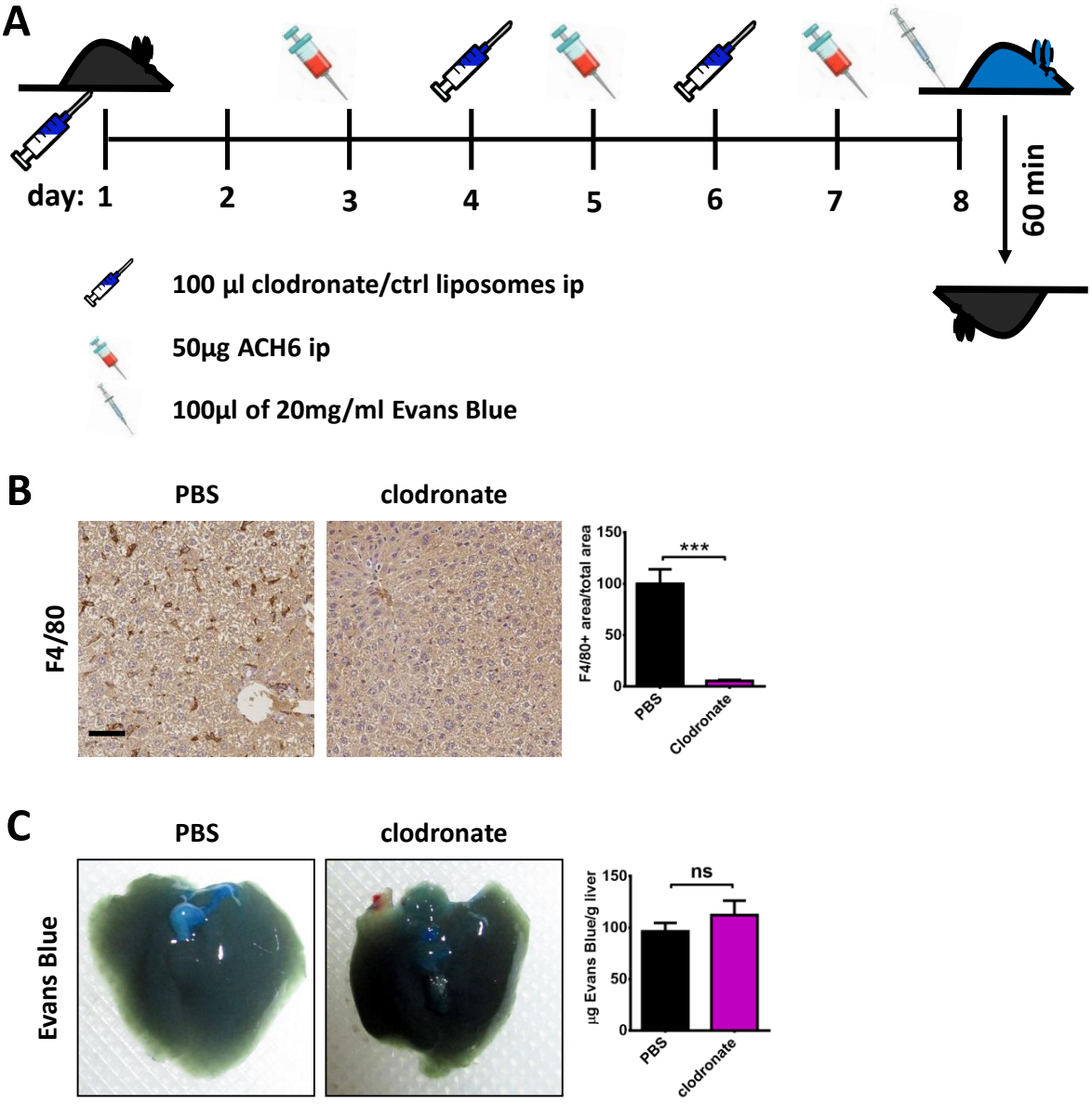

Figure 21: Kupffer cells are not important for LT induced metastasis formation in the liver

A) Schematic of the experimental setup for the clodronate depletion LTßR agonization experiments. C57BL/6 mice were treated with 50 µg ACH6 (red syringe) and 100 µl clodronate or control liposomes (dark blue syringe) every other day in turn for one week. On the 8th day mice were injected with 2mg Evans Blue (light blue syringe) intravenously and sacrificed 60 minutes later. Livers were perfused with PBS and analysed.

B) Representative immunohistochemical pictures of F4/80 stainings of paraffin-embedded liver samples from mice pretreated with ACH6 and clodronate or control liposomes for 7 days and sacrificed 1 day later. F4/80 positive area was assessed by histological software (DIH). Sample size is n=4 for all groups. Scale bars are 80µm.

C) Representative macroscopical pictures of EvansBlue stained livers from DBA/2 mice subjected to an EvansBlue assay as described in A. Retained EvansBlue dye was extracted from homogenized livers and assessed by absorbance at 620nm. n=4 mice were used for all groups.

Animal experiments and pictures were done by Dr. Nicole Simonavicius and Dr. Bastian Seubert, data processing and presentation was done by me.

Data are expressed as mean + SEM and statistical significance was calculated using Student's t-Test (*** $p < 0.001$, ns=non-significant).

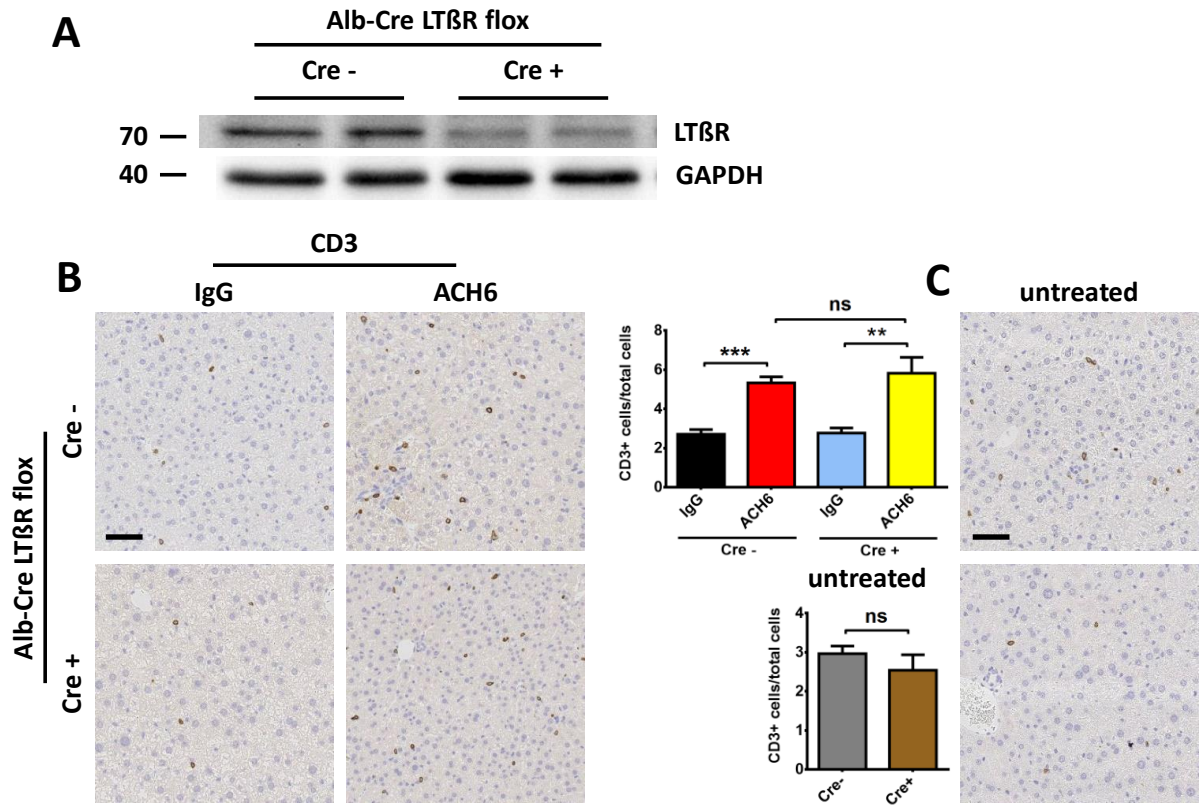

Figure 22: Hepatocytes are not important for LT induced metastasis formation of L-CI.5s in the liver
A) Representative immunoblot analysis of LTßR and GAPDH protein expression in isolated hepatocytes of Albumin-Cre LTßR floxed and Cre negative littermate control mice. *Western Blot was done by Dr. Monika Wolf.*
B, C) Representative immunohistochemical pictures of CD3 stainings of paraffin-embedded liver samples from Alb-Cre LTßR floxed or littermate control mice pretreated with ACH6 or IgG **(B)** or untreated **(C)**, injected with L-CI.5s cells and sacrificed 24 hours later. CD3 positive cells were assessed by histological software (DIH) and normalized to total cells analyzed. Sample size is n=6 for all groups. Scale bars are 80µm.
Data are expressed as mean + SEM and statistical significance was calculated using Student's t-Test (** $p < 0.01$, *** $p < 0.001$, ns=non-significant).

When subjected to a 24h experimental metastasis assay using L-CI.5 parental cells, no significant differences in the amount of tumor cells in the liver were found between cre- and cre+ animals, as assessed by immunohistochemical CD3 stainings (Figure 22B, C). Cre- and cre+ animals both showed roughly 3% of total cells with CD3+ staining when pretreated with IgG for 14 days. Pretreatment with ACH6 increased the relative amount of CD3+ cells to around 6% in both cases (Figure 22B). As an additional control, mice which received no pretreatment were used (Figure 22C). Like the IgG control group, cre- and cre+ animals were found to have roughly 3% CD3+ cells in the liver without pretreatment, suggesting that the IgG control antibody has no effect on its own. The results from the Albumin-Cre LTßR floxed mice suggest that hepatocyte-specific LTßR signaling is not relevant for the LT-induced increase of hepatic metastasis.

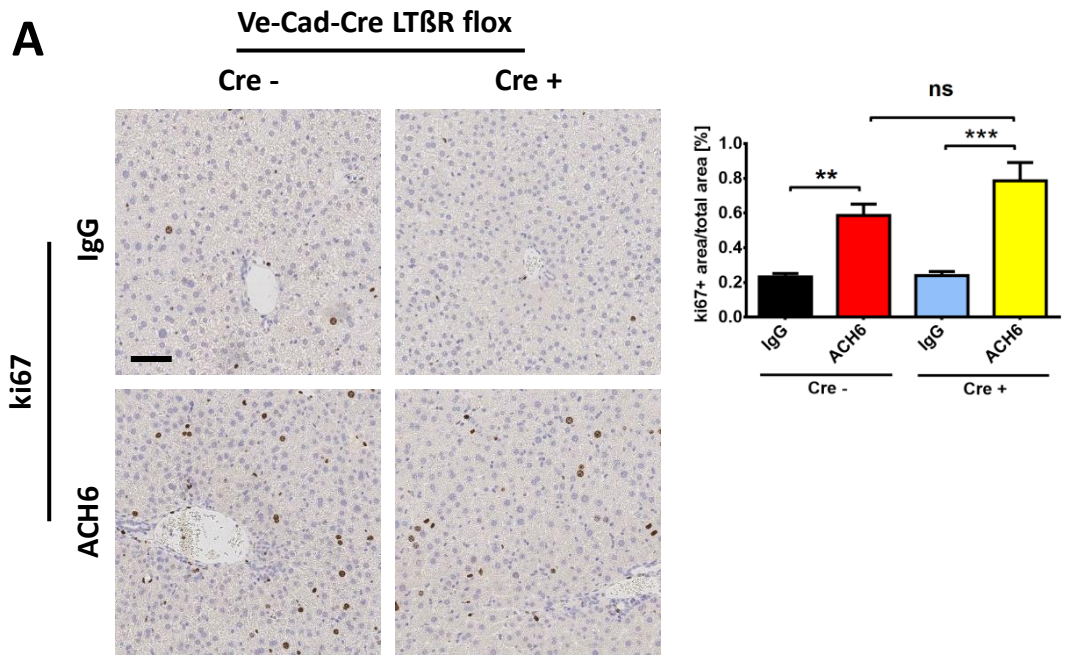

Figure 23: LSECs are not important for LT induced metastasis formation of L-CI.5s in the liver

A) Representative immunohistochemical pictures of ki67 stainings of paraffin-embedded liver samples from Ve-Cad-Cre LTßR floxed or littermate control mice pretreated with ACH6 or IgG, injected with L-CI.5s cells and sacrificed 24 hours later. Ki67 positive area was assessed by histological software (DIH) and normalized to total cells analyzed. Sample size is n=6 for all groups. Scale bars are 80µm.

Data are expressed as mean + SEM and statistical significance was calculated using Student's t-Test (** $p < 0.01$, *** $p < 0.001$, ns=non-significant).

LSEC specific LTßR signaling does not affect hepatic metastasis formation of L-CI.5s

To deduce whether LSEC specific LTßR signaling is needed for the LT-induced increase in liver metastasis, Ve-Cad-Cre LTßR floxed mice were used. These mice express the Cre recombinase under the endothelial cell-specific Ve-cadherin promoter, which leads to a deletion of the loxP flanked LTßR gene specifically in endothelial cells. This, however, had no effect on LT-induced hepatic metastasis formation as shown by a 24h experimental metastasis assay (Figure 23A). Tumor cells in the liver were assessed by immunohistochemical staining against ki67. Evaluating ki67+ liver area relative to the whole tissue area analysed, cre- and cre+ animals showed no significant differences after either IgG or ACH6 pretreatment for 14 days. Both showed roughly 0,25% ki67+ area in the liver after IgG pretreatment and 0,6 and 0,7% ki67+ area respectively after ACH6 pretreatment. This suggests that LSEC-specific LTßR signaling is not important for the LT-induced increase in hepatic metastasis.

Hepatic stellate cell-specific LTßR signaling significantly affects hepatic metastasis formation of L-CI.5s

Lastly, to deduce whether LSEC-specific LTßR signaling is needed for the LT induced increase in liver metastasis, GFAP-Cre LTßR floxed mice were used as a first model. These mice

express Cre recombinase under the GFAP promoter, which leads to a knockout of the loxP flanked LTßR gene in all GFAP expressing cells. In the liver this is specific to HSCs. However, outside of the liver it is also expressed in multiple other cell types, in the central nervous system[419,420] but also in kidney fibroblasts[421], keratinocytes[422], osteocytes and chondrocytes[423] and pancreatic stellate cells[424], amongst others. When pretreated with ACH6 for 14 days, GFAP-Cre LTßR floxed mice subjected to a 24h experimental metastasis assay with L-CI.5s showed a substantial decrease in the number of micrometastases as compared to cre- littermate control mice (Figure 24A). X-gal stained micrometastases dropped from 11 to 2 on average, indicating a critical role for HSC-specific LTßR signaling in LT-induced hepatic metastasis formation.

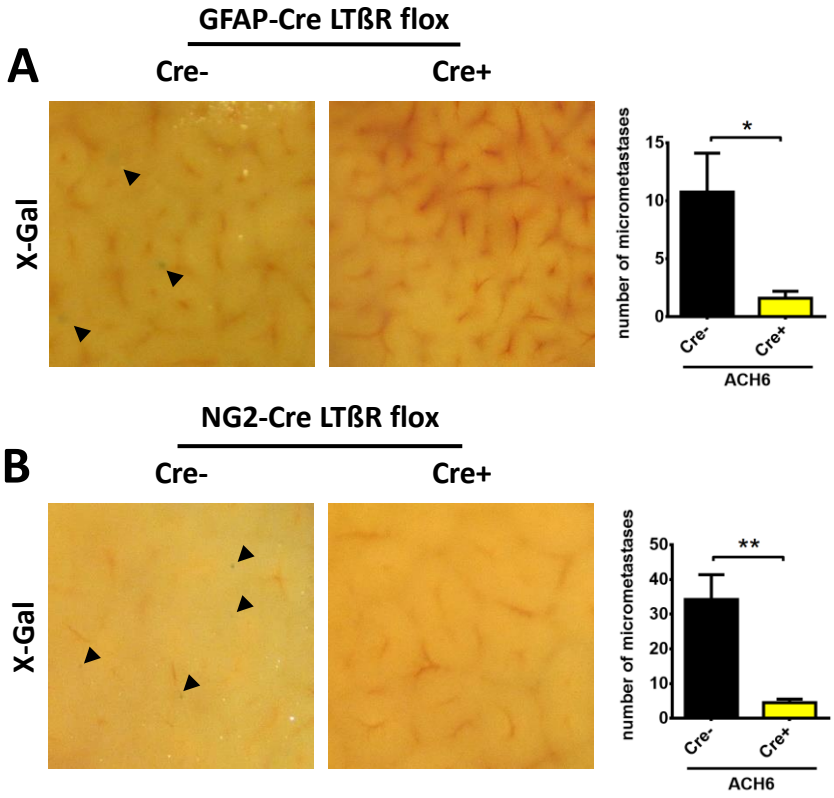

Figure 24: HSC specific LT signaling is crucial for LT induced hepatic metastasis of L-CI.5s

A, B) Representative macroscopical pictures of X-gal stained livers from GFAP-Cre LTßR floxed **(A)** or NG2-Cre LTßR floxed **(B)** or cre- littermate control mice pretreated for 14 days with ACH6, injected with L-CI.5s and sacrificed 24h later. Micrometastases were always calculated from the same lobes and are indicated by arrows. n≥4 mice were used for all groups.

Data are expressed as mean + SEM and statistical significance was calculated using Student's t-Test (* $p < 0.05$, ** $p < 0.01$).

As a second model for LTßR knockout in HSCs, NG2-Cre LTßR floxed mice were used. These mice express cre recombinase under the NG2 promoter. Like GFAP, NG2 is expressed exclusively in HSCs in the liver but is also expressed in various cell types outside the liver[425]. These cell types include mainly progenitor cell types like pericytes[426], oligodendrocyte progenitor cells[427], chondroblasts and myoblasts, but also cardiomyocytes, aortic smooth muscle cells and several tumors[428–430]. 24h experimental metastasis assays with NG2-Cre

LTßR floxed mice showed very similar results as GFAP-Cre LTßR floxed mice (Figure 24B). Again, cre+ LTßR floxed mice showed substantially fewer X-gal stained micrometastases in the liver when compared to cre- littermate controls. This corroborates the data from the GFAP-Cre LTßR floxed mice and strengthens the suggestion that HSC specific LTßR signaling is critical for LT-induced hepatic metastasis formation of L-CI.5s.

6.2.2 LT activates hepatic stellate cells in a non-fibrotic manner

To find out how hepatic stellate cells influence LT-mediated hepatic metastasis formation of L-CI.5s, cellular, morphological and functional changes of HSCs upon LTßR agonization were assessed as a first step. As a second step, molecular alterations and changes in expression patterns and protein phosphorylation were assessed, to identify potential signaling pathways mediating these effects.

LT induces classical activation markers in HSCs

Classical activation of hepatic stellate cells is accompanied by a strong upregulation of type-III intermediate filament proteins desmin (des) and vimentin (vim)[431,432]. Livers of mice that were treated with ACH6 for 14 days before being subjected to a 24h experimental metastasis assay with L-CI.5s showed a significant increase in both desmin and vimentin when compared to IgG pretreated animals (Figure 25A). Desmin staining was increased roughly 3-fold, while vimentin staining was only increased by around 40%. Furthermore, the same liver samples were analysed for expression of glial fibrillary acidic protein (GFAP) (Figure 25A). GFAP is expressed in quiescent HSCs and is downregulated during HSC activation[25]. Accordingly, ACH6 pretreated mice showed a roughly 4 times weaker GFAP staining than IgG pretreated control mice, corroborating the results from the desmin and vimentin stainings. Together, these results indicate that ACH6-induced LTßR agonization activates HSCs in a classical manner. 3D reconstruction of liver tissues from Lrat-tdTomato mice, which express the fluorescence marker *tdTomato* under the HSC-specific Lrat promoter, further corroborated these results (Figure 25B). Relative fluorescence of tdTomato was increased after ACH6 treatment compared to IgG, suggesting an increase in HSCs and/or morphological changes. Proliferation and morphological changes are both hallmarks of classical HSC activation, supporting the previous results.

To corroborate these findings in the other mouse models, and to make sure that HSC activation is not an artifact of ACH6 treatment but is directly related to HSC-specific LTßR signaling, desmin and vimentin expression was evaluated in additional mouse models (Figure 25C-E). When desmin expression was compared between livers of mice that had been subjected to a 7 day experimental metastasis assay using parental L-CI.5s, no tumor cells or L-CI.5s shLTαß, desmin expression was found to be significantly higher in mice injected with parental L-CI.5s (Figure 25C). These findings show that tumor cell-derived LT has a similar effect on desmin expression as ACH6. Of note, desmin expression was

unchanged in mice injected with L.CI-5s shLTαß compared to mice that were not injected at all.

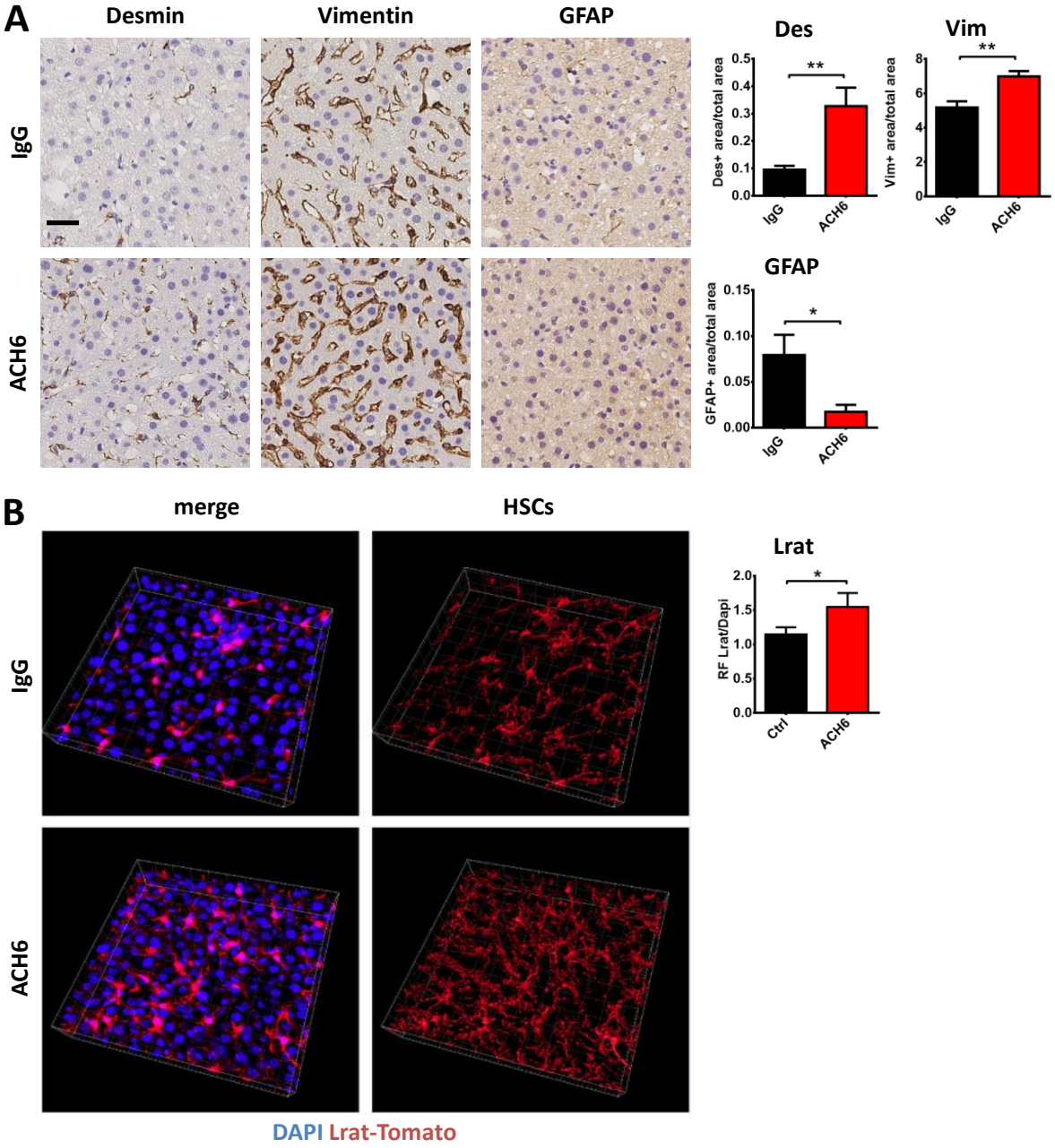

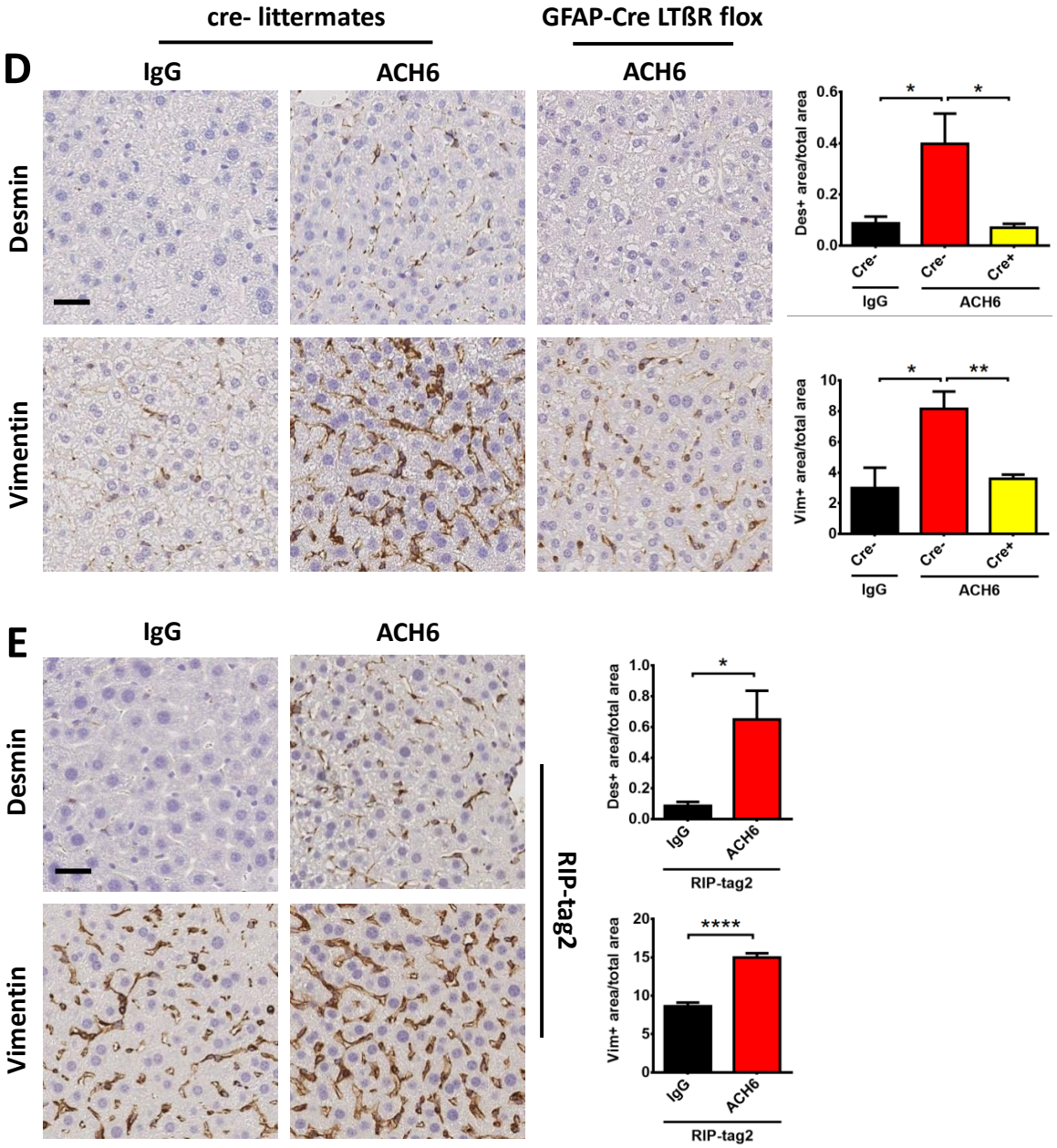

Figure 25: LTßR agonization on HSCs leads to increased expression of classical HSC activation markers

A) Representative immunohistochemical pictures of vimentin, desmin or GFAP stainings of paraffin-embedded liver samples from DBA/2 mice pretreated with ACH6 or IgG for 14 days, injected with L-CI.5s cells and sacrificed 7 days later. Vimentin, desmin and GFAP stained area was assessed by histological software (DIH) and normalized to total area analyzed. Sample size is n≥6 for all groups. Scale bars are 40µm.

B) Representative pictures of 3D reconstructed DAPI stainings of Lrat-tdTomato mice treated for 14 days with either IgG or ACH6. TdTomato expressing HSCs are shown in red, DAPI stained nuclei in blue. TdTomato fluorescence intensity per DAPI fluorescence intensity was assessed by ImageJ software. *3D reconstruction and images were done by Simone Joers (AG Geisler, Klinikum rechts der Isar, TU München, Germany).*

C-E) Representative immunohistochemical pictures of vimentin or desmin stainings of paraffin-embedded liver samples from DBA/2 **(C)**, GFAP-Cre LTßR floxed **(D)** or Rip-Tag2 **(E)** mice pretreated with ACH6 or IgG for 14 days **(D, E)** or untreated **(C)**, injected with L-CI.5s cells **(C, D)** or not **(E)** and sacrificed 24 hours **(D)**, 7 days **(C)** or 14 days **(E)** later. Vimentin and desmin stained areas were assessed by histological software (DIH) and normalized to total area analyzed. Sample size is n≥5 for all groups. Scale bars are 40µm.

Data are expressed as mean + SEM and statistical significance was calculated using Student's t-Test (* $p < 0.05$, ** $p < 0.01$, **** $p < 0.0001$).

Mice lacking LTßR on HSCs specifically (GFAP-Cre LTßR floxed) showed no increase of desmin or vimentin expression after 14 days ACH6 pretreatment when compared to cre- littermate controls pretreated with IgG (Figure 25D). Consequently, desmin and vimentin expression were significantly lower than in cre- littermate controls pretreated with ACH6. Together these data support the hypothesis that HSC-specific LTßR agoinzation leads to the activation of HSCs in our mouse models.

A significant increase in expression of desmin and vimentin was also visible in the livers of 14 days ACH6 treated RIP-tag2 mice when compared to IgG treated RIP-tag2 mice (Figure 25E). This corroborates the previous data, and also indicates that HSC activation is not dependant on L-CI.5s application.

LTßR-induced HSC activation is not fibrogenic

Besides the upregulation of desmin and vimentin, classical activation of HSCs is accompanied by a pro-fibrogenic phenotype, marked by a strong upregulation of alpha smooth muscle actin (a-sma) and fibrogenic collagens like collagen type-1, as already mentioned in the introduction. Surprisingly, no sign of fibrosis could be found after 2 weeks of ACH6 treatment, as evidenced by Sirius Red stainings (Figure 26A). Neither ACH6 nor IgG pretreated mice showed significant amounts of Sirius Red-stained collagen fibers within the liver parenchyma or sinusoids, as opposed to positive control mice with non-alcoholic steatohepatitis (NASH) pathology. We found similar results in mice that were subjected to a 7-day experimental metastasis assay with either parental, shLTαß or LTß overexpressing L-CI.5s (Figure 26B). None of the liver sections from these mice showed any significant amount of Sirius Red staining outside of vessel walls, and therefore much less than the control mice with NASH pathology.

As Sirius Red sensitive fibrotic collagen depositions only appear after HSCs have been fully activated and transformed, stainings for a-sma, one of the earliest markers of HSC activation and pro-fibrogenic transformation, were done as well. However, similar to the Sirius Red stainings, no significant amount of a-sma staining outside of vessel walls was found in either ACH6 or IgG pretreated mice (Figure 26C). In comparison, clearly visible a-sma staining was found around liver sinusoids in the positive control mice with NASH pathology. Finally, a small amount of collagen expression was detected using Lrat-TdTomato x col-GFP mice (Figure 26D). These mice express the fluorescence marker TdTomato under the HSC-specific *Lrat* promoter and the fluorescence marker GFP under the *Col1a1* promoter. A small amount of GFP expression was detected in IgG as well as ACH6 pretreated mice. The GFP expression colocalized with the TdTomato expressing HSCs and was around 30% higher in ACH6 treated mice, indicating an increase in collagen-I expression. However, TdTomato expression was also increased by around 30% (Figure 25B), indicating no net increase in collagen-I expression per HSC. Together, these results indicate that LTßR agonization leads to HSC activation in a non-fibrotic manner.

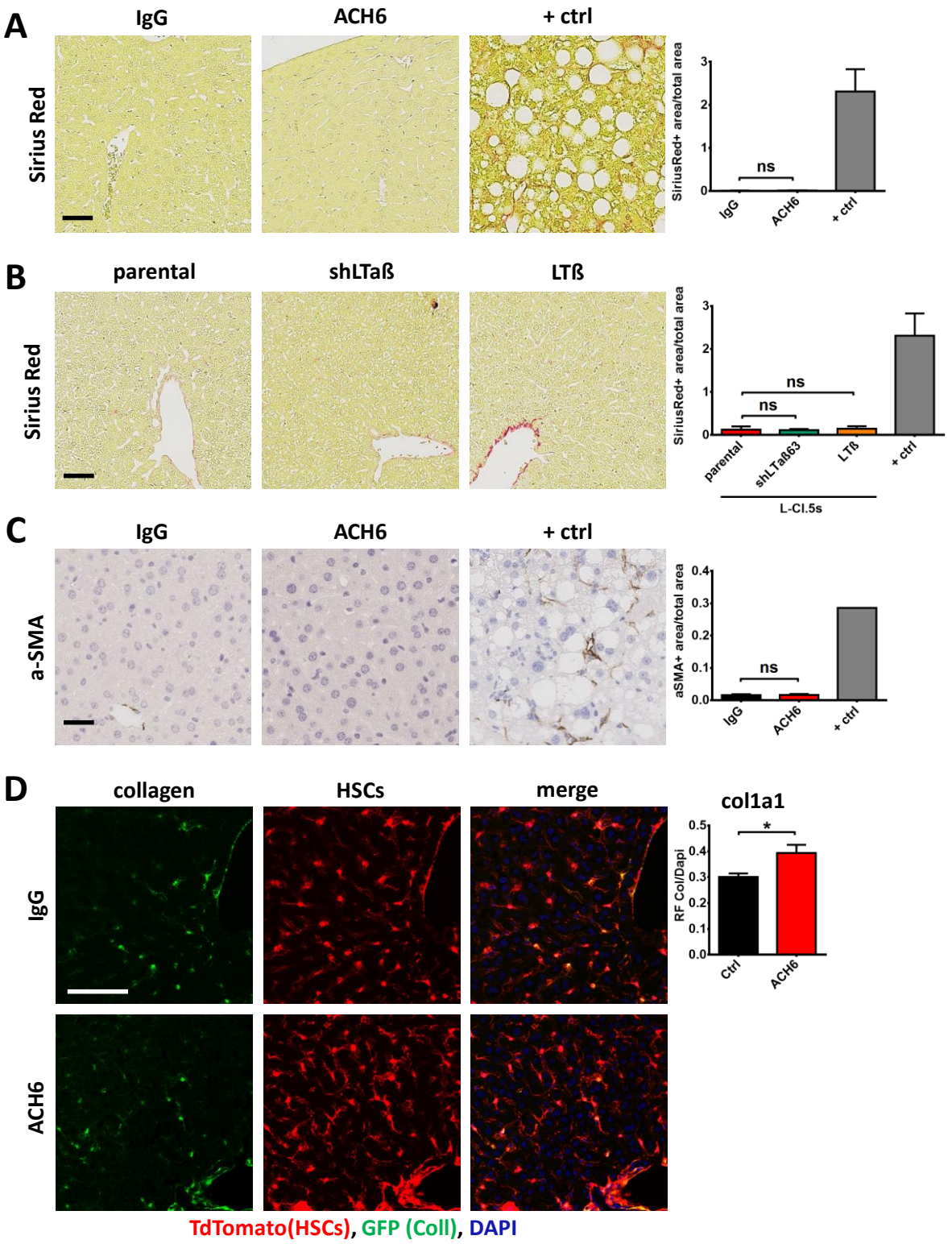

Figure 26: LT induced stellate cell activation does not lead to a fibrotic phenotype

A, B) Representative histochemical pictures of collagen stainings (Sirius Red) of paraffin-embedded liver samples from DBA/2 mice pretreated with ACH6 or IgG for 14 days **(A)** or untreated, injected with L-CI.5s P **(A, B)**, shLTaß or LTß **(B)** cells and sacrificed 7 days later. Sirius Red stained area was assessed by histological software (DIH) and normalized to total area analyzed. Liver samples from mice with NASH pathology were used as positive control (+ ctrl). Sample size is n≥6 for all groups and n=2 for + ctrl. Scale bars are 80µm.

C) Representative immunohistochemical pictures of a-sma stainings of paraffin-embedded liver samples from DBA/2 mice pretreated with ACH6 or IgG for 14 days, injected with L-CI.5s cells and sacrificed 7 days later. A-sma stained area was assessed by histological software (DIH) and normalized to total area analyzed. Liver samples from mice with NASH pathology were used as positive control (+ ctrl). Sample size is n≥6 for all groups and n=1 for + ctrl. Scale bars are 40µm.
D) Representative fluorescence microscopic images of collagen expressing cells and HSCs from cryo sections of liver samples from Lrat-TdTomato x col-GFP mice treated for 14 days with IgG or ACH6. Lrat expressing HSCs are stained red (TdTomato), collagen expressing cells are stained green and nuclei are stained blue (DAPI). GFP (col-GFP) fluorescence intensity per DAPI fluorescence intensity was assessed by ImageJ software. Sample size is n≥6 for all groups. Scale bars are 40µm. *Samples were provided by the lab of Prof. Robert Schwabe (Columbia University, New York, USA), pictures were made by Dr. Nicole Simonavicius, data processing and presentation was done by me.*
Data are expressed as mean + SEM and statistical significance was calculated using Student's t-Test (* $p < 0.05$).

6.2.3 LTßR agonization conveys pro-metastatic functions to HSCs *in vitro*

Murine C3H 10T1/2 and human LX-2 cells respond to LTßR agonization in a fashion similar to HSCs in vivo

To investigate the underlying mechanisms of LTßR-mediated HSC activation more thoroughly, *in vitro* assays were utilized. Therefore, murine C3H 10T1/2 (ATCC® CCL-226™) or human LX-2 cells[433] were used to model HSCs in the *in vitro* assays. C3H 10T1/2 cells treated with ACH6 for 24 hours showed a significant change in morphology compared to IgG-treated cells (Figure 27A). The size of the cells, as evaluated by multiplying length and width of each cell was decreased, while eccentricity, as evaluated by dividing length through width was increased. This change was accompanied by an increase in elasticity, as assessed by atomic force microscopy (Figure 27C). Cells treated with ACH6 showed a significant reduction in Apparent Youngs Modulus when compared to cells treated with IgG, indicating a decrease in cellular stiffness, and thus an increase in elasticity.

Real-time monitoring of the morphological changes using an xCELLigence (OLS OMNI Life Science) cell analyzer confirmed the morphological changes after ACH6 treatment (Figure 27D). Furthermore, real-time monitoring revealed that the changes started roughly four hours after ACH6 administration (t=21h). The morphological effect lasted roughly 15 hours (t=36h), whereafter it slowly declined back to the level of IgG treated cells (at t=44h). Similar results were observed with LX-2 cells treated with BS-1 (human LTßR agonist) or IvIG (control antibody) (Figure 27B). Cells treated with BS-1 showed a significant increase in eccentricity compared to cells treated with IvIG. However, size was not changed in LX-2 cells after BS-1 treatment. Taken together, both cell lines showed morphological signs of myofibroblastic transformation upon LTßR agonization.

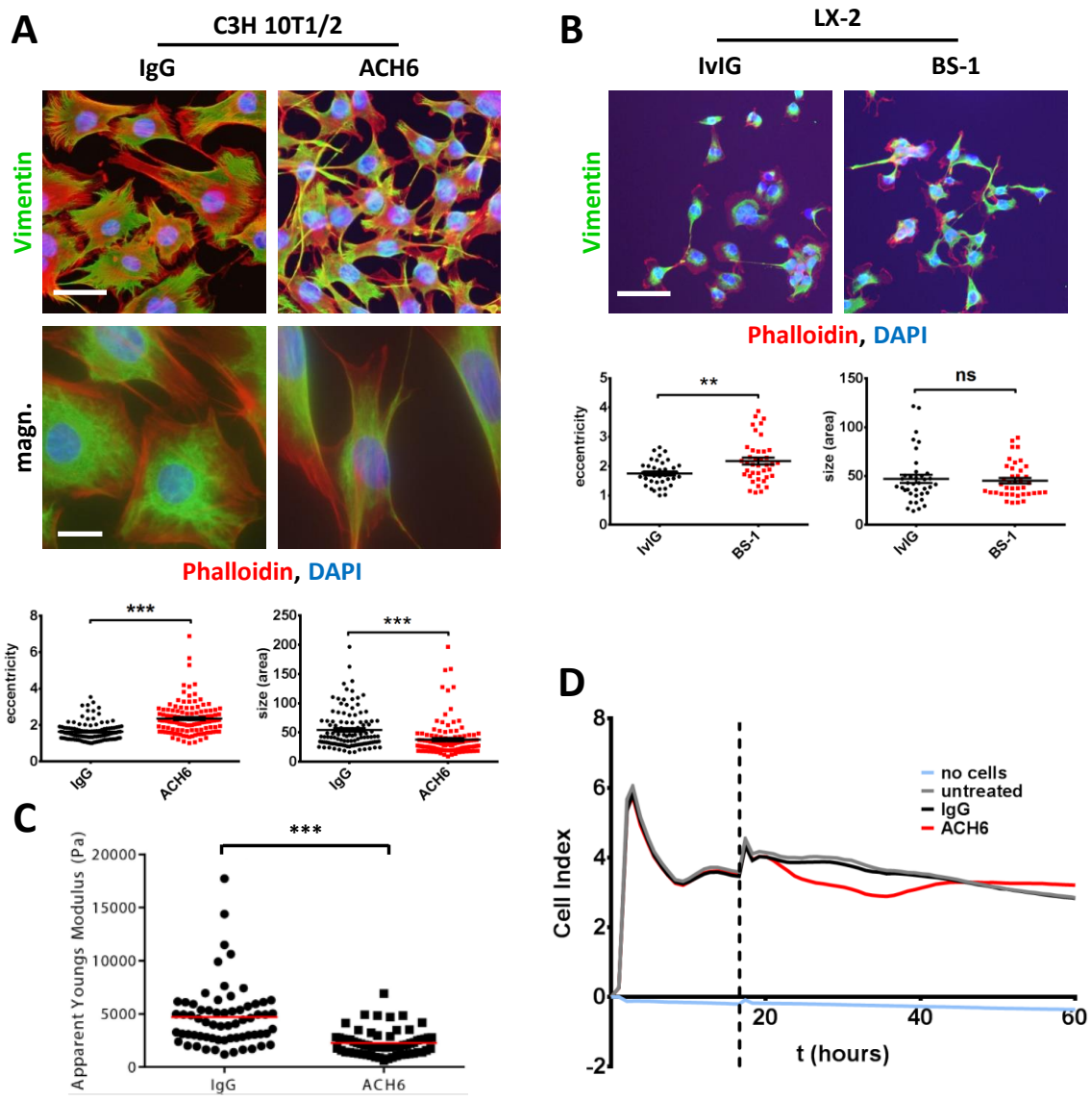

Figure 27: C3H 10T1/2 and LX-2 cells show transformation to myofibroblast-like cells after LTßR agonization

A, B) Representative fluorescence microscopy pictures of vimentin, phalloidin and DAPI stained 10T1/2 **(A)** or LX-2 **(B)** cells treated with ACH6 or IgG (10T1/2s) or IvIG or BS-1 (LX-2) for 24 hours. Lower row **(A)** shows higher magnifications. Eccentricity (length/width) and size (length x width) were assessed by manually measuring length and width of single cells in Photoshop software. Each dot (n≥60) represents one cell. Samples from at least 3 biological replicates were used for each group. Scale bars are 50µm and 20µm (inset).

C) Cellular stiffness of 10T1/2 cells treated with ACH6 or IgG for 24 hours as assessed by atomic force microscopy. Cellular stiffness is expressed by Apparent Youngs Modulus for each cell. Each dot represents one cell. *Experiments were done in the lab of Prof. Guck (TU Dresden, Germany).*

D) Morphological changes of 10T1/2 cells treated with ACH6 or IgG or untreated as assessed by an xCelligence cell analyzer. IgG or ACH6 treatment was done at t=17 hours (dotted line). Cell index was measured every 15 minutes (0-17 hours) or every minute (17-60 hours). No cells control was added to account for effects of cell culture medium. 1 representative experiment is shown. 6 biological replicates were done for each group.

Data are expressed as mean ± SEM and statistical significance was calculated using Student's t-Test (** $p < 0.01$, *** $p < 0.001$, ns=non-significant).

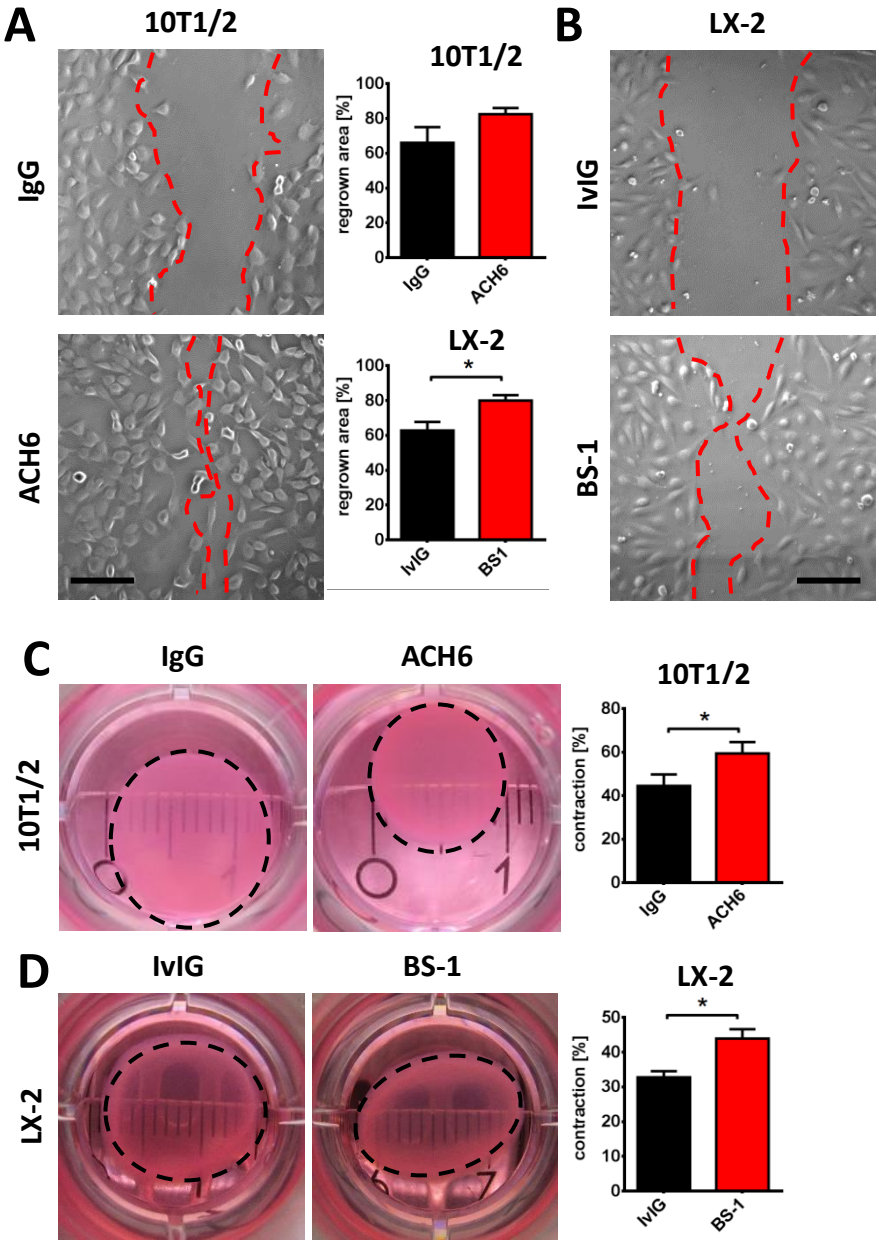

Figure 28: C3H 10T1/2 and LX-2 cells show increased contraction and wound healing capacity after LTßR agonization

A, B) Representative light microscopy pictures of a wound healing assay of 10T1/2 **(A)** or LX-2 **(B)** cells treated with ACH6 or IgG (10T1/2) or IvIG or BS-1 (LX-2) taken 24 hours after inducing the wound (scratch). Wound healing capacity (regrown area) was assessed by measuring the cell-free area between the growth fronts (dotted red lines) on each side with ImageJ software and substracting it from the cell-free area at wound induction (t=0). 3 biological replicates were done for all groups. Scale bars are 100µm.

C, D) Representative digital camera picture of collagen lattices (dotted black lines) from a collagen I contraction assay of C3H 10T1/2 **(C)** or LX-2 **(D)** cells treated with ACH6 or IgG (10T1/2) or IvIG or BS-1 (LX-2) taken after 24 hours of contraction. Contractility was assessed by calculating reduction of lattice circumference relative to lattice circumference before contraction (t=0, ≙well circumference). 3 biological replicates were done for all groups.

Data are expressed as mean + SEM and statistical significance was calculated using Student's t-Test (* $p < 0.05$).

Furthermore, experiments investigating functional properties of myofibroblastic transformation in these cell lines were performed. During liver regeneration and wound-healing processes *in vivo*, activated stellate cells need to proliferate and acquire a migratory phenotype as part of their myofibroblastic transformation and to reach the site of tissue damage[434,435]. To analyze these properties in 10T1/2 and LX-2 cells *in vitro*, wound healing assays were performed. Both celllines showed an increased capacity to recolonize a scratched area when treated with LTßR agonists during the process as compared to cells treated with the respective control antibodies (Figure 28A, B). In both cases the growth front of the re-growing monolayers was significantly farther advanced after 24h as indicated by the dotted red lines in Figure 28 A and B. A second feature of activated stellate cells and myofibroblasts is their contractility[15,43]. Using a collagen-I contraction assay kit, LTßR agonization via ACH6 or BS-1 was found to significantly increase the contractility of 10T1/2 or LX-2 cells (Figure 28 C, D). In both cases pretreatment with LTßR agonist caused a significantly stronger contraction of the collagen-I discs after 24h, as indicated by a stronger reduction in diameter (black dotted lines in Fig. 22 C, D). Taken together, C3H 10T1/2 as well as LX-2 cells show two typical functional changes towards a myfibroblastic phenotype after LTßR agonization, corroborating their usefulness as *in vitro* models for primary HSCs.

LTßR agonization increases pro-metastatic functional properties in C3H 10T1/2 cells in vitro

To unravel the role of hepatic stellate cell specific LTßR signaling during liver metastasis formation, functional changes that are tied to tumor cell metastasis were investigated. Adhesion and transmigration at the site of metastasis are crucial events during the metastatic cascade and potentially rate-limiting[79,152,155,271]. A simple adhesion assay was used to show that LTßR agonization increases the capacity of C3H 10T1/2 cells to bind tumor cells *in vitro* (Figure 29 A). 10T1/2 cells that had been pretreated with ACH6 for 48 hours could bind roughly twice as many tumor cells as 10T1/2 cells pretreated with IgG control antibody within 30 minutes of tumor cell seeding. Surprisingly, pretreating 10T1/2 cells with 2.5ng/ml TGFß1, one of the main drivers of fibrogenic HSC activation, did not increase their ability to bind tumor cells but rather decreased it (Figure 29 B). Still, a change towards a strong myofibroblastic phenotype, even more pronounced than after LTßR agonization, could be observed on the brightfield images (Figure 29 B). A strong morphological change upon TGFß1 stimulation could also be measured using an xCelligence cell analyzer (Figure 29D). Similar results were obtained when using L-CI.5s shNT and L-CI.5s shLTαß cells instead of parental L-CI.5s. ACH6 induced LTßR agonization in 10T1/2 cells increased their potential to bind L-CI.5s shNT as well as shLTαß (Figure 29 C). Interestingly, a significantly lower number of L-CI.5s shLTαß adhered to 10T1/2s when compared to L-CI.5s shNT after ACH6 or IgG pretreatment, indicating a direct role of tumor cell-derived LT in this process. This was corroborated by the finding that LTß overexpressing L-CI.5s show increased binding to 10T1/2s when compared to L-CI.5s EGFP control cells (Figure 29E). Finally, BS-1-mediated LTßR agonization of LX-2 cells also increased the adhesion of L-CI.5s two-fold (Figure 29F),

indicating that the mechanism is not unique to C3H 10T1/2 cells but also applies to human immortalized stellate cells. Together these data indicate that LTßR agonization directly correlates with the potential of C3H 10T1/2 or LX-2 cells to bind lymphoma cells *in vitro* and that preemptive LTßR agonization but also direct effects of tumor cell-derived LT play a role.

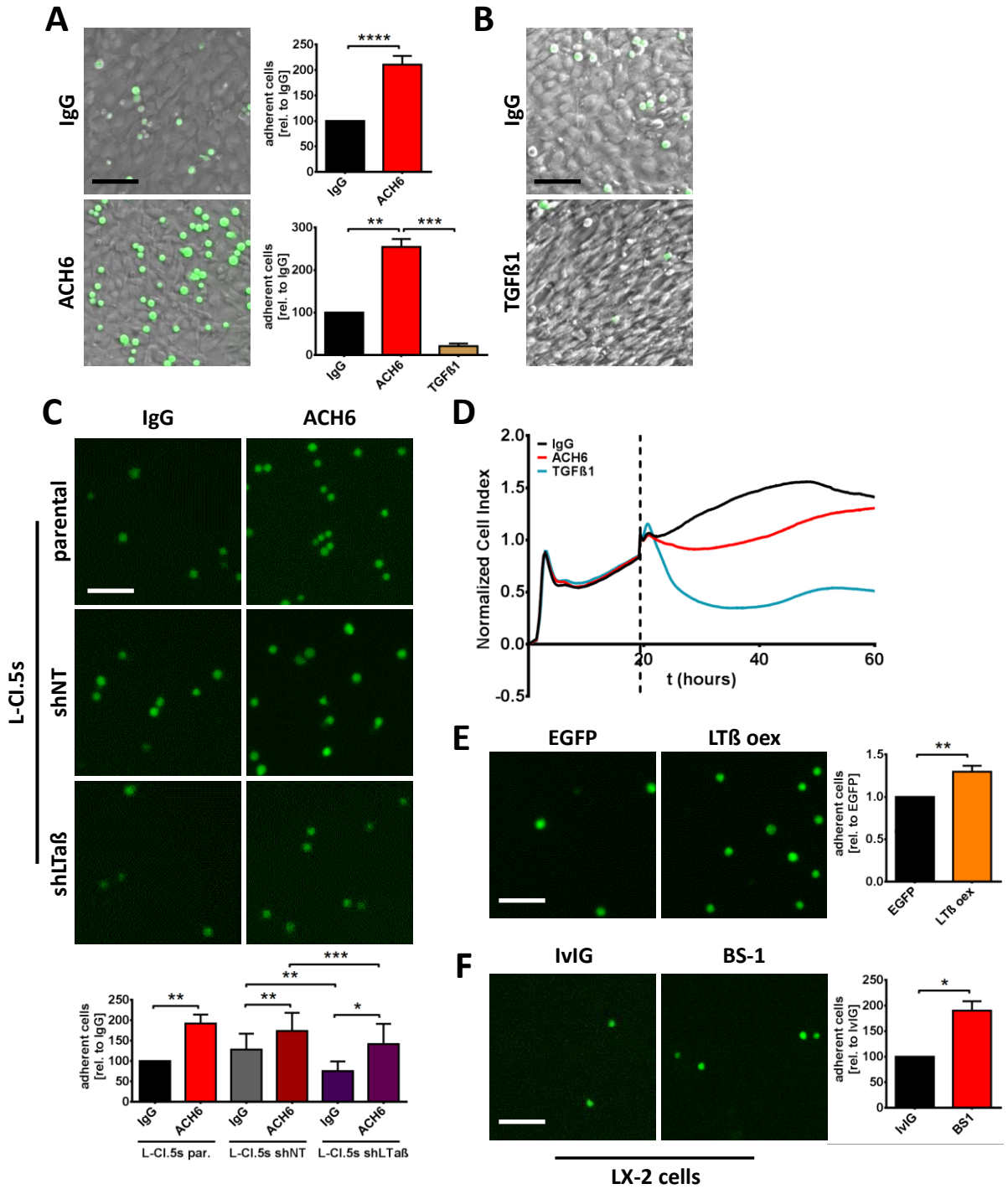

Figure 29: LTßR agonization of C3H 10T1/2 or LX-2 cells increases adhesion of tumor cells

A, B) Representative overlays of light and fluorescence microscopy pictures of adhesion assays showing green stained L-Cl.5s adhered to 10T1/2 cells pretreated with ACH6 or IgG **(A)** or TGFß1 **(B)**. 4 biological replicates were done for all groups. Scale bars are 100µm.

C) Representative fluorescence microscopy pictures of adhesion assays showing green stained L-CI.5s P, shNT or shLTαß adhered to 10T1/2 cells pretreated with ACH6 or IgG. 3 biological replicates were done for all groups. Scale bars are 100µm.
D) Morphological changes of 10T1/2 cells treated with IgG, ACH6 or TGFß1 as assessed by an xCelligence cell analyzer. IgG, ACH6 or TGFß1 treatment was done at t=19 hours (dotted line). Cell index was measured every 15 minutes (0-19 hours) or every minute (19-60 hours) and later normalized to the cell index at t=19 hours. 1 representative experiment is shown. At least 3 biological replicates were done for all groups.
E) Representative fluorescence microscopy pictures of adhesion assays showing green stained L-CI.5s EGFP or LTß adhered to 10T1/2 cells. At least 4 biological replicates were done for all groups. Scale bars are 100µm.
F) Representative fluorescence microscopy pictures of adhesion assays showing green stained L-CI.5s adhered to LX-2 cells pretreated with IvIG or BS-1. At least 4 biological replicates were done for all groups. Scale bars are 100µm.
For all adhesion assays five random pictures were taken per well and adherent cells were counted using ImageJ software and normalized to IgG (10T1/2) or IvIG (LX-2) control group. Data are expressed as mean + SEM and statistical significance was calculated using Student's t-Test (* $p < 0.05$, ** $p < 0.01$, *** $p < 0.001$, **** $p < 0.0001$).

Alongside the increased capacity to bind tumor cells, ACH6-stimulated C3H 10T1/2 cells also enable an increased transmigration of tumor cells through a synthetic endothelial barrier *in vitro*, as evidenced by a trans-endothelial migration assay (Figure 30A). For this assay a classical transwell inset was used and 10T1/2 cells were grown on the bottom side of the membrane while a HUVEC monolayer was grown on the top side, recreating to some extent the cellular structure of the endothelium in the liver. Pretreating the 10T1/2-HUVEC endothelial layer with ACH6 for 24 hours increased the amount of cell tracker green-stained L-CI.5s that were able to transmigrate to the bottom side of the transwell membrane within 24 hours almost two-fold, similar to the increase in adhesion seen in Figure 29A. As ACH6 only targets murine LTßR and not human LTßR, ACH6 pretreatment can only affect 10T1/2 cells but not HUVECs. Therefore, the data suggests that 10T1/2 specific LTßR signaling increases the potential of tumor cells to transmigrate in this setting. Supporting this hypothesis, ACH6 pretreatment was found to have no effect when using a HUVEC monolayer (EC) in the upper chamber only, without the support of 10T1/2 cells grown on the bottom side (ECPC) of the transwell membrane (Figure 30B, EC). There was no significant difference in transmigrated L-CI.5s after 24h between the ACH6-pretreated and the IgG-pretreated group, in contrast to the significant difference between ACH6 and IgG pretreated groups when using a 10T1/2-HUVEC endothelial layer (Figure 30B, ECPC). Interestingly, the number of tumor cells that were able to transmigrate within 24 hours was much higher when using the 10T1/2-HUVEC layer as compared to HUVECs only, irrespective of the treatment used (Figure 30B). The amount of transmigrated tumor cells was two-fold higher when comparing the IgG pretreated groups and four-fold higher when comparing the ACH6 pretreated groups. This finding corroborates the hypothesis that the 10T1/2 cells are crucial for the process of tumor cell transmigration in this setting. Additional transmigration assays using a 10T1/2-HUVEC endothelial layer (ECPC) and L-CI.5s with LTα, LTß or LTαß knockdown or control cells showed that tumor cell-derived LT affects their trans-endothelial

migration (Figure 30C). All four LT-knockdown cell lines showed a 30-50% reduced number of transmigrated cells when compared to the non-targeting control cells.

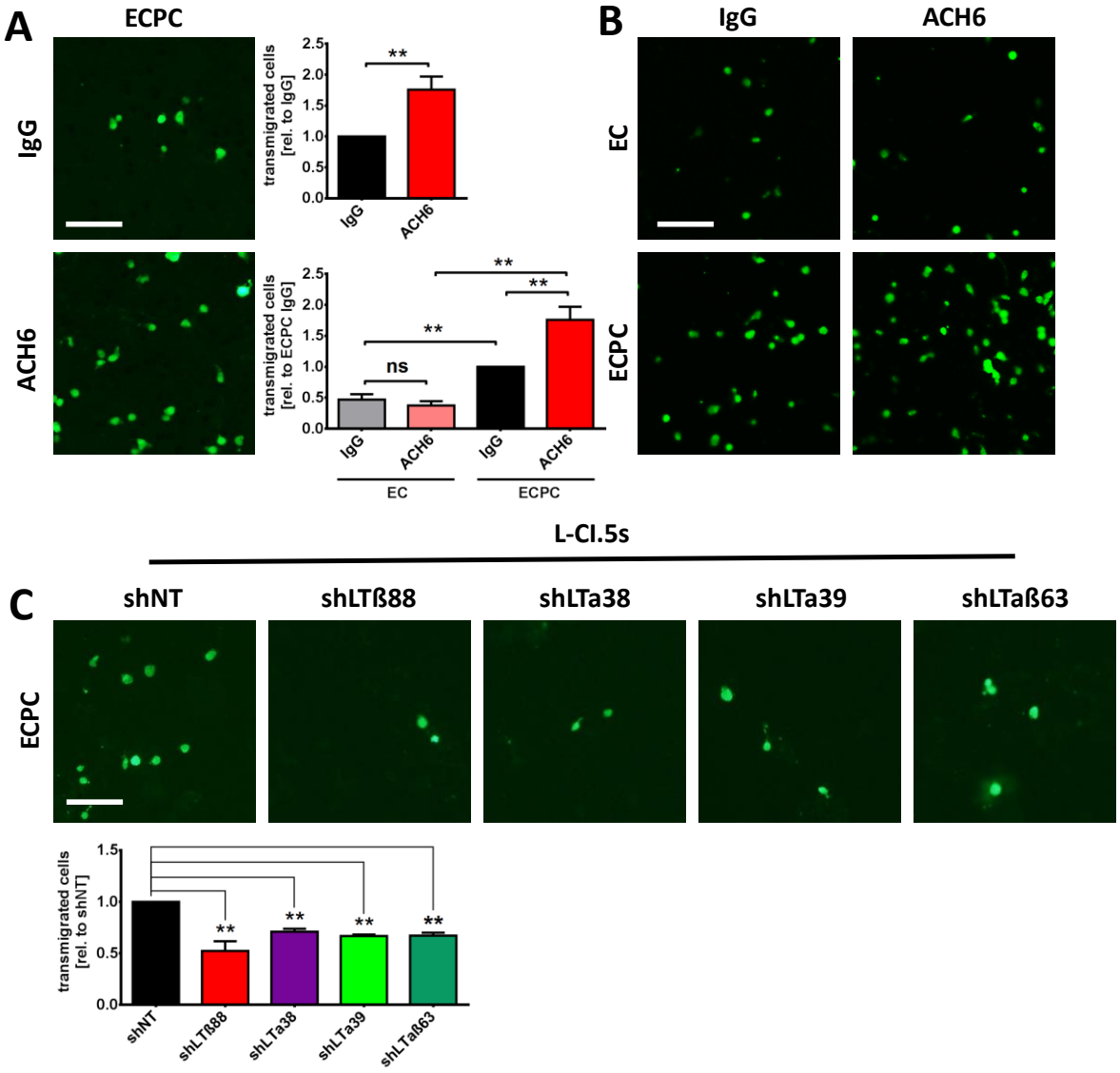

Figure 30: LTßR agonization of C3H 10T1/2 cells increases trans-endothelial migration of tumor cells

A) Representative fluorescence microscopy pictures of trans-endothelial migration assays showing green stained L-CI.5s after 24 hours transmigration period through a 10T1/2-HUVEC endothelial layer pretreated with ACH6 or IgG. At least 9 biological replicates were done for all groups. Scale bars are 100µm.

B) Representative fluorescence microscopy pictures of trans-endothelial migration assays showing green stained L-CI.5s after 24 hours transmigration period through a HUVEC monolayer (EC) or a 10T1/2-HUVEC endothelial layer (ECPC) pretreated with ACH6 or IgG. At least 3 biological replicates were done for all groups. Scale bars are 100µm.

C) Representative fluorescence microscopy pictures of trans-endothelial migration assays showing green stained L-CI.5s shNT, shLTß88, shLTα38, shLTα39 or shLTαß63 after 24 hours transmigration period through a 10T1/2-HUVEC endothelial layer. At least 3 biological replicates were done for all groups. Scale bars are 100µm. For all trans-endothelial migration assays five random pictures were taken per inset, transmigrated cells were counted using ImageJ software and then normalized to IgG (ECPC) control group. Data are expressed as mean + SEM and statistical significance was calculated using Student's t-Test (** $p < 0.01$, ns=non-significant).

6.3 Downstream signaling and effector functions are mediated by NIK and NF-kB2/RelB translocation

6.3.1 LTßR agonization induces NF-kB2 processing and RelB translocation in C3H 10T1/2 and LX-2 cells

LTßR agonization most prominently leads to activation and translocation of NF-kB2/Rel-B downstream[318]. Using protein lysates of 10T1/2 or LX-2 cells treated with LTßR agonist or a control antibody for four hours, western blots against p100/p52 and GAPDH were performed (Figure 31A). LTßR agonization led to a strong increase in p100 to p52 processing, which is also shown by the strong increase in p52/p100 ratio. A 5-fold increase of p52/p100 ratio in LX-2 and a 10-fold increase in 10T1/2 cells were observed. This suggests increased p52/RelB translocation into the nucleus, indicative of increased non-canonical NF-kB signaling. This was corroborated by immunocytochemical staining of phosphorylated RelB in ACH6 treated 10T1/2 cells (Figure 31B). Phosphorylated RelB could be observed in the nuclei of ACH6 treated cells but not in IgG treated cells.

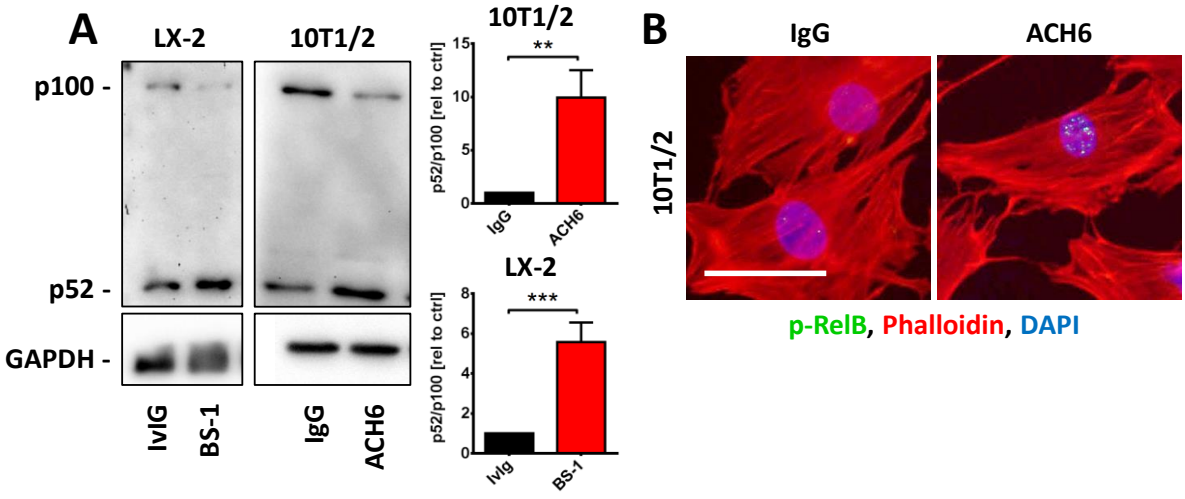

Figure 31: LTßR agonization of C3H 10T1/2 or LX-2 cells increases p100 processing and RelB translocation

A) Representative immunoblot analysis of p100, p52 and GAPDH protein expression in LX-2 or 10T1/2 cells treated with IvIG or BS-1 (LX-2) or IgG and ACH6 (10T1/2). Protein expression was assessed densitometrically, p52/p100 ratio was calculated and normalized to IgG control group. At least 9 biological replicates were done for all groups.

B) Representative fluorescence microscopy pictures of phospho-RelB, phalloidin and DAPI stained 10T1/2 cells treated with ACH6 or IgG for 24 hours. Scale bars are 50µm.

Data are expressed as mean + SEM and statistical significance was calculated using Student's t-Test (** $p < 0.01$, *** $p < 0.001$).

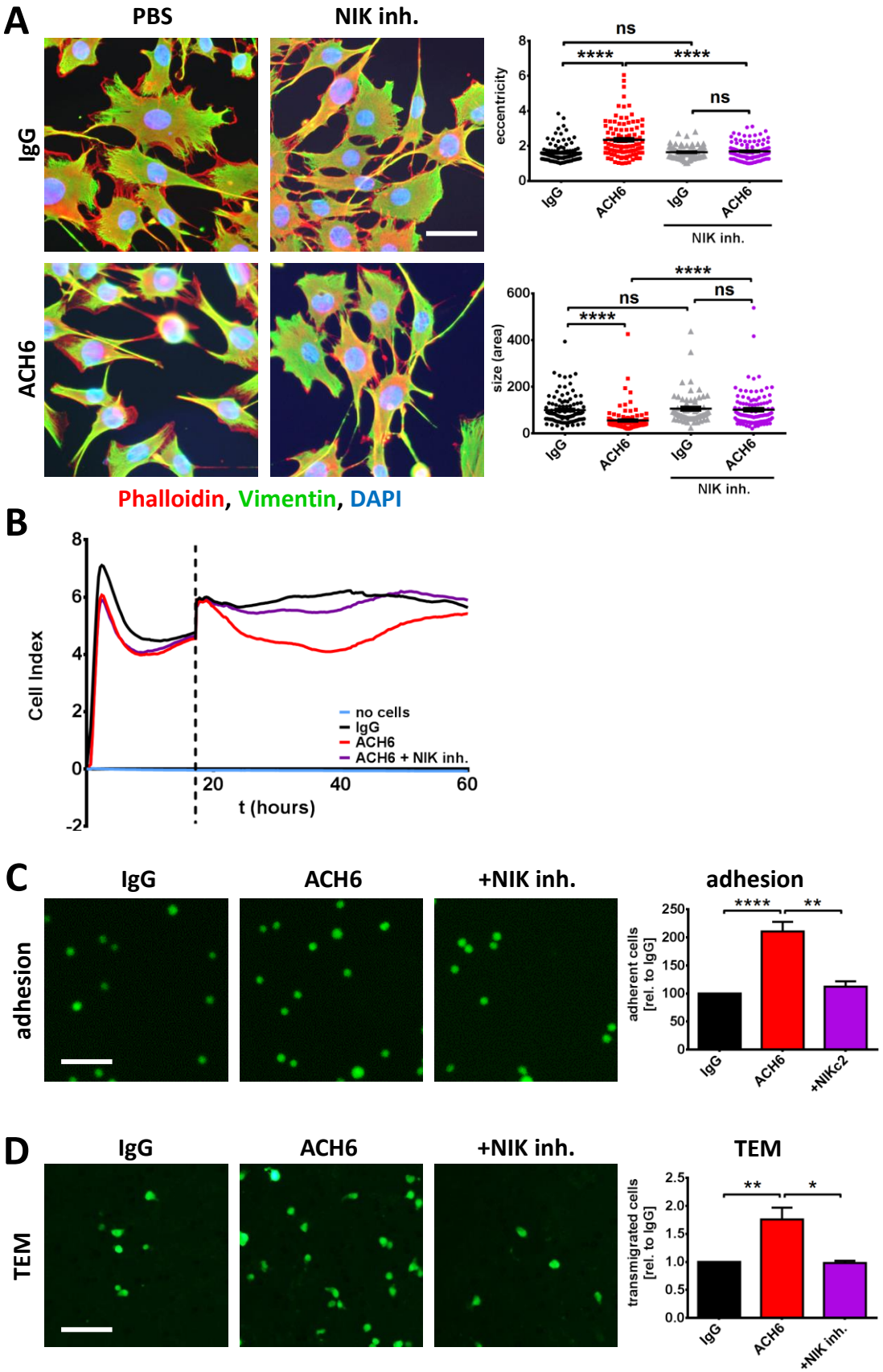

Figure 32: NIK inhibition in C3H 10T1/2 cells blocks morphological and functional effects of ACH6 stimulation
A) Representative fluorescence microscopy pictures of vimentin, phalloidin and DAPI stained 10T1/2 cells treated with ACH6 or IgG and with or without NIK inhibitor for 24 hours. Eccentricity (length/width) and size

(length x width) were assessed by manually measuring length and width of single cells with Photoshop software. Each dot (n≥60) represents one cell. Samples from at least 3 biological replicates were used for each group. Scale bars are 50µm.

B) Morphological changes of 10T1/2 cells treated with IgG or ACH6 with or without NIK inhibitor as assessed by an xCelligence cell analyzer. Treatments were administered at t=18 hours (dotted line). Cell index was measured every 15 minutes (0-18 hours) or every minute (18-60 hours). 1 representative experiment is shown. At least 3 biological replicates were done for all groups.

C) Representative fluorescence microscopy pictures of adhesion assays showing green stained L-CI.5s adhered to 10T1/2 cells pretreated with IgG or ACH6 with or without NIK inhibitor. At least 7 biological replicates were done for all groups. Scale bars are 100µm.

D) Representative fluorescence microscopy pictures of trans-endothelial migration assays showing green stained L-CI.5s after 24 hours transmigration period through a 10T1/2-HUVEC endothelial layer pretreated with IgG or ACH6 with or without NIK inhibitor. At least 3 biological replicates were done for all groups. Scale bars are 100µm.

For all adhesion and trans-endothelial migration assays five random pictures were taken per well or inset, adhered or transmigrated cells were counted using ImageJ software and then normalized to IgG control group. Data are expressed as mean ± SEM and statistical significance was calculated using Student's t-Test (* $p < 0.05$, ** $p < 0.01$, **** $p < 0.0001$, ns=non-significant).

6.3.2 NIK is critical for mediating morphologic changes and downstream effector functions after LTßR agonization *in vitro*

One of the key molecules in mediating non-canonical NF-kB signaling through LTßR is NIK[318]. To investigate whether the LTßR-induced morphological and functional changes in 10T1/2 cells described above were mediated by non-canonical NF-kB signaling, a NIK inhibitor was used (Figures 32, 33, 34). Neither the ACH6-induced increase of eccentricity nor the reduction of size could be observed when NIK inhibitor was added alongside ACH6 (Figure 32A). No difference in eccentricity or size was measured between ACH6- or IgG-treated groups when NIK inhibitor was administered in addition. NIK inhibitor itself had no effect on these morphological features, as no difference was measured between IgG + NIK inhibitor and IgG only treated groups. Real-time monitoring of morphological changes using an *xCelligence* cell analyzer confirmed that NIK inhibition suppressed ACH6-induced morphological changes throughout the entire duration of the experiment, up to 40 hours post antibody administration (Figure 32B). Suppression of morphological changes following LTßR agonization was also observed in LX-2 cells when NIK inhibitor was administered alongside BS-1 (Figure 33C). When NIK inhibitor was added alongside ACH6 during the 48 hours pretreatment period of an adhesion assay, ACH6-induced increase in adhesion of L-CI.5s towards a 10T1/2 monolayer was prevented (Figure 32C). A similar result was observed for trans-endothelial migration of L-CI.5s through a 10T1/2-HUVEC endothelial layer. Administration of NIK inhibitor alongside ACH6 completely abrogated the ACH6-induced increase in trans-endothelial migration (Figure 32D).

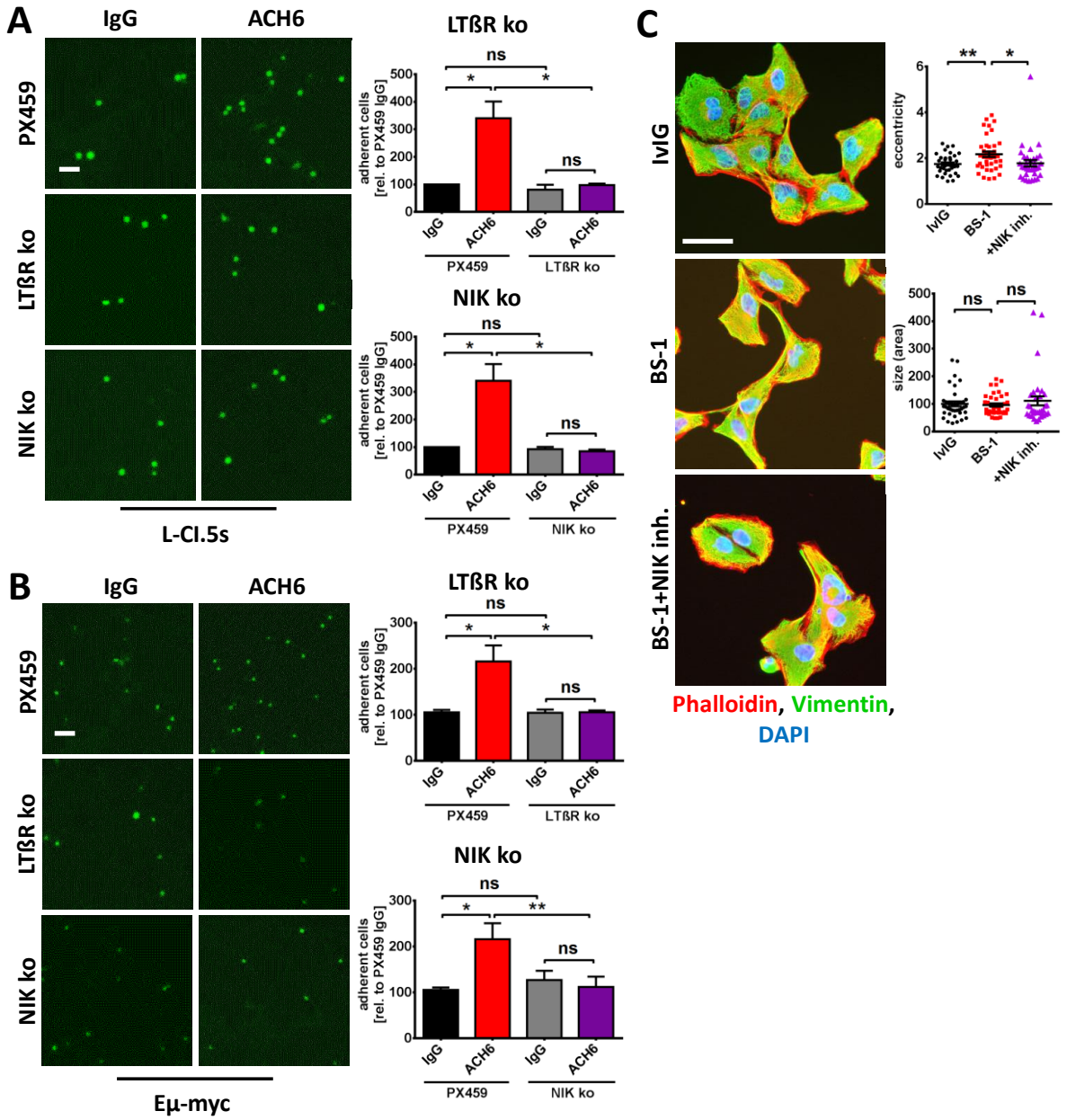

Figure 33: NIK inhibition in C3H 10T1/2 cells blocks morphological and functional effects of ACH6 stimulation

A, B) Representative fluorescence microscopy pictures of adhesion assays showing green stained L-CI.5s **(A)** or Eμ-myc **(B)** cells adhered to 10T1/2 PX459, LTßR ko or NIK ko cells pretreated with IgG or ACH6. 5 (A) or 4 (B) biological replicates were done for all groups. Scale bars are 100μm.

C) Representative fluorescence microscopy pictures of vimentin, phalloidin and DAPI stained LX-2 cells treated with IvIG or BS-1 with or without NIK inhibitor for 24 hours. Eccentricity (length/width) and size (length x width) were assessed by manually measuring length and width of single cells with Photoshop software. Each dot (n≥60) represents one cell. Samples from at least 3 biological replicates were used for each group. Scale bars are 50μm.

For all adhesion assays five random pictures were taken per well, adhered cells were counted using ImageJ software and then normalized to 10T1/2 PX459 IgG control group. Data are expressed as mean + SEM and statistical significance was calculated using Student's t-Test (* $p < 0.05$, ** $p < 0.01$, ns=non-significant).

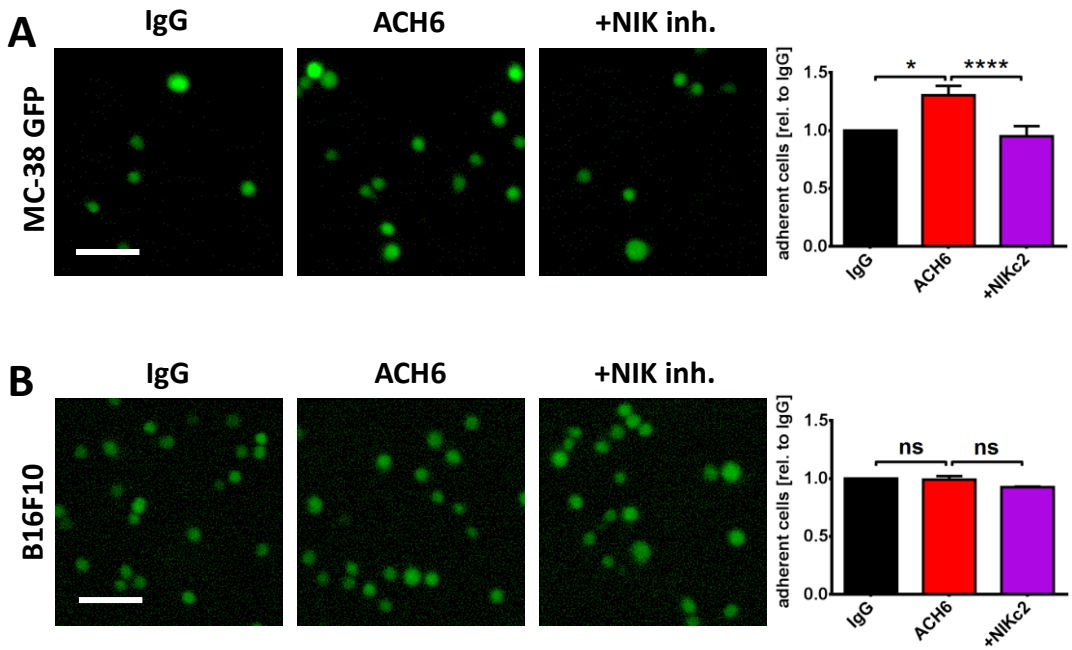

Figure 34: Adhesion of MC-38 GFP and B16F10 tumor cells towards C3H 10T1/2 cells after LTßR agonization
A, B) Representative fluorescence microscopy pictures of adhesion assays showing green stained MC38-GFP **(A)** or B16F10 **(B)** cells adhered to 10T1/2 cells pretreated with IgG or ACH6 with or without NIK inhibitor. 4 (A) or 2 (B) biological replicates were done for all groups. Scale bars are 100µm. Five random pictures were taken per well, adhered cells were counted using ImageJ software and then normalized to IgG control group. Data are expressed as mean + SEM and statistical significance was calculated using Student's t-Test (* $p < 0.05$, **** $p < 0.0001$).

To exclude that the results gained with the NIK inhibitor were caused by experimental artifacts or side-effects from the NIK inhibitor unrelated to LTßR agonization, LTßR or NIK were knocked out in C3H 10T1/2 cells using CRISPR/Cas9 recombination. Adhesion assays using 10T1/2 NIK ko or LTßR ko showed that ACH6 stimulation had no effect anymore on subsequent adhesion of L-CI.5s cells towards these 10T1/2s. In contrast, ACH6 stimulation of 10T1/2 cells transfected with a control construct (PX459) increased adhesion of L-CI.5s compared to IgG treatment (Figure 33A). These effects could be fully recreated using Eµ-myc B-cell lymphoma cells instead of L-CI.5s. LTßR as well as NIK knockout suppressed the ACH6-induced increase in adhesion (Figure 33B) observed in the PX459 control cells, corroborating the crucial role of NIK in mediating LTßR downstream signaling.

The effects of ACH6 and NIK inhibition on adhesion to 10T1/2 cells were completely reproducible using MC-38 GFP colon carcinoma cells (Figure 34A). ACH6 pretreatment of 10T1/2 cells increased subsequent adhesion of MC-38 GFP cells within 30 minutes of seeding by around 35%. This effect was again fully abrogated by adding NIK inhibitor together with ACH6. The murine B16F10 melanoma cell line on the other hand showed no reaction following ACH6 or NIK inhibitor treatment (Figure 34B). Neither ACH6 only nor ACH6 + NIK inhibitor pretreatment of 10T1/2 cells showed a significant change in subsequent adhesion of B16F10 melanoma cells to the 10T1/2 cells when compared to IgG control treated cells. Together these results indicate the importance of NIK in the

downstream transmission of LTßR signaling following LTßR agonization in 10T1/2 and LX-2 cells, and suggest that the effects of LTßR agonization in this model are mediated by NF-kB2 translocation. Furthermore, they show that this mechanism applies to other tumor entities than T-cell lymphoma as well, although not to all.

6.3.3 HSC-derived MMP-9 and MAdCAM-1 affect pro-metastatic downstream effector functions

Gene expression profiling of 10T1/2s, LX-2s and primary HSCs reveals potential downstream effector molecules

To discover potential downstream effector targets that mediate the effects observed after LTßR agonization, several different gene expression analyses were performed using isolated mRNA samples from 10T1/2, LX-2 or isolated primary hepatic stellate cells after LTßR agonization (Figure 35A). Quantitative real-time PCR was performed with 10T1/2 and LX-2 samples, a real-time PCR-based TaqMan LDA assay was done with 10T1/2 and primary stellate cells and RNA sequencing was done with primary hepatic stellate cells from Lrat-TdTomato mice. At this point, not all of the selected genes have been tested with all methods for all samples yet. Genes were selected with respect to their role in HSC activation, fibrosis, cytokine signaling, chemotaxis or adhesion. HSC activation genes showed only small differences in expression in 10T1/2 and LX-2 cells but much more pronounced differences in primary HSCs. As already observed with IHC staining, *Acta2* (a-sma) was not or only marginally upregulated after LTßR stimulation. *Des*, *Vim*, *Edn1* (endothelin-1) and *Lox* were all strongly upregulated in primary HSCs but only marginally or not at all in 10T1/2s or LX-2s. *Myocd* (myocardin) was slightly upregulated in 10T1/2s and LX-2 and not tested in primary HSCs and *Uchl1* was unchanged in 10T1/2s and LX-2s but slightly increased in primary HSCs. *Gfap* was consistently downregulated in 10T1/2s and primary HSCs while *Pparg* showed no significant changes in mRNA expression in either sample group. These results corroborate data shown earlier that LTßR agonization activates HSCs *in vivo*.

Col1a1, in some contrast to data shown earlier, and *Col4a4* were slightly upregulated in primary HSCs but mostly unchanged in cell culture samples. *Fn1* (fibronectin) showed no significant change in expression. *Mmp2* and *Mmp3* showed a slight upregulation in cell culture and in vivo, while *Mmp13* was strongly reduced in primary HSCs and not tested *in vitro*. Surprisingly, *Mmp9* showed a very strong upregulation in all 3 cell types. *Timp1* and *Timp3* showed reduced or unchanged expression *in vitro* and *in vivo*, which fits well to the increased expression of some of their target MMPs. Pro-inflammatory and pro-fibrotic cytokines *Il6*, *Pdgfb* and *Tgfb1* as well as *Pdgfrb* showed only mild changes. *Il6* was consistently slightly upregulated, but *Pdgfb*, *Pdgfrb* and *Tgfb1* were slightly upregulated in some and slightly downregulated in other cases, not allowing for any clear correlation with LTßR stimulation. Together, these results indicate, in line with results shown earlier, that LTßR agonization does not induce a strong pro-fibrotic response in HSC, but a mild at most.

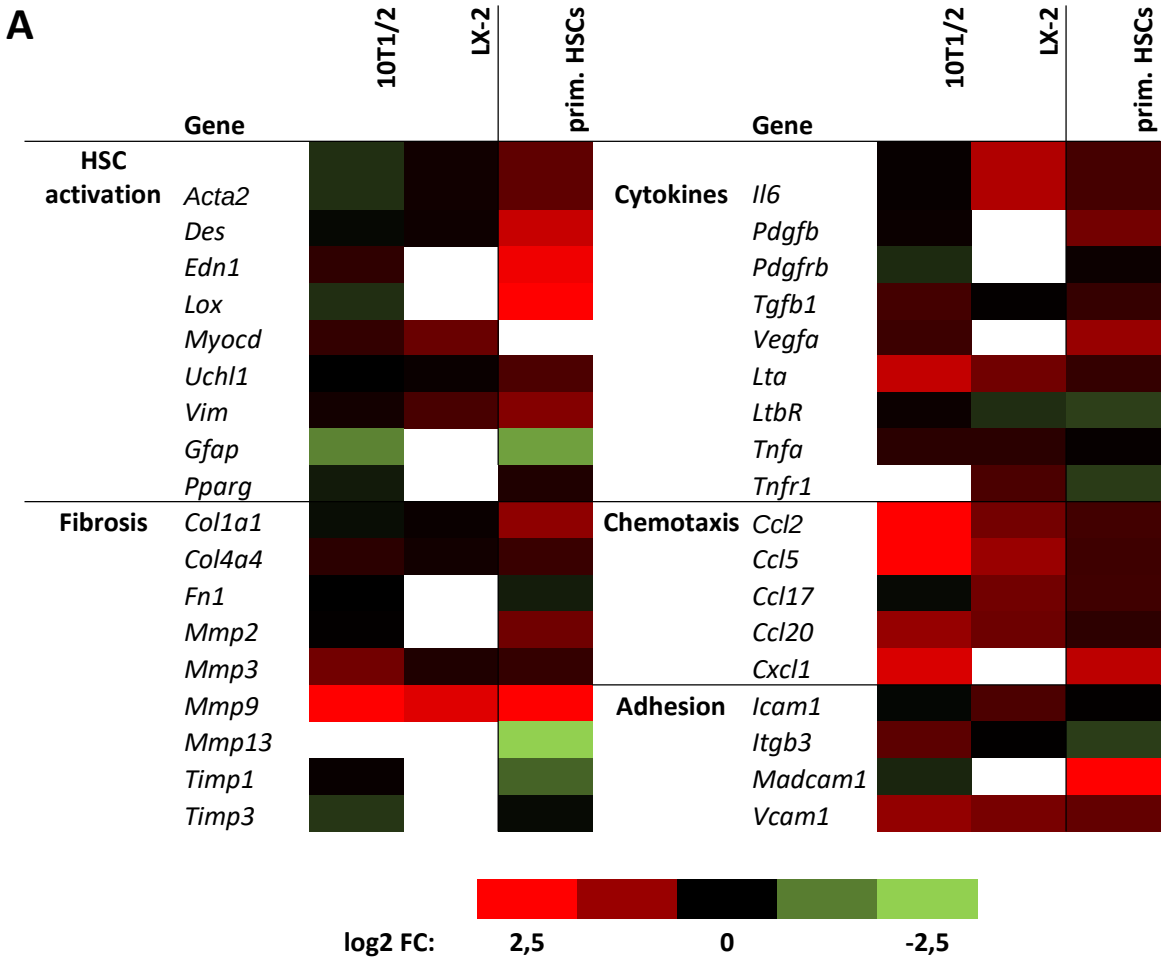

Figure 35: LTßR agonizatioin of C3H 10T1/2 cells, LX-2 cells or hepatic stellate cells in vivo leads to a unique gene expression signature

A) Relative mRNA expression of selected genes as assessed by RT-qPCR (10T1/2, LX-2), TaqMan LDA assay (10T1/2, prim. HSC) or RNA-Seq (prim. HSC) of cell lysates from 10T1/2s, LX-2s or isolated primary HSCs. Results show log2 fold change (log2FC) of cells treated with LTßR agonist (ACH6 or BS-1 (LX-2)) compared to control antibody (IgG or IvIG (LX-2)). mRNA expression was normalized to GAPDH housekeeping gene. Results of RT-qPCR and LDA assay (10T1/2) and LDA assay and RNA-Seq (prim. HSC) were pooled. *RNA Seq was done at the lab of Prof. Robert Schwabe (Columbia University, New York, USA), LDA assay was done by Dr. Nicole Simonavicius, RT-qPCRs, data processing and presentation was done by me.*

Data are expressed as heat map with expression levels being shown as color code with red indicating increased expression, green indicating reduced expression and black indicating unchanged expression. Statistical significance is not indicated.

Vegfa and *Lta* were slightly upregulated in most cases, whereas *Ltbr* was slightly downregulated and *Tnfa* and *Tnfr1* were unchanged. All tested chemokines were upregulated to some degree. *Ccl2* and *Ccl5* were strongly upregulated *in vitro* and to a lesser extent *in vivo*. *Ccl17*, *Ccl20* and *Cxcl1* were slightly upregulated consistently with all used methods. Furthermore, *Icam1*, *Madcam1* and *Vcam1* were upregulated to varying degrees *in vitro* and *in vivo*, supporting immune cell infiltration together with the increase in chemokines. *Itgb3* (integrin-ß3) expression was not chganed significantly. Taken together, these results suggest MMP-9 as a downstream effector molecule of LTßR agonization in

HSCs as it is the strongest and most consistently upregulated gene. Chemokines in general and CCL2 and CCL5 in particular were also substantially upregulated, suggesting immune cell infiltration as part of the mechanism. The consistent upregulation of pro-inflammatory adhesion molecules ICAM-1, VCAM-1 and MAdCAM-1 support this hypothesis. The strong upregulation of MAdCAM-1 *in vivo* was very striking, as MAdCAM-1 is not usually expressed in HSCs.

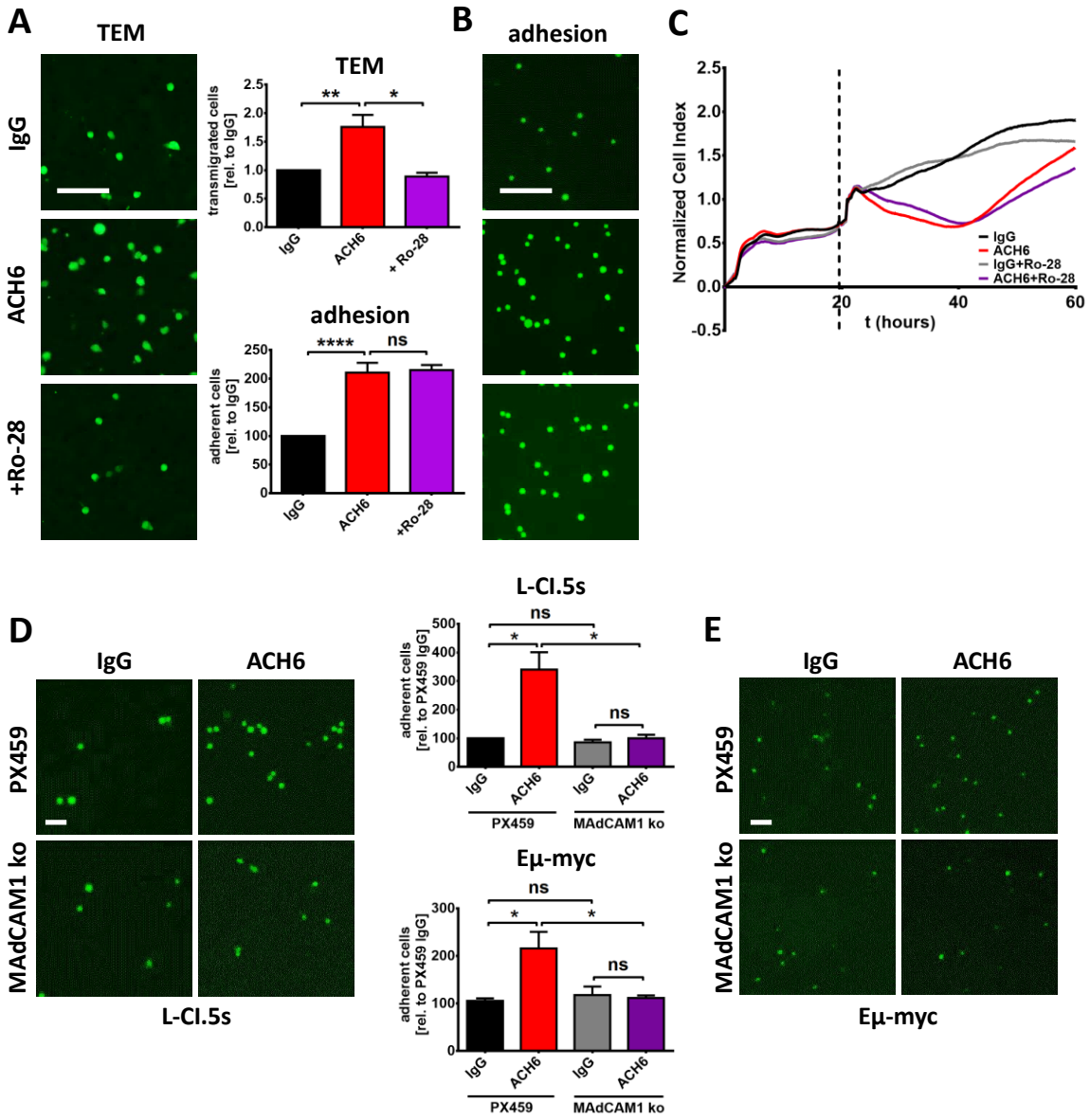

Figure 36: Influence of MMP-9 and MAdCAM-1 on ACH6 induced functional changes of C3H 10T1/2 cells

A) Representative fluorescence microscopy pictures of trans-endothelial migration assays showing green stained L-CI.5s after 24 hours transmigration period through a 10T1/2-HUVEC endothelial layer pretreated with IgG or ACH6 with or without MMP-9 inhibitor (Ro-28). At least 3 biological replicates were done for all groups. Scale bars are 100µm.

B) Representative fluorescence microscopy pictures of adhesion assays showing green stained L-CI.5s adhered to 10T1/2 cells pretreated with IgG or ACH6 with or without MMP-9 inhibitor (Ro-28). At least 3 biological replicates were done for all groups. Scale bars are 100µm.

C) Morphological changes of 10T1/2 cells treated with IgG or ACH6 and with or without MMP-9 inhibitor (Ro-28) as assessed by an xCelligence cell analyzer. Treatments were administered at t=20 hours (dotted line). Cell index was measured every 15 minutes (0-20 hours) or every minute (20-60 hours). At least 3 biological replicates were done for all groups.
D, E) Representative fluorescence microscopy pictures of adhesion assays showing green stained L-CI.5s **(D)** or Eμ-myc cells **(E)** adhered to 10T1/2 PX459 or MAdCAM1 ko cells pretreated with IgG or ACH6. 5 (L-CI.5s) or 4 (Eμ-myc) biological replicates were done for all groups. Scale bars are 100μm.
For all trans-endothelial migration and adhesion assays five random pictures were taken per well, adhered or transmigrated cells were counted using ImageJ software and then normalized to (10T1/2 PX459) IgG control group. Data are expressed as mean + SEM and statistical significance was calculated using Student's t-Test (* $p < 0.05$, ** $p < 0.01$, **** $p < 0.0001$, ns=non-significant).

MMP-9 and MAdCAM-1 affect ACH6 induced functional changes in C3H 10T1/2 cells by increasing adhesion or transmigration of tumor cells

To investigate a possible role of MMP-9 as a downstream effector upon LTßR agonization of HSCs, functional trans-endothelial migration and adhesion assays were performed using the selective MMP inhibitor Ro 28-2653 (Ro-28). Addition of the MMP inhibitor alongside ACH6 in trans-endothelial migration assays completely negated the ACH6-induced increase in transmigration of L-CI.5s through a 10T1/2-HUVEC endothelial layer (Figure 36A). On the other hand, Ro-28 had no effect on adhesion of L-CI.5s to 10T1/2 cells when administered alongside ACH6 to pretreat the 10T1/2 cells (Figure 36B). This result was supported by the fact that MMP inhibitor administration did not affect ACH6-induced morphological changes in C3H 10T1/2 cells, as assessed by an xCelligence cell analyzer (Figure 36C). Taken together, these results support a role for MMP-9 in mediating trans-endothelial migration of L-CI.5s and that the underlying mechanism is not directly dependant on morphological changes or adhesion to HSCs.

To investigate a possible role of MAdCAM-1 as downstream effector after LTßR agonization of HSCs, functional adhesion assays were performed using 10T1/2 cells with CRISPR/Cas9 mediated MAdCAM-1 knockout (MAdCAM1 ko). Indeed, ACH6 pretreatment of 10T1/2 MAdCAM1 ko cells did not increase subsequent adhesion of L-CI.5s compared to IgG treated MAdCAM1 ko cells (Figure 36D). In contrast, 10T1/2 cells transfected with a control construct (PX459) showed a significantly increased adhesion of L-CI.5s after ACH6 pretreatment compared to IgG pretreatment. These results could be fully reproduced using Eμ-myc B-cell lymphoma cells instead of L-CI.5s (Figure 36E), corroborating the effect of MAdCAM-1 knockout on adhesion. Accordingly, these results support a role for MAdCAM-1 as downstream effector after LTßR agonization in HSCs by increasing adhesion of L-CI.5s to HSCs.

6.3.4 ERK1/2 phosphorylation is potentially involved in mediating downstream signals after ACH6 stimulation in C3H 10T1/2 and LX-2 cells

To screen for signaling molecules involved in mediating downstream effects of LTßR agonization in HSCs, a phospho-kinase array (RnD Systems, USA) was performed using protein lysates from 10T1/2 cells treated for four hours with ACH6 or IgG or LX-2 cells treated for four hours with BS-1 or IvIG (Figure 37A). Six proteins showed differences in phosphorylation between ACH6 and IgG treated groups as illustrated by differing densitometric signal instensities. Phosphorylation of ERK-1 and -2 was increased after LTßR agonization in 10T1/2 and LX-2 cells, although the increase was very small between the LX-2 groups. GSK3α/ß, Akt1/2/3, CREB and ß-catenin also showed increased phosphorylation after ACH6 treatment in 10T1/2 cells but showed very little phosphorylation in LX-2 cells with no detectable differences between IvIG and BS-1 treated groups. On the other hand, increased phosphorylation at 3 different sites was detected for p53 in LX-2 cells after LTßR agonization but not in 10T1/2 cells. Taken together, only ERK1/2 showed increased phosphorylation in both 10T1/2 and LX-2 cells. To confirm this result, western blots against phospho-ERK1/2 (p-p44/p-p42) and total ERK1/2 were performed with protein lysates from 10T1/2 (Figure 37B) and LX-2 (Figure 37C) cells treated with LTßR agonist or control antibody. Both LX-2 and 10T1/2 cells showed significantly increased ERK1 and ERK2 phosphorylation relative to total ERK1 or ERK2 after LTßR agonisation. Total ERK1 and ERK2 levels were not increased significantly in 10T1/2 or LX-2 cells.

To confirm the role of ERK1/2 signaling in mediating downstream effects of LTßR agonization in HSCs, functional adhesion assays were performed using a MEK (UO126) or ERK1/2 (SCH77) inhibitor alongside ACH6 (Figure 37D). While ACH6 pretreatment of 10T1/2s again increased subsequent adhesion of L-CI.5s significantly, this effect was significantly reduced when administering MEK or ERK1/2 inhibitor in addition. Administering either inhibitor together with IgG did not have an effect on adhesion. Taken together, these results suggest a possible role for ERK1/2 in mediating downstream signals after LTßR agonisation in HSCs.

6.3.5 FAK but not Paxillin or Rac1 might be involved in mediating LTßR signaling-induced downstream effects

As earlier results in this thesis showed that LTßR agonization of 10T1/2 and LX-2 cells changed their morphology and increased motility, further experiments were performed to evaluate the contribution of morphology- and motility-related proteins FAK, Paxillin and Rac1 towards the downstream effects observed after LTßR agonization in 10T1/2 and LX-2 cells. Protein levels of FAK were not increased after LTßR agonization in 10T1/2 or LX-2 cells, but phosphorylation of tyrosines 576 and 577 was increased relative to total FAK levels in both cell lines after LTßR agonization (Figure 38A, B).

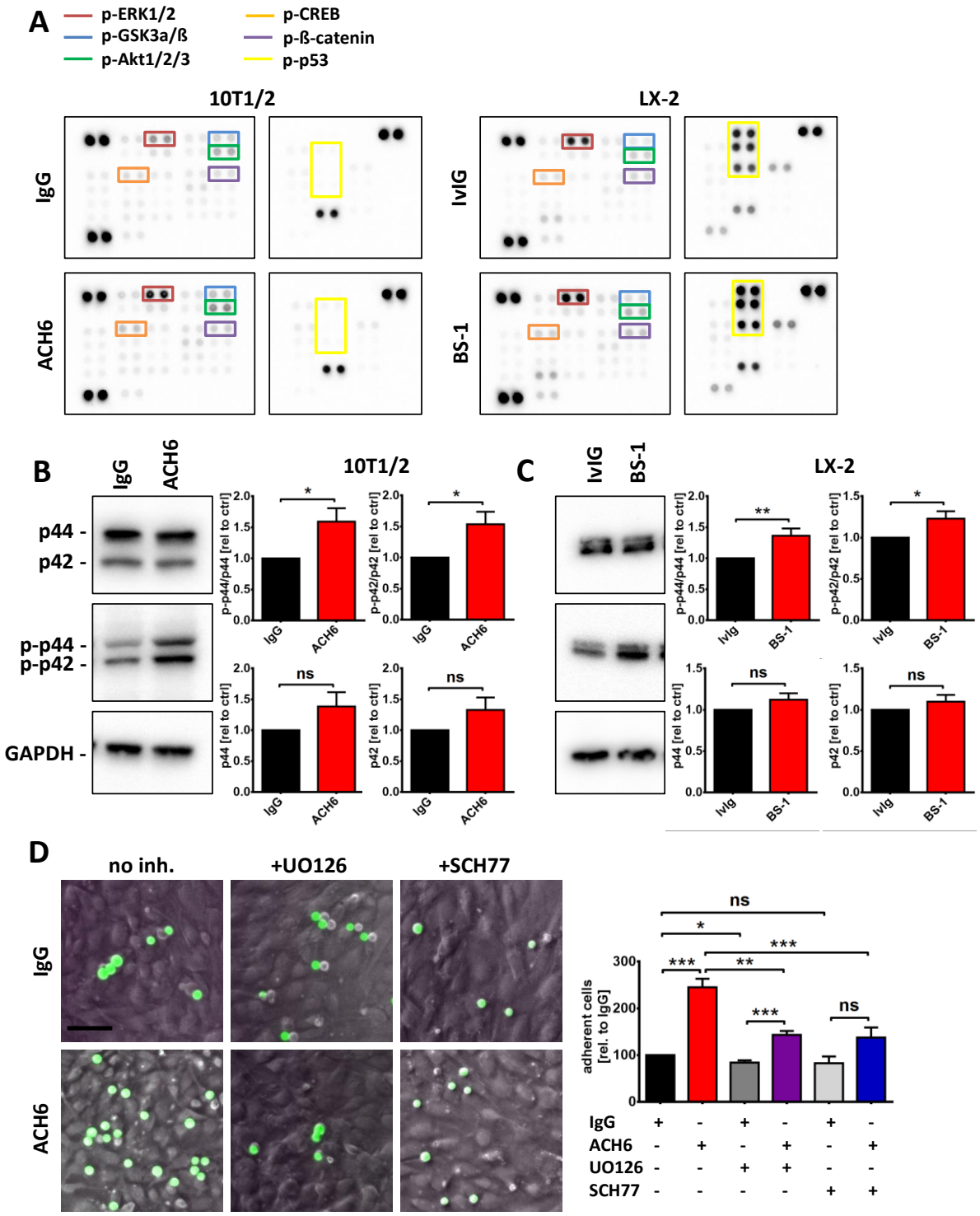

Figure 37: Activation of ERK1/2 may be involved in mediating downstream effects of LTßR agonization in C3H 10T1/2 and LX-2 cells

A) Representative RnD Proteome Profiler phospho-kinase array showing protein phosphorylation of various proteins in 10T1/2 (left) or LX-2 (right) cells treated with IgG and ACH6 (10T1/2) or IvIG or BS-1 (LX-2). Proteins with visible changes in phosphorylation signal strength between groups are highlighted with coloured boxes (see legend). 1 biological replicate was done for all groups.

B, C) Representative immunoblot analysis of p42, p44, phospho-p42 (p-p42), phospho-p44 (p-p44) and GAPDH protein expression in 10T1/2 **(B)** or LX-2 **(C)** cells treated with IgG or ACH6 (10T1/2) or IvIG or BS-1 (LX-2).

Protein expression was assessed densitometrically and normalized to IgG (10T1/2) or IvIG (LX-2) control group. Phospho-protein signals were normalized to respective unphosphorylated protein signals. At least 4 biological replicates were done for all groups.

D) Representative overlays of light and fluorescence microscopy pictures of adhesion assays showing green stained L-CI.5s adhered to 10T1/2 cells pretreated with IgG or ACH6 and with or without MEK (UO126) or ERK1/2 (SCH77) inhibitor. At least 4 biological replicates were done for all groups. Scale bars are 100µm. Five random pictures were taken per well, adhered cells were counted using ImageJ software and then normalized to IgG control group. Data are expressed as mean + SEM and statistical significance was calculated using Student's t-Test (* $p < 0.05$, ** $p < 0.01$, *** $p < 0.001$, ns=non-significant).

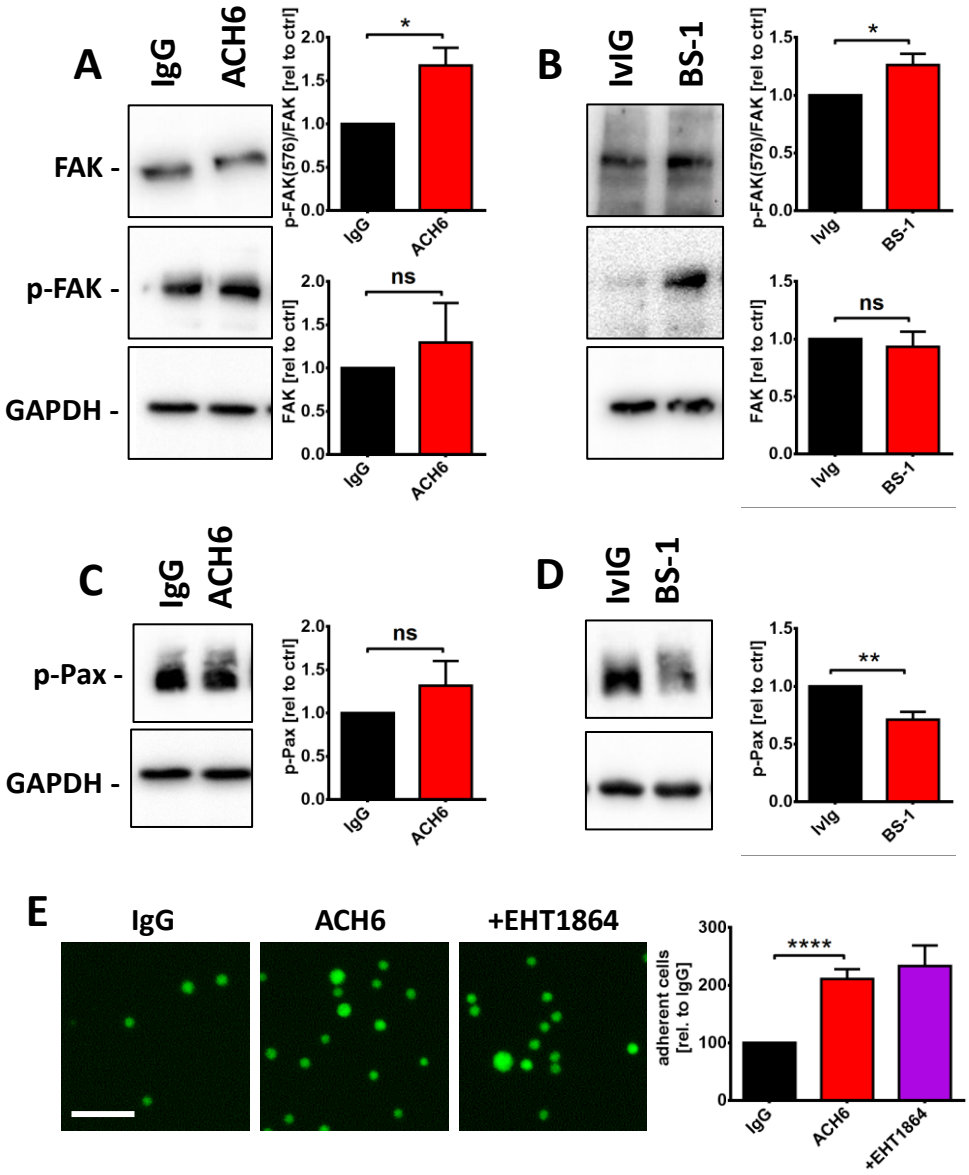

Figure 38: Influence of migration related proteins FAK, Pax and Rac1 on LTßR agonization induced functional changes in C3H 10T1/2 or LX-2 cells

A-D) Representative immunoblot analysis of FAK, phospho-FAK (p-FAK) and GAPDH **(A, B)** or phospho-pax (p-pax) and GAPDH **(C, D)** protein expression in 10T1/2 **(A, C)** or LX-2 **(B, D)** cells treated with IgG and ACH6 (10T1/2) or IvIG or BS-1 (LX-2). Protein expression was assessed densitometrically and normalized to IgG (10T1/2) or IvIG (LX-2) control group. Phospho-protein signals were normalized to respective unphosphorylated protein signals. At least 3 biological replicates were done for all groups.

E) Representative fluorescence microscopy pictures of adhesion assays showing green stained L-CI.5s adhered to 10T1/2 cells pretreated with IgG or ACH6 with or without Rac1 (EHT1864) inhibitor. At least 4 biological replicates were done for all groups. Scale bars are 100µm. Five random pictures were taken per well, adhered cells were counted using ImageJ software and then normalized to IgG control group.
Data are expressed as mean + SEM and statistical significance was calculated using Student's t-Test (* $p < 0.05$, ** $p < 0.01$, **** $p < 0.0001$, ns=non-significant).

Phosphorylated paxillin levels were reduced in LX-2 (Figure 38D) cells following LTßR agonization but were unchanged in 10T1/2s (Figure 38C). Rac1 effects were tested using the Rac1 inhibitor EHT1864 (Selleckchem). Rac1 inhibition had no effect on adhesion of L-CI.5s to 10T1/2 cells when administered together with ACH6 to pretreat 10T1/2 cells (Figure 38E). These results, although far from being complete, hint at a possible role for FAK in mediating LTßR-induced effects downstream.

6.3.6 ACH6-induced LTßR signaling leads to capillarization of sinusoidal endothelium in the liver

Capillarization of sinusoidal endothelium is a common feature of chronic liver damage[436]. As HSCs interact very closely with LSECs in the liver sinusoids, experiments were performed to investigate changes in LSECs after ACH6 treatment in mice (Figure 39). The classical endothelial marker CD31 was significantly increased after 2 weeks of ACH6 treatment on immunohistochemical level, indicating a transition from the highly specialized sinusoidal endothelium to normal endothelium. This was corroborated by a concomitant increase in collagen-IV staining, suggesting an increase in basement membrane, which is a feature of capillarized but not sinusoidal endothelium (Figure 39B). Furthermore, an increase in ICAM-1 and VCAM-1 staining was observed in 2 weeks ACH6-treated mice. While both adhesion molecules were also upregulated in HSCs (Figure 35A), the increase observed in immunohistochemical stainings (Figure 39A) was much more pronounced, especially in the case of ICAM-1. Lastly, to visualize the structure of sinusoidal endothelium after 2 weeks of ACH6 treatment, electron microscopic images of liver sinusoids from 2 weeks ACH6-treated mice were acquired in collaboration with the group of Prof. Marco Prinz (Universitätsklinik Freiburg, Germany) (Figure 39C). While IgG-treated mice showed the distinct fenestrated endothelium of a healthy liver, no fenestrations could be observed in the mice treated with ACH6 for 2 weeks, indicating a capillarization of the sinusoidal endothelium. Taken together, these results suggest that LTßR agonization in mice also changes morphology and function of LSECs.

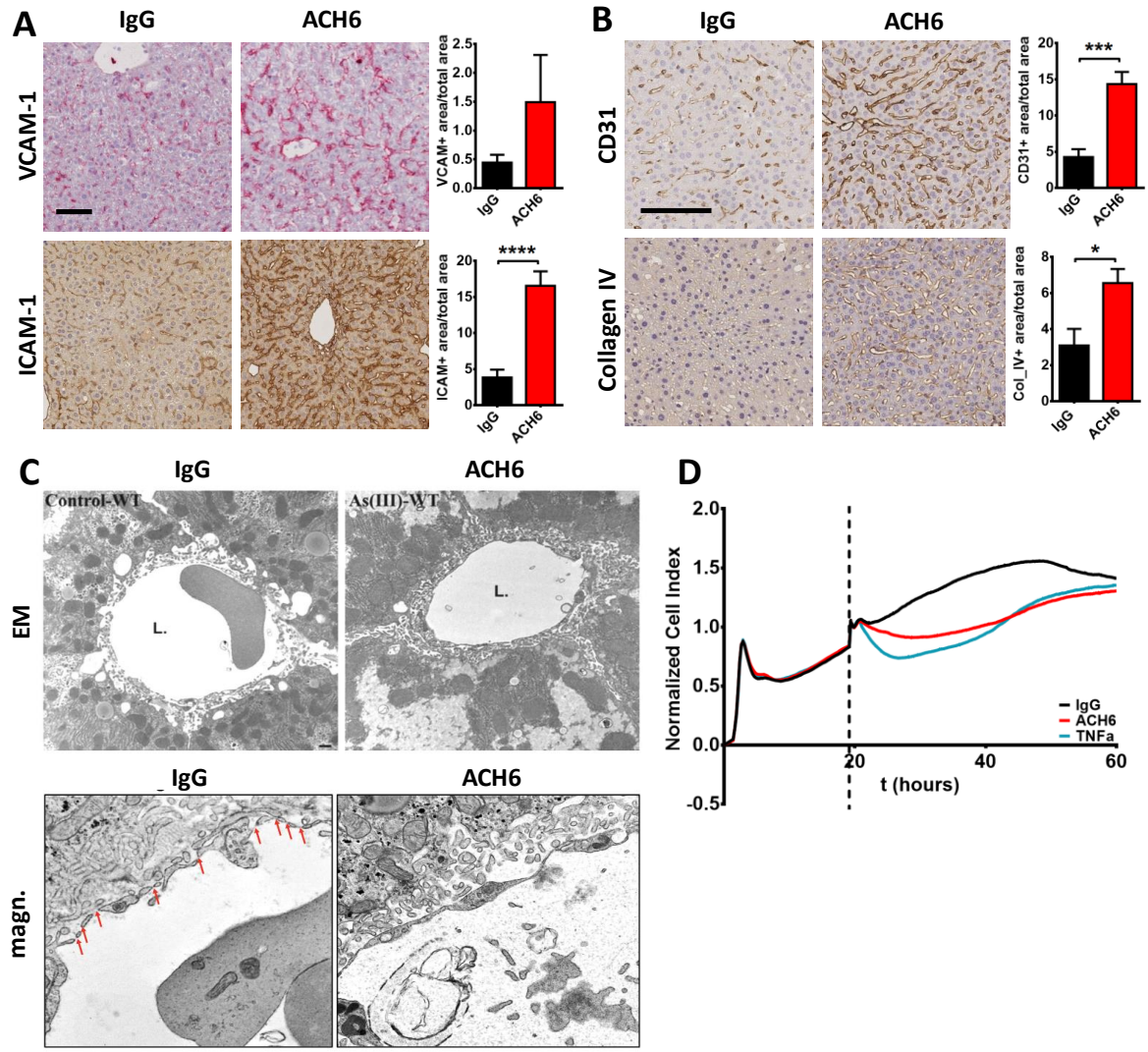

Figure 39: LTßR agonization leads to capillarization of liver sinusoidal endothelium in mice

A, B) Representative immunohistochemical pictures of VCAM-1 or ICAM-1 **(A)** or CD31 or collagen-IV **(B)** stainings of paraffin- (ICAM-1, CD31, collagen-IV) or cryo-embedded (VCAM-1) liver samples from DBA/2 mice pretreated with ACH6 or IgG for 14 days, injected with L-CI.5s cells and sacrificed 7 days later. Stained area was assessed by histological software (DIH) and normalized to total area analyzed. Sample size is n≥3 for all groups. Scale bars are 100µm.

C) Representative electron microscopic pictures from liver samples of DBA/2 mice treated with IgG or ACH6 for 14 days. Pictures show cross-sections of liver sinusoids. Fenestrae are indicated by red arrows. *Electron microscopy and pictures were done by the lab of Prof. Marco Prinz (University of Freiburg, Germany).*

D) Morphological changes of 10T1/2 cells treated with IgG, ACH6 or TNFα as assessed by an xCelligence cell analyzer. Treatments were administered at t=19 hours (dotted line). Cell index was measured every 15 minutes (0-19 hours) or every minute (19-60 hours). At least 3 biological replicates were done for all groups.

Data are expressed as mean + SEM and statistical significance was calculated using Student's t-Test (* $p < 0.05$, *** $p < 0.001$, **** $p < 0.0001$).

7. Discussion

Distant organ metastasis is responsible for the vast majority of cancer-related deaths. The liver is one of the organs most commonly affected by metastasis, and most hepatic malignancies are metastases and not primary hepatic cancers[437]. Still, therapeutic options for distant organ metastasis are very limited[90,95,231,232], owing in part to the fact that the underlying molecular and cellular mechanisms are still unclear. Here, evidence is presented that hepatic stellate cell-specific LTßR signaling is supporting metastatic spread of lymphoma and other tumor cells to the liver. The presented database research indicates that LT overexpression can be found in several human primary tumor entities with correlation to decreased overall patient survival in some of these, like AML and uveal melanoma. This is also supported by results from other groups showing that increased LT expression increases tumor incidence and disease severity in liver[60], lung[357], bladder[358], prostate[361] and endometrial[359] cancer and also in multiple myeloma[363] and leukemia[360]. Unfortunately, while a large amount of database research can be done on primary malignancies, the data available for metastatic cancers is virtually non-existent. Nevertheless, experimental data from human samples in this manuscript show that LT expression is significantly higher in secondary lymphoma manifestations in the liver than in primary manifestations. Even though the term “metastasis” is not used for lymphomas in a clinical setting, secondary lymphoma manifestations have much in common with metastasis, as both represent the spread of tumor cells from a primary to a secondary site. Therefore, the fact that LT is highly expressed or overexpressed in a variety of cancers, and the fact that the results in this thesis show LT expression correlates with secondary spread to the liver, suggests that LT can support metastatic spread of tumor cells to the liver. Although very few results have been published on the role of LTßR signaling in tumor metastasis, there is published evidence that LTßR signaling may support lymph node metastasis[438] and homing of T-cell leukemia cells to the bone marrow[366]. This is also supported by the finding that overexpression of LTs in some primary tumor entities (uveal melanoma, AML) correlates with decreased patient survival. Provided LT overexpression facilitates metastatic spread to the liver, overexpression of LT in the primary site would decrease patient survival by increasing the risk of hepatic metastasis. Taken together, the presented data supports the hypothesis that LT signaling is involved in hepatic metastasis in human cancer patients, but only by correlative means, not by clear causative evidence.

To investigate the role of lymphotoxins in hepatic metastasis, a murine T-cell lymphoma line (L.CI-5s) is successfully used as a model. As lymphoma cells, they express high levels of LTα and LTß and evidence is presented that these cells colonize the liver after intravenous injection into the tail vein, making them a very suitable model for this thesis. Using this model it is shown that lymphotoxin expression is closely correlated to the amount of lymphoma manifestations in the liver after tail vein injection. This holds true for increased

but also decreased tumor cell-derived lymphotoxin expression, and similar results were obtained when triggering LTßR signaling by means of agonizing antibodies and host-derived LTαß. These results not only support the hypothesis that LT facilitates hepatic metastasis formation, but also show that the source of LT does not affect the outcome. This finding is meaningful from a clinical perspective, as increased LT levels can be readily provided by host cells in a plethora of conditions, like inflammatory disorders or infections. It gains even more relevance in light of the findings that the same phenotype can be observed using B-cell lymphoma or even colon carcinoma cells, and that it also applies to the spontaneous formation of liver metastasis from insulinomas in Rip-Tag2 mice.

Furthermore, increased hepatic metastasis is not only observed after 7 days, but also increased seeding of tumor cells in the liver after 24h. The differences between the treated and control groups are very similar at both time points in the same experimental setting, indicating that the pro-metastatic effect of LT in the liver acts on the early steps of liver infiltration, such as extravasation and seeding. The data from in vitro XTT assays and ki67 stainings from murine liver samples show that LT is not involved in metastatic outgrowth and tumor cell proliferation in a significant manner in this model, although its direct effect on cell proliferation has been shown to promote tumor growth in nasopharyngeal cancer, multiple myeloma, castration-resistant prostate cancer and leukemia, amongst others[360–363]. Whether LT acts directly during tumor cell extravasation and seeding or is involved in creating a favourable niche even before the tumor cells enter the liver cannot be deduced from these results. The short timeframe that tumor cells injected via tail vein spend in the circulation and the fact that differences in tumor cell-derived lymphotoxin have a significant effect on hepatic metastasis formation suggests a direct effect. On the other hand, it is perfectly possible that the effect occurs only after the tumor cells have left the circulation and supports tumor cell migration and survival within the postendothelial space of Disse and the liver parenchyma, arguing in favor of LTs supporting metastatic niche formation. Interestingly, no difference in the number of metastatic foci was detected when co-injecting low and high LT-expressing L-CI.5s lymphoma cells. This, alongside the data from our ACH6 and Alb-LTαß experiments shows that LT can also act in trans, allowing the possibility that the phenotype is triggered by a small subset of disseminated tumor cells with high LT expression.

In the second part of the project evidence is provided that LT, regardless of the source is first integrated by hepatic stellate cells in this model. However, the lack of an experimental metastasis assay after clodronate treatment leaves the possibility that Kupffer cells can also contribute to the mechanism by integrating LT signals. On the other hand, the strong inhibition (80-90%) of ACH6-induced hepatic metastasis formation in GFAP-Cre LTßR floxed or NG2-Cre LTßR floxed mice compared to their wild-type littermate controls suggest that hepatic stellate cells are the most important LT-responsive cells in this model. Previous studies have shown that activated hepatic stellate cells may support the formation of a favourable niche through immune cell recruitment[263,264], angiogenesis[265] and tumor cell

invasion through regulation and expression of MMPs and TIMPs[15,256]. Here, an activation of hepatic stellate cells following increased LTßR agonization in HSCs is shown as well, with increased expression of HSC activation markers like desmin, vimentin, endothelin-1 and Lox, and decreased expression of quiescence marker GFAP. Surprisingly, the activation did not entail a strong upregulation of fibrogenic genes, as the classical activation model would predict. *Acta2*, *col1a1* and *col4a4* were only marginally upregulated *in vivo* and unchanged *in vitro*. Other important pro-fibrotic markers like *Timp1* and *Mmp13* were not upregulated, or even downregulated. This was also confirmed with immunohistochemical stainings against a-sma and collagen (Sirius Red), which showed no significant amount of staining at all, especially when compared to fibrotic livers from mice with NASH. Furthermore, the HSC-activating pro-fibrotic cytokines TGFß1 and PDGFß as well as the PDGFRß, which are also produced by HSCs during fibrosis to fuel the self-perpetuating vicious cycle of HSC activation, are not consistently increased. These results suggest that LTßR agonization in hepatic stellate cells leads to an activation of HSCs without induction of fibrosis. While these findings are not supported by the classical model of HSC activation, similar results where presented by Ruddell *et al.* already in 2009[353] showing that LTß had no effect on HSC expression levels of *Acta2*, *Timp1*, *Tgfß1* or *col1a1*.

The finding that LTßR mediates LT-induced downstream effects in HSCs implies that membrane-bound $LT\alpha_1ß_2$ and not secreted $LT\alpha_3$ is important for the observed phenotype. Therefore, the signaling requires cell-cell contact between LT-expressing tumor cells and LTßR-expressing HSCs. Thus, signaling from the primary site in the context of pre-metastatic niche formation is unlikely to play a role. This fits to the observation that LT expression in human patients is higher in secondary compared to primary tumor sites. However, as disseminated tumor cells are constantly shedded from the primary site, and early CTCs could induce LTßR signaling in HSCs via cell-cell contact to initiate the crucial changes in the sinusoidal microenvironment needed for later CTCs to metastasize successfully, metastatic niche formation is still a possible mechanism. On the other hand, we observe clear differences in experimental metastasis between LT overexpressing, LT knockdown and parental tumor cells without preconditioning the mice. In this model all tumor cells are injected into the blood stream simultaneously, so the timeframe in which the critical changes are bound to happen has to be quite short. Another option is that direct and indirect (preconditioning, PMN) effects both support hepatic metastasis formation, independent from another. Interestingly, a preliminary xCelligence experiment with 10T1/2 cells suggests that TNFα stimulation can induce similar morphologic changes as ACH6, indicating that TNFR signaling, and thus $LT\alpha_3$ as well, might be involved in an alternative route.

The *in vitro* assays shown in this thesis were performed using murine C3H 10T1/2 or human LX-2 cells as surrogates for primary HSCs. While LX-2 cells are derived from a spontaneously immortalized human HSC line[433], C3H 10T1/2 are murine embryonic fibroblasts. Nontheless, both cell lines display several features of activated stellate cells after LTßR agonization.

These include morphologic changes like increased eccentricity and decreased size, but also increased contractility and migration. These are all features of activated HSCs and myofibroblast-like cells. On a transcriptional level, the response to LTßR agonization of many genes involved in HSC activation was much more attenuated compared to the results from primary HSCs. The reason for that could be the well-known auto-activation that many cells undergo when seeded on plastic. This auto-activation might well interfere with LTßR-mediated activation by already triggering the upregulation of some of the LTßR target genes. Nontheless, gene expression levels in general were quite comparable between 10T1/2, LX-2 and primary HSCs. This, together with the similarities in morphological and functional changes, indicates that both cell lines can serve as suitable surrogates for primary HSCs in cell culture experiments.

At this point we know that LTs and LTßR signaling support metastatic spread of tumor cells to the liver and that this happens through an alternative, non-fibrotic activation of HSCs. Still, the question remains how HSC-specific LTßR signaling actually supports hepatic metastasis formation on a cellular and molecular level. In this thesis, data is provided supporting several different modes of action, although in the end, none can be proven completely within the scope of this thesis.

LTßR most prominently signals via the non-canonical NF-kB signaling pathway, activating NIK and NF-kB2/RelB. Here, NF-kB2 (p100) processing and phospho-RelB translocation into the nucleus are observed *in vitro*, suggesting that downstream effects are dependent on non-canonical NF-kB signaling. This is further corroborated by the fact that NIK inhibition almost completely negates all morphological and functional changes induced by LTßR agonization *in vitro*, showing that NIK activation is critical for mediating downstream effects. Further results in this manuscript suggest an involvement of MAPK/ERK signaling in mediating downstream effects. Phosphorylation of ERK1/2 is consistently observed after LTßR agonization, and blocking MEK (MAP2K) or ERK1/2 attenuates functional changes after LTßR agonization. Other studies have already shown that ERK1/2 can be activated downstream of NF-kB[439]. Furthermore, its central role in controlling cell proliferation and cell death[440] make it a likely candidate in activated hepatic stellate cells, as proliferation is one of the key features of activated HSCs. Nonetheless, these results only show a correlation between LTßR signaling and ERK1/2 activation, and ERK1/2 activation and downstream effects. This is no direct proof of causation, and so the possibility remains that ERK1/2 activation is not required for mediating downstream effects of LTßR agonization, but is rather involved in a parallel pathway. This might seem unlikely, but it is important to keep in mind that only one downstream effect (adhesion) was tested, and that the central role of the MEK-ERK signaling pathway in many cellular mechanisms makes it hard to exclude side-effects when evaluating its effects using inhibitors.

The increased activation of focal adhesion kinase that we observe after LTßR agonization might be involved in mediating downstream effects, or be involved in effector functions

itself, as FAK plays a role in morphologic changes. The data set presented in this manuscript does not allow a more detailed analysis, and more experiments would be needed to understand how FAK activation is involved in the processes we observe or if it is only a side-effect.

A very interesting result is the strong upregulation of *Madcam1* in hepatic stellate cells after LTßR agonization. Historically, MAdCAM-1 is known for its role in the recruitment of integrin-$\alpha_4ß_7$ expressing lymphocytes to the gut. More recently its expression has been discovered in HEVs during lymphoid organ neogenesis[335] and in chronically inflamed liver endothelium as well[441,442]. Expression of MAdCAM-1 on HEVs is regulated by LTs during this process[330,335], indicating that MAdCAM-1 can be activated by NF-kB signaling. This is supported by the data from the adhesion assays shown here, which indicate a consistent and significant increase of adhesion from lymphoma cells to 10T1/2 cells after LTßR stimulation. This increase in adhesion is abgrogated when MAdCAM-1 is knocked out in 10T1/2 cells, just as it is abrogated when LTßR or NIK are knocked out or inhibited, indicating that MAdCAM-1 could be one of the effector molecules downstream of the LTßR-NF-kB2 pathway responsible for the increased adhesion. As the main function of MAdCAM-1 is the binding of lymphocytes, it is well conceivable that an increase in MAdCAM-1 expression may help lymphoma cells or other integrin-$\alpha_4ß_7$ expressing cells to infiltrate the liver by facilitating their adhesion to the vessel wall. Here however, expression is observed in hepatic stellate cells and not in endothelial cells. Nonetheless, it is possible that increased MAdCAM-1 expression on hepatic stellate cells within the subendothelial space of Disse can increase retention of extravasated tumor cells by preventing their re-entry into the circulation. As intra- and extravasation are less of an obstacle in the fenestrated endothelium of the liver sinusoids, such a retention mechanism might be a large advantage for the tumor cells. The perivascular space not only protects DTCs from shear stress and immune surveillance, but it has recently emerged as an important niche often found to support DTCs and metastasis[177,443].

Another interesting result is the strong upregulation of *Mmp9* in hepatic stellate cells after LTßR agonization. The ability of HSCs to express significant amounts of MMP-9 in the liver besides macrophages and Kupffer cells has already been described in other studies[133,444]. However, the role of MMP-9 in liver fibrosis or indeed in fibrosis in general is not clear yet. No difference in fibrosis was observed in this thesis despite the strong increase in MMP-9. This is in line with other studies showing that MMP-$9^{-/-}$ mice have reduced fibrosis in the kidney, presumably due to reduced a-sma expression and reduced myofibroblast activation[445], but show no change in fibrosis in the liver or lung[446,447]. Its ability to activate latent TGFß1 has pro-fibrotic effects[448,449], but other studies show that MMP-9 overexpression attenuates fibrosis in the lung[450], and Kupffer cell-derived MMP-9 supports fibrosis resolution in the liver[451]. MMP-9 supports HSC transdifferentiation[452] but also HSC apoptosis[453] thus supporting both fibrosis initiation and resolution. Multiple studies have highlighted the role of MMP-9 in chemokine activation and lymphocyte influx in the lung

and liver[454–456]. Furthermore, several studies show its role in supporting metastatic spread of tumor cells to the lung[164] by inducing vascular remodeling[299]. This thesis shows that MMP-9 increases tumor cell trans-endothelial migration *in vitro* on one hand, but has no impact on adhesion of tumor cells to 10T1/2 cells *in vitro* on the other hand. This implies, that while MMP-9 has a potential effect on hepatic metastasis formation, it acts via a mechanism different from the one proposed for MAdCAM-1. One possibility is that MMP-9 induces changes in endothelial cells that promote increased tumor cell trans-endothelial migration. LSECs, just as HSCs, are very reactive to the surrounding ECM and ECM remodeling, which is known to affect LSEC differentiation[457]. Here, data is presented that indicates LTßR agonization leads to transdifferentiation and capillarization of LSECs. Capillarization is a well-established mechanism in chronic liver injury and usually preceeds fibrosis. As LT signaling is first integrated by HSCs and not LSECs in the models presented here, the changes in LSECs that affect tumor metastasis would have to be mediated by HSCs. This is also supported by the results of the transmigration assays shown here, where the effect of ACH6 treatment is only observed when using a HUVEC-10T1/2 layer but not with HUVECs alone. MMP-9 is a likely candidate to induce the observed LSEC capillarization, as it would also explain the results from the *in vitro* experiments, where MMP-9 inhibition only influences the EC containing trans-endothelial migration assay but not the adhesion assay, as no ECs are used in the latter.

Capillarization could facilitate tumor cell metastasis in various ways. While loss of fenestrations makes extravasation arguably more difficult for tumor cells, it also makes it more difficult for tumor cells to intravasate back across the endothelial barrier. Furthermore, the transdifferentiation of LSECs during capillarization changes their gene expression signature. This also affects adhesion molecules, whose presence can be critical for tumor cell survival and extravasation. A four- to five-fold increase of VCAM-1 and ICAM-1 in liver sinusoids after LTßR agonization is reported here using immunohistochemical stainings. This increase is only partially reflected by the marginal increase of *Icam1* and the two- to three-fold increase of *Vcam1* we observe in HSCs on the transcriptional level. Therefore, it is likely that ICAM-1 and VCAM-1 are also upregulated in endothelial cells. Both molecules are known to be constantly expressed on LSECs and upregulated under inflammatory conditions[458–460]. Furthermore, both are important mediators of trans-endothelial migration of leukocytes, and their expression on LSECs has been correlated with liver metastasis[458–460]. In summary, a possible mechanism based on the data we have could be the following: LTßR signaling in HSCs induces expression and secretion of MMP-9, the secreted MMP-9 induces a remodeling of the ECM in the space of Disse, triggering integrin-mediated transdifferentiation and capillarization of LSECs. Capillarized LSECs increase expression of ICAM-1 and VCAM-1, amongst others, thereby facilitating tumor cell attachment, adhesion and transmigration, while the loss of fenestrations makes re-entry of tumor cells into the circulation more difficult.

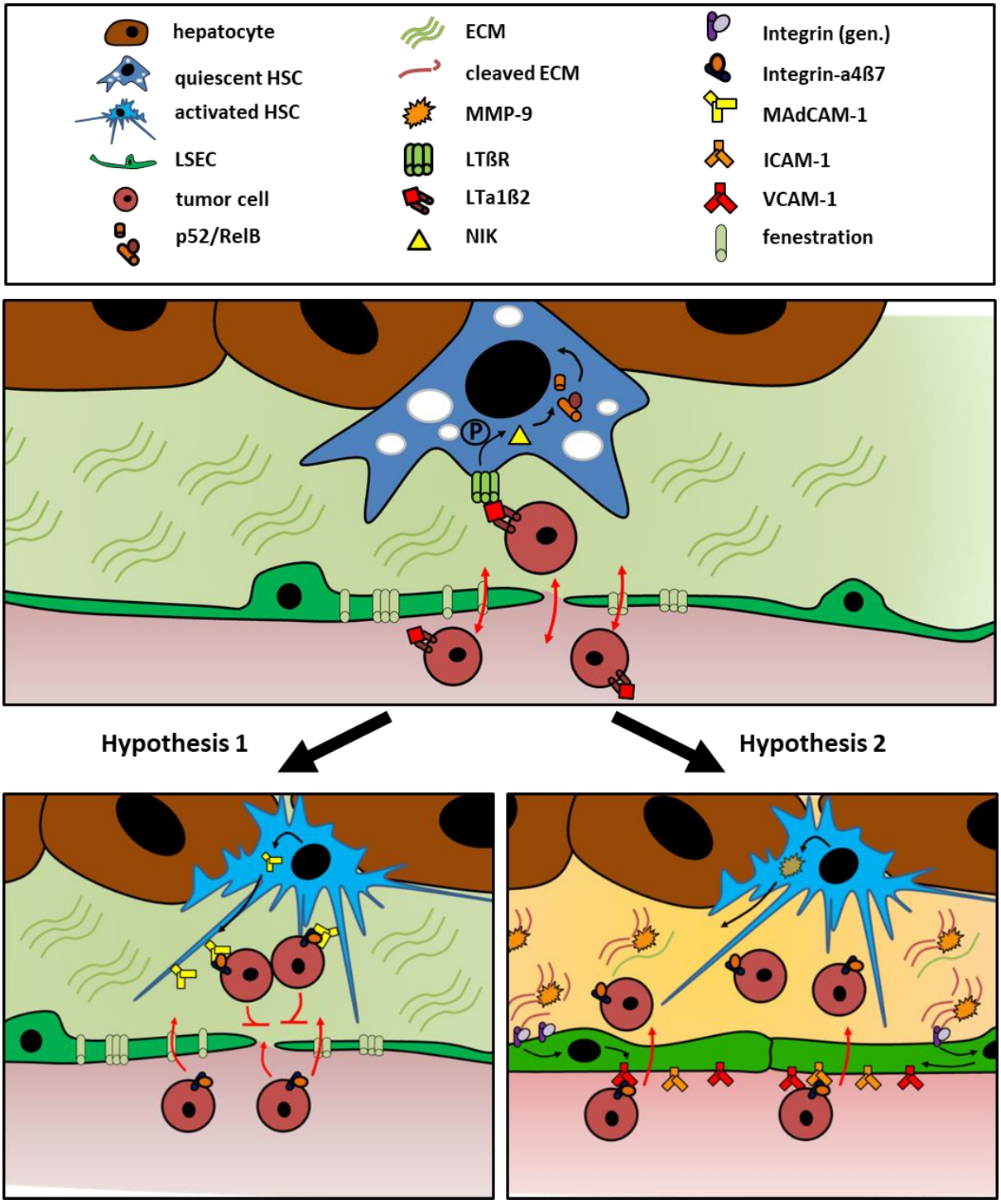

Figure 40: Possible mechanisms for increased hepatic metastasis after HSC-specific LTßR agonization
Two possible molecular mechanisms are conceivable and supported by the data shown in this manuscript.
Top schematic: Tumor cell derived LTα1ß2 binds to HSC expressed LTßR, activating NIK and NF-kB2/RelB. NF-kB2/RelB translocates into the nucleus
Hypothesis 1: NF-kB2/RelB translocation activates HSCs leading to a strong upregulation of MAdCAM-1. MAdCAM-1 retains extravasated tumor cells in the space of Disse preventing them from re-entering the circulation.
Hypothesis 2: NF-kB2/RelB translocation activates HSCs leading to a strong upregulation of MMP-9. MMP-9 remodels the ECM in the space of Disse, which leads to integrin-mediated transdifferentiation and

capillarization of LSECs with increased expression of adhesion molecules, facilitating tumor cell attachment and adhesion and thus subsequent extravasation as well.

Another interesting path to explore would follow the increased expression of chemokines observed after LTßR agonization. A strong increase of CCL-2 and CCL-5 and more moderate increases in CXCL-1, CCL-20 and CCL-17 are shown here. All of these chemokines have the potential to increase tumor cell metastasis in several ways, by supporting tumor cell homing and retention or by inducing immune cell infiltration and niche formation. However, without further experiments no conclusive remarks can be made on their role here.

In conclusion, this thesis shows that LT-LTßR signaling supports tumor cell metastasis to the liver for several different tumor entities in humans and in mice. Furthermore, it shows that hepatic stellate cell-specific LTßR signaling is most important to integrate LT and provide downstream effects. Interfering with HSC-specific LTßR signaling or reducing LT in the system reduces metastatic spread to the liver, making LTßR a potential target for therapeutic intervention. HSCs get activated in a non-fibrotic manner upon LTßR stimulation with subsequent transdifferentiation to a myofibroblast-like phenotype. Potential molecular mechanisms that would explain increased hepatic metastasis formation include MAdCAM-1-mediated tumor cell retention in the space of Disse, MMP-9-mediated transdifferentiation and capillarization of LSECs and chemokine-chemokine receptor interactions. These options open up exciting opportunities for further research on these mechanisms.

References:

1. Bray F, Ferlay J, Soerjomataram I, Siegel RL, Torre LA, Jemal A. Global cancer statistics 2018: GLOBOCAN estimates of incidence and mortality worldwide for 36 cancers in 185 countries. *CA Cancer J Clin*. September 2018. doi:10.3322/caac.21492

2. Momin BR, Pinheiro PS, Carreira H, Li C, Weir HK. Liver cancer survival in the United States by race and stage (2001-2009): Findings from the CONCORD-2 study. *Cancer*. 2017;123:5059-5078. doi:10.1002/cncr.30820

3. Ahmed I, Lobo DN. Malignant tumours of the liver. *Surg*. 2009;27(1):30-37. doi:10.1016/j.mpsur.2008.12.005

4. Yokoyama I, Todo S, Iwatsuki S, Starzl TE, Iwatsuki S. Liver transplantation in the treatment of primary liver cancer. *Hepatogastroenterology*. 1990;37(2):188-193. http://www.ncbi.nlm.nih.gov/pubmed/2160421. Accessed May 4, 2019.

5. Bosch F, Ribes J, Borràs J. Epidemiology of Primary Liver Cancer. *Semin Liver Dis*. 1999;19(03):271-285. doi:10.1055/s-2007-1007117

6. Zhang Y, Ren J-S, Shi J-F, et al. International trends in primary liver cancer incidence from 1973 to 2007. *BMC Cancer*. 2015;15(1):94. doi:10.1186/s12885-015-1113-4

7. Marengo A, Rosso C, Bugianesi E. Liver Cancer: Connections with Obesity, Fatty Liver, and Cirrhosis. *Annu Rev Med*. 2016;67(1):103-117. doi:10.1146/annurev-med-090514-013832

8. Alison MR, Lin W-R. Hepatocyte turnover and regeneration: Virtually a virtuoso performance. Kowdley K, McCaughan G, Trautwein C, eds. *Hepatology*. 2011;53(4):1393-1396. doi:10.1002/hep.24252

9. Higgins G, Anderson R. Experimental pathology of liver: restoration of liver in white rat following partial surgical removal. January 1931. https://www.scienceopen.com/document?vid=57858414-5eff-4c8d-a028-ccb3fc1c44a6. Accessed October 27, 2018.

10. Blachier M, Leleu H, Peck-Radosavljevic M, Valla D-C, Roudot-Thoraval F. *The Burden of Liver Disease in Europe*.; 2013. http://www.easl.eu/medias/EASLimg/Discover/EU/54ae845caec619f_file.pdf. Accessed October 27, 2018.

11. Marrone G, Shah VH, Gracia-Sancho J. Sinusoidal communication in liver fibrosis and regeneration. *J Hepatol*. 2016;65(3):608-617. doi:10.1016/j.jhep.2016.04.018

12. Frevert U, Engelmann S, Zougbédé S, et al. Intravital Observation of Plasmodium berghei Sporozoite Infection of the Liver. Egwang T, ed. *PLoS Biol*. 2005;3(6):e192. doi:10.1371/journal.pbio.0030192

13. Braet F, Wisse E. Structural and functional aspects of liver sinusoidal endothelial cell fenestrae: a review. *Comp Hepatol*. 2002;1(1):1. doi:10.1186/1476-5926-1-1

14. Friedman SL, Roll FJ, Boyles J, Bissell DM. Hepatic lipocytes: the principal collagen-producing cells of normal rat liver. *Proc Natl Acad Sci U S A*. 1985;82(24):8681-8685. http://www.ncbi.nlm.nih.gov/pubmed/3909149. Accessed September 24, 2018.

15. Friedman SL. Hepatic Stellate Cells: Protean, Multifunctional, and Enigmatic Cells of the Liver. *Physiol Rev*. 2008;88(1):125-172. doi:10.1152/physrev.00013.2007

16. Sato M, Suzuki S, Senoo H. Hepatic stellate cells: unique characteristics in cell biology and phenotype. *Cell Struct Funct*. 2003;28(2):105-112. http://www.ncbi.nlm.nih.gov/pubmed/12808230. Accessed October 28, 2018.

17. Wake K. Cell-cell organization and functions of "sinusoids" in liver microcirculation system. *J Electron Microsc (Tokyo)*. 1999;48(2):89-98. http://www.ncbi.nlm.nih.gov/pubmed/10356785. Accessed September 20, 2018.

18. Pinzani M, Gentilini P. Biology of Hepatic Stellate Cells and Their Possible Relevance in the Pathogenesis of Portal Hypertension in Cirrhosis. *Semin Liver Dis*. 1999;19(04):397-410. doi:10.1055/s-2007-1007128

19. Blomhoff R, Green MH, Berg T, Norum KR. Transport and storage of vitamin A. *Science*. 1990;250(4979):399-404. http://www.ncbi.nlm.nih.gov/pubmed/2218545. Accessed October 15, 2018.

20. Maher JJ. Interactions between hepatic stellate cells and the immune system. *Semin Liver Dis*. 2001;21(3):417-426. doi:10.1055/s-2001-17555

21. Paik Y, Schwabe RF, Bataller R, Russo MP, Jobin C, Brenner DA. Toll-Like receptor 4 mediates inflammatory signaling by bacterial lipopolysaccharide in human hepatic stellate cells. *Hepatology*. 2003;37(5):1043-1055. doi:10.1053/jhep.2003.50182

22. Winau F, Hegasy G, Weiskirchen R, et al. Ito cells are liver-resident antigen-presenting cells for activating T cell responses. *Immunity*. 2007;26(1):117-129. doi:10.1016/j.immuni.2006.11.011

23. Liaskou E, Wilson D V, Oo YH. Innate immune cells in liver inflammation. *Mediators Inflamm*. 2012;2012:949157. doi:10.1155/2012/949157

24. Bilzer M, Roggel F, Gerbes AL. Role of Kupffer cells in host defense and liver disease. *Liver Int*. 2006;26(10):1175-1186. doi:10.1111/j.1478-3231.2006.01342.x

25. Geerts A. History, heterogeneity, developmental biology, and functions of quiescent hepatic stellate cells. *Semin Liver Dis*. 2001;21(3):311-335. doi:10.1055/s-2001-17550

26. Jezequel AM, Novelli G, Venturini C, Orlandi F. Quantitative Analysis of the Perisinusoidal Cells in Human Liver: The Lipocytes. In: ; :85-90. doi:10.1159/000408420

27. Giampieri MP, Jezequel AM, Orlandi F. The Lipocytes in Normal Human Liver. *Digestion*. 1981;22(4):165-169. doi:10.1159/000198640

28. Marra F, Pinzani M. Role of hepatic stellate cells in the pathogenesis of portal hypertension. *Nefrologia*. 2002;22 Suppl 5:34-40.

http://www.ncbi.nlm.nih.gov/pubmed/12107915. Accessed October 15, 2018.

29. Melton AC, Yee HF. Hepatic stellate cell protrusions couple platelet-derived growth factor-BB to chemotaxis. *Hepatology*. 2007;45(6):1446-1453. doi:10.1002/hep.21606

30. Wake K. ?Sternzellen? in the liver: Perisinusoidal cells with special reference to storage of vitamin A. *Am J Anat*. 1971;132(4):429-461. doi:10.1002/aja.1001320404

31. Ballardini G, Groff P, Badiali de Giorgi L, Schuppan D, Bianchi FB. Ito cell heterogeneity: desmin-negative Ito cells in normal rat liver. *Hepatology*. 1994;19(2):440-446. http://www.ncbi.nlm.nih.gov/pubmed/7507464. Accessed September 24, 2018.

32. Ramm GA, Britton RS, O'Neill R, Blaner WS, Bacon BR. Vitamin A-poor lipocytes: a novel desmin-negative lipocyte subpopulation, which can be activated to myofibroblasts. *Am J Physiol*. 1995;269(4 Pt 1):G532-41. doi:10.1152/ajpgi.1995.269.4.G532

33. Ballardini G, Groff P, Badiali de Giorgi L, Schuppan D, Bianchi FB. Ito cell heterogeneity: desmin-negative Ito cells in normal rat liver. *Hepatology*. 1994;19(2):440-446.

34. D'Ambrosio DN, Walewski JL, Clugston RD, Berk PD, Rippe RA, Blaner WS. Distinct populations of hepatic stellate cells in the mouse liver have different capacities for retinoid and lipid storage. *PLoS One*. 2011;6(9):e24993. doi:10.1371/journal.pone.0024993

35. Mullhaupt B, Feren A, Fodor E, Jones A. Liver expression of epidermal growth factor RNA. Rapid increases in immediate-early phase of liver regeneration. *J Biol Chem*. 1994;269(31):19667-19670. http://www.ncbi.nlm.nih.gov/pubmed/7519599. Accessed April 13, 2019.

36. Schirmacher P, Geerts A, Pietrangelo A, Dienes HP, Rogler CE. Hepatocyte growth factor/hepatopoietin A is expressed in fat-storing cells from rat liver but not myofibroblast-like cells derived from fat-storing cells. *Hepatology*. 1992;15(1):5-11. http://www.ncbi.nlm.nih.gov/pubmed/1530788. Accessed April 13, 2019.

37. YOSHINO R, MIURA K, SEGAWA D, et al. Epimorphin expression and stellate cell status in mouse liver injury. *Hepatol Res*. 2006;34(4):238-249. doi:10.1016/j.hepres.2005.12.011

38. Asahina K, Sato H, Yamasaki C, et al. Pleiotrophin/Heparin-Binding Growth-Associated Molecule as a Mitogen of Rat Hepatocytes and Its Role in Regeneration and Development of Liver. *Am J Pathol*. 2002;160(6):2191-2205. doi:10.1016/S0002-9440(10)61167-4

39. Schwabe RF, Bataller R, Brenner DA. Human hepatic stellate cells express CCR5 and RANTES to induce proliferation and migration. *Am J Physiol Gastrointest Liver Physiol*. 2003;285(5):G949-58. doi:10.1152/ajpgi.00215.2003

40. Unanue ER. Ito cells, stellate cells, and myofibroblasts: new actors in antigen presentation. *Immunity*. 2007;26(1):9-10. doi:10.1016/j.immuni.2007.01.001

41. Viñas O, Bataller R, Sancho-Bru P, et al. Human hepatic stellate cells show features of antigen-presenting cells and stimulate lymphocyte proliferation. *Hepatology*. 2003;38(4):919-929. doi:10.1053/jhep.2003.50392

42. Kobayashi S, Seki S, Kawada N, et al. Apoptosis of T cells in the hepatic fibrotic tissue of the rat: a possible inducing role of hepatic myofibroblast-like cells. *Cell Tissue Res*. 2003;311(3):353-364. doi:10.1007/s00441-002-0670-4

43. Gressner AM. Transdifferentiation of hepatic stellate cells (Ito cells) to myofibroblasts: a key event in hepatic fibrogenesis. *Kidney Int Suppl*. 1996;54:S39-45. http://www.ncbi.nlm.nih.gov/pubmed/8731193. Accessed October 31, 2018.

44. Friedman SL. Mechanisms of Hepatic Fibrogenesis. *Gastroenterology*. 2008;134(6):1655-1669. doi:10.1053/j.gastro.2008.03.003

45. Canbay A, Friedman S, Gores GJ. Apoptosis: The nexus of liver injury and fibrosis. *Hepatology*. 2004;39(2):273-278. doi:10.1002/hep.20051

46. Bachem MG, Melchior R, Gressner AM. The role of thrombocytes in liver fibrogenesis: effects of platelet lysate and thrombocyte-derived growth factors on the mitogenic activity and glycosaminoglycan synthesis of cultured rat liver fat storing cells. *J Clin Chem Clin Biochem*. 1989;27(9):555-565. http://www.ncbi.nlm.nih.gov/pubmed/2607320. Accessed April 13, 2019.

47. Nieto N, Friedman SL, Cederbaum AI. Cytochrome P450 2E1-derived Reactive Oxygen Species Mediate Paracrine Stimulation of Collagen I Protein Synthesis by Hepatic Stellate Cells. *J Biol Chem*. 2002;277(12):9853-9864. doi:10.1074/jbc.M110506200

48. Jarnagin WR, Rockey DC, Koteliansky VE, Wang SS, Bissell DM. Expression of variant fibronectins in wound healing: cellular source and biological activity of the EIIIA segment in rat hepatic fibrogenesis. *J Cell Biol*. 1994;127(6 Pt 2):2037-2048. http://www.ncbi.nlm.nih.gov/pubmed/7806580. Accessed November 5, 2018.

49. Enzan H, Hayashi Y, Miyazaki E, et al. Morphological Aspects of Hepatic Fibrosis and Ito Cells (Hepatic Stellate Cells), with Special Reference to Their Myofibroblastic Transformation. In: *Liver Diseases and Hepatic Sinusoidal Cells*. Tokyo: Springer Japan; 1999:219-231. doi:10.1007/978-4-431-67935-6_18

50. Friedman SL. Mechanisms of disease: Mechanisms of hepatic fibrosis and therapeutic implications. *Nat Clin Pract Gastroenterol Hepatol*. 2004;1(2):98-105. doi:10.1038/ncpgasthep0055

51. Gracia-Sancho J, Laviña B, Rodríguez-Vilarrupla A, García-Calderó H, Bosch J, García-Pagán JC. Enhanced vasoconstrictor prostanoid production by sinusoidal endothelial cells increases portal perfusion pressure in cirrhotic rat livers. *J Hepatol*. 2007;47(2):220-227. doi:10.1016/j.jhep.2007.03.014

52. Steib CJ, Gerbes AL, Bystron M, et al. Kupffer cell activation in normal and fibrotic livers increases portal pressure via thromboxane A2. *J Hepatol*. 2007;47(2):228-238. doi:10.1016/j.jhep.2007.03.019

53. Malhi H, Guicciardi ME, Gores GJ. Hepatocyte Death: A Clear and Present Danger. *Physiol Rev*. 2010;90(3):1165-1194. doi:10.1152/physrev.00061.2009

54. Canbay A, Feldstein AE, Higuchi H, et al. Kupffer cell engulfment of apoptotic bodies stimulates death ligand and cytokine expression. *Hepatology*. 2003;38(5):1188-1198. doi:10.1053/jhep.2003.50472

55. Jiang JX, Mikami K, Venugopal S, Li Y, Török NJ. Apoptotic body engulfment by hepatic stellate cells promotes their survival by the JAK/STAT and Akt/NF-kappaB-dependent pathways. *J Hepatol*. 2009;51(1):139-148. doi:10.1016/j.jhep.2009.03.024

56. Rippe RA, Brenner DA. From quiescence to activation: Gene regulation in hepatic stellate cells. *Gastroenterology*. 2004;127(4):1260-1262. http://www.ncbi.nlm.nih.gov/pubmed/15481004. Accessed November 5, 2018.

57. Weber A, Boege Y, Reisinger F, Heikenwälder M. Chronic liver inflammation and hepatocellular carcinoma: persistence matters. *Swiss Med Wkly*. 2011;141:w13197. doi:10.4414/smw.2011.13197

58. Mehal WZ, Friedman SL. The Role of Inflammation and Immunity in the Pathogenesis of Liver Fibrosis. In: *Liver Immunology*. Totowa, NJ: Humana Press; 2007:111-121. doi:10.1007/978-1-59745-518-3_10

59. Li Q, Verma IM. NF-κB regulation in the immune system. *Nat Rev Immunol*. 2002;2(10):725-734. doi:10.1038/nri910

60. Haybaeck J, Zeller N, Wolf MJ, et al. A Lymphotoxin-Driven Pathway to Hepatocellular Carcinoma. *Cancer Cell*. 2009;16(4):295-308. doi:10.1016/j.ccr.2009.08.021

61. Budhu A, Wang XW. The role of cytokines in hepatocellular carcinoma. *J Leukoc Biol*. 2006;80(6):1197-1213. doi:10.1189/jlb.0506297

62. El-Serag HB, Rudolph KL. Hepatocellular carcinoma: epidemiology and molecular carcinogenesis. *Gastroenterology*. 2007;132(7):2557-2576. doi:10.1053/j.gastro.2007.04.061

63. García-Pagán J-C, Gracia-Sancho J, Bosch J. Functional aspects on the pathophysiology of portal hypertension in cirrhosis. *J Hepatol*. 2012;57(2):458-461. doi:10.1016/j.jhep.2012.03.007

64. Virchow R. Die Cellularpathologie in ihrer Begrundung auf physiologische und pathologische Gewebelehre. 1858. https://scholar.google.com/scholar?q=Virchow+R.+Die+Cellularpathologie+in+Ihrer+Begründung+auf+Physiologische+und+Pathologische+Gewebelehre+1858+A.+Hirschwald+Berlin+pp+xvi,+440+. Accessed April 13, 2019.

65. Balkwill F, Mantovani A. Inflammation and cancer: back to Virchow? *Lancet (London, England)*. 2001;357(9255):539-545. doi:10.1016/S0140-6736(00)04046-0

66. Virchow R. An Address on the Value of Pathological Experiments. *Br Med J*. 1881;2(1075):198-203. http://www.ncbi.nlm.nih.gov/pubmed/20749954. Accessed

November 5, 2018.

67. Demaria S, Pikarsky E, Karin M, et al. Cancer and Inflammation: Promise for Biologic Therapy. *J Immunother*. 2010;33(4):335-351. doi:10.1097/CJI.0b013e3181d32e74

68. Coussens LM, Werb Z. Inflammation and cancer. *Nature*. 2002;420(6917):860-867. doi:10.1038/nature01322

69. Kuper H, Adami HO, Trichopoulos D. Infections as a major preventable cause of human cancer. *J Intern Med*. 2000;248(3):171-183. http://www.ncbi.nlm.nih.gov/pubmed/10971784. Accessed November 5, 2018.

70. Grivennikov SI, Greten FR, Karin M. Immunity, Inflammation, and Cancer. *Cell*. 2010;140(6):883-899. doi:10.1016/j.cell.2010.01.025

71. Wolf MJ, Seleznik GM, Zeller N, Heikenwalder M. The unexpected role of lymphotoxin β receptor signaling in carcinogenesis: from lymphoid tissue formation to liver and prostate cancer development. *Oncogene*. 2010;29(36):5006-5018. doi:10.1038/onc.2010.260

72. Hanahan D, Weinberg RA. The hallmarks of cancer. *Cell*. 2000;100(1):57-70. http://www.ncbi.nlm.nih.gov/pubmed/10647931. Accessed May 14, 2018.

73. Hanahan D, Weinberg RA. Hallmarks of cancer: the next generation. *Cell*. 2011;144(5):646-674. doi:10.1016/j.cell.2011.02.013

74. Karin M, Greten FR. NF-kappaB: linking inflammation and immunity to cancer development and progression. *Nat Rev Immunol*. 2005;5(10):749-759. doi:10.1038/nri1703

75. Li Q, Withoff S, Verma IM. Inflammation-associated cancer: NF-kappaB is the lynchpin. *Trends Immunol*. 2005;26(6):318-325. doi:10.1016/j.it.2005.04.003

76. Liu ZG, Hsu H, Goeddel D V, Karin M. Dissection of TNF receptor 1 effector functions: JNK activation is not linked to apoptosis while NF-kappaB activation prevents cell death. *Cell*. 1996;87(3):565-576. http://www.ncbi.nlm.nih.gov/pubmed/8898208. Accessed November 5, 2018.

77. Wang CY, Mayo MW, Baldwin AS. TNF- and cancer therapy-induced apoptosis: potentiation by inhibition of NF-kappaB. *Science*. 1996;274(5288):784-787. http://www.ncbi.nlm.nih.gov/pubmed/8864119. Accessed November 5, 2018.

78. Karin M, Lin A. NF-kappaB at the crossroads of life and death. *Nat Immunol*. 2002;3(3):221-227. doi:10.1038/ni0302-221

79. Gupta GP, Massagué J. Cancer Metastasis: Building a Framework. *Cell*. 2006;127(4):679-695. doi:10.1016/j.cell.2006.11.001

80. de Visser KE, Eichten A, Coussens LM. Paradoxical roles of the immune system during cancer development. *Nat Rev Cancer*. 2006;6(1):24-37. doi:10.1038/nrc1782

81. Kalluri R, Zeisberg M. Fibroblasts in cancer. *Nat Rev Cancer*. 2006;6(5):392-401.

doi:10.1038/nrc1877

82. Condeelis J, Pollard JW. Macrophages: Obligate Partners for Tumor Cell Migration, Invasion, and Metastasis. *Cell*. 2006;124(2):263-266. doi:10.1016/j.cell.2006.01.007

83. Zou W. Immunosuppressive networks in the tumour environment and their therapeutic relevance. *Nat Rev Cancer*. 2005;5(4):263-274. doi:10.1038/nrc1586

84. Karin M. Nuclear factor-kappaB in cancer development and progression. *Nature*. 2006;441(7092):431-436. doi:10.1038/nature04870

85. Lee JS, Semela D, Iredale J, Shah VH. Sinusoidal remodeling and angiogenesis: a new function for the liver-specific pericyte? *Hepatology*. 2007;45(3):817-825. doi:10.1002/hep.21564

86. Olaso E, Salado C, Egilegor E, et al. Proangiogenic role of tumor-activated hepatic stellate cells in experimental melanoma metastasis. *Hepatology*. 2003;37(3):674-685. doi:10.1053/jhep.2003.50068

87. Kang N, Gores GJ, Shah VH. Hepatic stellate cells: Partners in crime for liver metastases? *Hepatology*. 2011;54(2):707-713. doi:10.1002/hep.24384

88. Brodt P. Role of the Microenvironment in Liver Metastasis: From Pre- to Prometastatic Niches. *Clin Cancer Res*. 2016;22(24):5971-5982. doi:10.1158/1078-0432.CCR-16-0460

89. Bissell DM. Sex and hepatic fibrosis. *Hepatology*. 1999;29(3):988-989. doi:10.1002/hep.510290351

90. Lambert AW, Pattabiraman DR, Weinberg RA. Emerging Biological Principles of Metastasis. *Cell*. 2017;168(4):670-691. doi:10.1016/j.cell.2016.11.037

91. Weiss L. Metastatic Inefficiency. *Adv Cancer Res*. 1990;54:159-211. doi:10.1016/S0065-230X(08)60811-8

92. Chambers AF, Groom AC, MacDonald IC. Dissemination and growth of cancer cells in metastatic sites. *Nat Rev Cancer*. 2002;2(8):563-572. doi:10.1038/nrc865

93. Cairns J. Mutation selection and the natural history of cancer. *Nature*. 1975;255(5505):197-200. http://www.ncbi.nlm.nih.gov/pubmed/1143315. Accessed September 16, 2018.

94. Nowell PC. The clonal evolution of tumor cell populations. *Science*. 1976;194(4260):23-28. http://www.ncbi.nlm.nih.gov/pubmed/959840. Accessed September 16, 2018.

95. Fidler IJ. The pathogenesis of cancer metastasis: The “seed and soil” hypothesis revisited. *Nat Rev Cancer*. 2003;3(6):453-458. doi:10.1038/nrc1098

96. Cifone MA, Fidler IJ. Increasing metastatic potential is associated with increasing genetic instability of clones isolated from murine neoplasms. *Proc Natl Acad Sci U S A*. 1981;78(11):6949-6952. http://www.ncbi.nlm.nih.gov/pubmed/6947269. Accessed

June 24, 2018.

97. Maser RS, DePinho RA. Connecting Chromosomes, Crisis, and Cancer. *Science (80-)*. 2002;297(5581):565-569. doi:10.1126/science.297.5581.565

98. Baylin SB, Ohm JE. Epigenetic gene silencing in cancer – a mechanism for early oncogenic pathway addiction? *Nat Rev Cancer*. 2006;6(2):107-116. doi:10.1038/nrc1799

99. Feinberg AP, Ohlsson R, Henikoff S. The epigenetic progenitor origin of human cancer. *Nat Rev Genet*. 2006;7(1):21-33. doi:10.1038/nrg1748

100. Hussain SP, Hofseth LJ, Harris CC. Radical causes of cancer. *Nat Rev Cancer*. 2003;3(4):276-285. doi:10.1038/nrc1046

101. Semenza GL. Targeting HIF-1 for cancer therapy. *Nat Rev Cancer*. 2003;3(10):721-732. doi:10.1038/nrc1187

102. Staller P, Sulitkova J, Lisztwan J, Moch H, Oakeley EJ, Krek W. Chemokine receptor CXCR4 downregulated by von Hippel-Lindau tumour suppressor pVHL. *Nature*. 2003;425(6955):307-311. doi:10.1038/nature01874

103. Paszek MJ, Zahir N, Johnson KR, et al. Tensional homeostasis and the malignant phenotype. *Cancer Cell*. 2005;8(3):241-254. doi:10.1016/j.ccr.2005.08.010

104. Garraway LA, Lander ES. Lessons from the Cancer Genome. *Cell*. 2013;153(1):17-37. doi:10.1016/j.cell.2013.03.002

105. Vogelstein B, Papadopoulos N, Velculescu VE, Zhou S, Diaz LA, Kinzler KW. Cancer Genome Landscapes. *Science (80-)*. 2013;339(6127):1546-1558. doi:10.1126/science.1235122

106. Vanharanta S, Massagué J. Origins of Metastatic Traits. *Cancer Cell*. 2013;24(4):410-421. doi:10.1016/j.ccr.2013.09.007

107. Naxerova K, Jain RK. Using tumour phylogenetics to identify the roots of metastasis in humans. *Nat Rev Clin Oncol*. 2015;12(5):258-272. doi:10.1038/nrclinonc.2014.238

108. Liotta LA. Tumor invasion and metastases--role of the extracellular matrix: Rhoads Memorial Award lecture. *Cancer Res*. 1986;46(1):1-7. http://www.ncbi.nlm.nih.gov/pubmed/2998604. Accessed June 24, 2018.

109. Cavallaro U, Christofori G. Cell adhesion and signalling by cadherins and Ig-CAMs in cancer. *Nat Rev Cancer*. 2004;4(2):118-132. doi:10.1038/nrc1276

110. Guo W, Giancotti FG. Integrin signalling during tumour progression. *Nat Rev Mol Cell Biol*. 2004;5(10):816-826. doi:10.1038/nrm1490

111. Thiery JP. Epithelial–mesenchymal transitions in tumour progression. *Nat Rev Cancer*. 2002;2(6):442-454. doi:10.1038/nrc822

112. Kalluri R, Weinberg RA. The basics of epithelial-mesenchymal transition. *J Clin Invest*.

2009;119(6):1420-1428. doi:10.1172/JCI39104

113. Nieto MA, Huang RY-J, Jackson RA, Thiery JP. EMT: 2016. *Cell*. 2016;166(1):21-45. doi:10.1016/j.cell.2016.06.028

114. Thiery JP. Epithelial–mesenchymal transitions in tumour progression. *Nat Rev Cancer*. 2002;2(6):442-454. doi:10.1038/nrc822

115. Mani SA, Guo W, Liao M-J, et al. The epithelial-mesenchymal transition generates cells with properties of stem cells. *Cell*. 2008;133(4):704-715. doi:10.1016/j.cell.2008.03.027

116. Brabletz T, Jung A, Spaderna S, Hlubek F, Kirchner T. Opinion: migrating cancer stem cells - an integrated concept of malignant tumour progression. *Nat Rev Cancer*. 2005;5(9):744-749. doi:10.1038/nrc1694

117. Fan F, Samuel S, Evans KW, et al. Overexpression of Snail induces epithelial-mesenchymal transition and a cancer stem cell-like phenotype in human colorectal cancer cells. *Cancer Med*. 2012;1(1):5-16. doi:10.1002/cam4.4

118. Rasheed ZA, Yang J, Wang Q, et al. Prognostic significance of tumorigenic cells with mesenchymal features in pancreatic adenocarcinoma. *J Natl Cancer Inst*. 2010;102(5):340-351. doi:10.1093/jnci/djp535

119. Kong D, Banerjee S, Ahmad A, et al. Epithelial to mesenchymal transition is mechanistically linked with stem cell signatures in prostate cancer cells. Creighton C, ed. *PLoS One*. 2010;5(8):e12445. doi:10.1371/journal.pone.0012445

120. Gupta PB, Onder TT, Jiang G, et al. Identification of selective inhibitors of cancer stem cells by high-throughput screening. *Cell*. 2009;138(4):645-659. doi:10.1016/j.cell.2009.06.034

121. Kurrey NK, Jalgaonkar SP, Joglekar A V, et al. Snail and slug mediate radioresistance and chemoresistance by antagonizing p53-mediated apoptosis and acquiring a stem-like phenotype in ovarian cancer cells. *Stem Cells*. 2009;27(9):2059-2068. doi:10.1002/stem.154

122. Friedl P, Locker J, Sahai E, Segall JE. Classifying collective cancer cell invasion. *Nat Cell Biol*. 2012;14(8):777-783. doi:10.1038/ncb2548

123. Grosse-Wilde A, Fouquier d'Hérouël A, McIntosh E, et al. Stemness of the hybrid Epithelial/Mesenchymal State in Breast Cancer and Its Association with Poor Survival. Ben-Jacob E, ed. *PLoS One*. 2015;10(5):e0126522. doi:10.1371/journal.pone.0126522

124. Li W, Kang Y. Probing the Fifty Shades of EMT in Metastasis. *Trends in cancer*. 2016;2(2):65-67. doi:10.1016/j.trecan.2016.01.001

125. Nieto MA, Huang RY-J, Jackson RA, Thiery JP. EMT: 2016. *Cell*. 2016;166(1):21-45. doi:10.1016/j.cell.2016.06.028

126. Friedl P, Wolf K. Tumour-cell invasion and migration: diversity and escape mechanisms. *Nat Rev Cancer*. 2003;3(5):362-374. doi:10.1038/nrc1075

127. Liotta LA, Kohn EC. The microenvironment of the tumour-host interface. *Nature*. 2001;411(6835):375-379. doi:10.1038/35077241

128. Condeelis J, Segall JE. Intravital imaging of cell movement in tumours. *Nat Rev Cancer*. 2003;3(12):921-930. doi:10.1038/nrc1231

129. Friedl P, Locker J, Sahai E, Segall JE. Classifying collective cancer cell invasion. *Nat Cell Biol*. 2012;14(8):777-783. doi:10.1038/ncb2548

130. Cheung KJ, Gabrielson E, Werb Z, Ewald AJ. Collective invasion in breast cancer requires a conserved basal epithelial program. *Cell*. 2013;155(7):1639-1651. doi:10.1016/j.cell.2013.11.029

131. Westcott JM, Prechtl AM, Maine EA, et al. An epigenetically distinct breast cancer cell subpopulation promotes collective invasion. *J Clin Invest*. 2015;125(5):1927-1943. doi:10.1172/JCI77767

132. Ye X, Tam WL, Shibue T, et al. Distinct EMT programs control normal mammary stem cells and tumour-initiating cells. *Nature*. 2015;525(7568):256-260. doi:10.1038/nature14897

133. Egeblad M, Werb Z. New functions for the matrix metalloproteinases in cancer progression. *Nat Rev Cancer*. 2002;2(3):161-174. doi:10.1038/nrc745

134. Overall CM, Kleifeld O. Tumour microenvironment — Opinion: Validating matrix metalloproteinases as drug targets and anti-targets for cancer therapy. *Nat Rev Cancer*. 2006;6(3):227-239. doi:10.1038/nrc1821

135. Hanahan D, Folkman J. Patterns and emerging mechanisms of the angiogenic switch during tumorigenesis. *Cell*. 1996;86(3):353-364. http://www.ncbi.nlm.nih.gov/pubmed/8756718. Accessed June 18, 2018.

136. Azzi S, Hebda JK, Gavard J. Vascular permeability and drug delivery in cancers. *Front Oncol*. 2013;3:211. doi:10.3389/fonc.2013.00211

137. Schaaf MB, Garg AD, Agostinis P. Defining the role of the tumor vasculature in antitumor immunity and immunotherapy. *Cell Death Dis*. 2018;9(2):115. doi:10.1038/s41419-017-0061-0

138. Headley MB, Bins A, Nip A, et al. Visualization of immediate immune responses to pioneer metastatic cells in the lung. *Nature*. 2016;531(7595):513-517. doi:10.1038/nature16985

139. Aceto N, Bardia A, Miyamoto DT, et al. Circulating tumor cell clusters are oligoclonal precursors of breast cancer metastasis. *Cell*. 2014;158(5):1110-1122. doi:10.1016/j.cell.2014.07.013

140. Palumbo JS, Talmage KE, Massari J V, et al. Platelets and fibrin(ogen) increase metastatic potential by impeding natural killer cell-mediated elimination of tumor cells. *Blood*. 2005;105(1):178-185. doi:10.1182/blood-2004-06-2272

141. Labelle M, Hynes RO. The initial hours of metastasis: the importance of cooperative

host-tumor cell interactions during hematogenous dissemination. *Cancer Discov*. 2012;2(12):1091-1099. doi:10.1158/2159-8290.CD-12-0329

142. Nash GF, Turner LF, Scully MF, Kakkar AK. Platelets and cancer. *Lancet Oncol*. 2002;3(7):425-430. doi:10.1016/S1470-2045(02)00789-1

143. Labelle M, Begum S, Hynes RO. Direct signaling between platelets and cancer cells induces an epithelial-mesenchymal-like transition and promotes metastasis. *Cancer Cell*. 2011;20(5):576-590. doi:10.1016/j.ccr.2011.09.009

144. Köhler S, Ullrich S, Richter U, Schumacher U. E-/P-selectins and colon carcinoma metastasis: first in vivo evidence for their crucial role in a clinically relevant model of spontaneous metastasis formation in the lung. *Br J Cancer*. 2010;102(3):602-609. doi:10.1038/sj.bjc.6605492

145. Coffelt SB, Kersten K, Doornebal CW, et al. IL-17-producing γδ T cells and neutrophils conspire to promote breast cancer metastasis. *Nature*. 2015;522(7556):345-348. doi:10.1038/nature14282

146. Spiegel A, Brooks MW, Houshyar S, et al. Neutrophils Suppress Intraluminal NK Cell-Mediated Tumor Cell Clearance and Enhance Extravasation of Disseminated Carcinoma Cells. *Cancer Discov*. 2016;6(6):630-649. doi:10.1158/2159-8290.CD-15-1157

147. Cools-Lartigue J, Spicer J, McDonald B, et al. Neutrophil extracellular traps sequester circulating tumor cells and promote metastasis. *J Clin Invest*. 2013;123(8):3446-3458. doi:10.1172/JCI67484

148. Spicer JD, McDonald B, Cools-Lartigue JJ, et al. Neutrophils promote liver metastasis via Mac-1-mediated interactions with circulating tumor cells. *Cancer Res*. 2012;72(16):3919-3927. doi:10.1158/0008-5472.CAN-11-2393

149. Spiegel A, Brooks MW, Houshyar S, et al. Neutrophils Suppress Intraluminal NK Cell-Mediated Tumor Cell Clearance and Enhance Extravasation of Disseminated Carcinoma Cells. *Cancer Discov*. 2016;6(6):630-649. doi:10.1158/2159-8290.CD-15-1157

150. Douma S, Van Laar T, Zevenhoven J, Meuwissen R, Van Garderen E, Peeper DS. Suppression of anoikis and induction of metastasis by the neurotrophic receptor TrkB. *Nature*. 2004;430(7003):1034-1039. doi:10.1038/nature02765

151. Müller A, Homey B, Soto H, et al. Involvement of chemokine receptors in breast cancer metastasis. *Nature*. 2001;410(6824):50-56. doi:10.1038/35065016

152. Wolf MJ, Hoos A, Bauer J, et al. Endothelial CCR2 signaling induced by colon carcinoma cells enables extravasation via the JAK2-Stat5 and p38MAPK pathway. *Cancer Cell*. 2012;22(1):91-105. doi:10.1016/j.ccr.2012.05.023

153. Al-Mehdi AB, Tozawa K, Fisher AB, Shientag L, Lee A, Muschel RJ. Intravascular origin of metastasis from the proliferation of endothelium-attachedtumor cells: a new model for metastasis. *Nat Med*. 2000;6(1):100-102. doi:10.1038/71429

154. Padua D, Zhang XH-F, Wang Q, et al. TGFbeta primes breast tumors for lung metastasis seeding through angiopoietin-like 4. *Cell*. 2008;133(1):66-77. doi:10.1016/j.cell.2008.01.046

155. Weis SM, Cheresh DA. Pathophysiological consequences of VEGF-induced vascular permeability. *Nature*. 2005;437(7058):497-504. doi:10.1038/nature03987

156. Criscuoli ML, Nguyen M, Eliceiri BP. Tumor metastasis but not tumor growth is dependent on Src-mediated vascular permeability. *Blood*. 2005;105(4):1508-1514. doi:10.1182/blood-2004-06-2246

157. Strilic B, Yang L, Albarrán-Juárez J, et al. Tumour-cell-induced endothelial cell necroptosis via death receptor 6 promotes metastasis. *Nature*. 2016;536(7615):215-218. doi:10.1038/nature19076

158. Paget S. The distribution of secondary growths in cancer of the breast. *Lancet*. 1889;1:571-573.

159. Hart IR, Fidler IJ. Role of organ selectivity in the determination of metastatic patterns of B16 melanoma. *Cancer Res*. 1980;40(7):2281-2287. http://www.ncbi.nlm.nih.gov/pubmed/7388794. Accessed June 26, 2018.

160. Tarin D, Price JE, Kettlewell MG, Souter RG, Vass AC, Crossley B. Mechanisms of human tumor metastasis studied in patients with peritoneovenous shunts. *Cancer Res*. 1984;44(8):3584-3592. http://www.ncbi.nlm.nih.gov/pubmed/6744281. Accessed June 26, 2018.

161. Hoshino A, Costa-Silva B, Shen T-L, et al. Tumour exosome integrins determine organotropic metastasis. *Nature*. 2015;527(7578):329-335. doi:10.1038/nature15756

162. Kaplan RN, Riba RD, Zacharoulis S, et al. VEGFR1-positive haematopoietic bone marrow progenitors initiate the pre-metastatic niche. *Nature*. 2005;438(7069):820-827. doi:10.1038/nature04186

163. Psaila B, Lyden D. The metastatic niche: adapting the foreign soil. *Nat Rev Cancer*. 2009;9(4):285-293. doi:10.1038/nrc2621

164. Hiratsuka S, Nakamura K, Iwai S, et al. MMP9 induction by vascular endothelial growth factor receptor-1 is involved in lung-specific metastasis. *Cancer Cell*. 2002;2(4):289-300. http://www.ncbi.nlm.nih.gov/pubmed/12398893. Accessed June 20, 2018.

165. Peinado H, Zhang H, Matei IR, et al. Pre-metastatic niches: organ-specific homes for metastases. *Nat Rev Cancer*. 2017;17(5):302-317. doi:10.1038/nrc.2017.6

166. McAllister SS, Weinberg RA. The tumour-induced systemic environment as a critical regulator of cancer progression and metastasis. *Nat Cell Biol*. 2014;16(8):717-727. doi:10.1038/ncb3015

167. Costa-Silva B, Aiello NM, Ocean AJ, et al. Pancreatic cancer exosomes initiate pre-metastatic niche formation in the liver. *Nat Cell Biol*. 2015;17(6):816-826.

doi:10.1038/ncb3169

168. Peinado H, Alečković M, Lavotshkin S, et al. Melanoma exosomes educate bone marrow progenitor cells toward a pro-metastatic phenotype through MET. *Nat Med*. 2012;18(6):883-891. doi:10.1038/nm.2753

169. Peinado H, Zhang H, Matei IR, et al. Pre-metastatic niches: organ-specific homes for metastases. *Nat Rev Cancer*. 2017;17(5):302-317. doi:10.1038/nrc.2017.6

170. Kitamura T, Qian B-Z, Pollard JW. Immune cell promotion of metastasis. *Nat Rev Immunol*. 2015;15(2):73-86. doi:10.1038/nri3789

171. Pantel K, Brakenhoff RH. Dissecting the metastatic cascade. *Nat Rev Cancer*. 2004;4(6):448-456. doi:10.1038/nrc1370

172. Braun S, Vogl FD, Naume B, et al. A Pooled Analysis of Bone Marrow Micrometastasis in Breast Cancer. *N Engl J Med*. 2005;353(8):793-802. doi:10.1056/NEJMoa050434

173. Aguirre-Ghiso JA. Models, mechanisms and clinical evidence for cancer dormancy. *Nat Rev Cancer*. 2007;7(11):834-846. doi:10.1038/nrc2256

174. Malladi S, Macalinao DG, Jin X, et al. Metastatic Latency and Immune Evasion through Autocrine Inhibition of WNT. *Cell*. 2016;165(1):45-60. doi:10.1016/j.cell.2016.02.025

175. Giancotti FG. Mechanisms governing metastatic dormancy and reactivation. *Cell*. 2013;155(4):750-764. doi:10.1016/j.cell.2013.10.029

176. Sosa MS, Bragado P, Aguirre-Ghiso JA. Mechanisms of disseminated cancer cell dormancy: an awakening field. *Nat Rev Cancer*. 2014;14(9):611-622. doi:10.1038/nrc3793

177. Ghajar CM. Metastasis prevention by targeting the dormant niche. *Nat Rev Cancer*. 2015;15(4):238-247. doi:10.1038/nrc3910

178. Shiozawa Y, Pedersen EA, Havens AM, et al. Human prostate cancer metastases target the hematopoietic stem cell niche to establish footholds in mouse bone marrow. *J Clin Invest*. 2011;121(4):1298-1312. doi:10.1172/JCI43414

179. Ghajar CM, Peinado H, Mori H, et al. The perivascular niche regulates breast tumour dormancy. *Nat Cell Biol*. 2013;15(7):807-817. doi:10.1038/ncb2767

180. Ghajar CM. Metastasis prevention by targeting the dormant niche. *Nat Rev Cancer*. 2015;15(4):238-247. doi:10.1038/nrc3910

181. Hanahan D, Coussens LM. Accessories to the crime: functions of cells recruited to the tumor microenvironment. *Cancer Cell*. 2012;21(3):309-322. doi:10.1016/j.ccr.2012.02.022

182. Quail DF, Joyce JA. Microenvironmental regulation of tumor progression and metastasis. *Nat Med*. 2013;19(11):1423-1437. doi:10.1038/nm.3394

183. Wan L, Pantel K, Kang Y. Tumor metastasis: moving new biological insights into the

clinic. *Nat Med*. 2013;19(11):1450-1464. doi:10.1038/nm.3391

184. Nguyen DX, Bos PD, Massagué J. Metastasis: from dissemination to organ-specific colonization. *Nat Rev Cancer*. 2009;9(4):274-284. doi:10.1038/nrc2622

185. Obenauf AC, Massagué J. Surviving at a Distance: Organ-Specific Metastasis. *Trends in Cancer*. 2015;1(1):76-91. doi:10.1016/j.trecan.2015.07.009

186. Sethi N, Kang Y. Unravelling the complexity of metastasis - molecular understanding and targeted therapies. *Nat Rev Cancer*. 2011;11(10):735-748. doi:10.1038/nrc3125

187. Minn AJ, Gupta GP, Siegel PM, et al. Genes that mediate breast cancer metastasis to lung. *Nature*. 2005;436(7050):518-524. doi:10.1038/nature03799

188. Minn AJ, Kang Y, Serganova I, et al. Distinct organ-specific metastatic potential of individual breast cancer cells and primary tumors. *J Clin Invest*. 2005;115(1):44-55. doi:10.1172/JCI22320

189. Valiente M, Obenauf AC, Jin X, et al. Serpins promote cancer cell survival and vascular co-option in brain metastasis. *Cell*. 2014;156(5):1002-1016. doi:10.1016/j.cell.2014.01.040

190. Takeda K, Hayakawa Y, Smyth MJ, et al. Involvement of tumor necrosis factor-related apoptosis-inducing ligand in surveillance of tumor metastasis by liver natural killer cells. *Nat Med*. 2001;7(1):94-100. doi:10.1038/83416

191. Bao S, Ouyang G, Bai X, et al. Periostin potently promotes metastatic growth of colon cancer by augmenting cell survival via the Akt/PKB pathway. *Cancer Cell*. 2004;5(4):329-339. http://www.ncbi.nlm.nih.gov/pubmed/15093540. Accessed June 20, 2018.

192. Loo JM, Scherl A, Nguyen A, et al. Extracellular Metabolic Energetics Can Promote Cancer Progression. *Cell*. 2015;160(3):393-406. doi:10.1016/j.cell.2014.12.018

193. Piskounova E, Agathocleous M, Murphy MM, et al. Oxidative stress inhibits distant metastasis by human melanoma cells. *Nature*. 2015;527(7577):186-191. doi:10.1038/nature15726

194. Shibue T, Brooks MW, Inan MF, Reinhardt F, Weinberg RA. The outgrowth of micrometastases is enabled by the formation of filopodium-like protrusions. *Cancer Discov*. 2012;2(8):706-721. doi:10.1158/2159-8290.CD-11-0239

195. Aceto N, Bardia A, Miyamoto DT, et al. Circulating tumor cell clusters are oligoclonal precursors of breast cancer metastasis. *Cell*. 2014;158(5):1110-1122. doi:10.1016/j.cell.2014.07.013

196. Barkan D, El Touny LH, Michalowski AM, et al. Metastatic growth from dormant cells induced by a col-I-enriched fibrotic environment. *Cancer Res*. 2010;70(14):5706-5716. doi:10.1158/0008-5472.CAN-09-2356

197. Cox TR, Erler JT. Molecular pathways: connecting fibrosis and solid tumor metastasis. *Clin Cancer Res*. 2014;20(14):3637-3643. doi:10.1158/1078-0432.CCR-13-1059

198. Kitamura T, Qian B-Z, Pollard JW. Immune cell promotion of metastasis. *Nat Rev Immunol*. 2015;15(2):73-86. doi:10.1038/nri3789

199. De Cock JM, Shibue T, Dongre A, Keckesova Z, Reinhardt F, Weinberg RA. Inflammation Triggers Zeb1-Dependent Escape from Tumor Latency. *Cancer Res*. 2016;76(23):6778-6784. doi:10.1158/0008-5472.CAN-16-0608

200. Gupta PB, Kuperwasser C, Brunet J-P, et al. The melanocyte differentiation program predisposes to metastasis after neoplastic transformation. *Nat Genet*. 2005;37(10):1047-1054. doi:10.1038/ng1634

201. Perou CM, Sørlie T, Eisen MB, et al. Molecular portraits of human breast tumours. *Nature*. 2000;406(6797):747-752. doi:10.1038/35021093

202. Oskarsson T, Batlle E, Massagué J. Metastatic stem cells: sources, niches, and vital pathways. *Cell Stem Cell*. 2014;14(3):306-321. doi:10.1016/j.stem.2014.02.002

203. Malanchi I, Santamaria-Martínez A, Susanto E, et al. Interactions between cancer stem cells and their niche govern metastatic colonization. *Nature*. 2012;481(7379):85-89. doi:10.1038/nature10694

204. Morel A-P, Lièvre M, Thomas C, Hinkal G, Ansieau S, Puisieux A. Generation of breast cancer stem cells through epithelial-mesenchymal transition. Klefstrom J, ed. *PLoS One*. 2008;3(8):e2888. doi:10.1371/journal.pone.0002888

205. Mani SA, Guo W, Liao M-J, et al. The epithelial-mesenchymal transition generates cells with properties of stem cells. *Cell*. 2008;133(4):704-715. doi:10.1016/j.cell.2008.03.027

206. Lawson DA, Bhakta NR, Kessenbrock K, et al. Single-cell analysis reveals a stem-cell program in human metastatic breast cancer cells. *Nature*. 2015;526(7571):131-135. doi:10.1038/nature15260

207. Malladi S, Macalinao DG, Jin X, et al. Metastatic Latency and Immune Evasion through Autocrine Inhibition of WNT. *Cell*. 2016;165(1):45-60. doi:10.1016/j.cell.2016.02.025

208. Hüsemann Y, Geigl JB, Schubert F, et al. Systemic spread is an early step in breast cancer. *Cancer Cell*. 2008;13(1):58-68. doi:10.1016/j.ccr.2007.12.003

209. Podsypanina K, Du Y-CN, Jechlinger M, Beverly LJ, Hambardzumyan D, Varmus H. Seeding and propagation of untransformed mouse mammary cells in the lung. *Science*. 2008;321(5897):1841-1844. doi:10.1126/science.1161621

210. Rhim AD, Mirek ET, Aiello NM, et al. EMT and dissemination precede pancreatic tumor formation. *Cell*. 2012;148(1-2):349-361. doi:10.1016/j.cell.2011.11.025

211. Harper KL, Sosa MS, Entenberg D, et al. Mechanism of early dissemination and metastasis in Her2+ mammary cancer. *Nature*. 2016;540(7634):588-592. doi:10.1038/nature20609

212. Klein CA. Parallel progression of primary tumours and metastases. *Nat Rev Cancer*. 2009;9(4):302-312. doi:10.1038/nrc2627

213. Canellos GP. Lymphoma: present and future challenges. *Semin Hematol*. 2004;41(4 Suppl 7):26-31. http://www.ncbi.nlm.nih.gov/pubmed/15768476. Accessed November 9, 2018.

214. Tzankov A, Dirnhofer S. Pathobiology of Classical Hodgkin Lymphoma. *Pathobiology*. 2006;73(3):107-125. doi:10.1159/000095558

215. Noronha V, Shafi NQ, Obando JA, Kummar S. Primary non-Hodgkin's lymphoma of the liver. *Crit Rev Oncol Hematol*. 2005;53(3):199-207. doi:10.1016/j.critrevonc.2004.10.010

216. Caccamo D, Pervez NK, Marchevsky A. Primary lymphoma of the liver in the acquired immunodeficiency syndrome. *Arch Pathol Lab Med*. 1986;110(6):553-555. http://www.ncbi.nlm.nih.gov/pubmed/3010899. Accessed November 9, 2018.

217. Vannata B, Zucca E. Primary extranodal B-cell lymphoma: current concepts and treatment strategies. *Chinese Clin Oncol*. 2015;4(1). doi:10.21037/cco.v4i1.5458

218. Zelenetz AD, Abramson JS, Advani RH, et al. NCCN Clinical Practice Guidelines in Oncology: non-Hodgkin's lymphomas. *J Natl Compr Canc Netw*. 2010;8(3):288-334. http://www.ncbi.nlm.nih.gov/pubmed/20202462. Accessed November 9, 2018.

219. NHL incidence UK 1993-2015. https://www.cancerresearchuk.org/health-professional/cancer-statistics/statistics-by-cancer-type/non-hodgkin-lymphoma/incidence#heading-Two. Accessed November 7, 2018.

220. HL incidence UK 1993-2015. https://www.cancerresearchuk.org/health-professional/cancer-statistics/statistics-by-cancer-type/hodgkin-lymphoma/incidence#heading-Two. Accessed November 7, 2018.

221. Zinzani PL. Lymphoma: Diagnosis, staging, natural history, and treatment strategies. *Semin Oncol*. 2005;32(1 Suppl 1):4-10. doi:10.1053/j.seminoncol.2005.01.008

222. Loddenkemper C, Longerich T, Hummel M, et al. Frequency and diagnostic patterns of lymphomas in liver biopsies with respect to the WHO classification. *Virchows Arch*. 2007;450(5):493-502. doi:10.1007/s00428-007-0384-9

223. Baumhoer D, Tzankov A, Dirnhofer S, Tornillo L, Terracciano LM. Patterns of liver infiltration in lymphoproliferative disease. *Histopathology*. 2008;53(1):81-90. doi:10.1111/j.1365-2559.2008.03069.x

224. El-fattah MA. Original Article Non-Hodgkin Lymphoma of the Liver : A US Population-based Analysis. *J Clin Transl Hepatol*. 2017;5(2):83-91. doi:10.14218/JCTH.2017.00015

225. Jaffe E. Malignant Lymphomas: Pathology of Hepatic Involvement. *Semin Liver Dis*. 1987;7(03):257-268. doi:10.1055/s-2008-1040581

226. Kim H, Dorfman RF. Morphological studies of 84 untreated patients subjected to laparotomy for the staging of non-Hodgkin's lymphomas. *Cancer*. 1974;33(3):657-674. http://www.ncbi.nlm.nih.gov/pubmed/4592903. Accessed November 9, 2018.

227. Santos ES, Raez LE, Salvatierra J, Morgensztern D, Shanmugan N, Neff GW. Primary

hepatic non-Hodgkin's lymphomas: case report and review of the literature. *Am J Gastroenterol*. 2003;98(12):2789-2793. doi:10.1111/j.1572-0241.2003.08766.x

228. Prabhu RM, Medeiros LJ, Kumar D, et al. Primary hepatic low-grade B-cell lymphoma of mucosa-associated lymphoid tissue (MALT) associated with primary biliary cirrhosis. *Mod Pathol*. 1998;11(4):404-410. http://www.ncbi.nlm.nih.gov/pubmed/9578094. Accessed November 9, 2018.

229. Möhler M, Gutzler F, Kallinowski B, Goeser T, Stremmel W. Primary hepatic high-grade non-Hodgkin's lymphoma and chronic hepatitis C infection. *Dig Dis Sci*. 1997;42(11):2241-2245. doi:10.1023/A:1018858415936

230. Dippel E, Assaf C, Hummel M, et al. Clonal T-cell receptor ?-chain gene rearrangement by PCR-based GeneScan analysis in advanced cutaneous T-cell lymphoma: a critical evaluation. *J Pathol*. 1999;188(2):146-154. doi:10.1002/(SICI)1096-9896(199906)188:2<146::AID-PATH334>3.0.CO;2-7

231. Brabletz T, Lyden D, Steeg PS, Werb Z. Roadblocks to translational advances on metastasis research. *Nat Med*. 2013;19(9):1104-1109. doi:10.1038/nm.3327

232. Holohan C, Van Schaeybroeck S, Longley DB, Johnston PG. Cancer drug resistance: An evolving paradigm. *Nat Rev Cancer*. 2013;13(10):714-726. doi:10.1038/nrc3599

233. Ding L, Ellis MJ, Li S, et al. Genome remodelling in a basal-like breast cancer metastasis and xenograft. *Nature*. 2010;464(7291):999-1005. doi:10.1038/nature08989

234. Yachida S, Jones S, Bozic I, et al. Distant metastasis occurs late during the genetic evolution of pancreatic cancer. *Nature*. 2010;467(7319):1114-1117. doi:10.1038/nature09515

235. Yates LR, Gerstung M, Knappskog S, et al. Subclonal diversification of primary breast cancer revealed by multiregion sequencing. *Nat Med*. 2015;21(7):751-759. doi:10.1038/nm.3886

236. Acharyya S, Oskarsson T, Vanharanta S, et al. A CXCL1 paracrine network links cancer chemoresistance and metastasis. *Cell*. 2012;150(1):165-178. doi:10.1016/j.cell.2012.04.042

237. Gilbert LA, Hemann MT. DNA damage-mediated induction of a chemoresistant niche. *Cell*. 2010;143(3):355-366. doi:10.1016/j.cell.2010.09.043

238. Riihimäki M, Hemminki A, Sundquist J, Hemminki K. Patterns of metastasis in colon and rectal cancer. *Sci Rep*. 2016;6:29765. doi:10.1038/srep29765

239. Acharyya S, Oskarsson T, Vanharanta S, et al. A CXCL1 paracrine network links cancer chemoresistance and metastasis. *Cell*. 2012;150(1):165-178. doi:10.1016/j.cell.2012.04.042

240. Goss PE, Chambers AF. Does tumour dormancy offer a therapeutic target? *Nat Rev Cancer*. 2010;10(12):871-877. doi:10.1038/nrc2933

241. Yachida S, Iacobuzio-Donahue CA. The Pathology and Genetics of Metastatic Pancreatic Cancer. *Arch Pathol Lab Med—Vol*. 2009;133. http://www.archivesofpathology.org/doi/pdf/10.1043/1543-2165-133.3.413?code=coap-site. Accessed May 15, 2018.

242. Hess KR, Varadhachary GR, Taylor SH, et al. Metastatic patterns in adenocarcinoma. *Cancer*. 2006;106(7):1624-1633. doi:10.1002/cncr.21778

243. Ma R, Feng Y, Lin S, et al. Mechanisms involved in breast cancer liver metastasis. *J Transl Med*. 2015;13:64. doi:10.1186/s12967-015-0425-0

244. Tas F. Metastatic Behavior in Melanoma: Timing, Pattern, Survival, and Influencing Factors. *J Oncol*. 2012;2012:1-9. doi:10.1155/2012/647684

245. Lu X, Kang Y. Organotropism of breast cancer metastasis. *J Mammary Gland Biol Neoplasia*. 2007;12(2-3):153-162. doi:10.1007/s10911-007-9047-3

246. Horak CE, Steeg PS. Metastasis gets site specific. *Cancer Cell*. 2005;8(2):93-95. doi:10.1016/j.ccr.2005.07.013

247. Colombo M, Raposo G, Théry C. Biogenesis, Secretion, and Intercellular Interactions of Exosomes and Other Extracellular Vesicles. *Annu Rev Cell Dev Biol*. 2014;30(1):255-289. doi:10.1146/annurev-cellbio-101512-122326

248. Paku S, Döme B, Tóth R, Timár J. Organ-specificity of the extravasation process: an ultrastructural study. *Clin Exp Metastasis*. 2000;18(6):481-492. http://www.ncbi.nlm.nih.gov/pubmed/11592305. Accessed November 20, 2018.

249. Hiratsuka S, Watanabe A, Aburatani H, Maru Y. Tumour-mediated upregulation of chemoattractants and recruitment of myeloid cells predetermines lung metastasis. *Nat Cell Biol*. 2006;8(12):1369-1375. doi:10.1038/ncb1507

250. Huang Y, Song N, Ding Y, et al. Pulmonary vascular destabilization in the premetastatic phase facilitates lung metastasis. *Cancer Res*. 2009;69(19):7529-7537. doi:10.1158/0008-5472.CAN-08-4382

251. Hiratsuka S, Watanabe A, Sakurai Y, et al. The S100A8–serum amyloid A3–TLR4 paracrine cascade establishes a pre-metastatic phase. *Nat Cell Biol*. 2008;10(11):1349-1355. doi:10.1038/ncb1794

252. Peinado H, Lavotshkin S, Lyden D. The secreted factors responsible for pre-metastatic niche formation: Old sayings and new thoughts. *Semin Cancer Biol*. 2011;21(2):139-146. doi:10.1016/j.semcancer.2011.01.002

253. Wang HH, McIntosh AR, Hasinoff BB, et al. B16 melanoma cell arrest in the mouse liver induces nitric oxide release and sinusoidal cytotoxicity: a natural hepatic defense against metastasis. *Cancer Res*. 2000;60(20):5862-5869. http://www.ncbi.nlm.nih.gov/pubmed/11059784. Accessed November 20, 2018.

254. Hehlgans T, Pfeffer K. The intriguing biology of the tumour necrosis factor/tumour necrosis factor receptor superfamily: players, rules and the games. *Immunology*.

2005;115(1):1-20. doi:10.1111/j.1365-2567.2005.02143.x

255. Braet F, Nagatsuma K, Saito M, Soon L, Wisse E, Matsuura T. The hepatic sinusoidal endothelial lining and colorectal liver metastases. *World J Gastroenterol*. 2007;13(6):821-825. http://www.ncbi.nlm.nih.gov/pubmed/17352008. Accessed November 20, 2018.

256. Van den Eynden GG, Majeed AW, Illemann M, et al. The multifaceted role of the microenvironment in liver metastasis: biology and clinical implications. *Cancer Res*. 2013;73(7):2031-2043. doi:10.1158/0008-5472.CAN-12-3931

257. Ou J, Peng Y, Deng J, et al. Endothelial cell-derived fibronectin extra domain A promotes colorectal cancer metastasis via inducing epithelial-mesenchymal transition. *Carcinogenesis*. 2014;35(7):1661-1670. doi:10.1093/carcin/bgu090

258. Glinskii O V, Huxley VH, Glinsky G V, Pienta KJ, Raz A, Glinsky V V. Mechanical entrapment is insufficient and intercellular adhesion is essential for metastatic cell arrest in distant organs. *Neoplasia*. 2005;7(5):522-527. http://www.ncbi.nlm.nih.gov/pubmed/15967104. Accessed November 20, 2018.

259. Witz IP. The selectin–selectin ligand axis in tumor progression. *Cancer Metastasis Rev*. 2008;27(1):19-30. doi:10.1007/s10555-007-9101-z

260. Elliott VA, Rychahou P, Zaytseva YY, Evers BM. Activation of c-Met and upregulation of CD44 expression are associated with the metastatic phenotype in the colorectal cancer liver metastasis model. André F, ed. *PLoS One*. 2014;9(5):e97432. doi:10.1371/journal.pone.0097432

261. Georges R, Bergmann F, Hamdi H, et al. Sequential biphasic changes in claudin1 and claudin4 expression are correlated to colorectal cancer progression and liver metastasis. *J Cell Mol Med*. 2012;16(2):260-272. doi:10.1111/j.1582-4934.2011.01289.x

262. Khatib AM, Kontogiannea M, Fallavollita L, Jamison B, Meterissian S, Brodt P. Rapid induction of cytokine and E-selectin expression in the liver in response to metastatic tumor cells. *Cancer Res*. 1999;59(6):1356-1361. http://www.ncbi.nlm.nih.gov/pubmed/10096570. Accessed November 20, 2018.

263. Muhanna N, Doron S, Wald O, et al. Activation of hepatic stellate cells after phagocytosis of lymphocytes: A novel pathway of fibrogenesis. *Hepatology*. 2008;48(3):963-977. doi:10.1002/hep.22413

264. Zhao W, Zhang L, Xu Y, et al. Hepatic stellate cells promote tumor progression by enhancement of immunosuppressive cells in an orthotopic liver tumor mouse model. *Lab Investig*. 2014;94(2):182-191. doi:10.1038/labinvest.2013.139

265. Taura K, De Minicis S, Seki E, et al. Hepatic Stellate Cells Secrete Angiopoietin 1 That Induces Angiogenesis in Liver Fibrosis. *Gastroenterology*. 2008;135(5):1729-1738. doi:10.1053/j.gastro.2008.07.065

266. Levental KR, Yu H, Kass L, et al. Matrix Crosslinking Forces Tumor Progression by

Enhancing Integrin Signaling. *Cell*. 2009;139(5):891-906. doi:10.1016/j.cell.2009.10.027

267. Goetz JG, Minguet S, Navarro-Lérida I, et al. Biomechanical Remodeling of the Microenvironment by Stromal Caveolin-1 Favors Tumor Invasion and Metastasis. *Cell*. 2011;146(1):148-163. doi:10.1016/j.cell.2011.05.040

268. Wang J, Fallavollita L, Brodt P. Inhibition of experimental hepatic metastasis by a monoclonal antibody that blocks tumor-hepatocyte interaction. *J Immunother Emphasis Tumor Immunol*. 1994;16(4):294-302. http://www.ncbi.nlm.nih.gov/pubmed/7881638. Accessed November 21, 2018.

269. Roos E, Dingemans KP, Van de Pavert I V, Van den Bergh-Weerman MA. Mammary-carcinoma cells in mouse liver: infiltration of liver tissue and interaction with Kupffer cells. *Br J Cancer*. 1978;38(1):88-99. http://www.ncbi.nlm.nih.gov/pubmed/687522. Accessed November 21, 2018.

270. Zvibel I, Wagner A, Pasmanik-Chor M, et al. Transcriptional profiling identifies genes induced by hepatocyte-derived extracellular matrix in metastatic human colorectal cancer cell lines. *Clin Exp Metastasis*. 2013;30(2):189-200. doi:10.1007/s10585-012-9527-8

271. Enns A, Korb T, Schlüter K, et al. αvβ5-Integrins mediate early steps of metastasis formation. *Eur J Cancer*. 2005;41(7):1065-1072. doi:10.1016/j.ejca.2004.12.031

272. Hiratsuka S, Goel S, Kamoun WS, et al. Endothelial focal adhesion kinase mediates cancer cell homing to discrete regions of the lungs via E-selectin up-regulation. *Proc Natl Acad Sci*. 2011;108(9):3725-3730. doi:10.1073/pnas.1100446108

273. Harburger DS, Calderwood DA. Integrin signalling at a glance. *J Cell Sci*. 2009;122(2):159-163. doi:10.1242/jcs.018093

274. Balkwill F. Cancer and the chemokine network. *Nat Rev Cancer*. 2004;4(7):540-550. doi:10.1038/nrc1388

275. Kim J, Mori T, Chen SL, et al. Chemokine Receptor CXCR4 Expression in Patients With Melanoma and Colorectal Cancer Liver Metastases and the Association With Disease Outcome. *Ann Surg*. 2006;244(1):113-120. doi:10.1097/01.sla.0000217690.65909.9c

276. Müller A, Homey B, Soto H, et al. Involvement of chemokine receptors in breast cancer metastasis. *Nature*. 2001;410(6824):50-56. doi:10.1038/35065016

277. Ham B, Wang N, D'Costa Z, et al. TNF Receptor-2 Facilitates an Immunosuppressive Microenvironment in the Liver to Promote the Colonization and Growth of Hepatic Metastases. *Cancer Res*. 2015;75(24):5235-5247. doi:10.1158/0008-5472.CAN-14-3173

278. Weiss L. Biomechanical interactions of cancer cells with the microvasculature during hematogenous metastasis. *Cancer Metastasis Rev*. 1992;11(3-4):227-235. http://www.ncbi.nlm.nih.gov/pubmed/1423815. Accessed March 10, 2019.

279. Kemperman H, Wijnands YM, Roos E. αV Integrins on HT-29 Colon Carcinoma Cells: Adhesion to Fibronectin Is Mediated Solely by Small Amounts of αVβ6, and αVβ5 Is Codistributed with Actin Fibers. *Exp Cell Res*. 1997;234(1):156-164. doi:10.1006/excr.1997.3599

280. Haler J, Nasralla M, Nicolson GL. Different adhesion properties of highly and poorly metastatic HT-29 colon carcinoma cells with extracellular matrix components: Role of integrin expression and cytoskeletal components. *Br J Cancer*. 1999. doi:10.1038/sj.bjc.6690614

281. Eble JA, Haier J. Integrins in cancer treatment. *Curr Cancer Drug Targets*. 2006;6(2):89-105. http://www.ncbi.nlm.nih.gov/pubmed/16529540. Accessed March 10, 2019.

282. Gooding JM, Yap KL, Ikura M. The cadherin-catenin complex as a focal point of cell adhesion and signalling: new insights from three-dimensional structures. *BioEssays*. 2004;26(5):497-511. doi:10.1002/bies.20033

283. Thiery JP, Acloque H, Huang RYJ, Nieto MA. Epithelial-Mesenchymal Transitions in Development and Disease. *Cell*. 2009;139(5):871-890. doi:10.1016/j.cell.2009.11.007

284. Polyak K, Weinberg RA. Transitions between epithelial and mesenchymal states: acquisition of malignant and stem cell traits. *Nat Rev Cancer*. 2009;9(4):265-273. doi:10.1038/nrc2620

285. Coussens LM, Werb Z. Inflammation and cancer. *Nature*. 2002;420(6917):860-867. doi:10.1038/nature01322

286. Crusz SM, Balkwill FR. Inflammation and cancer: advances and new agents. *Nat Rev Clin Oncol*. 2015;12(10):584-596. doi:10.1038/nrclinonc.2015.105

287. Coffelt SB, de Visser KE. Inflammation lights the way to metastasis. *Nature*. 2014;507(7490):48-49. doi:10.1038/nature13062

288. Wu Y, Zhou BP. Inflammation: a driving force speeds cancer metastasis. *Cell Cycle*. 2009;8(20):3267-3273. doi:10.4161/cc.8.20.9699

289. Cuzick J, Otto F, Baron JA, et al. Aspirin and non-steroidal anti-inflammatory drugs for cancer prevention: an international consensus statement. *Lancet Oncol*. 2009;10(5):501-507. doi:10.1016/S1470-2045(09)70035-X

290. Rayburn ER, Ezell SJ, Zhang R. Anti-Inflammatory Agents for Cancer Therapy. *Mol Cell Pharmacol*. 2009;1(1):29-43. doi:10.4255/mcpharmacol.09.05

291. Khatib A-M, Fallavollita L, Wancewicz E V, Monia BP, Brodt P. Inhibition of hepatic endothelial E-selectin expression by C-raf antisense oligonucleotides blocks colorectal carcinoma liver metastasis. *Cancer Res*. 2002;62(19):5393-5398. http://www.ncbi.nlm.nih.gov/pubmed/12359742. Accessed March 10, 2019.

292. Zhang C, Zhou C, Wu X-J, et al. Human CD133-positive hematopoietic progenitor cells initiate growth and metastasis of colorectal cancer cells. *Carcinogenesis*.

2014;35(12):2771-2777. doi:10.1093/carcin/bgu192

293. Galdiero MR, Bonavita E, Barajon I, Garlanda C, Mantovani A, Jaillon S. Tumor associated macrophages and neutrophils in cancer. *Immunobiology*. 2013;218(11):1402-1410. doi:10.1016/j.imbio.2013.06.003

294. Mills CD. Anatomy of a discovery: m1 and m2 macrophages. *Front Immunol*. 2015;6:212. doi:10.3389/fimmu.2015.00212

295. Sionov RV, Fridlender ZG, Granot Z. The Multifaceted Roles Neutrophils Play in the Tumor Microenvironment. *Cancer Microenviron*. 2015;8(3):125-158. doi:10.1007/s12307-014-0147-5

296. Keskinov AA, Shurin MR. Myeloid regulatory cells in tumor spreading and metastasis. *Immunobiology*. 2015;220(2):236-242. doi:10.1016/j.imbio.2014.07.017

297. Seubert B, Grünwald B, Kobuch J, et al. Tissue inhibitor of metalloproteinases (TIMP)-1 creates a premetastatic niche in the liver through SDF-1/CXCR4-dependent neutrophil recruitment in mice. *Hepatology*. 2015;61(1):238-248. doi:10.1002/hep.27378

298. Meyer C, Cagnon L, Costa-Nunes CM, et al. Frequencies of circulating MDSC correlate with clinical outcome of melanoma patients treated with ipilimumab. *Cancer Immunol Immunother*. 2014;63(3):247-257. doi:10.1007/s00262-013-1508-5

299. Yan HH, Pickup M, Pang Y, et al. Gr-1+CD11b+ Myeloid Cells Tip the Balance of Immune Protection to Tumor Promotion in the Premetastatic Lung. *Cancer Res*. 2010;70(15):6139-6149. doi:10.1158/0008-5472.CAN-10-0706

300. Im JH, Fu W, Wang H, et al. Coagulation Facilitates Tumor Cell Spreading in the Pulmonary Vasculature during Early Metastatic Colony Formation. *Cancer Res*. 2004;64(23):8613-8619. doi:10.1158/0008-5472.CAN-04-2078

301. Ware CF. The TNF superfamily. *Cytokine Growth Factor Rev*. 14(3-4):181-184. http://www.ncbi.nlm.nih.gov/pubmed/12787557. Accessed March 10, 2019.

302. Locksley RM, Killeen N, Lenardo MJ. The TNF and TNF receptor superfamilies: integrating mammalian biology. *Cell*. 2001;104(4):487-501. http://www.ncbi.nlm.nih.gov/pubmed/11239407. Accessed March 10, 2019.

303. Williams TW, Granger GA. Lymphocyte in vitro cytotoxicity: Mechanism of human lymphotoxin-induced target cell destruction. *Cell Immunol*. 1973;6(2):171-185. doi:10.1016/0008-8749(73)90020-8

304. GRANGER GA, WILLIAMS TW. Lymphocyte Cytotoxicity in vitro: Activation and Release of a Cytotoxic Factor. *Nature*. 1968;218(5148):1253-1254. doi:10.1038/2181253a0

305. Ruddle NH, Waksman BH. Cytotoxic effect of lymphocyte-antigen interaction in delayed hypersensitivity. *Science*. 1967;157(3792):1060-1062. http://www.ncbi.nlm.nih.gov/pubmed/6036235. Accessed March 10, 2019.

306. Ware CF. NETWORK COMMUNICATIONS: Lymphotoxins, LIGHT, and TNF. *Annu Rev Immunol*. 2005;23(1):787-819. doi:10.1146/annurev.immunol.23.021704.115719

307. Jones EY, Stuart DI, Walker NPC. Structure of tumour necrosis factor. *Nature*. 1989;338(6212):225-228. doi:10.1038/338225a0

308. Browning JL, Androlewicz MJ, Ware CF. Lymphotoxin and an associated 33-kDa glycoprotein are expressed on the surface of an activated human T cell hybridoma. *J Immunol*. 1991;147(4):1230-1237. http://www.ncbi.nlm.nih.gov/pubmed/1714477. Accessed March 10, 2019.

309. Seleznik G, Seeger H, Bauer J, et al. The lymphotoxin β receptor is a potential therapeutic target in renal inflammation. *Kidney Int*. 2016;89(1):113-126. doi:10.1038/ki.2015.280

310. Seleznik GM, Reding T, Romrig F, et al. Lymphotoxin β Receptor Signaling Promotes Development of Autoimmune Pancreatitis. *Gastroenterology*. 2012;143(5):1361-1374. doi:10.1053/j.gastro.2012.07.112

311. Ware CF, VanArsdale TL, Crowe PD, Browning JL. The ligands and receptors of the lymphotoxin system. *Curr Top Microbiol Immunol*. 1995;198:175-218. http://www.ncbi.nlm.nih.gov/pubmed/7774281. Accessed March 10, 2019.

312. Browning JL, Ngam-ek A, Lawton P, et al. Lymphotoxin beta, a novel member of the TNF family that forms a heteromeric complex with lymphotoxin on the cell surface. *Cell*. 1993;72(6):847-856. http://www.ncbi.nlm.nih.gov/pubmed/7916655. Accessed March 10, 2019.

313. Mauri DN, Ebner R, Montgomery RI, et al. LIGHT, a new member of the TNF superfamily, and lymphotoxin alpha are ligands for herpesvirus entry mediator. *Immunity*. 1998;8(1):21-30. http://www.ncbi.nlm.nih.gov/pubmed/9462508. Accessed March 10, 2019.

314. Montgomery RI, Warner MS, Lum BJ, Spear PG. Herpes simplex virus-1 entry into cells mediated by a novel member of the TNF/NGF receptor family. *Cell*. 1996;87(3):427-436. http://www.ncbi.nlm.nih.gov/pubmed/8898196. Accessed March 10, 2019.

315. Oeckinghaus A, Hayden MS, Ghosh S. Crosstalk in NF-κB signaling pathways. *Nat Immunol*. 2011;12(8):695-708. doi:10.1038/ni.2065

316. Schall TJ, Lewis M, Koller KJ, et al. Molecular cloning and expression of a receptor for human tumor necrosis factor. *Cell*. 1990;61(2):361-370. http://www.ncbi.nlm.nih.gov/pubmed/2158863. Accessed March 10, 2019.

317. Coope HJ, Atkinson PGP, Huhse B, et al. CD40 regulates the processing of NF-kappaB2 p100 to p52. *EMBO J*. 2002;21(20):5375-5385. http://www.ncbi.nlm.nih.gov/pubmed/12374738. Accessed March 10, 2019.

318. Dejardin E, Droin NM, Delhase M, et al. The lymphotoxin-beta receptor induces different patterns of gene expression via two NF-kappaB pathways. *Immunity*. 2002;17(4):525-535. http://www.ncbi.nlm.nih.gov/pubmed/12387745. Accessed

March 10, 2019.

319. Browning JL, French LE. Visualization of lymphotoxin-beta and lymphotoxin-beta receptor expression in mouse embryos. *J Immunol*. 2002;168(10):5079-5087. http://www.ncbi.nlm.nih.gov/pubmed/11994460. Accessed March 11, 2019.

320. Remouchamps C, Boutaffala L, Ganeff C, Dejardin E. Biology and signal transduction pathways of the Lymphotoxin-αβ/LTβR system. *Cytokine Growth Factor Rev*. 2011;22(5-6):301-310. doi:10.1016/j.cytogfr.2011.11.007

321. Gommerman JL, Browning JL. Lymphotoxin/LIGHT, lymphoid microenvironments and autoimmune disease. *Nat Rev Immunol*. 2003;3(8):642-655. doi:10.1038/nri1151

322. De Togni P, Goellner J, Ruddle NH, et al. Abnormal development of peripheral lymphoid organs in mice deficient in lymphotoxin. *Science*. 1994;264(5159):703-707. http://www.ncbi.nlm.nih.gov/pubmed/8171322. Accessed March 11, 2019.

323. Koni PA, Sacca R, Lawton P, Browning JL, Ruddle NH, Flavell RA. Distinct roles in lymphoid organogenesis for lymphotoxins alpha and beta revealed in lymphotoxin beta-deficient mice. *Immunity*. 1997;6(4):491-500. http://www.ncbi.nlm.nih.gov/pubmed/9133428. Accessed March 11, 2019.

324. Nishikawa S-I, Honda K, Vieira P, Yoshida H. Organogenesis of peripheral lymphoid organs. *Immunol Rev*. 2003;195:72-80. http://www.ncbi.nlm.nih.gov/pubmed/12969311. Accessed March 11, 2019.

325. Ansel KM, Ngo VN, Hyman PL, et al. A chemokine-driven positive feedback loop organizes lymphoid follicles. *Nature*. 2000;406(6793):309-314. doi:10.1038/35018581

326. Fu YX, Molina H, Matsumoto M, Huang G, Min J, Chaplin DD. Lymphotoxin-alpha (LTalpha) supports development of splenic follicular structure that is required for IgG responses. *J Exp Med*. 1997;185(12):2111-2120. http://www.ncbi.nlm.nih.gov/pubmed/9182683. Accessed March 11, 2019.

327. Gommerman JL, Mackay F, Donskoy E, Meier W, Martin P, Browning JL. Manipulation of lymphoid microenvironments in nonhuman primates by an inhibitor of the lymphotoxin pathway. *J Clin Invest*. 2002;110(9):1359-1369. doi:10.1172/JCI15975

328. Lu TT, Cyster JG. Integrin-Mediated Long-Term B Cell Retention in the Splenic Marginal Zone. *Science (80-)*. 2002;297(5580):409-412. doi:10.1126/science.1071632

329. Lorenz RG, Chaplin DD, McDonald KG, McDonough JS, Newberry RD. Isolated lymphoid follicle formation is inducible and dependent upon lymphotoxin-sufficient B lymphocytes, lymphotoxin beta receptor, and TNF receptor I function. *J Immunol*. 2003;170(11):5475-5482. http://www.ncbi.nlm.nih.gov/pubmed/12759424. Accessed March 11, 2019.

330. Browning JL, Allaire N, Ngam-ek A, et al. Lymphotoxin-β Receptor Signaling Is Required for the Homeostatic Control of HEV Differentiation and Function. *Immunity*. 2005;23(5):539-550. doi:10.1016/j.immuni.2005.10.002

331. Iizuka K, Chaplin DD, Wang Y, et al. Requirement for membrane lymphotoxin in natural killer cell development. *Proc Natl Acad Sci U S A*. 1999;96(11):6336-6340. http://www.ncbi.nlm.nih.gov/pubmed/10339588. Accessed March 11, 2019.

332. Wu Q, Wang Y, Wang J, Hedgeman EO, Browning JL, Fu YX. The requirement of membrane lymphotoxin for the presence of dendritic cells in lymphoid tissues. *J Exp Med*. 1999;190(5):629-638. http://www.ncbi.nlm.nih.gov/pubmed/10477548. Accessed March 11, 2019.

333. McCarthy DD, Summers-Deluca L, Vu F, Chiu S, Gao Y, Gommerman JL. The Lymphotoxin Pathway: Beyond Lymph Node Development. *Immunol Res*. 2006;35(1-2):41-54. doi:10.1385/IR:35:1:41

334. Kang H-S, Blink SE, Chin RK, et al. Lymphotoxin Is Required for Maintaining Physiological Levels of Serum IgE That Minimizes Th1-mediated Airway Inflammation. *J Exp Med*. 2003;198(11):1643-1652. doi:10.1084/jem.20021784

335. Drayton DL, Ying X, Lee J, Lesslauer W, Ruddle NH. Ectopic LT alpha beta directs lymphoid organ neogenesis with concomitant expression of peripheral node addressin and a HEV-restricted sulfotransferase. *J Exp Med*. 2003;197(9):1153-1163. doi:10.1084/jem.20021761

336. Chin RK, Lo JC, Kim O, et al. Lymphotoxin pathway directs thymic Aire expression. *Nat Immunol*. 2003;4(11):1121-1127. doi:10.1038/ni982

337. Zhu M, Chin RK, Christiansen PA, et al. NF-κB2 is required for the establishment of central tolerance through an Aire-dependent pathway. *J Clin Invest*. 2006;116(11):2964-2971. doi:10.1172/JCI28326

338. Ware CF, Crowe PD, Grayson MH, Androlewicz MJ, Browning JL. Expression of surface lymphotoxin and tumor necrosis factor on activated T, B, and natural killer cells. *J Immunol*. 1992;149(12):3881-3888. http://www.ncbi.nlm.nih.gov/pubmed/1281193. Accessed March 11, 2019.

339. Drayton DL, Liao S, Mounzer RH, Ruddle NH. Lymphoid organ development: from ontogeny to neogenesis. *Nat Immunol*. 2006;7(4):344-353. doi:10.1038/ni1330

340. Kratz A, Campos-Neto A, Hanson MS, Ruddle NH. Chronic inflammation caused by lymphotoxin is lymphoid neogenesis. *J Exp Med*. 1996;183(4):1461-1472. http://www.ncbi.nlm.nih.gov/pubmed/8666904. Accessed March 11, 2019.

341. Gommerman JL, Giza K, Perper S, et al. A role for surface lymphotoxin in experimental autoimmune encephalomyelitis independent of LIGHT. *J Clin Invest*. 2003;112(5):755-767. doi:10.1172/JCI18648

342. Kang H-S, Chin RK, Wang Y, et al. Signaling via LTβR on the lamina propria stromal cells of the gut is required for IgA production. *Nat Immunol*. 2002;3(6):576-582. doi:10.1038/ni795

343. Fava RA, Notidis E, Hunt J, et al. A role for the lymphotoxin/LIGHT axis in the pathogenesis of murine collagen-induced arthritis. *J Immunol*. 2003;171(1):115-126.

http://www.ncbi.nlm.nih.gov/pubmed/12816989. Accessed March 11, 2019.

344. Körner H, Riminton DS, Strickland DH, Lemckert FA, Pollard JD, Sedgwick JD. Critical points of tumor necrosis factor action in central nervous system autoimmune inflammation defined by gene targeting. *J Exp Med*. 1997;186(9):1585-1590. http://www.ncbi.nlm.nih.gov/pubmed/9348316. Accessed March 11, 2019.

345. Olsen NJ, Stein CM. New Drugs for Rheumatoid Arthritis. Wood AJJ, ed. *N Engl J Med*. 2004;350(21):2167-2179. doi:10.1056/NEJMra032906

346. Browning JL. Inhibition of the lymphotoxin pathway as a therapy for autoimmune disease. *Immunol Rev*. 2008;223(1):202-220. doi:10.1111/j.1600-065X.2008.00633.x

347. Ekström K, Hjalgrim H, Brandt L, et al. Risk of malignant lymphomas in patients with rheumatoid arthritis and in their first-degree relatives. *Arthritis Rheum*. 2003;48(4):963-970. doi:10.1002/art.10939

348. Guo Z, Wang J, Meng L, et al. Cutting edge: membrane lymphotoxin regulates CD8(+) T cell-mediated intestinal allograft rejection. *J Immunol*. 2001;167(9):4796-4800. http://www.ncbi.nlm.nih.gov/pubmed/11673481. Accessed March 11, 2019.

349. Markey KA, Burman AC, Banovic T, et al. Soluble lymphotoxin is an important effector molecule in GVHD and GVL. *Blood*. 2010;115(1):122-132. doi:10.1182/blood-2009-01-199927

350. Upadhyay V, Poroyko V, Kim T, et al. Lymphotoxin regulates commensal responses to enable diet-induced obesity. *Nat Immunol*. 2012;13(10):947-953. doi:10.1038/ni.2403

351. Hamid YH, Urhammer SA, Gl&#xfffd;mer C, et al. The common T60N polymorphism of the lymphotoxin-? gene is associated with type 2 diabetes and other phenotypes of the metabolic syndrome. *Diabetologia*. 2005;48(3):445-451. doi:10.1007/s00125-004-1659-1

352. Tumanov A V., Koroleva EP, Christiansen PA, et al. T Cell-Derived Lymphotoxin Regulates Liver Regeneration. *Gastroenterology*. 2009;136(2):694-704.e4. doi:10.1053/j.gastro.2008.09.015

353. Ruddell RG, Knight B, Tirnitz-Parker JEE, et al. Lymphotoxin-β receptor signaling regulates hepatic stellate cell function and wound healing in a murine model of chronic liver injury. *Hepatology*. 2009;49(1):227-239. doi:10.1002/hep.22597

354. Seet BT, Johnston JB, Brunetti CR, et al. Poxviruses and immune evasion. *Annu Rev Immunol*. 2003;21(1):377-423. doi:10.1146/annurev.immunol.21.120601.141049

355. Luftig M, Yasui T, Soni V, et al. Epstein-Barr virus latent infection membrane protein 1 TRAF-binding site induces NIK/IKK -dependent noncanonical NF- B activation. *Proc Natl Acad Sci*. 2004;101(1):141-146. doi:10.1073/pnas.2237183100

356. Spear PG. Herpes simplex virus: receptors and ligands for cell entry. *Cell Microbiol*. 2004;6(5):401-410. doi:10.1111/j.1462-5822.2004.00389.x

357. Takei K, Ikeda S, Arai T, Tanaka N, Muramatsu M, Sawabe M. Lymphotoxin-alpha

polymorphisms and presence of cancer in 1,536 consecutive autopsy cases. *BMC Cancer*. 2008;8(1):235. doi:10.1186/1471-2407-8-235

358. NONOMURA N, TOKIZANE T, NAKAYAMA M, et al. Possible correlation between polymorphism in the tumor necrosis factor-beta gene and the clinicopathological features of bladder cancer in Japanese patients. *Int J Urol*. 2006;13(7):971-976. doi:10.1111/j.1442-2042.2006.01450.x

359. Niwa Y, Ito H, Matsuo K, et al. Lymphotoxin-α polymorphisms and the risk of endometrial cancer in Japanese subjects. *Gynecol Oncol*. 2007;104(3):586-590. doi:10.1016/j.ygyno.2006.09.007

360. Yamagishi M, Nakano K, Miyake A, et al. Polycomb-Mediated Loss of miR-31 Activates NIK-Dependent NF-κB Pathway in Adult T Cell Leukemia and Other Cancers. *Cancer Cell*. 2012;21(1):121-135. doi:10.1016/j.ccr.2011.12.015

361. Ammirante M, Luo J-L, Grivennikov S, Nedospasov S, Karin M. B-cell-derived lymphotoxin promotes castration-resistant prostate cancer. *Nature*. 2010;464(7286):302-305. doi:10.1038/nature08782

362. Or YY-Y, Chung GT-Y, To K-F, et al. Identification of a novel 12p13.3 amplicon in nasopharyngeal carcinoma. *J Pathol*. 2010;220(1):97-107. doi:10.1002/path.2609

363. Keats JJ, Fonseca R, Chesi M, et al. Promiscuous Mutations Activate the Noncanonical NF-κB Pathway in Multiple Myeloma. *Cancer Cell*. 2007;12(2):131-144. doi:10.1016/j.ccr.2007.07.003

364. Browning JL, Miatkowski K, Sizing I, et al. Signaling through the lymphotoxin beta receptor induces the death of some adenocarcinoma tumor lines. *J Exp Med*. 1996;183(3):867-878. http://www.ncbi.nlm.nih.gov/pubmed/8642291. Accessed March 11, 2019.

365. Ito D, Back TC, Shakhov AN, Wiltrout RH, Nedospasov SA. Mice with a targeted mutation in lymphotoxin-alpha exhibit enhanced tumor growth and metastasis: impaired NK cell development and recruitment. *J Immunol*. 1999;163(5):2809-2815. http://www.ncbi.nlm.nih.gov/pubmed/10453025. Accessed March 11, 2019.

366. Rehm A, Mensen A, Schradi K, et al. Cooperative function of CCR7 and lymphotoxin in the formation of a lymphoma-permissive niche within murine secondary lymphoid organs. *Blood*. 2011;118(4):1020-1033. doi:10.1182/blood-2010-11-321265

367. Hehlgans T, Stoelcker B, Stopfer P, et al. Lymphotoxin-beta receptor immune interaction promotes tumor growth by inducing angiogenesis. *Cancer Res*. 2002;62(14):4034-4040. http://www.ncbi.nlm.nih.gov/pubmed/12124338. Accessed March 11, 2019.

368. Pahl HL. Activators and target genes of Rel/NF-κB transcription factors. *Oncogene*. 1999;18(49):6853-6866. doi:10.1038/sj.onc.1203239

369. Barnes PJ, Karin M. Nuclear Factor-κB — A Pivotal Transcription Factor in Chronic Inflammatory Diseases. Epstein FH, ed. *N Engl J Med*. 1997;336(15):1066-1071.

doi:10.1056/NEJM199704103361506

370. Ben-Neriah Y, Karin M. Inflammation meets cancer, with NF-κB as the matchmaker. *Nat Immunol*. 2011;12(8):715-723. doi:10.1038/ni.2060

371. Ruland J. Return to homeostasis: downregulation of NF-κB responses. *Nat Immunol*. 2011;12(8):709-714. doi:10.1038/ni.2055

372. Lawrence T, Gilroy DW, Colville-Nash PR, Willoughby DA. Possible new role for NF-κB in the resolution of inflammation. *Nat Med*. 2001;7(12):1291-1297. doi:10.1038/nm1201-1291

373. Guttridge DC, Albanese C, Reuther JY, Pestell RG, Baldwin AS. NF-kappaB controls cell growth and differentiation through transcriptional regulation of cyclin D1. *Mol Cell Biol*. 1999;19(8):5785-5799. http://www.ncbi.nlm.nih.gov/pubmed/10409765. Accessed March 13, 2019.

374. La Rosa FA, Pierce JW, Sonenshein GE. Differential regulation of the c-myc oncogene promoter by the NF-kappa B rel family of transcription factors. *Mol Cell Biol*. 1994;14(2):1039-1044. http://www.ncbi.nlm.nih.gov/pubmed/8289784. Accessed March 13, 2019.

375. Duckett CS. Apoptosis and NF-kappa B: the FADD connection. *J Clin Invest*. 2002;109(5):579-580. doi:10.1172/JCI15197

376. Collins T, Read MA, Neish AS, Whitley MZ, Thanos D, Maniatis T. Transcriptional regulation of endothelial cell adhesion molecules: NF-kappa B and cytokine-inducible enhancers. *FASEB J*. 1995;9(10):899-909. http://www.ncbi.nlm.nih.gov/pubmed/7542214. Accessed March 13, 2019.

377. Caamaño J, Hunter CA. NF-kappaB family of transcription factors: central regulators of innate and adaptive immune functions. *Clin Microbiol Rev*. 2002;15(3):414-429. doi:10.1128/CMR.15.3.414-429.2002

378. Nickols JC, Valentine W, Kanwal S, Carter BD. Activation of the transcription factor NF-κB in Schwann cells is required for peripheral myelin formation. *Nat Neurosci*. 2003;6(2):161-167. doi:10.1038/nn995

379. Cao Y, Karin M. NF-kappaB in mammary gland development and breast cancer. *J Mammary Gland Biol Neoplasia*. 2003;8(2):215-223. http://www.ncbi.nlm.nih.gov/pubmed/14635796. Accessed March 13, 2019.

380. Snapper CM, Zelazowski P, Rosas FR, et al. B cells from p50/NF-kappa B knockout mice have selective defects in proliferation, differentiation, germ-line CH transcription, and Ig class switching. *J Immunol*. 1996;156(1):183-191. http://www.ncbi.nlm.nih.gov/pubmed/8598461. Accessed March 13, 2019.

381. Hayden MS, Ghosh S. NF-κB in immunobiology. *Cell Res*. 2011;21(2):223-244. doi:10.1038/cr.2011.13

382. Pasparakis M, Luedde T, Schmidt-Supprian M. Dissection of the NF-κB signalling

cascade in transgenic and knockout mice. *Cell Death Differ*. 2006;13(5):861-872. doi:10.1038/sj.cdd.4401870

383. Bonizzi G, Karin M. The two NF-κB activation pathways and their role in innate and adaptive immunity. *Trends Immunol*. 2004;25(6):280-288. doi:10.1016/j.it.2004.03.008

384. Kaser A, Zeissig S, Blumberg RS. Inflammatory Bowel Disease. *Annu Rev Immunol*. 2010;28(1):573-621. doi:10.1146/annurev-immunol-030409-101225

385. Neurath MF, Pettersson S, Meyer zum Büschenfelde KH, Strober W. Local administration of antisense phosphorothioate oligonucleotides to the p65 subunit of NF-kappa B abrogates established experimental colitis in mice. *Nat Med*. 1996;2(9):998-1004. http://www.ncbi.nlm.nih.gov/pubmed/8782457. Accessed March 13, 2019.

386. Tak PP, Gerlag DM, Aupperle KR, et al. Inhibitor of nuclear factor ?B kinase ? is a key regulator of synovial inflammation. *Arthritis Rheum*. 2001;44(8):1897-1907. doi:10.1002/1529-0131(200108)44:8<1897::AID-ART328>3.0.CO;2-4

387. Pasparakis M. Regulation of tissue homeostasis by NF-κB signalling: implications for inflammatory diseases. *Nat Rev Immunol*. 2009;9(11):778-788. doi:10.1038/nri2655

388. Eckmann L, Nebelsiek T, Fingerle AA, et al. Opposing functions of IKKbeta during acute and chronic intestinal inflammation. *Proc Natl Acad Sci U S A*. 2008;105(39):15058-15063. doi:10.1073/pnas.0808216105

389. Yin L, Wu L, Wesche H, et al. Defective Lymphotoxin-beta Receptor-Induced NF-kappa B Transcriptional Activity in NIK-Deficient Mice. *Science (80-)*. 2001;291(5511):2162-2165. doi:10.1126/science.1058453

390. Flier JS, Underhill LH, Dvorak HF. Tumors: Wounds That Do Not Heal. *N Engl J Med*. 1986;315(26):1650-1659. doi:10.1056/NEJM198612253152606

391. Karin M, Cao Y, Greten FR, Li Z-W. NF-κB in cancer: from innocent bystander to major culprit. *Nat Rev Cancer*. 2002;2(4):301-310. doi:10.1038/nrc780

392. Bredel M, Scholtens DM, Yadav AK, et al. NFKBIA Deletion in Glioblastomas. *N Engl J Med*. 2011;364(7):627-637. doi:10.1056/NEJMoa1006312

393. Vallabhapurapu S, Karin M. Regulation and Function of NF-κB Transcription Factors in the Immune System. *Annu Rev Immunol*. 2009;27(1):693-733. doi:10.1146/annurev.immunol.021908.132641

394. Neri A, Chang CC, Lombardi L, et al. B cell lymphoma-associated chromosomal translocation involves candidate oncogene lyt-10, homologous to NF-kappa B p50. *Cell*. 1991;67(6):1075-1087. http://www.ncbi.nlm.nih.gov/pubmed/1760839. Accessed March 13, 2019.

395. Gonzalez-Suarez E, Jacob AP, Jones J, et al. RANK ligand mediates progestin-induced mammary epithelial proliferation and carcinogenesis. *Nature*. 2010;468(7320):103-

107. doi:10.1038/nature09495

396. Schramek D, Leibbrandt A, Sigl V, et al. Osteoclast differentiation factor RANKL controls development of progestin-driven mammary cancer. *Nature*. 2010;468(7320):98-102. doi:10.1038/nature09387

397. Tan W, Zhang W, Strasner A, et al. Tumour-infiltrating regulatory T cells stimulate mammary cancer metastasis through RANKL–RANK signalling. *Nature*. 2011;470(7335):548-553. doi:10.1038/nature09707

398. Greten FR, Eckmann L, Greten TF, et al. IKKβ Links Inflammation and Tumorigenesis in a Mouse Model of Colitis-Associated Cancer. *Cell*. 2004;118(3):285-296. doi:10.1016/j.cell.2004.07.013

399. Grivennikov S, Karin E, Terzic J, et al. IL-6 and Stat3 Are Required for Survival of Intestinal Epithelial Cells and Development of Colitis-Associated Cancer. *Cancer Cell*. 2009;15(2):103-113. doi:10.1016/j.ccr.2009.01.001

400. Yu H, Kortylewski M, Pardoll D. Crosstalk between cancer and immune cells: role of STAT3 in the tumour microenvironment. *Nat Rev Immunol*. 2007;7(1):41-51. doi:10.1038/nri1995

401. Colotta F, Allavena P, Sica A, Garlanda C, Mantovani A. Cancer-related inflammation, the seventh hallmark of cancer: links to genetic instability. *Carcinogenesis*. 2009;30(7):1073-1081. doi:10.1093/carcin/bgp127

402. Hagemann T, Lawrence T, McNeish I, et al. “Re-educating” tumor-associated macrophages by targeting NF-κB. *J Exp Med*. 2008;205(6):1261-1268. doi:10.1084/jem.20080108

403. Erez N, Truitt M, Olson P, Hanahan D, Hanahan D. Cancer-Associated Fibroblasts Are Activated in Incipient Neoplasia to Orchestrate Tumor-Promoting Inflammation in an NF-κB-Dependent Manner. *Cancer Cell*. 2010;17(2):135-147. doi:10.1016/j.ccr.2009.12.041

404. Wu Y, Deng J, Rychahou PG, Qiu S, Evers BM, Zhou BP. Stabilization of snail by NF-kappaB is required for inflammation-induced cell migration and invasion. *Cancer Cell*. 2009;15(5):416-428. doi:10.1016/j.ccr.2009.03.016

405. He G, Yu G-Y, Temkin V, et al. Hepatocyte IKKbeta/NF-kappaB inhibits tumor promotion and progression by preventing oxidative stress-driven STAT3 activation. *Cancer Cell*. 2010;17(3):286-297. doi:10.1016/j.ccr.2009.12.048

406. Sakurai T, He G, Matsuzawa A, et al. Hepatocyte Necrosis Induced by Oxidative Stress and IL-1α Release Mediate Carcinogen-Induced Compensatory Proliferation and Liver Tumorigenesis. *Cancer Cell*. 2008;14(2):156-165. doi:10.1016/j.ccr.2008.06.016

407. Inokuchi S, Aoyama T, Miura K, et al. Disruption of TAK1 in hepatocytes causes hepatic injury, inflammation, fibrosis, and carcinogenesis. *Proc Natl Acad Sci*. 2010;107(2):844-849. doi:10.1073/pnas.0909781107

408. Bettermann K, Vucur M, Haybaeck J, et al. TAK1 Suppresses a NEMO-Dependent but NF-κB-Independent Pathway to Liver Cancer. *Cancer Cell*. 2010;17(5):481-496. doi:10.1016/j.ccr.2010.03.021

409. Dajee M, Lazarov M, Zhang JY, et al. NF-κB blockade and oncogenic Ras trigger invasive human epidermal neoplasia. *Nature*. 2003;421(6923):639-643. doi:10.1038/nature01283

410. Acosta JC, O'Loghlen A, Banito A, et al. Chemokine Signaling via the CXCR2 Receptor Reinforces Senescence. *Cell*. 2008;133(6):1006-1018. doi:10.1016/j.cell.2008.03.038

411. Lee D-F, Hung M-C. Advances in Targeting IKK and IKK-Related Kinases for Cancer Therapy. *Clin Cancer Res*. 2008;14(18):5656-5662. doi:10.1158/1078-0432.CCR-08-0123

412. Nakanishi C, Toi M. Nuclear factor-κB inhibitors as sensitizers to anticancer drugs. *Nat Rev Cancer*. 2005;5(4):297-309. doi:10.1038/nrc1588

413. Carvajal RD, Schwartz GK, Tezel T, Marr B, Francis JH, Nathan PD. Metastatic disease from uveal melanoma: treatment options and future prospects. *Br J Ophthalmol*. 2017;101(1):38-44. doi:10.1136/bjophthalmol-2016-309034

414. Grossniklaus HE. Progression of ocular melanoma metastasis to the liver: the 2012 Zimmerman lecture. *JAMA Ophthalmol*. 2013;131(4):462-469. doi:10.1001/jamaophthalmol.2013.2547

415. Krüger A, Schirrmacher V, Hoegen P Von. Scattered micrometastases visualized at the single-cell level: Detection and re-isolation of lacZ-labeled metastasized lymphoma cells. *Int J Cancer*. 1994;58(2):275-284. doi:10.1002/ijc.2910580222

416. Adams JM, Harris AW, Pinkert CA, et al. The c-myc oncogene driven by immunoglobulin enhancers induces lymphoid malignancy in transgenic mice. *Nature*. 1985;318(6046):533-538. doi:10.1038/318533a0

417. Bichi R, Shinton SA, Martin ES, et al. Human chronic lymphocytic leukemia modeled in mouse by targeted TCL1 expression. *Proc Natl Acad Sci*. 2002;99(10):6955-6960. doi:10.1073/pnas.102181599

418. Hanahan D. Heritable formation of pancreatic beta-cell tumours in transgenic mice expressing recombinant insulin/simian virus 40 oncogenes. *Nature*. 315(6015):115-122. http://www.ncbi.nlm.nih.gov/pubmed/2986015. Accessed December 30, 2018.

419. Jacque CM, Vinner C, Kujas M, Raoul M, Racadot J, Baumann NA. Determination of glial fibrillary acidic protein (GFAP) in human brain tumors. *J Neurol Sci*. 1978;35(1):147-155. doi:10.1016/0022-510X(78)90107-7

420. Roessmann U, Velasco ME, Sindely SD, Gambetti P. Glial fibrillary acidic protein (GFAP) in ependymal cells during development. An immunocytochemical study. *Brain Res*. 1980;200(1):13-21. doi:10.1016/0006-8993(80)91090-2

421. Buniatian G, Traub P, Albinus M, et al. The immunoreactivity of glial fibrillary acidic

protein in mesangial cells and podocytes of the glomeruli of rat kidney in vivo and in culture. *Biol Cell*. 1998;90(1):53-61. doi:10.1016/S0248-4900(98)80232-3

422. von Koskull H. Rapid identification of glial cells in human amniotic fluid with indirect immunofluorescence. *Acta Cytol*. 28(4):393-400. http://www.ncbi.nlm.nih.gov/pubmed/6205529. Accessed January 5, 2019.

423. Kasantikul V, Shuangshoti S. Positivity to glial fibrillary acidic protein in bone, cartilage, and chordoma. *J Surg Oncol*. 1989;41(1):22-26. http://www.ncbi.nlm.nih.gov/pubmed/2654484. Accessed January 5, 2019.

424. Apte M V, Haber PS, Applegate TL, et al. Periacinar stellate shaped cells in rat pancreas: identification, isolation, and culture. *Gut*. 1998;43(1):128-133. http://www.ncbi.nlm.nih.gov/pubmed/9771417. Accessed January 5, 2019.

425. Nishiyama A, Dahlin KJ, Prince JT, Johnstone SR, Stallcup WB. The primary structure of NG2, a novel membrane-spanning proteoglycan. *J Cell Biol*. 1991;114(2):359-371. http://www.ncbi.nlm.nih.gov/pubmed/1906475. Accessed January 5, 2019.

426. Ozerdem U, Grako KA, Dahlin-Huppe K, Monosov E, Stallcup WB. NG2 proteoglycan is expressed exclusively by mural cells during vascular morphogenesis. *Dev Dyn*. 2001;222(2):218-227. doi:10.1002/dvdy.1200

427. Levine JM, Reynolds R, Fawcett JW. The oligodendrocyte precursor cell in health and disease. *Trends Neurosci*. 2001;24(1):39-47. http://www.ncbi.nlm.nih.gov/pubmed/11163886. Accessed January 5, 2019.

428. Al-Mayhani MTF, Grenfell R, Narita M, et al. NG2 expression in glioblastoma identifies an actively proliferating population with an aggressive molecular signature. *Neuro Oncol*. 2011;13(8):830-845. doi:10.1093/neuonc/nor088

429. Stallcup WB. The NG2 proteoglycan: past insights and future prospects. *J Neurocytol*. 31(6-7):423-435. http://www.ncbi.nlm.nih.gov/pubmed/14501214. Accessed January 5, 2019.

430. Levine JM, Nishiyama A. The NG2 chondroitin sulfate proteoglycan: a multifunctional proteoglycan associated with immature cells. *Perspect Dev Neurobiol*. 1996;3(4):245-259. http://www.ncbi.nlm.nih.gov/pubmed/9117258. Accessed January 5, 2019.

431. Niki T, Pekny M, Hellemans K, et al. Class VI intermediate filament protein nestin is induced during activation of rat hepatic stellate cells. *Hepatology*. 1999;29(2):520-527. doi:10.1002/hep.510290232

432. Puche JE, Saiman Y, Friedman SL. Hepatic Stellate Cells and Liver Fibrosis. In: *Comprehensive Physiology*. Vol 3. Hoboken, NJ, USA: John Wiley & Sons, Inc.; 2013:1473-1492. doi:10.1002/cphy.c120035

433. Xu L, Hui AY, Albanis E, et al. Human hepatic stellate cell lines, LX-1 and LX-2: New tools for analysis of hepatic fibrosis. *Gut*. 2005. doi:10.1136/gut.2004.042127

434. Das D, Barnes MA, Nagy LE. Anaphylatoxin C5a modulates hepatic stellate cell

migration. *Fibrogenesis Tissue Repair*. 2014;7:9. doi:10.1186/1755-1536-7-9

435. Yang C, Zeisberg M, Mosterman B, et al. Liver fibrosis: Insights into migration of hepatic stellate cells in response to extracellular matrix and growth factors. *Gastroenterology*. 2003;124(1):147-159. doi:10.1053/gast.2003.50012

436. Boulanger C, Durand F, Moreau R, et al. Liver sinusoidal endothelial cells: Physiology and role in liver diseases. *J Hepatol*. 2016;66(1):212-227. doi:10.1016/j.jhep.2016.07.009

437. Fielding L. Current imaging strategies of primary and secondary neoplasms of the liver. *Semin Intervent Radiol*. 2006;23(1):3-12. doi:10.1055/s-2006-939836

438. Wu X, Takekoshi T, Sullivan A, Hwang ST. Inflammation and tumor microenvironment in lymph node metastasis. *Cancers (Basel)*. 2011;3(1):927-944. doi:10.3390/cancers3010927

439. Sironi L, Banfi C, Brioschi M, et al. Activation of NF-kB and ERK1/2 after permanent focal ischemia is abolished by simvastatin treatment. *Neurobiol Dis*. 2006;22(2):445-451. doi:10.1016/J.NBD.2005.12.004

440. Mebratu Y, Tesfaigzi Y. How ERK1/2 activation controls cell proliferation and cell death: Is subcellular localization the answer? *Cell Cycle*. 2009;8(8):1168-1175. doi:10.4161/cc.8.8.8147

441. Ala A, Brown D, Khan K, et al. Mucosal Addressin Cell Adhesion Molecule (MAdCAM-1) Expression Is Upregulated in the Cirrhotic Liver and Immunolocalises to the Peribiliary Plexus and Lymphoid Aggregates. *Dig Dis Sci*. 2013;58(9):2528-2541. doi:10.1007/s10620-013-2755-1

442. Grant A, Lalor PF, Hübscher SG, Briskin M, Adams DH. MAdCAM-1 expressed in chronic inflammatory liver disease supports mucosal lymphocyte adhesion to hepatic endothelium (MAdCAM-1 in chronic inflammatory liver disease). *Hepatology*. 2001;33(5):1065-1072. doi:10.1053/jhep.2001.24231

443. Seano G. Targeting the perivascular niche in brain tumors. *Curr Opin Oncol*. 2018;30(1):54-60. doi:10.1097/CCO.0000000000000417

444. Knittel T, Mehde M, Kobold D, Saile B, Dinter C, Ramadori G. Expression patterns of matrix metalloproteinases and their inhibitors in parenchymal and non-parenchymal cells of rat liver: regulation by TNF-alpha and TGF-beta1. *J Hepatol*. 1999;30(1):48-60. http://www.ncbi.nlm.nih.gov/pubmed/9927150. Accessed April 8, 2019.

445. Wang X, Zhou Y, Tan R, et al. Mice lacking the matrix metalloproteinase-9 gene reduce renal interstitial fibrosis in obstructive nephropathy. *Am J Physiol Physiol*. 2010;299(5):F973-F982. doi:10.1152/ajprenal.00216.2010

446. Kaviratne M, Hesse M, Leusink M, et al. IL-13 activates a mechanism of tissue fibrosis that is completely TGF-beta independent. *J Immunol*. 2004;173(6):4020-4029. http://www.ncbi.nlm.nih.gov/pubmed/15356151. Accessed April 8, 2019.

447. Betsuyaku T, Fukuda Y, Parks WC, Shipley JM, Senior RM. Gelatinase B Is Required for Alveolar Bronchiolization after Intratracheal Bleomycin. *Am J Pathol*. 2000;157(2):525. doi:10.1016/S0002-9440(10)64563-4

448. Yu Q, Stamenkovic I. Cell surface-localized matrix metalloproteinase-9 proteolytically activates TGF-beta and promotes tumor invasion and angiogenesis. *Genes Dev*. 2000;14(2):163-176. http://www.ncbi.nlm.nih.gov/pubmed/10652271. Accessed April 8, 2019.

449. Lee CG, Homer RJ, Zhu Z, et al. Interleukin-13 induces tissue fibrosis by selectively stimulating and activating transforming growth factor beta(1). *J Exp Med*. 2001;194(6):809-821. http://www.ncbi.nlm.nih.gov/pubmed/11560996. Accessed April 8, 2019.

450. Cabrera S, Gaxiola M, Arreola JL, et al. Overexpression of MMP9 in macrophages attenuates pulmonary fibrosis induced by bleomycin☆. *Int J Biochem Cell Biol*. 2007;39(12):2324-2338. doi:10.1016/j.biocel.2007.06.022

451. Feng M, Ding J, Wang M, Zhang J, Zhu X, Guan W. Kupffer-derived matrix metalloproteinase-9 contributes to liver fibrosis resolution. *Int J Biol Sci*. 2018;14(9):1033-1040. doi:10.7150/ijbs.25589

452. Han Y-P, Yan C, Zhou L, Qin L, Tsukamoto H. A Matrix Metalloproteinase-9 Activation Cascade by Hepatic Stellate Cells in Trans-differentiation in the Three-dimensional Extracellular Matrix * Downloaded from. *J Biol Chem*. 2007;282(17):12928-12939. doi:10.1074/jbc.M700554200

453. Ramachandran P, Iredale JP. Liver fibrosis: a bidirectional model of fibrogenesis and resolution. *QJM*. 2012;105(9):813-817. doi:10.1093/qjmed/hcs069

454. CORRY DB, KISS A, SONG L-Z, et al. Overlapping and independent contributions of MMP2 and MMP9 to lung allergic inflammatory cell egression through decreased CC chemokines. *FASEB J*. 2004;18(9):995-997. doi:10.1096/fj.03-1412fje

455. Greenlee KJ, Corry DB, Engler DA, et al. Proteomic identification of in vivo substrates for matrix metalloproteinases 2 and 9 reveals a mechanism for resolution of inflammation. *J Immunol*. 2006;177(10):7312-7321. http://www.ncbi.nlm.nih.gov/pubmed/17082650. Accessed April 8, 2019.

456. Coito AJ. Leukocyte transmigration across endothelial and extracellular matrix protein barriers in liver ischemia/reperfusion injury. *Curr Opin Organ Transplant*. 2011;16(1):34-40. doi:10.1097/MOT.0b013e328342542e

457. Natarajan V, Harris EN, Kidambi S. SECs (Sinusoidal Endothelial Cells), Liver Microenvironment, and Fibrosis. *Biomed Res Int*. 2017;2017:4097205. doi:10.1155/2017/4097205

458. Chen Q, Massagué J. Molecular pathways: VCAM-1 as a potential therapeutic target in metastasis. *Clin Cancer Res*. 2012;18(20):5520-5525. doi:10.1158/1078-0432.CCR-11-2904

459. Kong D-H, Kim YK, Kim MR, Jang JH, Lee S. Emerging Roles of Vascular Cell Adhesion Molecule-1 (VCAM-1) in Immunological Disorders and Cancer. *Int J Mol Sci*. 2018;19(4). doi:10.3390/ijms19041057

460. Benedicto A, Romayor I, Arteta B. Role of liver ICAM-1 in metastasis. *Oncol Lett*. 2017;14(4):3883-3892. doi:10.3892/ol.2017.6700

List of Figures

Publications

1. “Single cell polarity in liquid phase facilitates tumour metastasis.”

Anna Lorentzen, **Paul F. Becker**, Jan Kosla, Massimo Saini, Kathrin Weidele, Paolo Ronchi, Corinna Klein, Monika J. Wolf, Felix Geist, Bastian Seubert, Marc Ringelhan, Daniela Mihic-Probst, Knud Esser, Marko Roblek, Felix Kuehne, Gaia Bianco, Tracy O’Connor, Quentin Müller, Kathleen Schuck, Sebastian Lange, Daniel Hartmann, Saskia Spaich, Olaf Groß, Jochen Utikal, Sebastian Haferkamp, Martin R. Sprick, Amruta Damle-Vartak, Alexander Hapfelmeier, Norbert Hüser, Ulrike Protzer, Andreas Trumpp, Dieter Saur, Nachiket Vartak, Christoph A. Klein, Bernhard Polzer, Lubor Borsig & Mathias Heikenwalder. *Nat Commun*. 2018;9(1):887. doi:10.1038/s41467-018-03139-6

2. “CCL2 is a vascular permeability factor inducing CCR2-dependent endothelial retraction during lung metastasis.”

Marko Roblek, Darya Protsyuk, **Paul F. Becker**, Cristina Stefanescu, Christian Gorzelanny, Jesus F. Glaus Garzon, Lucia Knopfova, Mathias Heikenwalder, Bruno Luckow, Stefan W Schneider and Lubor Borsig. *Mol Cancer Res*. December 2018:molcanres.0530.2018. doi:10.1158/1541-7786.MCR-18 0530

3. “Hepatic stellate cell-specific LTßR-signaling drives hepatic metastasis formation.”

Paul F. Vandersee, Jan Kosla, Suchira U. Gallage, Bastian Seubert, Nicole Simonavicius, Tracy O’Connor, Maria Garcia-Beccaria, Gaia Bianco, Katharina Kober, Silvia Affo, Anna Lorentzen, Dirk Wohlleber, Torsten Haferlach, Angela Krackhardt, Jeff Browning, Kristian Pietras, Robert Schwabe, Thomas Longerich, Matthias Matter, Achim Krüger, Lubor Borsig & Mathias Heikenwälder.

Manuscript in preparation

Achnowledgements

With the conclusion of my PhD thesis a whole chapter of my life will end and a long-lived dream will come true. Looking back I have to humbly acknowledge all the help I got and how much more one can achieve with support from good people and friends. I am incredibly grateful for all the people who helped and supported me in everywhich way during my PhD thesis in- and outside of the lab. It has been a long journey with many ups and downs and I would not have been able to go the distance without the support from my family and friends, the guidance and counsel from my thesis committee and collaborators and the helping hands from my colleagues.

First, I want to thank my parents as well as my brother and my sister for supporting me my entire life. They have always been there when I needed help, backed me up in my decisions and enabled me to pursue my studies and my career which have lead to this PhD thesis. They helped me broaden my horizon and sharpen my wits in countless discussions and shaped the way I am today. Without them I would certainly not be at this point today.

Second, I would like to thank my wife Nicole for her love and caring throughout these past years. For her incredible support in good and in bad times, for her patience and understanding when my work and the thesis seemed to consume all my time, and I couldn't spend as much time with her as she deserved. Also for being a great mother to my daughter Charlotte, who has been the joy of my life ever since she was born two years ago and who has made my life and my work so much easier by cheering me up every single day and by motivating me to be a better man.

Then, I would like to thank my awesome colleagues and lab members in Munich and Heidelberg who have made my life at work so much easier by supporting me in many different ways. I want to thank Robert, Ruth, Daniel, Olga, Reiner, Jenny and Danijela for their technical support and know-how and I want to thank Tjeerd, Patrick and Ulli for their support in the animal facilities. I want to thank Jan, Suchira, Flo, Jessi, Judith, Detian, Sukumar, Arlind and Marc for always having an open ear and helping hands and being fantastic colleagues. And of course I want to thank Anna, Nicole and Basti who have helped me tremendously and mentored me during a considerable amount of time of this thesis. Not to forget, I want to thank Monika and Marko from our collaborating lab in Zurich. Special thanks go to my office mates Tracy, Elena and Valentina for great discussions on scientific matters and beyond, for many cheerful moments and so much support.

I would also like to thank my collaboration partners for their support, input and critical discussions that have helped me to develop as a scientist and push my projects. Most notably I want to thank Prof. Robert Schwabe, Prof. Ulrich Keller, Prof. Thomas Longerich and Prof. Lubor Borsig.

I would like to thank Dr. Axel Szabowski and Dr. Almut Barden who have helped me tremendously with organizational and official matters when I had sore need and without whom I wouldn't have been able to finish my thesis the way I did.

Finally, I want to give my sincere gratitude to all members of my PhD committee. First and foremost to Prof. Mathias Heikenwälder for taking me into his lab and giving me the opportunity to do my PhD research and develop myself as a scientist and a person in general. For his counsel and guideance, for keeping me motivated and pushing me to my limits. Without him, all this would not have been possible. Furthermore, I want to thank Prof. Percy Knolle for taking up the position as first advisor after Prof. Heikenwälder moved to the DKFZ, for scientific input and support when needed. Then, I want to thank Prof. Lubor Borsig and Prof. Hans Hauner for their counsel during thesis committee meetings and critical input in general.

To all those mentioned above and all those I might have forgotten to mention – to everyone who helped me in everywhich way – I say: "Thank you from the bottom of my heart"!